13974
14.12.55

DATE LABEL

18 JUL 1978			
8 AUG 1979			

Call No. 535.1 M855P

Date 14.11.55

Accpunt No. 13974

J. & K. UNIVERSITY LIBRARY

This book should be returned on or before the last stamped above. An overdue charges of 6 nP. will be levied for each day. The book is kept beyond that day.

ATMA RAM & SONS
BOOKSELLERS
Kashmere Gate, DELHI-6

PHOTOCONDUCTIVITY

PHOTOCONDUCTIVITY
IN THE ELEMENTS

TREVOR SIMPSON MOSS, M.A., PH.D.

LONDON
BUTTERWORTHS SCIENTIFIC PUBLICATIONS
1952

BUTTERWORTHS PUBLICATIONS LTD., BELL YARD,
TEMPLE BAR, LONDON W.C.2

BUTTERWORTH AND CO. (AFRICA) LTD., DURBAN

BUTTERWORTH AND CO. (AUSTRALIA) LTD.
SYDNEY: MELBOURNE: WELLINGTON: AUCKLAND

BUTTERWORTH AND CO. (CANADA) LTD., TORONTO

U.S.A. Edition published by—
ACADEMIC PRESS INC., PUBLISHERS
125 EAST 23RD STREET
NEW YORK 10, N.Y.

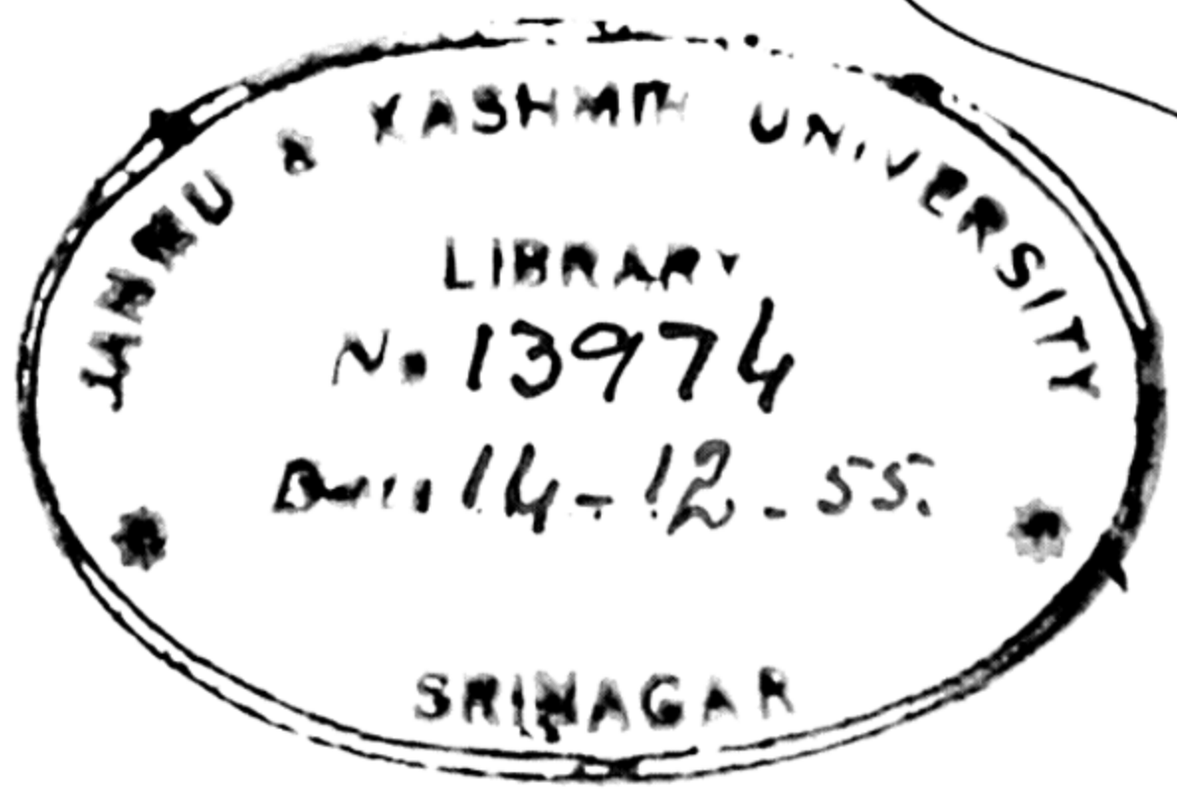

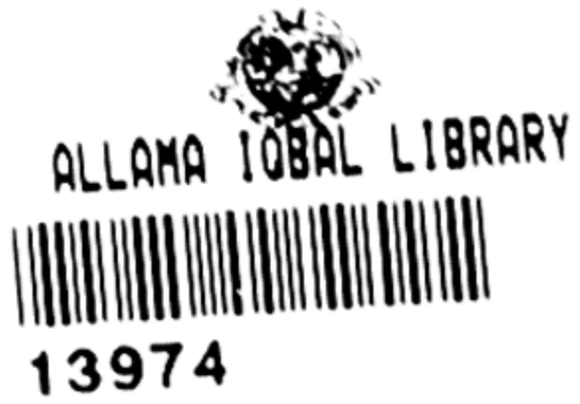

Set in Monotype Baskerville Type
Printed in Great Britain by Love & Malcomson Ltd, Redhill, Surrey

PREFACE

During the past few years there has been a great expansion of both academic and commercial interest in the properties of photoconducting and semiconducting materials, with a corresponding increase in the amount of theoretical and experimental work devoted to such materials and in our knowledge concerning them. The aim of this book, which arose from a thesis presented for the degree of Doctor of Philosophy of the University of Cambridge in 1950, is to consider the various photoconductive and other photoelectric effects, together with those electrical and optical properties of non-metals which have a direct bearing on these effects.

Part I discusses the theoretical aspects of the electrical and optical properties of semiconductors and insulators, and of the occurrence and behaviour of photocurrents. Part II provides an up-to-date review of such properties in the elements, assessed from the published literature—to which extensive references are given—or from the author's own experimental work, much of which is as yet unpublished except in the aforementioned dissertation. Although the non-metallic elements are much fewer in number than the corresponding compounds, they comprise some of the materials of the greatest technical interest at the present time, and the study of them has added greatly to our knowledge of conductive and photoconductive processes.

Acknowledgment is made to the Chief Scientist, Ministry of Supply, for permission to publish this book; to G. E. Kimball and the *Journal of Chemical Physics*, to G. L. Pearson and the American Institute of Electrical Engineers, to G. Busch and his co-workers, and to the Physical Society, for permission to reproduce *Figures 1*, *22*, *26*, and *49* and *50* respectively. I also wish to thank Dr. L. Pincherle for reading part of the manuscript, and my wife for checking the manuscript and proofs and preparing the diagrams.

T. S. M.

Malvern
August, 1952

CONTENTS

PART I

THEORY

INTRODUCTION

Solids are customarily divided into three classes on the basis of their electrical properties, namely metals, insulators and semiconductors. Metals are characterized by high conductivities, lying generally in the range 10^4 to $10^6\,\Omega^{-1}\,cm^{-1}$. The conductivity is only slightly temperature dependent, falling slowly as the temperature is raised. Insulators have very low conductivities under normal conditions, values of 10^{-12} to $10^{-18}\,\Omega^{-1}\,cm^{-1}$ are typical. Intermediate values of conductivity are found in semiconductors, the values being widely dependent on impurities and temperature, and the conductivity increasing rapidly with rising temperature. Furthermore in contradistinction to metals the conductivity increases with impurity content. Values between $10\,\Omega^{-1}\,cm^{-1}$ and $10^{-10}\,\Omega^{-1}\,cm^{-1}$ are commonly encountered.

The essential difference between metals and insulators lies in the number of electrons which are *free* to conduct. In metals the number of conducting electrons is of the order of 1 per atom *i.e.* about 10^{22} per cm^3, whereas in insulators, although a correspondingly large number of electrons are potentially available to carry current, the vast majority are not normally permitted to do so. It is now considered that all crystalline materials are capable of electronic conductivity if *free* electrons can be produced in them. These electrons can then move, more or less unimpeded, through the crystals.

Such free electrons may be produced in a variety of ways, for example by bombardment of the crystal with high speed electrons. More commonly the conduction electrons are produced by freeing the bound electrons already within the crystal by thermal agitation or illumination, the first of these processes resulting in semiconduction, and the second in photoconduction.

Optical properties also provide a means of distinguishing the three classes of materials. For example, metals have very high absorption coefficients from the ultra-violet to very long

wavelengths. They are therefore opaque, but good reflectors. Insulators are generally transparent in the visible region (or at least part of it) but possess strong selective absorption bands both at shorter and longer wavelengths, and have low reflection coefficients. Semiconductors are generally opaque in the visible, but transparent in the near infra-red region of the spectrum.

1

ENERGY BANDS IN SOLIDS

TWO DIFFERENT METHODS have been used in theoretical calculations of the energy levels in solids. For a detailed treatment of the quantum mechanical considerations underlying these theories, see, for example, SEITZ (1940). In the first method the atoms of the solid are considered to be widely separated initially, and the behaviour of the wave functions is investigated as the atoms are brought closer together and interaction between them increases.

If an assembly of $\mathcal{N}_a$ atoms is considered, then initially the allowed energy levels will be sharp lines as for a single atom, merely duplicated $\mathcal{N}_a$ times. As the atomic spacing is reduced and the individual wave functions overlap, the lines broaden into bands of levels which extend throughout the crystal, the number of levels in each band corresponding to the number of atomic levels from which the band was produced. Since by the Pauli principle each level can accommodate two electrons with opposite spins, there will be a total of $2\mathcal{N}_a$ quantum states available in each band for each original atomic energy level.

This method is not readily applicable to the study of electrical phenomena in solids, and most of the theoretical treatment of electrical properties is based on results obtained from the second method, which uses the so-called collective electron model. Here the valence electrons of the atoms are not considered as bound to the parent atoms, but are considered to be moving through the lattice, any individual electron being treated as moving in the combined field of the ions plus the average field of the remaining electrons.

The ions are considered to be fixed at their normal lattice sites, so that the resultant field is periodic with the periodicity of the crystal lattice. Now it may be shown by quantum mechanics that an electron may travel unimpeded in a *perfectly periodic* field, such as would exist in a crystal if there were no lattice irregularities and the atoms were at rest. It is

further found that such an electron has only certain permitted energy values, the energy spectrum consisting of bands of allowed energies separated by forbidden zones in which there exist no wavefunctions extending throughout the crystal. In the allowed bands the discrete energy levels lie so close to each other as to be effectively a continuum. The number of energy states in each band is limited to a small multiple of the number of atoms in the lattice, and by the exclusion principle only one electron may occupy each state. Thus, in the simpler cases, a band will normally be either completely occupied (with the next band above empty) or just half full.

In the latter case when in the highest band the states are only partly occupied, the energies of some electrons may be increased by application of an electric field *i.e.* the electrons may be accelerated in the direction of the field, so that a net charge transfer (and hence conduction) occurs. Such conditions occur for sodium for example, where the 3*s* level of the atom becomes a band containing two quantum states per atom in the crystal. As sodium has only one valence electron per atom, this 3*s* band is consequently only half full, and typical metallic conductivity results. Experimental evidence of the distribution of energy levels in metals is given by soft x-ray spectroscopy (see SKINNER, 1938). Bombardment of the metal in the x-ray tube ejects electrons from the inner x-ray levels of the ions of the crystal. These levels are then filled by electrons from the upper (valence) band, which emit soft x-ray quanta as they fall to the lower energy levels. As the inner x-ray levels are sharp, the spectrum of the emitted radiation gives an indication of the distribution of energy levels in the upper band.

If, however, there are just sufficient electrons present to occupy all the states in the highest occupied band, then there can be no net acceleration of the electrons by an applied field and consequently no current, so that the material is an insulator. An example of this type of crystal is furnished by diamond, where the behaviour of the two highest energy levels as calculated by KIMBALL (1935) is illustrated in *Figure 1*. At a lattice spacing of about 10 Å the 2*s* and 2*p* levels begin to broaden into bands. At the normal lattice spacing for diamond the two bands are separated by a zone several electron

volts wide in which no levels exist. For carbon there are eight quantum states per atom, which at the observed lattice spacing of diamond are distributed with four states in each of the two bands. As there are four valence electrons per atom, the bottom band of levels is exactly filled, and the upper band empty. Hence diamond is normally an insulator.

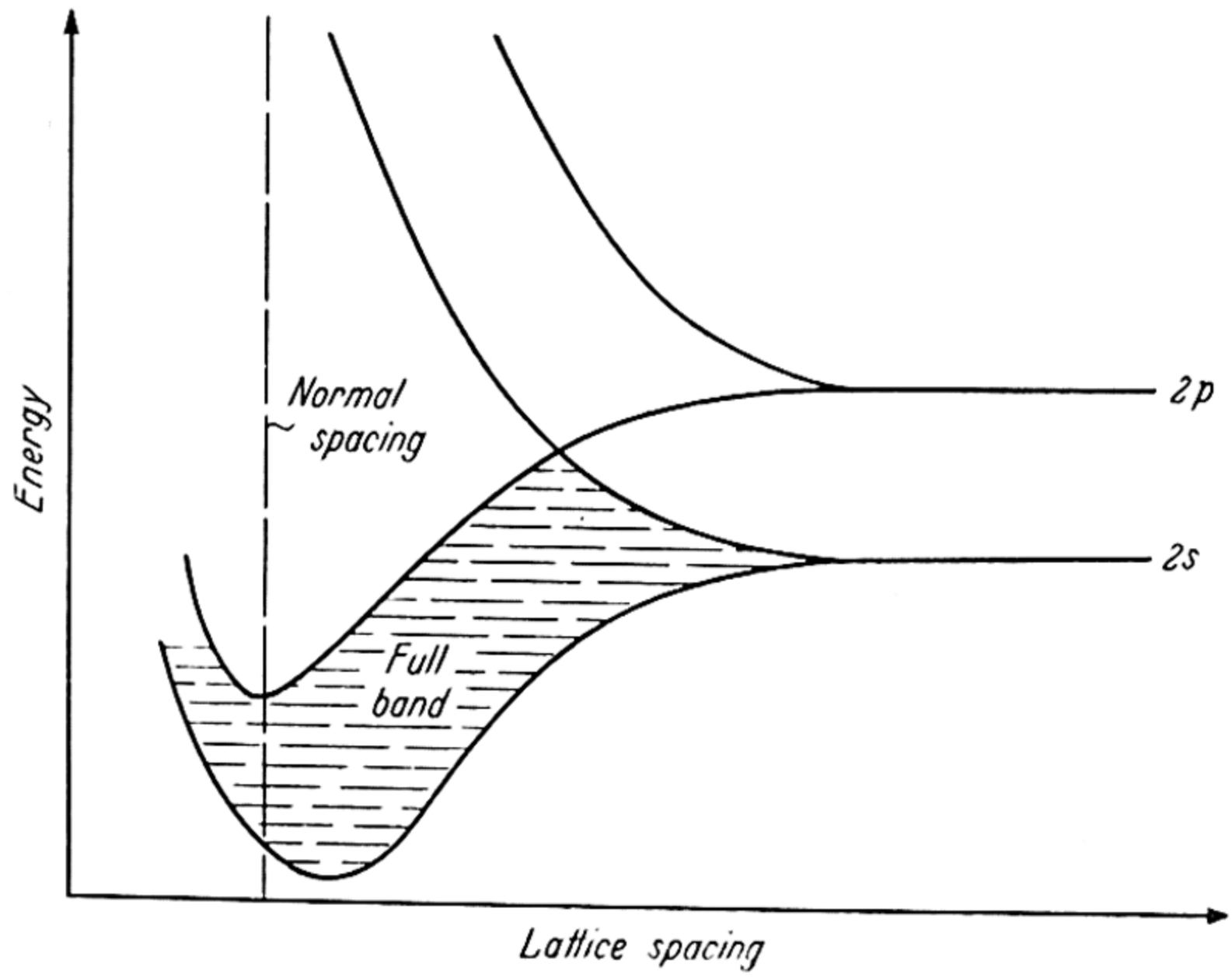

Figure 1. Diamond band structure (*from* KIMBALL)

In such a material however, conductivity may occur if by some means electrons are raised from the highest filled band into the empty band above, where they may be freely accelerated. In addition to the conductivity due to such electrons raised into the normally empty conduction band, there will be a contribution from the movement of the 'positive holes' left in the originally full band. By virtue of other electrons in the full band moving into the vacancies, the positive holes effectively drift through the material (under the applied field) in the opposite direction to the electrons. In general therefore, a positive hole may be treated as an electron of positive charge, although the effective mass will not normally equal the free electron mass*.

* The effective mass of a conduction electron may also differ from the free electron mass.

Two ways in which electrons may be excited from the full band into the conduction band are:

a thermally,

b optically, by the absorption of radiation quanta.

X-rays or electron bombardment may also be used. If the width of the forbidden zone is relatively small, then appreciable numbers of electrons will be raised by thermal agitation into the conduction levels at room temperature or above, and consequently such a material will be a partial or semi-conductor. There is thus no difference in principle between an insulator and a semiconductor; it is merely a question of the width of the forbidden zone.

I.I. TYPES OF SEMICONDUCTOR

The above type of semiconductor, where the electrons in the conduction band come from the full band, is known as 'intrinsic'. In 'extrinsic' semiconductors the electrons originate at impurity centres of some kind, these centres giving localized energy levels within the forbidden zone. Two kinds of impurity levels are possible, donor levels and acceptor levels. At zero temperature the former are occupied by electrons which may be excited into the conduction band as the temperature is raised, giving 'electron' conductivity. On the other hand, acceptor levels are empty at zero temperature, but electrons may be excited thermally to these levels from the full band, the positive holes thus created giving 'hole' conductivity. SAXON and HUTNER (1949), by use of a simple one-dimensional lattice model, have shown how energy levels are produced in the forbidden zone by either substitutional or interstitial impurities, or vacant lattice sites.

The possible arrangements of energy levels are shown in *Figure* 2a. If neither set of impurity levels is present, the material is an intrinsic semiconductor, an activation energy E being required to raise electrons into the conduction band. If donor levels only are present, then an 'electron' semiconductor with activation energy ΔE_1 results; whereas acceptor levels give a hole conductor with activation energy ΔE_2. The energy of impurity centres has been discussed by SERIN (1946)

while the probability of the ionization of impurity centres by single or multiple phonons has been treated theoretically by GOODMAN *et alii* (1947). *Figure 2*b shows the density of states function, *i.e.* the distribution of permitted levels on the energy diagram.

In the case of germanium, donor or acceptor centres are produced simply by replacing germanium atoms by atoms with one more valence electron or one less. Substitution by an arsenic atom with five valence electrons means that four electrons are used in satisfying the electron-pair valence bonds that give rise to the full band of energy levels, the remaining

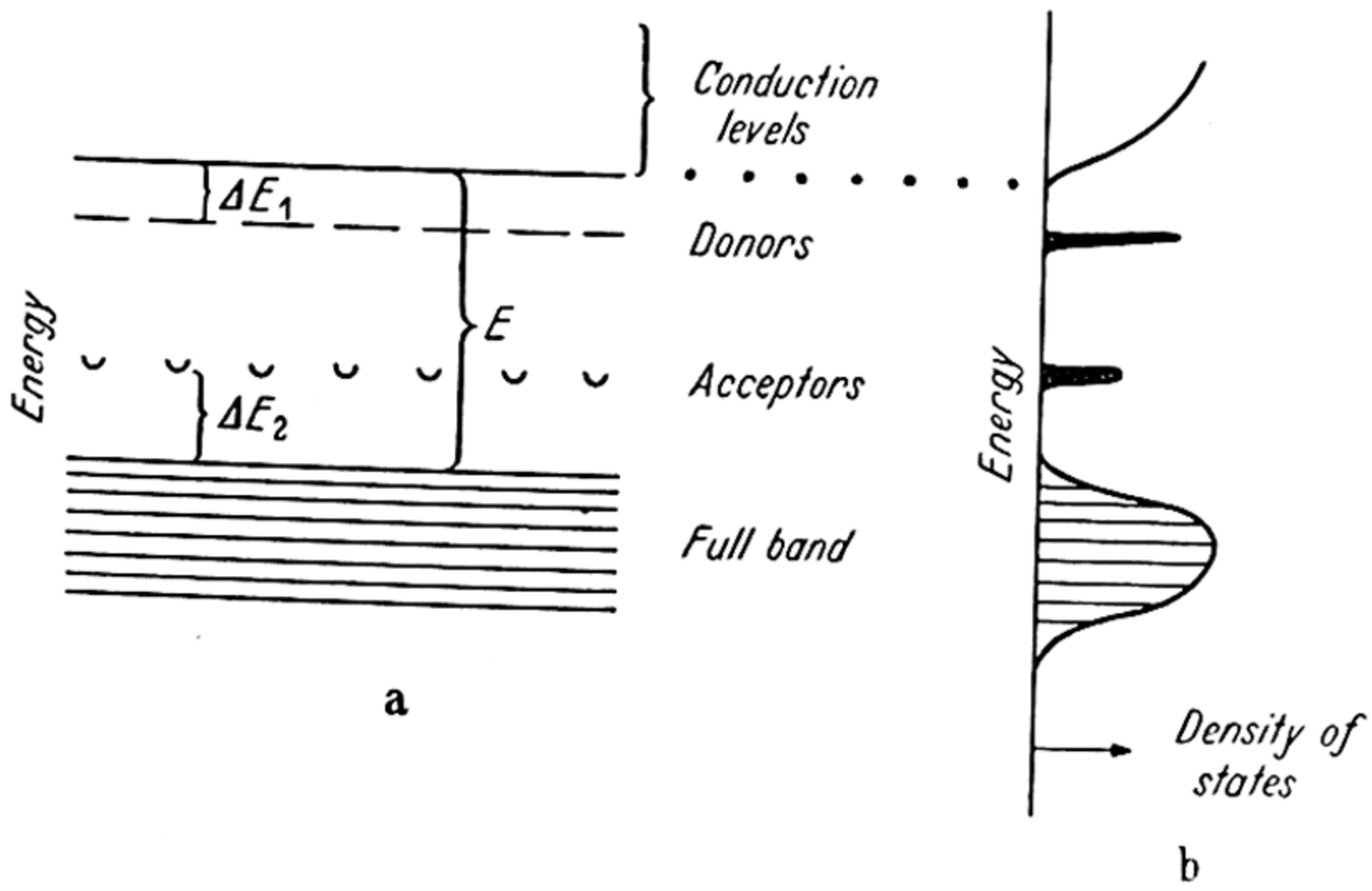

Figure 2. a *Energy levels in semiconductors.* b *Distribution of permitted levels*

excess electron being bound to the parent atom with very low binding energy. At room temperature thermal energies are more than sufficient to free this electron and raise it into the conduction band of levels. Similarly if a trivalent boron atom is used to replace a germanium atom, one of the valence bonds to a neighbouring germanium atom is incomplete. If an electron from a neighbouring electron-pair bond is used to complete the boron–germanium bond, the result is the production of a positive hole in the full band.

It has been shown experimentally for many materials that the activation energy of impurity centres decreases as the concentration of impurities increases. For silicon for example,

PEARSON and BARDEEN (1949) find the activation energy is effectively reduced to zero when the density of acceptor levels reaches 6×10^{18} per cm^3. Possible causes of this effect such as increasing interaction between impurity centres as their average separation decreases, or increased shielding of the impurity ion charge by conduction electrons, have been considered by VON HEYWANG (1949), PINCHERLE (1951), CASTELLAN and SEITZ (1951), and SAXON and HUTNER (1949).

2

HALL EFFECT AND CONDUCTIVITY

Both the conductivity and Hall effect (*i.e.* the transverse voltage produced when a current is passed through a conductor lying in a magnetic field at right angles to the current) are determined primarily by the number of current carriers in the material.

For an intrinsic semiconductor, the density of electrons in the conduction band at a given temperature T is found by statistical mechanics (see for example Fowler, 1936) to be

$$n = \Upsilon e^{-E/2kT} \qquad \ldots\ldots(1)$$

where E is the activation energy, and

$$\Upsilon = \frac{2(2\pi mkT)^{3/2}}{h^3} \qquad \ldots\ldots(2)$$

where m is the effective mass of the electron in the conduction band, and the other constants have the usual significance. This result is only applicable as long as classical statistics can be used. The problem of highly impure semiconductors where the electron gas is to some degree degenerate has been treated fully by Shifrin (1944) and Labhart (1946). It will be seen that Υ is a slowly varying function of T, this variation being normally negligible in comparison with the exponential term.

The simplest treatment of the Hall effect indicates that for one type of current carrier only the Hall constant R (*i.e.* the transverse voltage produced by unit field and unit current in a specimen of unit thickness) is given by $R = \pm 3\pi/8nec$ where the negative sign applies to electrons and the positive sign to positive holes. The magnitude of the Hall constant thus yields the density of current carriers, whilst the sign of the Hall constant gives directly the sign of the carriers. Alternatively, the sign of the carriers may be determined by observation of the sign of the thermo-electric power of the material.

In order to determine the conductivity from the density of carriers, we need to know the carrier mobility *i.e.* the velocity

with which the carrier moves in unit applied electric field. Although the mobility is normally *defined* in the above manner, experimentally it appears in several different ways, and it is advisable to tabulate these different experimental concepts of mobility:

1 Conductivity— This mobility is expressed by $\sigma = neb_1$ where b_1 is the ' conductivity ' mobility. If n can be measured *directly* without use of the Hall effect—for example by radio-active tracers, as has been done for germanium—then b_1 is derivable from the conductivity.

2 Hall Effect— With the expression for the Hall constant given above, we have the ' Hall ' mobility given by

$$b_2 = \frac{8c}{3\pi} R\sigma \qquad \ldots\ldots(3)$$

Until recently the Hall effect was the only available method of measuring the mobility, so that most of the mobility values quoted in the literature are derived from this type of measurement.

3 Drift Velocity Measurements— Direct measurement of the drift velocities of electrons injected into germanium has now been carried out by observing the time required to traverse a given distance in the specimen in a known electric field. The mobility is then given simply by $b_3 =$ (velocity)/(field).

4 Magneto-Resistance Effect— Here the resistance change according to SEITZ (1950) is

$$\frac{\Delta\rho}{\rho} = 3{\cdot}8 \times 10^{-17} b_4^2 H^2 \qquad \ldots\ldots(4)$$

PEARSON and SUHL (1951) have found this law to give the correct field and temperature dependence of b_4.

Measurements made on these different aspects of mobility in germanium show that the differences in the three values obtained are not great, and as far as the present treatment is concerned we may continue to discuss the mobility as though it were a unique property of each material considered. It may be mentioned that SHOCKLEY (1950) has shown that the ' Hall ' mobility will be less than the ' drift ' or ' conductivity ' mobilities in cases where the energy surfaces of the Brillouin zones are concave or re-entrant, in contrast to the spherical

energy surfaces which are usually assumed in the theoretical evaluation of the Hall constant.

When both types of current carrier are present simultaneously, the expression for the Hall constant depends on the concentrations of both types of carrier and their mobilities. We then have*

$$R = -\frac{3\pi}{8ec}\left(\frac{n_e b_e^2 - n_h b_h^2}{(n_e b_e + n_h b_h)^2}\right) \qquad \ldots.(5)$$

For an intrinsic semiconductor where $n_e = n_h$ this reduces to

$$R = -\frac{3\pi}{8nec}\left(\frac{b_e - b_h}{b_e + b_h}\right) \qquad \ldots.(6)$$

2.1. TEMPERATURE DEPENDENCE

As the Hall constant is inversely proportional to the density of carriers, it will vary exponentially with temperature. More accurately $\log(RT^{3/2}) \propto E/2kT$. Thus a plot of $\log(RT^{3/2})$ against inverse temperature should give a straight line from the slope of which the activation energy E may be deduced.

For an impurity semiconductor with N_d donor levels per cm^3 situated ΔE below the conduction band, we find

$$n = (\Upsilon N_d)^{\frac{1}{2}} e^{-\Delta E/2kT} \dagger \qquad \ldots.(7)$$

in the low temperature region, where the number of intrinsic electrons is insignificant. Since the total density of conduction electrons is approximately

$$n = \Upsilon^{\frac{1}{2}}\left(\Upsilon^{\frac{1}{2}} e^{-E/2kT} + N_d^{\frac{1}{2}} e^{-\Delta E/2kT}\right) \qquad \ldots.(8)$$

where $\Upsilon \gg N_d$, it is clear that the second (impurity) term will predominate at low temperatures, while at sufficiently high temperatures the first term will of course be much the larger. Hence for an impurity semiconductor, the plot of $\log R$ against $1/T$ will in general consist of two straight lines. The slope in the low temperature region will be $\Delta E/2k$, and at high temperatures $E/2k$. Both activation energies may thus be determined from the curve. The more complicated problem of the distribution of electrons and holes in a semiconductor when

* See for example, BUSCH (1950).

† Assuming the Fermi level is not within kT of the conduction band.

both donor and acceptor centres are present at the same time has been treated by HUTNER *et alii* (1950).

For the conductivity,

$$\sigma = n_e e b_e + n_h e b_h \qquad \ldots\ldots(9)$$

We thus need to know the form of the temperature dependence of the mobility terms. The mobility may be expressed in terms of the mean free path l of the electrons (or holes) between collisions by the relation

$$b = \tfrac{4}{3} e l (2\pi m k T)^{-\frac{1}{2}} \qquad \ldots\ldots(10)$$

where for the electron mobility m is the effective mass of an electron and similarly for the hole mobility m is the effective mass of a hole.

In valence crystals the mean free path is determined by two forms of scattering, namely lattice scattering and impurity scattering. If the mean free paths determined by either form of scattering alone are l_L and l_I, then in general $1/l = 1/l_L + 1/l_I$*. It has been shown by SEITZ (1948) that $l_L \propto T^{-1}$. Hence in the temperature region where lattice scattering is predominant, the mobility $b \propto T^{-3/2}$. Such a relation has been verified experimentally for silicon (PEARSON and BARDEEN, 1949). Hence for the temperature variation of the conductivity we have simply $\sigma = \sigma_0 e^{-E/2kT}$. The intrinsic activation energy may thus be determined directly from a plot of log σ against reciprocal temperature. CONWELL and WEISSKOPF (1946) have shown that for impurity scattering the temperature dependence of the mean free path is given by

$$1/l_I \propto T^{-2} \log (1 + CT^2) \qquad \ldots\ldots(11)$$

where the CT^2 term generally may be neglected in comparison with unity. Hence $b \propto T^{3/2}$. Thus in the region of impurity scattering there will be a temperature term in the expression for conductivity in addition to the exponential term. However the effect of this term will be small compared with the exponential term except for very small activation energies. Methods of analysing mobility data to give the contributions of lattice and impurity scattering are discussed by KLAHR and HUNTER (1951).

* See TORREY and WHITMER (1948).

The magnitudes of the conductivities to be expected are of interest, and may readily be estimated. For intrinsic conductivity $\sigma = neb = \Upsilon eb e^{-E/2kT}$, where $b = b_e + b_h$. Near room temperature $\Upsilon = 2{\cdot}5 \times 10^{19}$ and hence $\sigma = 4be^{-E/2kT}$. The value of mobility found for bulk silicon for example is ~ 200 cm sec^{-1}/V cm^{-1}, so that $\sigma \sim 10^3 e^{-E/2kT}$. With a value of mobility as great as $b = 3000$, as has been observed for germanium, $\sigma_0 = 1{\cdot}2 \times 10^4$, so that considerable variation in σ_0 is possible.

For impurity conductivity, we have $\sigma_0 = be(\Upsilon N)^{\frac{1}{2}}$. Hence with $N = 10^{16}$ impurity centres/cm^3, for example, we have $\sigma_0 = 0{\cdot}08b$. In general the mobility will be considerably less than in intrinsic semiconductors, and even with high impurity concentrations (10^{18}/cm^3) it is unlikely that σ_0 will reach 100. Thus values of σ_0 approaching one thousand will signify intrinsic conductivity, where bulk specimens are concerned. For films however, mobilities are lower, and even for intrinsic semiconductors it is probable that b will be only ~ 50 cm sec^{-1}/V cm^{-1}. For germanium, for example, which has extremely high mobilities in the single crystal form, values of 1 to 50 cm sec^{-1}/V cm^{-1} are quoted for films by THORNHILL and LARK-HOROVITZ (1951). Thus for films, values of $\sigma_0 \sim 100$ indicate that the conductivity is probably intrinsic.

Impurity centres which provide the donor and acceptor levels are likely to be of one of the following types:

i Substitutional impurities of valency different from the valency of the main lattice atoms. For example, phosphorus or boron atoms in germanium.

ii Vacant lattice sites. These may occur in both valence and ionic crystals. In the latter, either anions or cations may be missing. A missing anion with an electron bound to the vacancy is known as an *F* centre.

iii Interstitial ions. In ZnO for example an excess of Zn is taken up interstitially.

iv Crystal dislocations.

3

OPTICAL PROPERTIES OF MATERIALS

THE OPTICAL PROPERTIES of a material can be specified by two parameters, the refractive index (n) and the absorption index (k). The two may be combined as the complex index of refraction, namely $n' = n - ik$.

The dielectric constant is the square of the refractive index, so that the *real* part of the dielectric constant is $\epsilon = n^2 - k^2$, which, when there is no absorption, gives $\epsilon = n^2$. The imaginary part of the dielectric constant, which causes the absorption, is $2nk$. This term is related to the high frequency conductivity (σ) by the equation $nk = \sigma/\nu$, where ν is the frequency (see, for example, SEITZ, 1940). The absorption constant K, which is the factor determined in practice from transmission measurements, represents the reciprocal of the distance in which the light intensity is attenuated to 1/e of its initial value *i.e.* the attenuation for a thickness x of the material is exp $(-Kx)$. The absorption constant is related to the absorption index by $K = 4\pi k/\lambda$.

3.1. ABSORPTION IN NON-METALS

In the region of the main lattice absorption of insulators or semiconductors, the absorption coefficient is very large, of the order of $10^6 cm^{-1}$. In general the absorption spectrum will consist of one or more discrete lines, with a continuous absorption band at higher frequencies. These discrete lines correspond to an electron being raised to an excited state in the field of the hole from which it originated. As the field round the positive hole will be similar to the Coulomb field of a simple positive charge, there will exist a series of bound states for the electron. Such a centre of excitation is termed an exciton*.

Thus the lowest frequency which can be absorbed will produce an exciton, but will not necessarily give rise to a free

* See WANNIER (1937) for the wave-mechanical concept of excitons.

hole and electron. The exciton as a whole may move through the crystal, and may thus have momentum. However the selection rules governing optical transitions state that absorption of a quantum of radiation can only produce an exciton of zero momentum, unless some energy is simultaneously given up to producing quanta of lattice vibrations (phonons), when the required rule is that the combined momentum of the exciton and phonon(s) is zero. Ideally the exciton formation would give rise to a sharp line, but in practice the lines are broadened by interaction with lattice vibrations and by the presence of crystal imperfections, and may well be merged into the edge of the continuous absorption band.

Radiation lying in the continuous absorption band will produce free electrons and positive holes, and hence under an applied field photoconductivity may occur. For absorption in the exciton bands, photoconductivity will not necessarily occur, although thermal energies from the lattice may be sufficient to raise the excited electrons into the conduction levels before they recombine with the positive holes.

It may be noted that the edge of the continuous absorption band does not correspond to the transition from the *top* of the full band to the *bottom* of the conduction band, as this transition is normally forbidden. However, owing to lattice defects and thermal vibrations, there is always *some* transition probability. Such a mechanism may be the explanation of the tail often found on the long-wave edge of the main absorption band. CHEESMAN (1952) supports this view, and discusses the transition probabilities of the nominally forbidden transitions when vibrations of the lattice ions are taken into account. His theoretical results agree reasonably well with the measured shape of the absorption edge for cadmium sulphide. Alternatively, the long-wave tail may be due to absorption by atoms on the surface or in cracks, or by impurities. The transitions possible on absorption of radiation are shown schematically on the energy level diagram in *Figure 3*.

It is of interest to estimate the absolute absorption coefficient resulting from a given concentration of absorbing centres. Suppose a centre has an absorption line of frequency width $\Delta\nu$. Then if the energy density of monochromatic radiation is

$\mathcal{J}$ erg/cm³, the probability per unit time that a quantum is absorbed is $\mathcal{J}\beta/\Delta\nu$ where β is the Einstein coefficient. The number of quanta incident on the surface is given by $n = \dfrac{\mathcal{J}c}{h\nu}$ per cm² per sec, or $\mathcal{J} = \dfrac{nh\nu.}{c}$ Thus if we have N_c

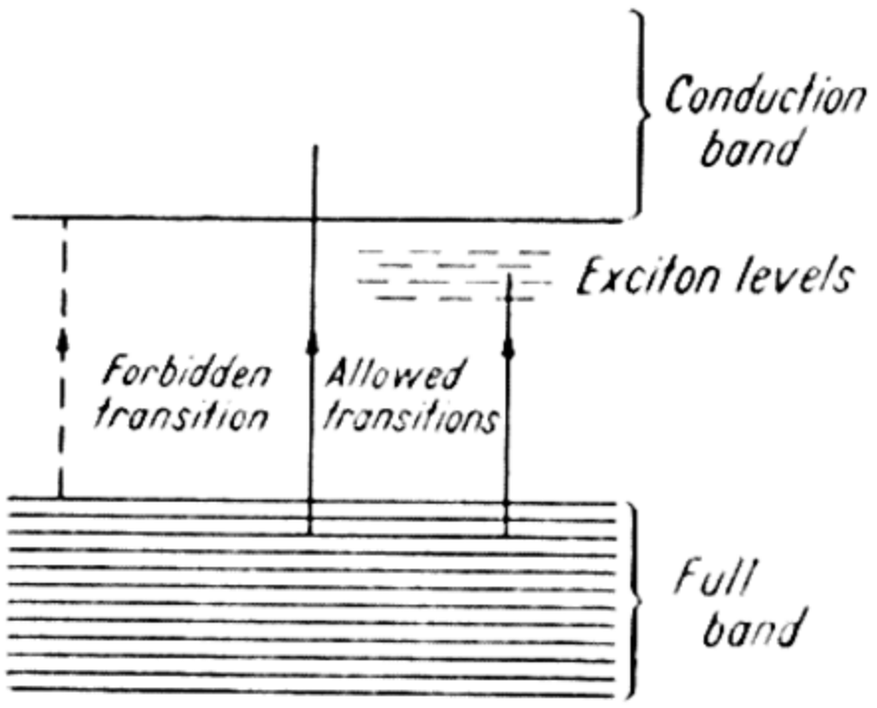

Figure 3. Optical absorption transitions

absorbing centres per cm³ the number of quanta absorbed (per sec) in a layer of thickness Δx will be $(nh\nu\beta/c\Delta\nu)\ N_c\Delta x$, so that the absorption constant K is given by:

$$1 - e^{-K\Delta x} = \frac{h\nu\beta N_c\Delta x}{c\Delta\nu} \qquad \ldots.(12)$$

If $K\Delta x$ is small this reduces to $K = h\nu\beta N_c/c\Delta\nu$. The value of β is $\pi e^2 f/(h\nu m)$ (see for example MOTT and SNEDDON, 1948) where f is the oscillator strength of the line. Hence

$$K = \frac{\pi e^2 f N_c}{mc\Delta\nu} = 10^{-16}N_c \text{ for } f = 1 \text{ and } h\Delta\nu = 1\text{eV} \qquad \ldots.(13)$$

This calculated value of K may be compared with data obtained by KLEINSCHROD (1936) for the impurity absorption band formed by F centres in KCl. For a particular case the density of impurity centres was 115×10^{16}/cm³, and the observed bandwidth of the line approximately 1/3 eV (at half maximum K). Hence the calculated $K = 345\ \text{cm}^{-1}$, which compares closely with the observed absorption maximum of $310\ \text{cm}^{-1}$. This example gives the typical order of magnitude of the absorption constant in an impurity absorption band.

The formula may also be correlated with the absorption constant found for main lattice absorption. For germanium for example, data from BRATTAIN and BRIGGS (1949), show the

bandwidth (at half maximum absorption) to be approximately 2·5 eV. Now germanium has $4{\cdot}5 \times 10^{22}$ atoms/cm^3. Hence the formula gives $K \simeq 2 \times 10^6 \text{cm}^{-1}$. The observed maximum value of K is $1 \times 10^6 \text{cm}^{-1}$, so that the agreement is reasonable. There is thus a pronounced difference in the magnitude of the absorption due to the main lattice or to impurity centres, and hence quantitative absorption measurements are often useful in deciding whether photoconductivity in a particular band is intrinsic or arises from impurities.

3.2. ABSORPTION BY CONDUCTION ELECTRONS

In addition to the frequency-selective absorption already discussed, there will also be absorption by any electrons in the conduction band, and in cases of high impurity or high temperature this will be considerable. As the magnitude is much less than that in the main lattice absorption region, this type of absorption is most obvious at long wavelengths, where the perfectly pure material with no thermally excited electrons would otherwise be transparent.

For carriers moving in a perfectly periodic field, absorption of radiation is theoretically forbidden. However, as the strict periodicity of the field is destroyed by lattice vibrations and imperfections, this restriction is relaxed and absorption occurs. The magnitude of the absorption is given by

$$nk\nu = \frac{e^2 N_c}{4\pi^2 m} \frac{2\pi\gamma}{\gamma^2 + \nu^2} \qquad \ldots\ldots(14)$$

where γ is the damping factor. Now $nk\nu$ is the specific conductivity of the material, and hence when $\nu \ll \gamma$, we have the low frequency conductivity $\sigma = e^2 N_c / 2\pi m\gamma$. Alternatively, $\sigma = N_c eb$ and hence γ may be expressed in terms of the mobility as $2\pi\gamma = e/mb$.

Hence $nk\nu = \sigma(1 + \nu^2/\gamma^2)^{-1} = Kcn/4\pi$ since $K = 4\pi k/\lambda$, giving

$$K = \frac{4\pi\sigma}{cn}(1 + \nu^2/\gamma^2)^{-1} \qquad \ldots\ldots(15)$$

Thus at not too long wavelengths where $\nu/\gamma \gg 1$, the absorption constant should vary as the square of the wavelength.

This is found to be so for silicon and germanium, and the lead chalcogenides, although (as discussed later) the absolute magnitude of the absorption is in error by several orders of magnitude.

As an illustration of the absorption of a semiconducting element over a wide range of wavelengths, *Figure 4* shows the data available for germanium. The values of the absorption constant cover a range of seven decades.

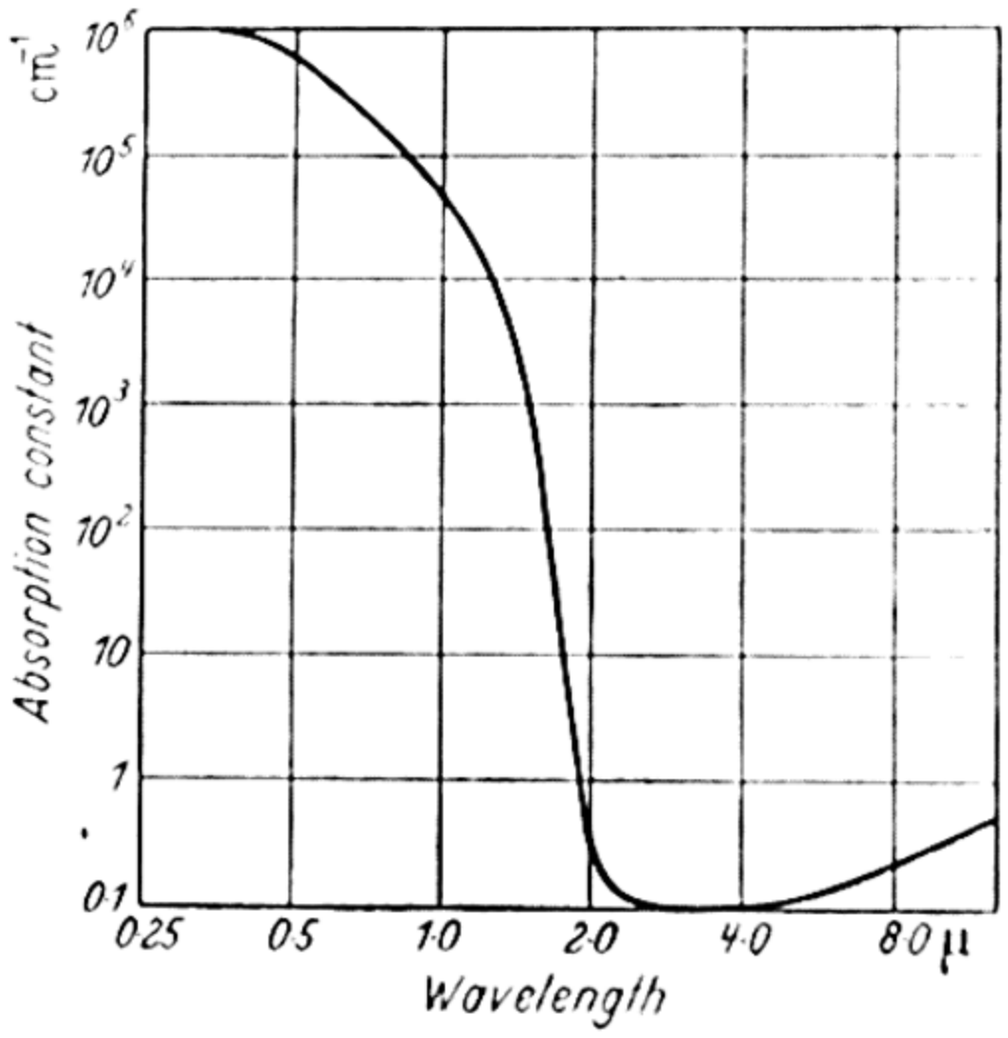

Figure 4. Absorption in germanium

3.3. REFRACTIVE INDEX THEORY FOR INSULATORS

In the Lorentz treatment of refractive index, the material is considered to contain electrons held in equilibrium positions by elastic forces. The equation of motion of an electron under an applied electrostatic field $Ee^{2\pi i\nu t}$ is then $m\ddot{x} + 2\pi m\gamma\dot{} + gx = -eEe^{2\pi i\nu t}$ where γ is the damping coefficient and g the force constant. Hence

$$x = -\frac{e}{4\pi^2 m\{(\nu_0^2 - \nu^2)^2 + \nu^2\gamma^2\}^{\frac{1}{2}}} \cdot \frac{\cos\phi - i\sin\phi}{} \cdot Ee^{2\pi i\nu t}$$

where $\nu_0^2 = g/4\pi^2 m$ is the resonant frequency, and the phase angle $\phi = \tan^{-1}\dfrac{\gamma\nu}{\nu_0^2 - \nu^2}$.

Now the current density associated with this motion is $-N_c e\dot{x} = (\sigma + 2\pi i\nu\alpha)Ee^{2\pi i\nu t}$ where σ is the specific conductivity, α the polarizability of the material, and N_c the density of oscillators. Hence the high frequency dielectric constant

$$\epsilon = 1 + 4\pi\alpha = 1 + \frac{N_c e^2}{m\pi} \frac{\nu_0^2 - \nu^2}{(\nu_0^2 - \nu^2)^2 + \gamma^2\nu^2} \quad \ldots\ldots(16)$$

At relatively long wavelengths where $\nu \to 0$, this becomes

$$\epsilon = 1 + \frac{N_c e^2}{m\pi\nu_0^2} \quad \ldots\ldots(17)$$

As an example of the applicability of this simple theory, we may estimate the value of ϵ for germanium. Now ν_0 is the frequency for the maximum value of $2nk$ (see SIMON, 1951), *i.e.* the imaginary part of the dielectric constant, for which the experimental value is $\nu_0 = 5 \times 10^{14}$c/s (BRATTAIN and BRIGGS, 1949). Inserting this value in equation 17 gives $\epsilon = 15$. This value is close to the square of the observed refractive index, namely $n^2 = 16$, and shows that even this simple theory can give the correct order of magnitude for the dielectric constant.

The simple theory above does not include the effect of the internal field produced by dipoles induced by the applied field E. When this correction is applied equation 16 is modified to give the Lorentz–Lorenz formula*

$$\frac{\epsilon - 1}{\epsilon + 2} = \frac{N_c e^2}{3m\pi} \frac{\nu_0^2 - \nu^2}{(\nu_0^2 - \nu^2)^2 + \gamma^2\nu^2} \quad \ldots\ldots(18)$$

For frequencies well removed from ν_0, the $\gamma^2\nu^2$ term may generally be neglected, giving $(\epsilon - 1)/(\epsilon + 2) = A/(\nu_0^2 - \nu^2)$ where A is a constant. Either of the dispersion formulae 16 or 18 may conveniently be rewritten in terms of refractive index and wavelengths as

$$1/(n^2 - 1) = a - b/\lambda^2 \quad \ldots\ldots(19)$$

The form of equation 16 obtained by this simple classical treatment is essentially the same as that obtained by quantum-mechanical treatments, except that the single term is replaced by a series of terms (for each absorption line), the terms being weighted by an appropriate oscillator strength for the line. Fuller treatment of dispersion theory is given in standard works, such as VAN VLECK (1932) and ROSENFELD (1951).

It should be noted that the real and imaginary parts of the

* However, MOTT and GURNEY (1948) maintain that the simple Drude formula of equation 16 is more accurate than the Lorentz–Lorenz formula.

dielectric constant are not independent, but that if either is known for all frequencies, then the other is completely specified (see BODE, 1945). For example if the imaginary part of the dielectric constant $2nk$ is known, then the real part

$$n_1^2 - k_1^2 = 1 - \frac{2}{\pi}\int_0^\infty \frac{2nk\nu - 2n_1k_1\nu_1}{\nu^2 - \nu_1^2}\,\mathrm{d}\nu$$

where ν_1 is the frequency at which it is desired to calculate the real part of the dielectric constant. It follows that the refractive index extrapolated to zero frequency, n_0, is given by $n_0^2 - 1 = \frac{2}{\pi}\int_0^\infty 2nk\mathrm{d}\lambda/\lambda$, a relation which has been given by BIRNBAUM (1949).

3.4. RELATION BETWEEN THERMAL AND OPTICAL ACTIVATION ENERGIES

By the Franck–Condon principle, when an electron is removed from an atom by the absorption of a light quantum, the surrounding ions do not have time to move during the process. The optical activation energy is thus the energy required to remove the electron with the ions stationary. After the absorption act however, the lattice ions will move to new equilibrium positions, the energy of the crystal being somewhat lowered in the process. The difference between this final energy state and the initial state before the absorption, represents the thermal activation energy. The optical activation energy will thus exceed the thermal by the amount of energy given out as the ions move to their new positions of equilibrium after the absorption process. For ionic crystals MOTT and GURNEY (1948) estimate that the energy given out per volume is $\left(\frac{1}{\epsilon} - \frac{1}{\epsilon_0}\right)\frac{e^2}{8\pi^4}$, where ϵ and ϵ_0 are the high frequency and zero frequency dielectric constants respectively. By postulating an effective volume for the centre, this expression can be integrated over that volume. The main characteristic of the resulting expression is that it is proportional to $1/\epsilon - 1/\epsilon_0$. There should thus be considerable difference in the activation energies for highly polar materials. However, for compounds where

$\epsilon \simeq \epsilon_0$, or for monatomic crystals (where ϵ and ϵ_0 should be equal) there should be negligible difference.

The validity of the assumption that ϵ and ϵ_0 are equal for elements will be discussed on the basis of the experimental data available in the chapters on the individual elements. Theoretically any absorption bands in the infra-red will contribute to the dielectric constant, and will result in $\epsilon > \epsilon_0$. A pure non-polar material has no strong absorption bands in the infra-red (in contrast to the vibrational bands associated with ionic crystals) but impurities giving absorption bands in this spectral region can produce small changes in the refractive index.

Seitz (1940) deduces the contribution to the refractive index (Δn) to be

$$\Delta n = \frac{N_c f e^2}{18\pi m} \cdot \frac{(n^2+2)^2}{n} \cdot \frac{\nu_0^2 - \nu^2}{\gamma^2\nu^2 + (\nu_0^2 - \nu^2)^2} \quad \ldots\ldots (20)$$

where ν_0 is the frequency of the impurity absorption band and γ the damping coefficient. Putting $\nu = 0$ to find the contribution to the low frequency index of refraction we have

$$\Delta n = \frac{N_c f e^2}{18\pi m \nu_0^2} \frac{(n^2+2)^2}{n}$$

Taking ν_0 at 1μ and $f=1$ we have $\Delta n = 5 \times 10^{-23} N_c (n^2+2)^2/n$. Hence for $n = 2$ and $N_c = 10^{18}/\text{cm}^3$ we have $\Delta n = 10^{-3}$. We may thus conclude that normal impurity concentrations will have a very small effect on the refractive index.

4

PHOTOCONDUCTIVITY

MUCH of the pioneer work on the investigation of photo-conductivity was done by GUDDEN and POHL and their co-workers (see GUDDEN, 1928), working mainly with insulating crystals. They recognized two types of photoconductive crystal, namely

I idiochromatic crystals whose properties are determined by the basic material alone and not by any artificially introduced impurities, and

II allochromatic crystals which are not photoconductive when pure, but become so when foreign atoms or particles are introduced into the crystal.

Crystals of type *I* are characterized by high refractive indices, and Gudden and Pohl found that for a material to be photo-conductive without artificially introduced impurity centres, the refractive index must be greater than about 2. Diamond is an example of a type *I* crystal, while both yellow and blue rocksalt are of type *II*; pure rocksalt itself being inactive. Even in the pure type *I* crystals Gudden and Pohl believed that photo-electrons originated only at preferred points in the lattice, and not at every atom. They also distinguished between primary and secondary photocurrents, and gave the following characteristic differences between the two:

	Primary Currents	*Secondary Currents*
a	*'Instantaneous' with illumination*	*Appreciable time lag*
b	*Little temperature dependence*	*Marked temperature dependence*
c	*Quantum efficiency unity*	*May exceed unity*
d	*Occur in perfect crystals*	*Usually larger in less perfect crystals*
e	*Proportional to light intensity*	*Often hysteresis effects*
f	*Current initially proportional to applied field, finally saturating*	*No simple function of applied field*

The primary current constitutes the pure photo-effect, whilst the secondary current is attributed to a lowering of electronic barriers by the primary current, thus permitting the

flow of additional electrons. The primary photocurrent is thus best studied in flawless single crystals, secondary currents being enhanced by intercrystalline barriers.

4.1. PRIMARY PHOTOCURRENTS IN INSULATORS

When the insulating crystal is illuminated by light of such a wavelength that electrons are raised to the conduction levels, they are then free to move through the crystal lattice under an applied field. The positive charges may also be mobile and, if so, they too contribute to the primary photocurrent.

The current obtained however, is not independent of the applied field, as the photoelectrons do not, in general, all succeed in reaching the anode. The explanation is that after travelling an irregular path through the crystal for some time, the electron becomes trapped at some crystal imperfection, or by recombination with a positive hole. The total distance travelled by an electron in this time may be large—the order of 1 cm—but unless the applied field is very high, the net movement towards the anode will be only a small fraction of this distance.

Initially the distance moved by the electron towards the anode is proportional to the field, *i.e.* net charge transfer between the electrodes (and hence photocurrent) is proportional to field. If the positive holes are immobile, it is clear that the photocurrent will saturate when the field is sufficiently high to drag all the photoelectrons to the anode before they are trapped.

An elementary equation for the form of the current/voltage curve may be obtained as follows. Consider a slab of crystal between parallel electrodes of separation h, illuminated so that N electrons/sec are produced uniformly over the area between the electrodes (see *Figure* 5a). Taking the distance d travelled by a photoelectron towards the anode before being trapped as proportional to the field, then $d = CV/h$ where C is a constant. Thus those electrons produced at a distance $> d$ from the anode will all travel a distance d, so that their contribution to the charge measured in the external circuit is $\frac{de}{h}\frac{(h-d)}{h}N$ per sec.

Those produced within the distance d of the anode will produce a charge contribution of

$$\int_0^d \frac{xe}{h}\frac{\Delta x\mathcal{N}}{h} = \frac{d^2\,\mathcal{N}e}{2h^2} \qquad \ldots\ldots(21)$$

Hence the total charge transfer is $q = (\mathcal{N}ed/h)\{1 - (d/2h)\}$. Now $d/h = V/V_0$ where V_0 is the voltage required to drive an electron fully across the crystal. Hence

$$q = \frac{\mathcal{N}eV}{V_0}\left\{1 - \frac{V}{2V_0}\right\} \qquad \ldots\ldots(22)$$

so that the curve of q against V should be a parabola. Some results given by GUDDEN and POHL (1921) for diamond are plotted in the form q/V against V in *Figure* 5b. The fact

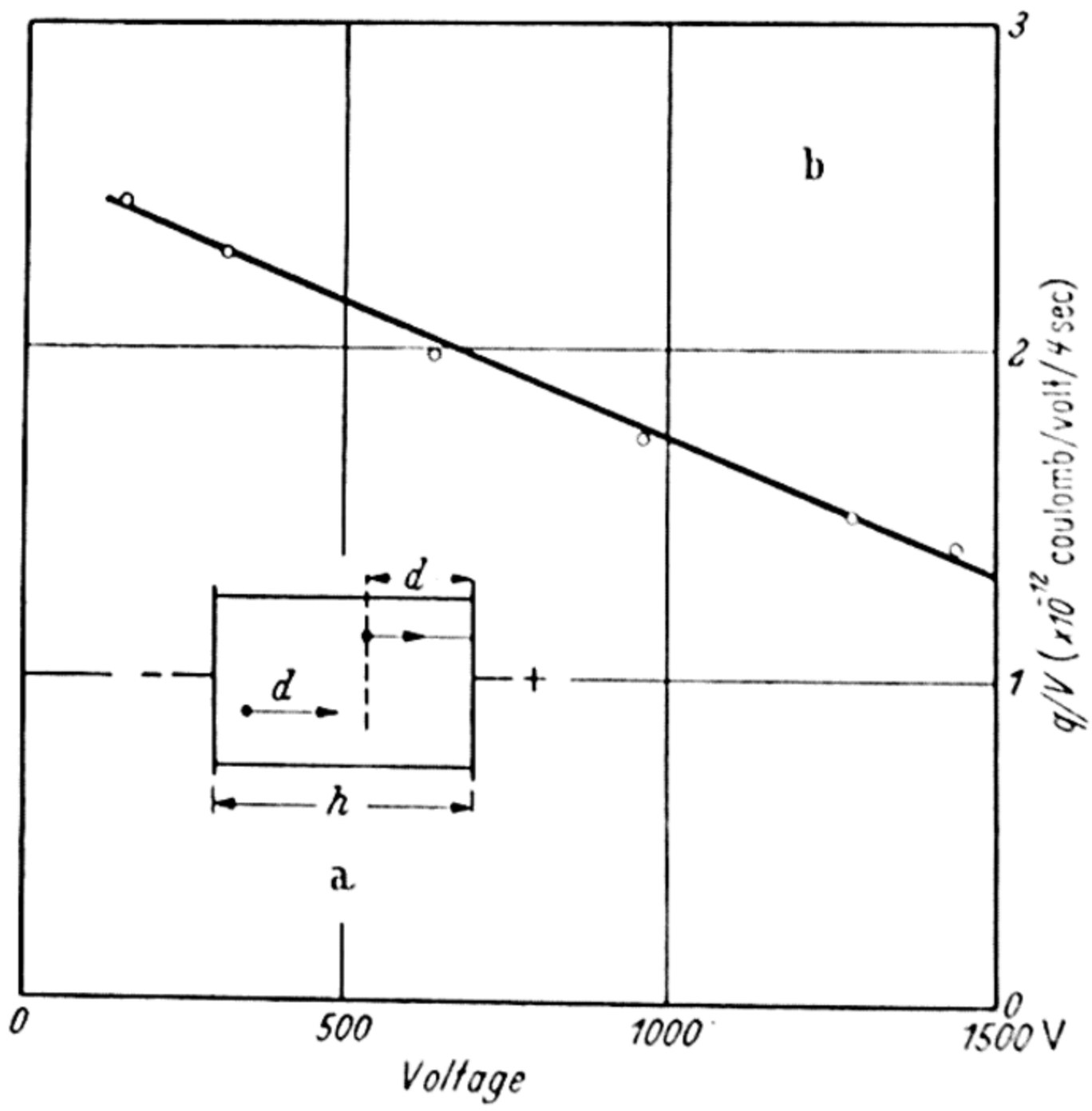

Figure 5. a *Motion of photoelectrons.* b *Charge–voltage relation for diamond*

that the points lie fairly close to a straight line shows that the above relation adequately represents the results. For the example shown, current saturation would occur at $V_0 = 1{,}560$ or 15,300 V/cm.

Gudden and Pohl showed that for diamond the photocurrent obtained with saturation field corresponded to the release of one electron for each absorbed light quantum. In these measurements it was found that the positive holes were normally immobile, but that they could be rendered free to travel through the crystal by illumination with intense infra-red irradiation. If this radiation was applied *at the same time* as the primary ultra-violet radiation, then the photocurrent due to the ultra-violet alone was practically doubled.

Alternatively, if the infra-red was applied *after* the ultra-violet was turned off, a supplementary current of similar magnitude was obtained. Application of the infra-red without pre-illumination gave no photocurrent. Typical figures obtained by Gudden and Pohl (1924) for the charge passing between the electrodes were:

Ultra-violet alone,	$3{\cdot}75 \times 10^{-10}$ C
Subsequent infra-red alone,	$3{\cdot}63 \times 10^{-10}$ C

It was later shown by Gyulai (1925) that for every quantum of short-wave light absorbed to produce the primary current, approximately one quantum of long-wave light had to be absorbed to produce the positive photocurrent.

Gudden and Pohl (1923) also established the principle of quantum equivalence. They found that under favourable conditions, the absorption of each quantum of radiation liberates one electron. The accuracy of their results is indicated by the fact that *assuming* the quantum efficiency to be unity, they calculated Planck's constant to be $h = 6{\cdot}8 \times 10^{-27}$ using diamond, and $h = 7{\cdot}0 \times 10^{-27}$ using a zinc blende crystal, as compared with the accepted value of $h = 6{\cdot}55 \times 10^{-27}$ erg sec. Recent measurements on germanium by Goucher (1950) show that for this material one electron and one positive hole are produced for each absorbed light quantum. For silver bromide, Lehfeldt (1935) found a quantum efficiency of about 60 per cent, and a similar value is given for Sb_2S_3 by Forgue, Goodrich and Cope (1951).

Measurements have been carried out on the Hall effect produced by photocurrents in diamond by Lenz (1925), who thus established that the photocurrents were electronic (and

not ionic) in character. From the magnitude of the Hall effect the mobility of the photoelectrons can be found.

If the positive holes produced by the illumination are immobile (as is to be expected if the photoelectrons originate at impurity centres) a space charge will build up in the crystal, and the photocurrent will gradually decrease with time. To avoid this effect, measurements on insulators are usually made using pulses of light of short duration.

4.2. PHOTOCONDUCTIVITY IN SEMICONDUCTORS

Most of the early measurements on photoconductivity in semiconductors were of a superficial nature. In general no attempt was made to separate primary and secondary currents, and most of the measurements were made on natural crystals of unknown purity content. For example COBLENTZ and KAHLER (1919) in their measurements on MoS_2 show response times of about 5 minutes, so that the currents must be secondary ones. Gudden and Pohl (see GUDDEN, 1928) showed that such long time effects occur in CdS, and they showed also that the shape of the spectral sensitivity curve for HgS was altered slightly according to whether primary or secondary currents were involved. The effects of secondary currents can be greatly reduced by carrying out measurements rapidly *i.e.* using either short pulses of illumination, or chopped radiation. The main differences between photoconductivity in semiconductors and in insulators arise from the fact that in the former there are already considerable numbers of conduction electrons (or holes) present in the un-illuminated material and the photocurrent is quite often only a fraction of the dark current.

The presence of electronic barriers which are modulated by the primary photoelectrons can lead to changes in the dark current which greatly exceed the primary photocurrent itself. In oxidized layers where such effects are particularly marked, effective quantum efficiencies of hundreds and even thousands may be found (FASSBENDER, 1947). This effect of the field current in amplifying the primary photocurrent has been discussed by STOCKMAN (1950).

In order to eliminate the effects of intercrystalline barriers, some workers have used the photoconducting material in a condenser and then measured the a.c. impedance of the condenser (PUTSEIKO, 1949). By making the a.c. measurements in the presence of a steady electric field, this worker was able to determine the sign of the current carriers. As regards spectral response curves, Putseiko's results do not differ significantly from those obtained by conventional methods.

Hall effect measurements show in copper oxide that the effect of illumination is simply to increase the number of current carriers, without altering the mobility (ENGELHARD, 1933) *i.e.* the mobility of the photoelectrons is the same as that of the thermally excited electrons.

In semiconductors the energies involved are small (otherwise thermal energies would not be sufficient to raise appreciable numbers of electrons to the conduction levels), and consequently the photoconductive wavelengths usually lie in the infra-red region of the spectrum.

5

SPECTRAL DISTRIBUTION OF PHOTOCONDUCTIVITY

RADIATION of frequency greater than that of the series limit of the absorption spectrum will produce free electrons and positive holes, and thus photoconductivity should result under an applied field. However, in the region of very high absorption where the absorption constant is $\sim 10^{-5}\text{cm}^{-1}$, the radiation can only penetrate a thin surface film, and thus can only produce photoconductivity in this film. Surface imperfections will tend to impede the flow of this current more than currents through the bulk of the material. Also, the fact that the radiation is absorbed in a thin surface film means that the *density* of photoelectrons produced will be high, and therefore the probability of recombination of holes and electrons will be high. For these reasons the photocurrent in the region of highest absorption is always less than near the absorption edge. For some crystals the photocurrent drops rapidly as the frequency exceeds that near the absorption edge, but the effect is usually much less pronounced if thin layers ($\sim 1\mu$ thick) are used.

For most materials investigated in the form of thin layers the spectral sensitivity curves (for an equal energy spectrum) are similar to that shown in *Figure 6*a, which represents results obtained for arsenic. For short wavelengths the sensitivity rises slowly as the wavelength increases, then, after reaching some ' threshold ' wavelength, starts to fall rapidly. It is found that if the spectral sensitivity curves are plotted as log (sensitivity) against linear wavelength, this fall is usually approximately a straight line *i.e.* an exponential fall in sensitivity with wavelength occurs. This relation was shown to be obeyed by lead sulphide (Moss, 1949b), and the majority of the curves for the elements given later in this volume will be seen to show the same behaviour.

5.1. DETERMINATION OF OPTICAL ACTIVATION ENERGY BY RELATION TO THE THERMAL ACTIVATION ENERGY

From measurements on the spectral distribution of the photoconductive effect (shown in many figures later) it is clear that no absolute threshold wavelength exists *i.e.* there is no wavelength at which the sensitivity vanishes completely. There is thus no significance about the longest wavelength at which the photoconductive effect can be measured, as this can in principle be extended indefinitely by using a more powerful source of radiation, or a higher gain amplifier (narrowing the bandwidth to reduce the noise, if necessary). For an arsenic layer for example (*Figure 6*a), the sensitivity falls steadily over

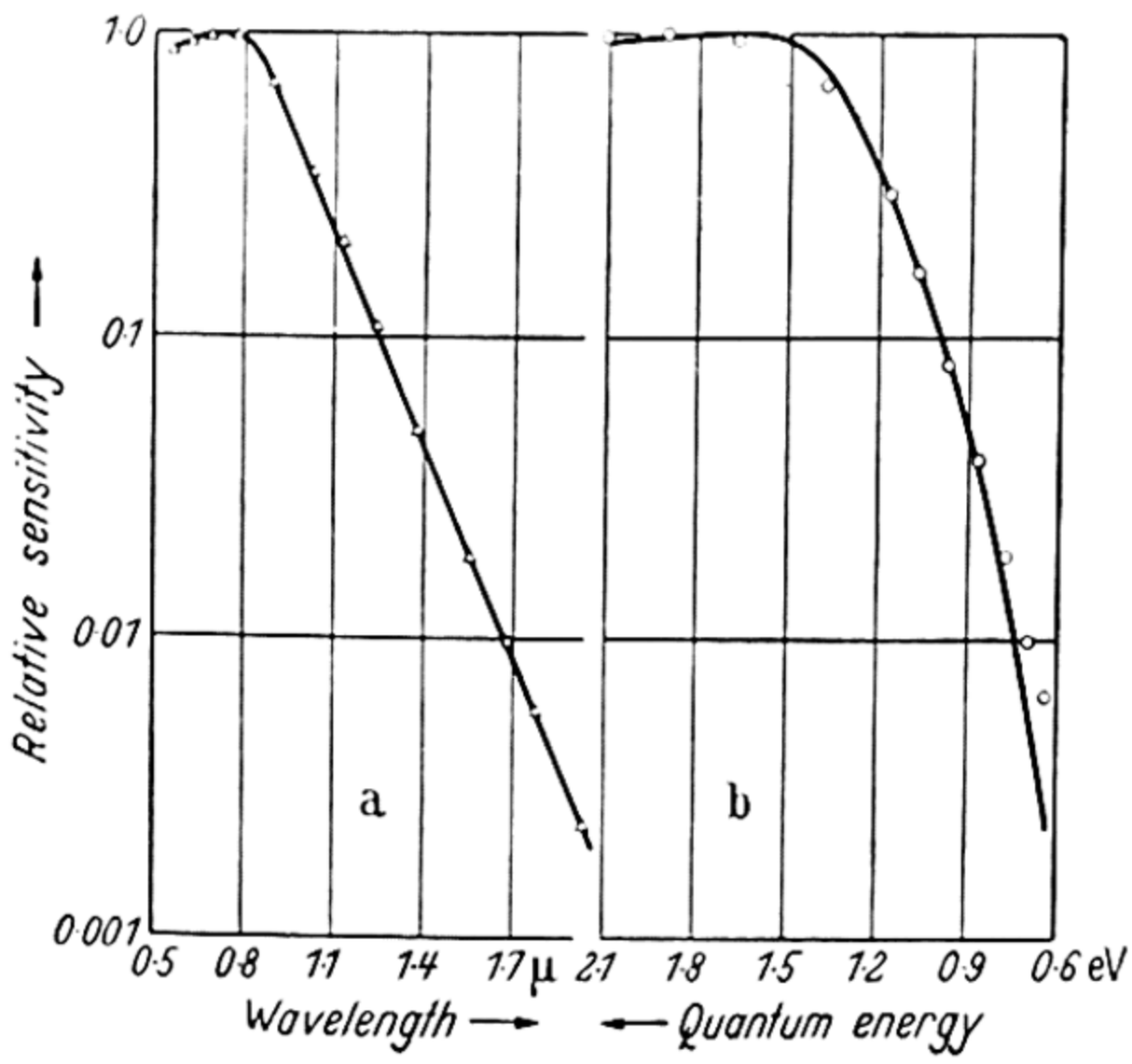

Figure 6. Spectral sensitivity curves for arsenic. b *Full line experiment. Points theory (equation* 23)

a range of 1,000 : 1; while for a PbS layer, the author has observed an exponential fall over a range of more than 10,000 : 1. However thermal measurements (Hall effect or conductivity) give a precise value of activation energy, and it is therefore necessary to define a ' threshold ' wavelength from which may be derived an optical activation energy for comparison with this energy.

We will consider a monatomic solid (that is an intrinsic

semiconductor), where there should be no difference in the thermal and optical activation energies in consequence of the Franck–Condon principle, because the material is non-polar and has the same dielectric constant at both low and high frequencies. For mathematical convenience we will represent the spectral sensitivity curve by the equation:

$$S(E) = \frac{1}{1 + \exp\{\beta(E_0 - E)\}} \qquad \ldots\ldots(23)$$

where β is a constant, E is the energy at any wavelength, and E_0 the energy at the 'threshold' wavelength. This curve has a flat response at short wavelengths, and an exponential fall with energy at long wavelengths. The experimental results are more accurately represented by an exponential fall with *wavelength* (see *Figure 6*a), but the difference is small as *Figure 6*b shows. Here the full line shows the experimental curve while the circles are points calculated from equation 23 with $\beta = 8{\cdot}0$, and $E_0 = 1{\cdot}27$eV.

It is assumed that the varying sensitivity results from the distribution of energy levels from which the photoelectrons originate (or alternatively to which they may go). Such a distribution of centres has been considered by Busch (1946) in another connection, and by Rose (1951). If the distribution is such that there are $N(E)\mathrm{d}E$ levels between E and $E + \mathrm{d}E$, then with radiation of a given quantum energy E_λ, the amount of absorption, and hence the sensitivity, will be proportional to the total number of centres of energy lower than E_λ; *i.e.* $\int_0^{E_\lambda} N(E)\mathrm{d}E$. Hence

$$\left.\begin{aligned} S(E) &\propto \int_0^{E_\lambda} N(E)\mathrm{d}E \\ \text{or} \qquad N(E) &= G\,\frac{\mathrm{d}S(E)}{\mathrm{d}E} \end{aligned}\right\} \qquad \ldots\ldots(24)$$

where G is a constant. By using the expression for $S(E)$ we obtain

$$N(E) = \frac{G\beta \exp\{\beta(E_0 - E)\}}{[1 + \exp\{\beta(E_0 - E)\}]^2} \qquad \ldots\ldots(25)$$

From this expression for the distribution of levels we can

calculate the number of electrons which will be present in the conduction band due to thermal excitation.

If in *Figure 7*, we take the zero of energy at the bottom of the conduction band, the number of electrons per cm² raised thermally to the conduction levels from the level E will be: $C\{N(E)\}^{\frac{1}{2}} \exp(-E/2kT)\mathrm{d}E$ where C is a constant, and the *total* number raised to the conduction band

$$n = \int C\{N(E)\}^{\frac{1}{2}} \exp(-E/2kT)\mathrm{d}E \qquad \ldots\ldots(26)$$

Putting $E_0 - E = \phi$, then

$$n = C(G\beta)^{\frac{1}{2}} \int_{-\infty}^{\infty} \frac{\exp(\beta\phi/2)\exp(\phi - E_0)/2kT}{1 + \exp(\beta\phi)}\,\mathrm{d}\phi.$$

The positive limit of integration is taken as infinity for convenience, although in reality ϕ should not exceed E_0. However,

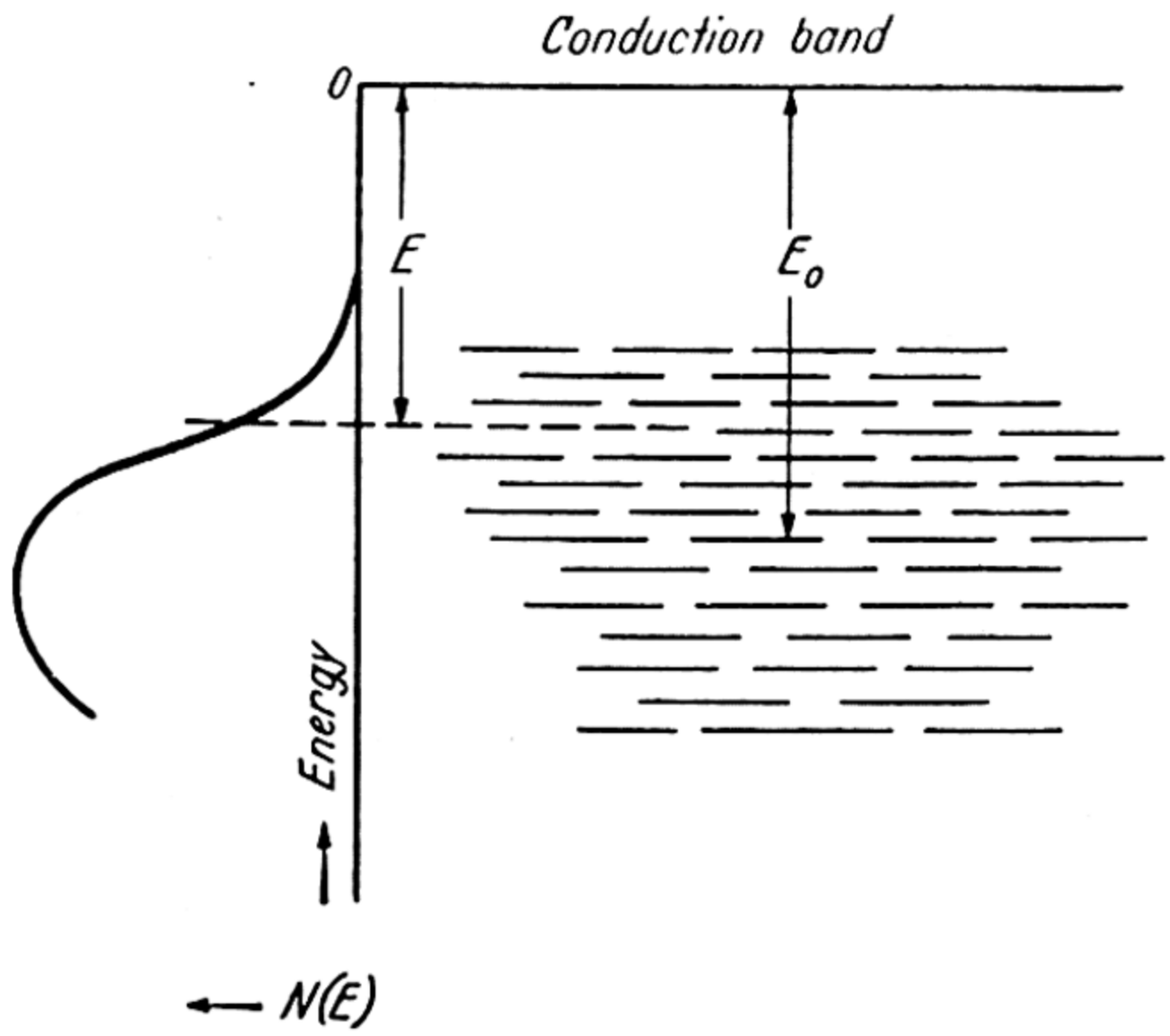

Figure 7. Distribution of energy levels

in practice the number of levels is zero at $\phi > E_0$, and even from the assumed formula for S we find $S \simeq e^{-30}$ at $E = 0$ for PbS for example. Hence

$$n = C(G\beta)^{\frac{1}{2}} \int_{-\infty}^{\infty} \frac{\exp\left[\frac{1}{2}\phi\{\beta + (1/kT)\}\right]\exp(-E_0/2kT)}{1 + \exp(\beta\phi)}\,\mathrm{d}\phi.$$

This expression can be arranged in the form of a known integral as follows:

Put $\beta\phi = x$, and $\phi\left(\beta + \frac{1}{kT}\right) = 2ax$

where $2a = 1 + \left(\frac{1}{\beta kT}\right)$

$$\therefore n = C\left(\frac{G}{\beta}\right)^{\frac{1}{2}} \exp\left(-\frac{E_0}{2kT}\right)\int_{-\infty}^{\infty} \frac{e^{ax}}{1+e^{x}}\,dx$$

Putting $e^x = y$, the integral gives $\int_0^\infty \left(\frac{y^{a-1}}{1+y}\right)dy$, which has the value $\pi/\sin \pi a$*. Thus

$$n = C\left(\frac{G}{\beta}\right)^{\frac{1}{2}} \frac{\pi}{\sin \pi a} \exp\left(-\frac{E_0}{2kT}\right) \qquad \ldots\ldots(27)$$

This corresponds to the expression occurring in the conductivity or Hall effect from the simple theory of electrons excited into the conduction band from one definite energy level, namely $n = n_0 \exp(-W/2kT)$ where W is the activation energy, or width of the forbidden zone for intrinsic conductivity.

Hence by comparison, $W = E_0$. Thus when $E = W$, the sensitivity is

$$S = [1 + \exp\{\beta(E_0 - W)\}]^{-1} = \tfrac{1}{2} \qquad \ldots\ldots(28)$$

We thus reach the important conclusion that, the activation energy is determined from the spectral sensitivity curve as the point where the sensitivity has fallen to half value, that is

$$E_0 = W = \text{quantum energy at } \lambda_{\frac{1}{2}}.$$

In cases where two or more bands of sensitivity are present, the activation energy of the longer wavelength bands will be determined from the wavelength where the sensitivity has fallen to half its value on the flat part of the curve immediately preceding the exponential fall.

5.2. METHOD OF PHOTOELECTRIC LINES

There is a second method which has been suggested for use in determining the threshold wavelength, the method being

* The function $\sin \pi a$ where $2a = 1 + (1/\beta kT)$ is a slowly varying function of T provided βkT is appreciably > 1. In all cases β must be $\gg 1/kT$, or the above theory is not applicable since it would imply semi-metallic properties in the material with energy gap ~ 0.

analogous to that used in photo-emission measurements to determine the work function of metals. RICHARDSON (1912) showed that if a metal surface be exposed to the total radiation from a black body at a temperature T, the total photo-emission from the surface should be given by

$$I = AT^2 e^{-h\nu_0/kT} \quad \ldots\ldots(29)$$

where ν_0 is the threshold frequency for the surface. Hence plots of log (I/T^2) as a function of inverse temperature should give straight lines, the slopes of which yield the work function. This method was used by ROY (1926) who found the plots to be straight lines, the work functions from which agree well with those obtained by the Fowler–DuBridge type of measurements. (See HUGHES and DUBRIDGE (1932).)

The suggestion has been made by LANGE (1938) and also by TREU* that a similar relation should hold for the internal electron 'emission' in a photoconductor. Thus the number of electrons raised to the conduction band, and hence the photo-current, should be proportional to $T^2 e^{-h\nu_0/kT}$ where T is the temperature of the black-body source. Both workers carried out experiments, and found that the 'photoelectric lines' plotted according to the above formula were indeed straight lines. By this method Lange found the activation energy for a selenium cell to be 1·46 eV, equivalent to a threshold wavelength of 0·84μ. This figure may be compared with spectral sensitivity measurements made on various selenium cells by BROWN and SIEG (1914) from whose curves it may be seen that the $\lambda_{\frac{1}{2}}$ values lie in the range 0·75μ to 0·85μ.

Results obtained by Treu on lead sulphide cells may be compared with $\lambda_{\frac{1}{2}}$ values obtained by the present author (Moss, 1949b) on similar cells:

TREU		AUTHOR	
Temperature	*Equiv. threshold*	*Temperature*	$\lambda_{\frac{1}{2}}$ *value*
17° to 20°C	2·7μ to 3·2μ	17°C	2·7μ to 2·9μ
− 70°C	3·1μ to 3·4μ	− 78°C	3·0μ to 3·3μ

The agreement between the two sets of results is very good—any systematic difference being smaller than the scatter in either set of measurements—and they can therefore be

* TREU, M. Report of war-time work at Erlangen University.

considered as experimental proof that the threshold wavelength found by the Richardson type plot and by the $\lambda_{\frac{1}{2}}$ value on the photoconductivity curve are the same.

It is interesting to note that measurements by Treu on one of his cells at 20°C and — 67°C gave a spectral shift of 0·3μ; which compares well with the value of 0·32μ found by the author (1949b). Values of $\lambda_{\frac{1}{2}}$ obtained from curves given by ROTH (1938) and Fischer *et alii* (1938) also give $\lambda_{\frac{1}{2}}$ values similar to the above.

It is concluded therefore from these two lines of approach that the ' threshold ' wavelength to be used to determine the optical activation energy is the wavelength where the sensitivity has fallen to half its value at either the maximum, or the flat part of the curve preceding the exponential fall. Confirmation is obtained from the generally good agreement found (in the results to be described in later chapters) between thermal and optical activation energies in the elements, where the two values would be expected to be approximately the same.

6

THEORY OF PHOTO-RESPONSE

6.1. RESPONSE TIME AND PHOTOCURRENT-INTENSITY RELATION

CALCULATIONS are carried out for a single crystal model on the basis that the rate at which the photocurrent builds up after illumination is applied, and the final steady value which it reaches, are determined by the recombination of the photo-electrons with the positive holes (produced at the same time as the photoelectrons) or with other trapping centres. Donor or acceptor impurity centres will both act as trapping centres when they are unoccupied.

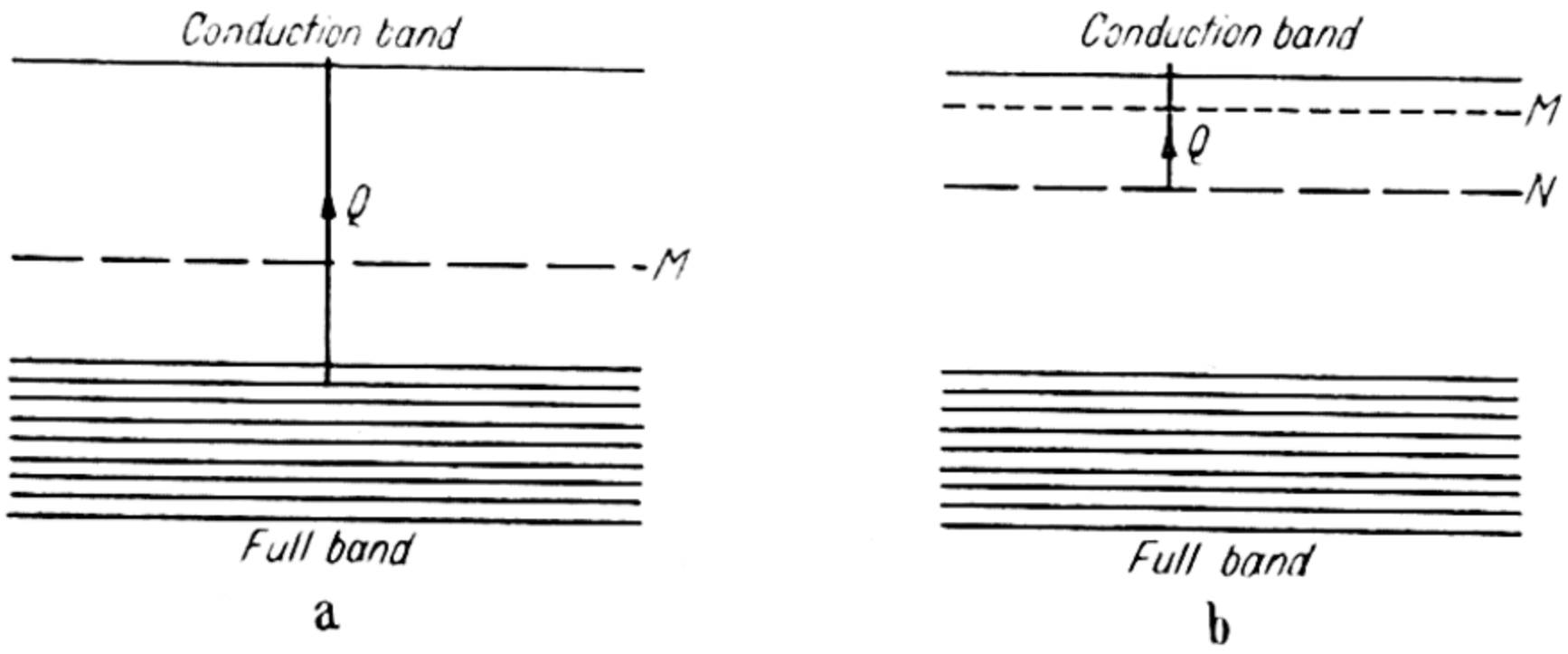

Figure 8

Consider a semiconductor as shown in *Figure 8*a, with M impurity levels per cm³ near the full band. The radiation raises Q photoelectrons from the full to the conduction band per cm³ per sec. Suppose that originally n' of the acceptor levels are occupied, leaving n' holes in the full band, and that the conduction band is empty. Let B be the recombination coefficient and n the density of photoelectrons in the conduction band. Then the equation for the build up of the signal is

$$dn/dt = Q - Bn(n + n' + M - n') = Q - Bn(n + M) \ldots . (30)$$

if the same recombination coefficient is taken for both holes in the full band and acceptor levels.

If n_1 is the density of conduction electrons when equilibrium has been attained, then

$$\mathrm{d}n/\mathrm{d}t = 0 = Q - Bn_1(n_1 + M)$$
$$\therefore n_1(n_1 + M) = Q/B$$

Hence for small signals, with $n_1 \ll M$, the final density of photo-electrons is $n_1 = Q/BM$. Thus we see that there is a linear relation between n_1 and Q at low levels. Since the photocurrent is proportional to n_1, and Q is proportional to the radiant power producing the signal, then the photocurrent must be proportional to the radiant power in this range. As all semiconductors contain *some* impurity levels, it is always possible to have n_1 small compared with M, and so for sufficiently small signals the photo-response should always vary linearly with incident power.

For large signals, with $n_1 \gg M$, the above equation gives $n_1^2 = Q/B$ or $n_1 = (Q/B)^{\frac{1}{2}}$. Thus for large signals, the photocurrent will be proportional to (Power)$^{\frac{1}{2}}$. Similar conclusions were reached by PICK (1948) for the signal-intensity relations. Recent measurements on cadmium sulphide (SMITH, 1951) show that at low levels of illumination the response is practically linear over several decades of energy, but that it follows approximately a (Power)$^{\frac{1}{2}}$ law at high intensities.

For very pure materials, M will be small and the change over from linear to (Power)$^{\frac{1}{2}}$ relation will occur at very small photocurrents. On the other hand when M is large, the photocurrent should be linear up to relatively high values of incident power. Integrating equation 30 we obtain

$$\frac{n_1 - n}{n_1 + n + M} = \frac{n_1}{n_1 + M} \exp\{-B(M + 2n_1)t\}$$

Thus for $n_1 \ll M$, $n/n_1 = 1 - \exp(-BMt)$, and the response time, defined as the time for the signal to reach $1 - 1/e$ of its maximum value, is $\tau = 1/BM$. A study of the build up of the signal when the bi-molecular recombination process applies has been published by VON HIPPEL and RITTNER (1946).

If there is some intrinsic conductivity in the dark, due to thermal excitation of the electrons at a rate of A/cm^3/sec, then equation 30 is replaced by

$$dn/dt = A + Q - Bn(n + M) \qquad \ldots.(31)$$

and $A = Bn_0(n_0 + M)$ where n_0 is the density of conduction electrons in the dark. Putting $\Delta n = n - n_0$,

$$dn/dt = Q - B\Delta n(\Delta n + X) \qquad \ldots.(32)$$

where $X = M + 2n_0$. Thus for small signals ($\Delta n \ll X$), the steady value of Δn is given by $\Delta n_1 = Q/BX$, so that the photocurrent is proportional to the power as before.

For large signals, $\Delta n \gg X$, $\Delta n_1^2 = B/Q$, so that again a (Power)$^{\frac{1}{2}}$ law will be reached at sufficiently high levels. Integrating equation 32 gives

$$\frac{\Delta n_1 - \Delta n}{\Delta n_1 + \Delta n + X} = \frac{\Delta n_1}{\Delta n_1 + X} \exp\{-B(X + 2\Delta n_1)t\}$$

Thus for Δn_1 small, $\Delta n/\Delta n_1 = 1 - \exp(-BXt)$, giving response time $\tau = 1/BX = 1/B(M + 2n_0)$. Thus both the response time τ and the signal Δn_1 will decrease as n_0 increases, the two bearing the simple relation

$$\Delta n_1 = Q\tau \qquad \ldots.(33)$$

This relation has been shown to hold by LASHKAREV *et alii* (1949).

Raising the temperature will increase n_0, the increase being rapid in the range of intrinsic conductivity, so both τ and the signal (or sensitivity) should decrease on heating. For a tellurium cell the sensitivity was found to decrease greatly on warming from liquid air temperature to room temperature (see Chapter 21). A similar variation in sensitivity in a germanium cell has been found by BECKER and FAN (1950). The photovoltage of their cell decreased by 10^4 between 100°K and 290°K, while the response time fell from 1,500μ sec to less than 12μ sec. Similar temperature variation of response time and sensitivity have previously been reported for lead sulphide (Moss, 1947), while for cuprous oxide RYVKIN (1949) has shown that τ varies exponentially with reciprocal temperature in the same way as the resistivity, *i.e.* $\tau \propto 1/\sigma \propto \exp(E/2kT)$.

The results derived for the defect conductor considered apply equally to an excess conductor. Also the same equations apply to a semiconductor where the photoelectrons originate at donor impurity levels, as opposed to the full band. For

example for the case illustrated in *Figure* 8b, if all the 'N' levels are occupied in the dark, there will be M electrons shared between the conduction band and the 'M' levels. Hence $dn/dt = Q - B(n + M)n$ which is identical with equation 30. For any of the above examples, the treatment becomes somewhat more complicated if different recombination coefficients are used for the different levels.

A lengthy treatment of the theory of the photo-response has been given recently by Rose (1951) in which he pays particular attention to the effect of trapping on the response times and photocurrents. He shows that trapping centres distributed exponentially with energy depth below the conduction band can give rise to exponents between unity and a half for the signal/intensity relation.

6.2. MAGNITUDES OF PHOTOCURRENTS AND RESPONSE TIMES

An idea of the values of B to be expected may be derived from estimates of the capture cross-section for an electron by a trap or positive hole. If this cross-section is c, then an electron moving with velocity u will sweep out an effective volume cu per second. This volume contains Mcu traps, so that the average time before recapture is $\tau = 1/Mcu$. But $\tau = 1/BM$, so we have $B = cu$. If c is comparable with normal atomic dimensions *i.e.* $\sim$ 1Å square, then for thermal velocities where $u \simeq 10^7$ cm/sec, we find that $B \simeq 10^{-9}$ cm^3/sec. With a density of centres $M = 10^{14}$ to 10^{18} per cm^3, the response time will be $\tau = 10^{-5}$ to 10^{-9} sec.

Measurements on germanium (Shockley *et alii*, 1949) show that in this material the capture cross-section is actually much smaller than the above estimate. The figure given is 10^{-18} cm^2, so that $B = 10^{-11}$. For thallous sulphide, B is about 10^{-11} to 10^{-12} (von Hippel and Rittner, 1946), for PbS, Pick (1948) finds 10^{-11}, and for CdS Fassbender and Lehmann (1949) give 10^{-10} to 10^{-14} cm^3/sec. Thus response times of 10^{-3} sec or more become feasible. The values of response times which have been measured for various photoconductors lie mostly between 10^{-6} and 10^{-3} seconds, although the

absence of shorter response times is no doubt largely due to the difficulties of measurement. There are indications that τ is only $\sim 10^{-8}$ sec in diamond (McKay, 1950). The theory thus gives the right order of magnitude for the response time.

For the photocurrent $\Delta n = Q/BM = \tau Q$, and $\Delta\sigma = \Delta neb$. For a layer 1 cm square, thickness d cm, with q quanta/sec absorbed, $Q = q/d$, and the photocurrent $\Delta i = dV\Delta neb = ebq\tau V$, where V is the applied voltage and unity quantum efficiency is assumed.

Thus for example, with $\tau = 1\mu$ sec, $q = 10^{16}$ (*i.e.* 2 milliwatt at 1μ wavelength) $b = 10$ cm sec^{-1}/V cm^{-1} and $V = 100$V, we find $\Delta i = 10^{-6}$ amp. High photocurrents will result when τ and b are large. For example, in high purity germanium $\tau \sim 100\mu$ sec and $b = 3{,}500$ cm sec^{-1}/V cm^{-1}, so that with other parameters as above $\Delta i = 50$ mA. At the other extreme the values might be as low as $\tau = 10^{-8}$ sec and $b = 1$ cm sec^{-1}/V cm^{-1}, so that the photocurrent would only be 10^{-9} amp even with a quantum efficiency of unity. Should the quantum efficiency be only 1 per cent, the photocurrent is proportionally reduced to 10^{-11} amp. These figures cover the general range of photocurrents met in practice.

In the above treatment, only recombination probabilities in the bulk of the material are considered. The effect of a different recombination probability for the surface has been discussed by Suhl and Shockley (1949), Becker and Fan (1950), and Haynes and Shockley (1951).

6.3. BARRIER THEORY OF PHOTOCONDUCTIVITY

The theory of § 6.1 assumes that the variation in conductivity on illumination results from a change in n, the density of conducting electrons or holes, as the case may be. A possible alternative explanation is that the number of conduction electrons is relatively unaffected by the illumination, but that the effective mobility is increased.

More specifically the theory (as outlined by Gibson, 1951 and Rittner, 1950, for example) supposes that the primary photoeffect is to excite a small number of electrons in the neighbourhood of potential barriers, these electrons causing a

reduction in the height of the barriers so that conduction by the large density of free electrons normally present is increased. This type of theory is applicable to oxidized microcrystalline films, particularly of the lead, thallium and cadmium sulphide types; and provides an explanation of the anomalously high values of apparent quantum efficiency which are sometimes found in these materials. For single crystals and films of elements prepared under high vacuum conditions there is no evidence that barrier modulation phenomena are important.

Gibson postulates that in the oxidation process, surface states are created which capture electrons from within the crystals, and thus set up space charge barriers of the Schottky type (SCHOTTKY, 1939 and 1941). Thus the contact between one microcrystal and another can be treated as two such barriers back to back. In the photoelectric process it is assumed that the number of electrons in the surface states is reduced, so that the barrier height is reduced, with consequent increase of conductivity.

Consider a material with a density M of donor impurities, and an area-density of surface states n_0, situated at a depth E below the conduction band. Let the height of the double Shottky barrier be ϕ. Then the number of surface states emptied thermally will vary exponentially with their depth below the Fermi level *i.e.* $\Delta n_0 = n_0 \exp\{(\phi - E)/kT\}$ if we take the Fermi level as coincident with the bottom of the conduction band, as is approximately the case when the impurity activation energy is very small. According to BARDEEN (1947) $\phi = (n_0 - \Delta n_0)^2 e^2/2\epsilon M$, and the surface charge

$$s = (n_0 - \Delta n_0)e = (2\epsilon M\phi)^{\frac{1}{2}} \qquad \ldots\ldots(34)$$

On illumination a further Δn surface states are emptied, and the surface charge and barrier height both decrease with $\Delta s = e\Delta n$ and $\Delta\phi = s\Delta s/\epsilon M$. Thus $\Delta n = \epsilon M\Delta\phi/es \simeq \epsilon M\,\Delta\phi/e^2 n_0 = H\Delta\phi$ say. Thus the change in barrier height is proportional to the number of surface states emptied by the illumination. Now if there are $\mathcal{N}$ electrons/cm^2 flowing across the barrier per second then $\mathcal{N}$ will vary exponentially with the barrier height as $\mathcal{N} = \mathcal{N}_0 \exp(-\phi/kT)$. Thus the change in electron flow for a small change in ϕ is given by $\Delta\mathcal{N}/\mathcal{N} = -\Delta n/HkT$.

In the dark, under equilibrium conditions, the recombination condition can now be written as $\nu n_0 \exp(-E/kT) = p\mathcal{N}\Delta n_0$ where p is the capture cross-section of a surface state and ν is a frequency (see MOTT and GURNEY, 1948). When illumination is applied which empties I electrons per unit area from the surface states (per second), then

$$I + \nu n_0 \exp(-E/kT) = p(\mathcal{N} + \Delta\mathcal{N}_1)(\Delta n_0 + \Delta n_1) \quad \ldots\ldots(35)$$

Hence

$$I = p\Delta\mathcal{N}_1(\Delta n_0 + \Delta n_1 + HkT) \simeq \Delta\mathcal{N}_1\left\{\frac{\nu n_0}{\mathcal{N}}\exp(-E/kT) + pHkT\right\} \quad \ldots\ldots(36)$$

if Δn_1 is small compared with Δn_0.

Now $\Delta\mathcal{N}_1$ is proportional to the photocurrent Δi, the current flow being given by the *difference* in electron currents across the barrier, while $\Delta\mathcal{N}_1$ is the *sum* of the electron currents crossing the barrier in both directions. The two are therefore related by the expression

$$\frac{e\Delta\mathcal{N}_1}{\Delta i} = \frac{\exp(eV/kT) + 1}{\exp(eV/kT) - 1}$$

where V is the voltage across the barrier*. Hence we see that at low levels of illumination the barrier theory shows that I is proportional to $\Delta\mathcal{N}_1$ and hence to the photocurrent; as found previously by the recombination theory in §6.1.

The behaviour during the build up of the signal will be given by an equation similar to 35

$$\frac{\mathrm{d}}{\mathrm{d}t}(\Delta n) = I + \nu n_0 \exp(-E/kT) - p(\mathcal{N} + \Delta\mathcal{N})(\Delta n_0 + \Delta n)$$

$$= I - \Delta\mathcal{N}\left\{\frac{\nu n_0}{\mathcal{N}}\exp(-E/kT) + pHkT\right\}$$

$$= I - \frac{\Delta n\mathcal{N}}{HkT}\left\{\frac{\nu n_0}{\mathcal{N}}\exp(-E/kT) + pHkT\right\}$$

$$\therefore \Delta n = \tau I\{1 - \exp(-t/\tau)\}$$

* See MOTT and GURNEY (1948), or standard works on rectifier theory.

where the time constant

$$\tau = \frac{HkT}{\rho HNkT + \nu n_0 \exp(-E/kT)} \qquad \ldots\ldots(37)$$

Hence we see that at $t = \infty$ $\Delta n = \Delta n_1 = \tau I$, which is the same relation as found already in equation 33. This same relation thus holds for a theory based on either number of current carriers, or on their mobility.

Gibson (1951) has found that these relations for the photo-current and time constant given by equations 36 and 37 give better agreement with the measured properties of oxidized lead sulphide layers than the simpler recombination theory based on numbers of carriers. The theory is probably applicable to any oxidized microcrystalline layers where the effect of intercrystalline barriers determines the resistance of the layers. For photoconductive layers which are prepared under good vacuum conditions barrier effects should not be important. Also, as by definition, barrier modulation constitutes a secondary photocurrent, it should not be effective in good single crystals.

6.4. WAVELENGTH DEPENDENCE

It has been pointed out in §6.1 that the relative magnitudes of n and M determine whether a linear or (Power)$^{\frac{1}{2}}$ law will occur. Now n is the *density* of photoelectrons, and hence may be expected to vary with the absorption constant for the material. For a given number of quanta incident on the photoconductor and a given quantum efficiency, n will be larger when all the photoelectrons are produced in a thin surface layer.

Thus at wavelengths where the absorption constant is very large, a (Power)$^{\frac{1}{2}}$ law should occur, even at low intensities, although the effect will only be marked when the photo-electrons are not able to diffuse far from the thin surface layer in which they are produced. This phenomena is probably responsible for the drop in photocurrent with decreasing wave-length which often occurs as the region of main lattice absorp-tion band is entered.

We might thus expect that using a moderate range of illuminating intensities, some materials would give linear response at long wavelengths where the absorption is low, but give a (Power)$^{\frac{1}{2}}$ relation in the short wavelength, high absorption region. Such behaviour is in fact encountered in selenium and phosphorus for example, the experimental data for which are discussed in the chapters devoted to the individual elements.

Consider radiation falling on to an infinitely thick slab having an absorption constant K. The number of quanta absorbed per unit volume in a thin layer at depth z is $QK\mathrm{e}^{-Kz}$ where the total absorbed radiation per unit area is $Q = \int_0^\infty QK\mathrm{e}^{-Kz}\mathrm{d}z$. Assuming unit quantum efficiency, the density of photoelectrons at the z level is $n(z)$ where $\mathrm{d}n(z)/\mathrm{d}t = QK\mathrm{e}^{-Kz} - Bn(z)\{n(z) + M\} = 0$ at equilibrium. Hence

$$Bn(z)\{n(z) + M\} = QK\mathrm{e}^{-Kz} \qquad \ldots\ldots(38)$$

and the total number of photoelectrons at equilibrium per unit area is

$$\mathcal{N} = \int_0^\infty n(z)\mathrm{d}z = \frac{2}{K}\left[\frac{M}{2}\log\left(n(z) + M\right) - n(z)\right]_{n(0)}^{n(\infty)}$$

$$= \frac{n(0)}{K}\left[2 - \frac{M}{n(0)}\log\left(1 + \frac{n(0)}{M}\right)\right] \qquad \ldots\ldots(39)$$

Thus for small values of K such that $4QK/B \ll M^2$ we have $\mathcal{N} = Q/BM$, and, as expected under these conditions of low absorption constant, the response will be linear, since the number of photoelectrons at equilibrium is proportional to the intensity of radiation. It will also be noted that the resulting value of $\mathcal{N}$ is independent of the absorption constant.

When K is large however, such that $4QK/B \gg M^2$ then

$$\mathcal{N} = (Q/KB)^{\frac{1}{2}}[2 - (BM^2/QK)^{\frac{1}{2}}\log\{1 + (QK/BM^2)^{\frac{1}{2}}\}]$$

As $M(B/QK)^{\frac{1}{2}}$ is small, the logarithmic term may be neglected, and

$$\mathcal{N} = 2(Q/BK)^{\frac{1}{2}} \qquad \ldots\ldots(40)$$

Thus for these conditions a Signal $\propto$ (Power)$^{\frac{1}{2}}$ law will result. Also we see that $N \propto K^{-\frac{1}{2}}$, so that as K increases, the photoconductivity will decrease, although both the number of quanta absorbed and the quantum efficiency remain constant.

The transition from linear to square root response will occur in the neighbourhood of $n(0) = M = (QK/B)^{\frac{1}{2}}$. Hence, for example, taking $M = 10^{14}$ traps/cm^3, $Q = 10^{16}$ quanta/cm^2/sec (*i.e.* 2 mW at 1μ) and $B = 10^{-9}$, we find $K = 10^3$ cm^{-1}. Thus for this case, only values of $K < 10^3$ would give a linear response, and as K rose above 10^3 cm^{-1} the measured spectral sensitivity would fall.

Typical spectral sensitivity curves which might be observed for a material with the absorption spectrum of curve A* in *Figure 9* are shown at B. Curve *1*, for very small incident energy, shows constant sensitivity out to the absorption edge; curve *2*, for medium incident energy, is flat for part of the range of wavelengths; while curve *3*, for high incident energy, has a sharp peak in the neighbourhood of the absorption edge. FASSBENDER (1949) has used this type of theory to explain the spectral sensitivity curves of cadmium sulphide.

6.5. EFFECT OF DIFFUSION

The effect of high absorption constant may be considerably modified by diffusion from the surface layers into the body of the material. Including the diffusion term, the general continuity equation for electrons may then be written

$$\frac{\partial n_e}{\partial_t} = q - Bn_e(n_h) - \frac{1}{e}\,\mathrm{div}\, I \qquad \ldots\ldots(41)$$

where I is the current density, and n_e, n_h are the density of electrons and holes respectively. Assume that the holes diffuse to the same extent as the electrons. As the diffusion constants $D_e/D_h = (b_e/b_h)^{\frac{1}{2}}$ there will be little difference if the mobilities are similar. Hence we may put $n_e = n_h = n$.

Assuming uniform conditions in the plane of the surface exposed to the radiation, we have div $I = \partial I/\partial z$ where the z direction is perpendicular to the surface. Now $I = -eD\partial n/\partial z$.

* A curve somewhat similar to this has been given for PbTe by GIBSON (1952).

Hence

$$\frac{\partial n}{\partial t} = q - Bn^2 + \frac{D\partial^2 n}{\partial z^2} \qquad \ldots\ldots(42)$$

At equilibrium, $\partial n/\partial t = 0$ and $q - Bn^2 + D(d^2n/dz^2) = 0$. If the absorption constant of the material is K then $q = QKe^{-Kz}$, where Q quanta per cm^2 per sec is the incident radiation. Use of this expression for q makes the equation difficult to solve, and to obtain an approximate solution we will assume that all

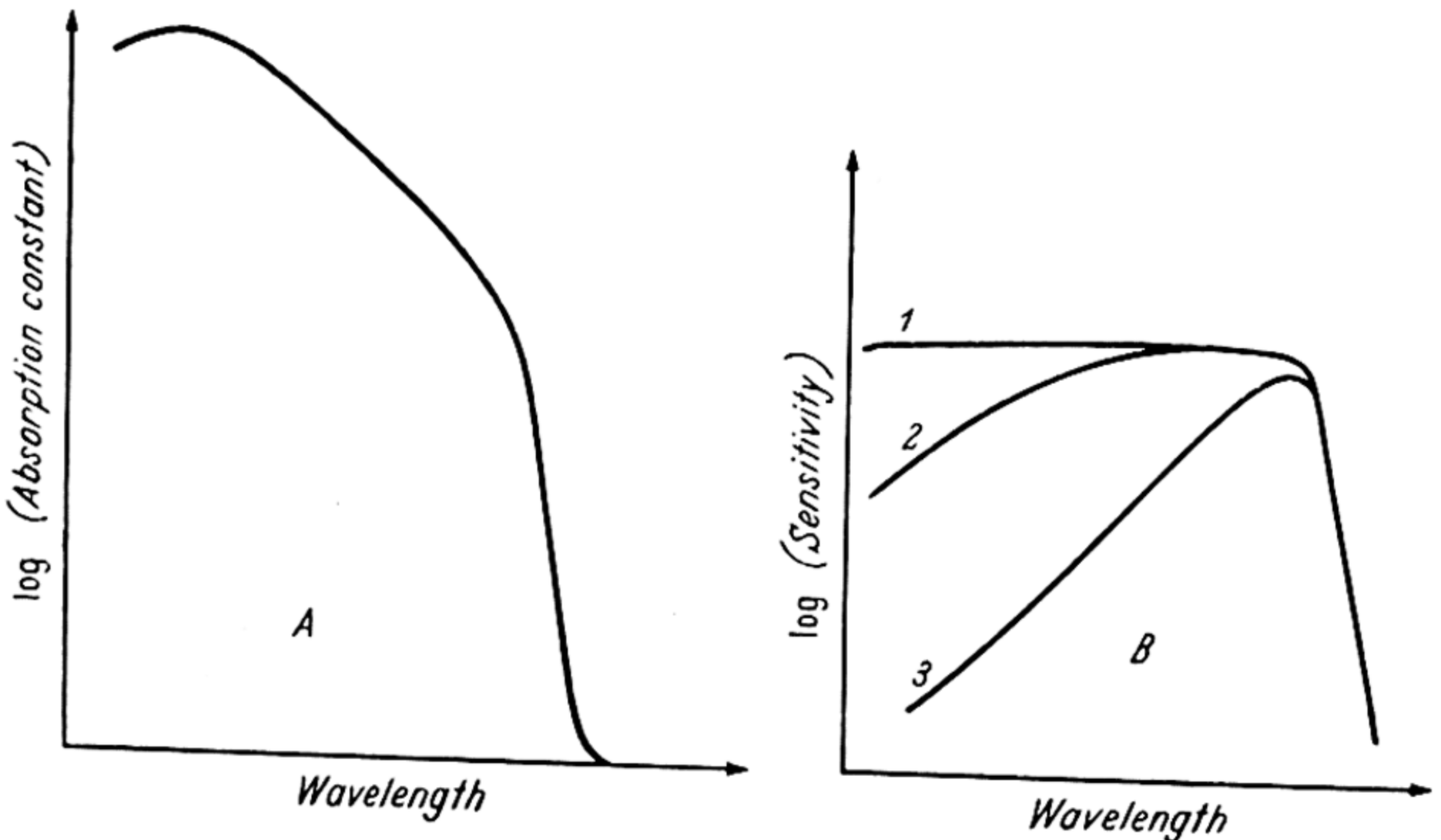

Figure 9. Theoretical spectral response curves

the radiation is absorbed in a very thin surface layer, so that q may be taken as zero except near $z = 0$, where it is $q = QK$. Hence $Dd^2n/\partial z^2 = Bn^2$ giving

$$n^{\frac{1}{2}} = \frac{1}{z\,(B/6D)^{\frac{1}{2}} + (B/QK)^{\frac{1}{2}}} \qquad \ldots\ldots(43)$$

Thus n will decrease to $1/4$ of its value at $x = 0$ in a distance z' where $z'\sqrt{(B/6D)} = (B/QK)^{\frac{1}{2}}$ or

$$z'^2 = 6D(QBK)^{-\frac{1}{2}} \qquad \ldots\ldots(44)$$

Taking $D = 80$ cm^{2}sec^{-1} (equivalent to a mobility of 3,200 cm sec^{-1}/V cm^{-1}*), $KQ = 10^{19}$ quanta/cm^3/sec (equivalent to 10^{-3} W of radiation of 2μ wavelength absorbed in 10^{-3} cm layer) and $B = 10^{-11}$, which is the order found for germanium, then $z' = 2$ mm. Thus for the case of germanium,

* D is related to the mobility b by the equation $b = De/kT$.

where D has a very high value and B a very low value, the diffusion depth will be large even for high values of incident energy, and therefore it would be expected that little fall in the photocurrent would take place even if the radiation were absorbed in a layer as thin as 10^{-3} cm. This result is borne out by experiments which show little fall in photo-sensitivity for wavelengths down to the visible region where the absorption constant exceeds $10^5\,\mathrm{cm}^{-1}$.

In the case of diamond however, where $D \sim 20\,\mathrm{cm}^2\,\mathrm{sec}^{-1}$ and B is much larger, perhaps $\sim 10^{-6}$ as estimated from the low response time of 10^{-8} secs, then we have $z' \simeq 10^{-3}$ cm. Thus there will be little diffusion of the photoelectrons into the bulk of the crystal, and consequently the photocurrent should fall markedly for wavelengths in the high absorption region. Such behaviour is in fact observed for diamond.

Integrating equation 43 we have the total number of photo-electrons $\mathcal{N} = \int_0^\infty n\mathrm{d}z$ giving $\mathcal{N}^2 = (6D/B)\sqrt{(QK/B)}$, treating the material as an infinitely thick slab of 1 cm² area. With no diffusion considered, we have simply $\mathcal{N}' = \int_0^{\frac{1}{k}} \sqrt{(QK/B)}\mathrm{d}z$ $= (Q/BK)^{\frac{1}{2}}$ or $\mathcal{N}'^2 = Q/BK$. For the data given above for germanium, the ratio $\mathcal{N}/\mathcal{N}'$ exceeds 1,000, thus emphasizing the importance of diffusion effects when the optical absorption is very high.

Fassbender (1949) has given a somewhat different theory for the case where the positive holes are immobile. As the distributions of electrons and holes throughout the material are no longer the same, an extra term must be introduced into the continuity equation to represent the field resulting from the net charge. The continuity equation for the photoelectrons then becomes:

$$QKe^{-Kz} - Bn_e n_h + \frac{D\mathrm{d}^2 n_e}{\mathrm{d}z^2} + \frac{b\mathrm{d}}{\mathrm{d}z}(n_e F) = 0 \quad \ldots\ldots(45)$$

where the field F is such that $\mathrm{d}F/\mathrm{d}z = (e/\epsilon)(n_h - n_e)$, ϵ being the dielectric constant. For the holes,

$$QKe^{-Kz} - Bn_e n_h = 0 \quad \ldots\ldots(46)$$

Hence

$$\frac{D\mathrm{d}^2 n_e}{\mathrm{d}z^2} + \frac{b\mathrm{d}}{\mathrm{d}z}(n_e F) = 0 \text{ or } \frac{D\mathrm{d}n_e}{\mathrm{d}z} + bn_e F = 0$$

Now for distances $> 1/K$, $n_h = 0$ since the holes do not diffuse, and hence with this condition $\mathrm{d}F/\mathrm{d}z = -(e/\epsilon)n_e$. Eliminating F and integrating we have

$$n_e = \frac{\mathcal{N}_0{}^2 \alpha}{(1 + \alpha \mathcal{N}_0 z)^2} \qquad \ldots\ldots(47)$$

where $\mathcal{N}_0 = \int_0^\infty n_e \mathrm{d}z$ and $\alpha = eb/2D\epsilon$.

Since $D = bkT/e$ we have $\alpha \simeq 10^{-7}$ cm for a dielectric constant $\epsilon = 20$. At $z = 0$ equation 46 gives

$$n_e(0) n_h(0) = \frac{QK}{B} \qquad \ldots\ldots(48)$$

Also, to maintain electrical neutrality $\mathcal{N}_0 = \int_0^\infty n_h \mathrm{d}z$, and as the holes will extend only to the same depth as the radiation *i.e.* $\sim 1/K$, we may say roughly $n_h = K\mathcal{N}_0$. With $n_e(0) = \mathcal{N}_0{}^2\alpha$, equation 48 becomes $\mathcal{N}_0{}^3 \alpha K = QK/B$ or $\mathcal{N}_0 = (Q/\alpha B)^{\frac{1}{3}}$. Thus

$$n_e = \frac{(\alpha Q^2/B^2)^{\frac{1}{3}}}{\{1 + (\alpha^2 Q/B)^{\frac{1}{3}} z\}^2}$$

which shows that n_e decays to $1/4$ of its value at the surface in a distance $z' = (\alpha^2 Q/B)^{\frac{1}{3}}$. This effective diffusion depth is thus independent of the absorption constant, so that however large K may be, the photoelectrons will always diffuse a distance z' into the material. With $Q = 10^{16}$ quanta/cm^2/sec and $B = 10^{-10}$ for example, then $z' = 1\mu$. For thick samples this diffusion depth would not greatly affect the spectral sensitivity curve, but for films only $\sim 1\mu$ thick it would be sufficient to prevent a fall of sensitivity in the high absorption region.

7

PHOTOVOLTAIC EFFECTS

In 1876 Adams and Day (1877) first discovered that a selenium rod was capable of generating a voltage when illuminated near either of the electrodes. The effect is essentially a barrier phenomenon and has been found to occur for many types of barrier arrangement. Semiconductor materials with soldered electrodes, sputtered electrodes, pressure contacts (including 'cats' whiskers'), insulating barrier layers and internal *p*–*n* junctions in single crystals, have all been found capable of generating a photovoltage. As regards spectral distribution of sensitivity and response time the photovoltaic and photoconductive effects are essentially similar, both being governed by the same fundamental absorption and recombination processes.

In general, the photovoltaic effect has not been the subject of such extensive research work as photoconductivity, although in view of the greater convenience of using a photovoltaic cell where no external battery is required, much technical development has been carried out, particularly on selenium and cuprous oxide cells.

From the theoretical point of view the photovoltage can be calculated more explicitly than the photoconductivity, since the voltage generated is largely independent of the geometry of the specimen and also independent of the mobility of the carriers. The simplest example to consider is that of a single crystal with an internal *p*–*n* junction, as the difficult questions of the precise nature of the surface barrier and the role of surface states do not then arise.

7.1. PHOTOVOLTAIC THEORY FOR *p*–*n* JUNCTION

Consider a sample of an amphoteric semiconductor which is an excess conductor (*n*-type) at one end and defect conductor (*p*-type) at the other, there being a sharp transition between

the two regions. The energy level diagram will be represented by *Figure 10*a.

In equilibrium there will be a potential ϕ across the junction such that no net current flow will take place. This condition will normally occur with the Fermi level lying between the top of the full band and the acceptor levels on the left of the junction, and between the donor levels and bottom of the conduction band on the right of the junction. The Fermi level, must of course be the same for both p and n regions, when the system is in equilibrium. Statistical theory gives the position of the Fermi level in the n-type material as $\psi_n = E_1 - kT \log (\Upsilon/n_e)$, and in the p-type material as $\psi_p = E_2' + kT \log (\Upsilon/n_h)$, where n_e and n_h are the concentrations of electrons and holes respectively, and Υ is given by equation 2. Assuming the centres to be fully ionized so that $n_e = N_d$ and $n_h = N_a$, we have on equating ψ_n and ψ_p

$$E_2' = E_1' - E = E_1 - kT \log (\Upsilon^2/N_d N_a)$$

$$\therefore \phi = E_1' - E_1 = E - kT \log (\Upsilon^2/N_a N_d)$$

For the simple case when the material is equally impure on each side of the junction, so that $N_a = N_d = N$, the above expression reduces to

$$\phi = E - 2kT \log (\Upsilon/N) \qquad \ldots.(49)$$

Thus for normal impurity concentrations, ϕ differs from E by only a few tenths of a volt.

Conventional rectifier theory (see for example HENISCH, 1949, or TORREY and WHITMER, 1948) shows that the current across such a p–n junction will be given by

$$I = I_1 e^{-\phi/kT} (1 - e^{-eV/kT}) + I_2 e^{-\phi/kT} (1 - e^{-eV/kT}) \ldots.(50)$$

when a potential V is applied across the junction, I_1 and I_2 representing the electron and hole contributions to the current flow. If the junction is now uniformly illuminated, so that Q photoelectrons and holes are produced per cm^3 per sec, then the concentrations of electrons and holes will change in the manner represented by the recombination equations of § 6.1.

For the model of *Figure 10*a the general recombination equations will be similar to equations 31 and 32; $A = Bn_0(n_0 + M)$ and $Q + A = Bn(n + M)$. Therefore $\Delta n/n = Q/Bn(2n + M)$.

Thus for holes, the photosensitivity, defined as $S_h = \Delta n_h / Q n_h$ is

$$S_h = \frac{1}{B n_h (N_d + 2n_h)} \qquad \ldots\ldots(51)$$

as the density of trapping centres for holes is $M = N_d$. Similarly for electrons $S_e = \Delta n_e / Q n_e = 1/B n_e (N_a + 2n_e)$. Thus for the p-type material on the left of the junction, where $N_d = 0$, $S(p)_h = 1/2Bn_h^2 = 1/2BN_a^2$ assuming the impurity centres to be fully ionized. Also $S(p)_e = 1/Bn_eN_a$ as $n_e \ll N_a$. Now the densities of holes and electrons in a given sample of semiconductor bear a simple reciprocal relation to each other such that $n_e n_h = n_i^2$ where n_i is the density of *intrinsic* carriers for the material. (See, for example, SHOCKLEY, 1950.)

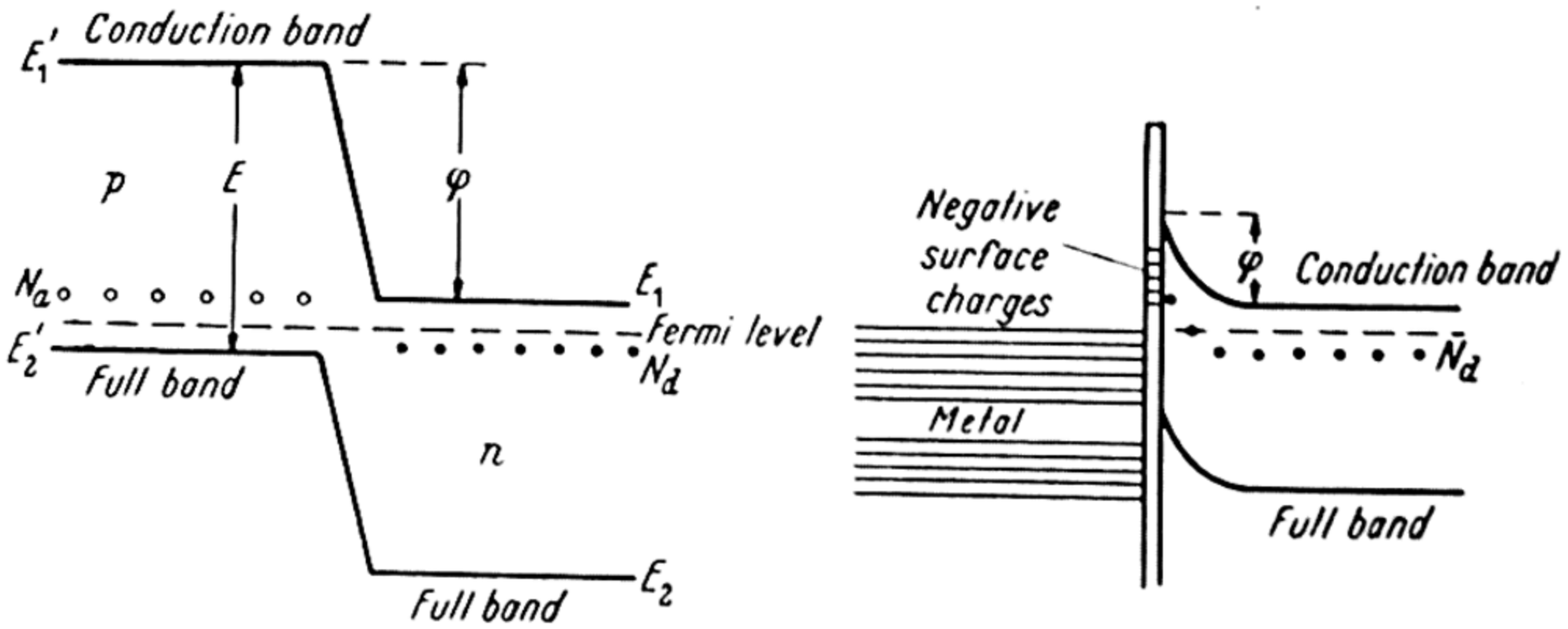

a) *p–n Junction* b) *Metal–Semiconductor contact*

Figure 10

Hence $n_e = n_i^2/n_h$ giving $S(p)_e = 1/Bn_i^2$. Now N_a is normally much greater than n_i, so that $Na^2 \gg n_i^2$ and hence $S(p)_e \gg S(p)_h$. Conversely we find for the n-type material that $S(n)_h \gg S(n)_e$. These results may be summarized by stating that variation in the density of *minority* carriers is the most important factor in the operation of p–n junctions.

Ignoring therefore the changes in the *majority* carrier densities, the current relation for the junction (equation 50) will be modified by the irradiation to give

$$I_L = I_1 e^{-\phi/kT}(1 + QS(p)_e - e^{-eV/kT}) + I_2 e^{-\phi/kT}(1 + QS(n)_h - e^{-eV/kT})$$

Thus, when $I_L = 0$, the photovoltage

$$V_p = -\frac{kT}{e} \log\,(1 + SQ) \qquad \ldots\ldots(52)$$

where $S = \{I_1 S(p)_e + I_2 S(n)_h\}/(I_1 + I_2)$. If the recombination coefficients are the same for holes, and electrons, then $S(p)_e = S(n)_h = 1/Bn_i^2$. Also $Bn_i^2 = A$, the rate of thermal generation of electrons and holes as by definition $M = 0$ when $n = n_i$. Thus $S = 1/A$ and the photovoltage

$$V_p = -\frac{kT}{e} \log \left(1 + \frac{Q}{A}\right) \qquad \ldots\ldots(53)$$

For small intensities of illumination the relation reduces to $V_p = -\frac{kT}{e} \cdot \frac{Q}{A}$ *i.e.* the response becomes linear.

A result similar to that of equation 53 has been obtained by FAN (1949) who finds

$$V_p = \frac{kT}{e} \log \left(1 + \frac{\Delta n(p)}{n(p)_0}\right)$$

the term in brackets being the relative increase of electron concentration in the p region *i.e.* the relative increase of the *minority* carrier concentration. Fan's relation may thus be expressed as $V_p = \frac{kT}{e} \log (1 + QS(p)_e)$ which is similar to equation 52.

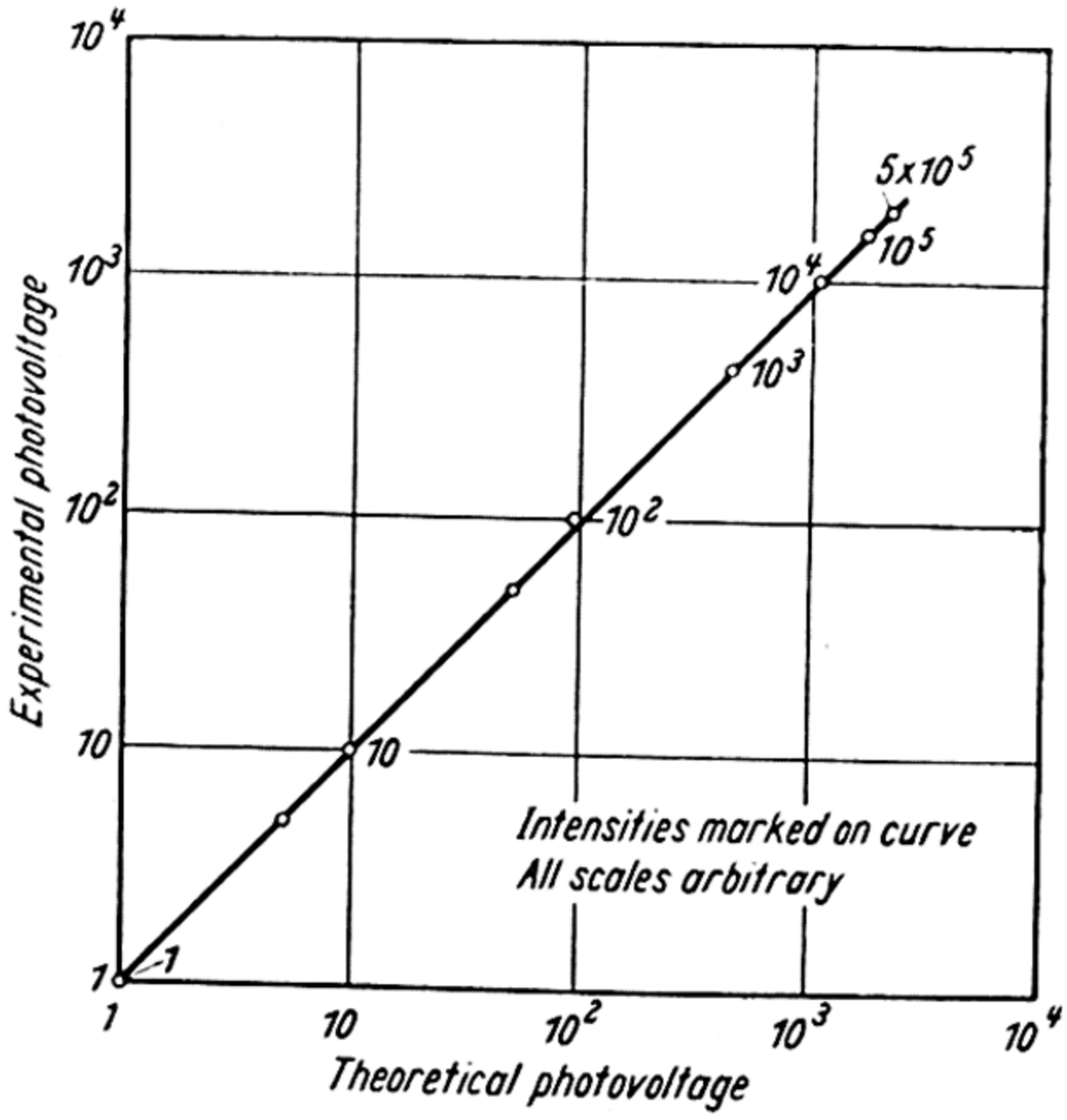

Figure 11. Intensity dependence of photovoltage

These results for the photovoltage are independent of the shape of the specimen, provided only that the area is large compared with the actual area of the transition region, and the transition region is thin *i.e.* thin compared with the diffusion length. For some *p–n* junctions, measurement of the photo-response shows this length to be as much as $\frac{1}{2}$ mm (GOUCHER *et alii*, 1951).

BECKER and FAN (1950) have carried out measurements of the photovoltage in a germanium *p–n* junction. They found the voltage to be proportional to the illuminating intensity (at low levels) over a range of 100 : 1 in intensity, whilst for stronger illumination the voltage increased less rapidly than the intensity. Plotting their results as the measured voltage against a theoretical voltage calculated from $V_p = V_0 \log (1 + QS)$ (using $S = 3{\cdot}5 \times 10^{-3}$ and $V_0 = 660$) the graph of *Figure 11* is obtained. It will be seen that the results lie well on a 45° line, showing that the experimental and theoretical voltages are equal over the whole range of nearly a million to one in intensity of illumination.

Excess-defect semiconductor contacts have also been reported by SOSNOWSKI (1947), and their properties have been treated in detail by SHOCKLEY (1949).

7.2. METAL–SEMICONDUCTOR JUNCTION

A rectifying contact between a metal and a semiconductor may exhibit photovoltaic effects in much the same way as a *p–n* junction.

The Schottky barrier (SCHOTTKY, 1939) formed at the junction of a metal and an *n*-type semiconductor may be represented by *Figure 10*b. According to BARDEEN (1947), capture of electrons in surface states gives the surface of the semiconductor a net negative charge, a corresponding equal and opposite charge appearing in the body of the material.

Assuming the physical gap between the semiconductor and metal to be thin enough to allow electron penetration by the quantum-mechanical tunnel effect, the current across the junction will again be given by an expression similar to equation 50, namely

$$I = I_0 e^{-e\phi/kT}(1 - e^{-eV/kT}) \qquad \ldots\ldots(54)$$

where V is the applied voltage. Following the same arguments as for the p–n junction we obtain $V_p = -(kT/e)\log(1 + S'Q)$* corresponding to equation 52. Thus again for very small light intensities $V_p \propto Q$, whilst when $S'Q \gg 1$, $V_p \propto \log Q$. LANGE (1938) has shown that such a logarithmic relation is well obeyed for selenium barrier cells over a range of more than 10,000 : 1 in illuminating intensity. It is also observed from other curves given by Lange that the transition from the linear law to the exponential law occurs in the neighbourhood of $V_p = 30\text{mV}$ (*ie.* $S'Q = 2{\cdot}5$) as would be expected from the theoretical formula.

From equation 49, the saturation photovoltage will occur when the illumination is so strong that the barrier vanishes *i.e.* $V_{p\,\max} = \phi$. A convenient alternative expression for the barrier height is $\phi = 2kT\log(N/n_i)$ where n_i is the concentration of *intrinsic* conduction electrodes. Thus at room temperature, for a concentration of impurity electrons 10^3 times intrinsic for example, the theory gives $V_{p\,\max} = 0{\cdot}35$ V, and for 10^6 times intrinsic, $V_{p\,\max} = 0{\cdot}7$ V. In practice, values of saturation photovoltages as great as $0{\cdot}5$ V are often found for selenium barrier layer cells.

7.3. SPECTRAL DISTRIBUTION OF THE PHOTOVOLTAIC EFFECT

Few measurements have been made on both photovoltaic and photoconductive effects in elements under comparable conditions. As the two phenomena depend on the same fundamental absorption process, the two spectral response curves must be similar. The two main causes of difference are:

i Geometry of specimen—photovoltaic measurements are normally carried out on bulk specimens, whereas thin layers are generally used for photoconductivity measurements.

ii The extremely high electric fields ($\sim 10^5$ V/cm) occurring at Schottky type barriers may substantially modify the

* A law of similar form has been derived by FRENKEL and JOFFÉ (1932) for a metal–semiconductor contact.

recombination probabilities. For wavelengths where the absorption constant is very high, with consequent high recombination probabilities (as discussed in § 6.3) for the photoconductive case, the high fields will separate the electron hole pairs formed in the photo-process and thus lessen the recombination rate. We would thus expect less fall in sensitivity at short wavelengths for the photovoltage than for the photoconductivity.

For lead telluride, measurements on the spectral response of the photovoltaic effect have been given by GIBSON (1952) who finds the threshold wavelength for five 'cats'-whisker' type photocells to be in the range $\lambda_{\frac{1}{2}} = 4{\cdot}8 - 5{\cdot}3\mu$. For photoconductive cells (at the same temperature of 90°K), the author (Moss, 1949b) has found values in the range $\lambda_{\frac{1}{2}} = 4{\cdot}9 - 5{\cdot}4\ \mu$. It is also worthy of note that the spectral shift with temperature of the threshold wavelength found by Gibson of $\mathrm{d}E/\mathrm{d}T = 5 \pm 1 \times 10^{-4}\mathrm{eV}/°\mathrm{C}$ agrees with the value found by the author for photoconductive layers within the accuracy of the experiments.

Values obtained for threshold wavelengths for photoconductive and photovoltaic effects in selenium and germanium will be compared in the chapters devoted to the individual elements.

8

TEMPERATURE DEPENDENCE OF SPECTRAL RESPONSE AND ACTIVATION ENERGY

It has been found experimentally that photoconductors show a certain spectral shift with temperature. The effect varies considerably in magnitude, and even in sign—the general tendency being for the threshold wavelength to decrease on cooling. The only materials so far known where the threshold wavelength increases on cooling are the PbS, PbSe, PbTe series (Moss, 1949b), Cd_3As_2 (Moss, 1950) and the element tellurium. The order of magnitude of the shift is 10^{-4} to 10^{-3} eV/°C.

This temperature change of the threshold wavelength clearly implies a change in the optical activation energy, and hence, for intrinsic photoconductors, a change in the energy gap between the bottom of the conduction band and the top of the full band. Such a variation in the energy gap can be attributed to two separate effects:

a variation of the bandwidths;

b relative movement of the energy bands.

Increasing temperature will always broaden the energy bands as a result of increasing lattice vibrations, so that the first effect gives dE/dT negative. The second effect will arise primarily from variation in lattice constant, and (assuming that the lattice always expands on heating) will give dE/dT negative for a material such as diamond where *Figure 1* shows the energy gap to decrease with increasing lattice constant. Alternatively, dE/dT will be positive if the energy bands approach each other as the lattice contracts *i.e.* the levels do not cross over as in *Figure 1*. The problem of the broadening of energy levels by lattice vibrations has been treated by Moglich *et alii* (1940), Radkowsky (1948) and Cheesman

(1952). Although Radkowsky's calculated shifts are in reasonable agreement with experiment for polar crystals, they are far too small for the case of the monatomic crystals with which we are concerned at present.

A more recent treatment has been given by FAN (1951), the results obtained being in fair agreement with the experimental values for silicon and germanium. The formula given by Fan for the energy shift is

$$\left(\frac{\delta E}{\delta T}\right)_1 = 4\pi^2\,(128\,\omega^2 k^3/243\,\pi^1)^{1/3}\,(m_e C_e^2 + m_h C_h^2)/(h^2 M u^2) \qquad \ldots\ldots(55)$$

where ω is the volume of the unit cell, M is the mass of an atom, u is the velocity of sound in the crystal, and the constants C_e and C_h are related to the mobilities of electrons and holes respectively.

The magnitude of the second effect, namely the relative movement of the energy bands with lattice dilatation has been estimated by BARDEEN and SHOCKLEY (1950). These workers considered the interaction of electrons and holes with 'deformation potentials' produced by the periodic dilatation of the lattice waves, thus relating the mobility of electrons and holes to the shifts of the conduction and filled bands (respectively). The result obtained may be conveniently expressed in terms of the same constants C_e and C_h as in equation 55:

$$\left(\frac{\delta E}{\delta T}\right)_2 = 2(\pm C_e \pm C_h)\,\beta \qquad \ldots\ldots(56)$$

where β is the coefficient of linear expansion, and the relation between C and the mobility is given by

$$b_e C_e^2 = 3eh^4 M u^2 (512\,\omega^2 k^3 T^3 m_e^5 \pi^7)^{-\frac{1}{2}} \qquad \ldots\ldots(57)$$

The signs to be taken in equation 56 depend on whether the energy levels rise or fall on dilatation. For diamond, silicon and germanium, Shockley and Bardeen conclude that both negative values should be taken, whilst for tellurium both positive values should be used.

For both formulae 55 and 56 it will be seen that the shift increases with the magnitude of C_e and C_h, and hence decreases with increasing mobility. Thus germanium, which has a very

high mobility, would be expected to show only slight temperature dependence of the activation energy. This expectation is confirmed by experiment, the shift for germanium being less than for any of the other elements which have so far been measured.

The experimental temperature dependence of the activation energy will be given by the sum of the values from equations 55 and 56, and it is not possible to separate the two contributions from temperature measurements alone. However, as the second term is determined only by dilatation, it may be evaluated by measurements of E at different *pressures*. We then have $(\partial E/\partial T)_2 = 3\beta V(\Delta E/\Delta V)$ since $\Delta V/V$ is the dilatation.

8.1. EXPERIMENTAL METHODS

There exist now a variety of experimental ways of obtaining information about the change in activation energy with temperature, or with dilatation alone. For most materials only one of these methods has been used, but for germanium, for example, several have been tried.

i This is the original method, namely the shift of the spectral sensitivity curve of the photoconductive or photovoltaic response with temperature. The analogous method of shift with pressure has not been reported.

ii Shift of the long wavelength absorption edge with temperature.

iii Shift of absorption edge with pressure.

iv Temperature variation of the thermal activation energy deduced from precise conductivity and Hall effect measurements in the range of intrinsic conductivity. For the intrinsic range of conductivity of a semiconductor, theory gives the concentration of carriers as

$$n_e = n_h = 2(2\pi mkT/h^2)^{3/2}\exp(-E/2kT) \quad \ldots\ldots(1)$$

if the effective masses are taken as equal to the free electron mass.

Careful measurements on silicon and germanium show that $n_e T^{-3/2}$ is an exponential function of reciprocal temperature as the equation requires, but that the

numerical factor obtained differs significantly from the value of $2(2\pi mk/h^2)^{3/2}$. The discrepancy is attributed to the temperature variation of the energy gap *i.e.* if $E = E_0 - \gamma T$ then the right-hand side of equation 1 is multiplied by the factor $\exp(-\gamma/2k)$. This factor, and hence γ, may be found from the observed discrepancy.

v Pressure dependence of the conductivity of a *p–n* junction. Equation 50 shows that the current across a *p–n* junction is $I \propto \exp(-\phi/kT)\{1 - \exp(-eV/kT)\}$ so that for a given applied voltage $I \propto \exp(-\phi/kT)$. Now, from equation 49 $\phi = E - 2kT \log \Upsilon/N$, so that in junctions with fairly high impurity concentrations $\phi \simeq E$. Hence $I \propto \exp(-E/kT)$ and the pressure dependence of I gives the pressure dependence of E. Using the same equation, the temperature dependence of E should be given by the temperature dependence of the resistance of the junction at very small applied voltages, since we then have $I \propto V \exp(-\phi/kT)$. However this method does not seem to have been used to date.

vi Pressure dependence of the activation energy may be obtained directly by measuring the conductivity/temperature at various pressures, in the range of intrinsic conductivity.

The comparison of the experimental values obtained by these various methods and the theoretical values will be given in the chapters devoted to the individual elements.

9

CORRELATION BETWEEN THRESHOLD WAVELENGTH AND REFRACTIVE INDEX

THE general theory of photoconductivity in *F* centres in alkali halides, shows that absorption of the optical quantum first raises an electron into an excited state without freeing it from the centre. The electron is then transferred to the conduction band by thermal energy from the lattice (MOTT and GURNEY, 1948). HELLER and MARCUS (1951) discuss the mobility of these 'excitons', and consider them a necessary intermediate stage in the photoelectric process. It has often been suggested that even in so-called pure materials, the photo-effect takes place only at preferred points in the lattice, such as vacant lattice sites, interstitial ions, or at atoms on the surface or in cracks *i.e.* at any discontinuity in the lattice (SMEKAL, 1929; ZWICKY, 1929; GUDDEN and POHL, 1926). Any of these imperfections will create potential holes in the lattice capable of trapping electrons.

An electron trapped at such a potential hole will be some-what similar to an electron in an isolated atom, except that it is immersed in a medium of dielectric constant equal to that of the bulk material. Thus all the energy levels of the electron will be scaled down by a factor $(1/\epsilon_{eff})^2$, where ϵ_{eff} is an 'effective' dielectric constant, which will approximate to the square of the refractive index (MOTT, 1949).

Hence the optical energy required to raise an electron at one of these irregularities into an excited state should be pro-portional to $1/\epsilon^2$. If therefore, the photoelectrons originate at such irregularities, we should expect that the threshold wave-length of the photoconductive effect, which is determined by the minimum energy required to raise an electron into an excited state, would vary as the fourth power of the refractive index.

Table I

Material	n	λ_c	n^4/λ_c	*References*	
				Refractive Index	*Wavelength*
PbO	2·53, 2·66	0·53	85	*Landolt-Bornstein*	*SIGESO*, 1945
HgS	2·58, 2·32	0·63	84	*Landolt-Bornstein*	*Gudden and Pohl*, 1920
	2·76, 3·06		113	*Int. Critical Tables*	
HgO	2·37, 2·5, 2·65	0·55	71	*Landolt-Bornstein*	*Dechene*, 1939
$PbCrO_4$	2·5	0·55	71	*Kapp*, 1935	*Kapp*, 1935
Cu_2O	2·56	0·63	68	*Landolt-Bornstein*	*Faltz*, 1937
Ag_2S	3·2 *approx*	1·35	78	*See note (e)*	*Coblentz and Kahler*, 1922
Sb_2S_3	2·9 *approx*	0·8	88	*Billings and Hyman*, 1947	*Coblentz*, 1920
MoS_2	5·57, 2·33	2·0	84	*Bailly*, 1938	*Coblentz and Kahler*, 1919
	3·3		59	*Coblentz and Kahler*, 1919	
CdS	2·43, 2·46	0·54	66	*Landolt-Bornstein*	*Gulden and Pohl*, 1920
PbS	3·9	2·8	83	*Handbk. Chem. Phys.*, 1948	*Moss*, 1947
PbSc	4·6*	5·0	88		*Gibson, Lawson and Moss*, 1951
Tl_2S	2·9 *approx*	1·0	71	*See note (e)*	*Hughes and Du-Bridge*, 1932
PbTe	5·0	3·6	170	*Avery*, 1951	*Moss*, 1949b
TlBr	2·33	0·41	72	*Hojendahl*, 1938	*Coblentz and Eckford*, 1923
HgI_2	2·58, 2·36	0·55	67	*Int. Critical Tables*	*Volmer*, 1917
TlI	2·55	0·46	92	*Gudden and Pohl*, 1928	*Coblentz and Eckford*, 1923
ZnS	2·34	0·38	79	*Landolt-Bornstein*	*Gudden and Pohl*, 1920
$PbMoO_4$	2·4, 2·3	0·46	66	*Landolt-Bornstein*	*SIGESO*, 1945
			Av. 77†		

* Private communication from D. G. Avery.

† For the simple hydrogen-like formula, with the effective mass taken as the free electron mass, the value of n^4/λ_c would be 11.

9.1. EXPERIMENTAL DATA ON COMPOUNDS

We will first survey the available data on photoconductive compounds. *Table 1* contains all such materials with high refractive indices (*i.e.* greater than 2·3) for which both spectral sensitivity and refractive index data are available, with the exception of a few complex mixed crystals. According to GUDDEN (1928) and to KURRELMEYER (1927) the refractive index must be greater than 2 for photoconductivity to occur without artificially produced impurity centres.

It will be seen that for the materials listed in *Table I* the values of n^4/λ_c are surprisingly consistent. With the exception of PbTe they all lie in the neighbourhood of 77 throughout a range of variation of n^4 of 30 to 440. Lead telluride is anomalous in that its threshold wavelength is less than for lead selenide. It may be noted that GIBSON (1952) has found that the long wavelength absorption edge in PbTe is at a shorter wavelength than in PbSe, although the wavelength of *maximum* absorption increases progressively for the series PbS, PbSe, PbTe (GIBSON, 1950).

The fact that the values are so similar for such a wide range of compounds indicates that the photoelectrons are originating from the same type of lattice imperfection in all cases, or alternatively, that the binding energies of the different types of centre are similar. Several different types of centre which would all give rise to hydrogen-like conditions can be visualized:

Notes to Table I

(*a*) It would be preferable to quote the refractive index in the region of the spectrum where the material is non-absorbing. However, few of the materials quoted have been measured over a large range of wavelengths, and so for consistency the index has been quoted for red light (0·65 to 0·75μ) whenever possible. For non-isotrophic media, the geometric mean has been used to calculate n^4/λ_c. (*b*) In order to be applicable to the various types of spectrum sensitivity curves which have been reported, the characteristic wavelength is taken as the point where the sensitivity finally begins to decrease rapidly. When the spectral curve is sharply peaked this wavelength is taken as the wavelength of maximum sensitivity. For materials where the sensitivity is roughly constant over a range of wavelengths, PbS for example, it is the point where the exponential drop begins on the long wavelength side. (*c*) Schonwald (1932), has reported that for Cu_2O there is an additional band at longer wavelengths. It is of relatively low sensitivity and has not been included in the data of *Table I*. (*d*) It should be remarked that most of the measurements have been carried out on natural crystals, and both n and λ_c often vary from specimen to specimen, or as reported by different observers. (*e*) Estimated from reflectivity and data on mixed crystals with As_2S_3.

1 An *F* centre *i.e.* a missing negative ion replaced by an electron.

2 The analogous centre consisting of a missing positive ion with a bound ' positive hole ' (*i.e.* an electron missing from one of the adjacent negative ions) is also possible according to MOTT and GURNEY (1948).

3 A substituted foreign atom which has one valency electron more than the number required to satisfy the valence bonds in the lattice.

4 Similarly an atom with one *less* valence electron than the lattice atoms.

PEARSON and BARDEEN (1949) have calculated the excitation energies of boron impurities in silicon, assuming the energies to be scaled down by a factor ϵ^2, from the Bohr formula for the ionization energy of the hydrogen atom. The energy therefore is $E = 2\pi^2 m^* e^4/\epsilon^2 h^2$. Putting $m^* = m$, the free electron mass, gives for holes, $E_h = 0{\cdot}09$ eV as $\epsilon = 12$. Experimentally the value for the impurity activation energy was found by Pearson and Bardeen to be 0·08 eV, so the two values are in agreement. For electrons the effective mass must be lower, as the mobility of electrons exceeds that of holes, and hence the theoretical value of the energy will be lower. With $m_e/m_h = 2/3$ as indicated by the relative mobilities, $E_e = 0{\cdot}054$ eV. BALTENSPERGER (1951) has computed the wave functions for a phosphorus atom in silicon, and obtains a somewhat greater activation energy, namely 0·065 eV. The experimental value found by Pearson and Bardeen is approximately 0·06 eV. Also from the simple hydrogen-like treatment the radius of the orbit should be $\epsilon \times$ the Bohr radius for hydrogen *i.e.* $12 \times 0{\cdot}53 = 6{\cdot}4$ Å, which agrees well with Baltensperger's value of 7 Å.

SIMPSON (1949) has used a wave mechanical treatment for centres in ionic crystals (where ϵ and ϵ_0 are not equal), and obtains energies $W \propto (1/\epsilon + 2{\cdot}2/\epsilon_0)\ (1/\epsilon_0 + 15/\epsilon)$ *i.e.* $W \propto \epsilon^{-2}(1 + 2{\cdot}2\epsilon/\epsilon_0)$ to an accuracy of a few per cent. Similar results have been obtained by KUBO (1948). Thus again the energies are found to be approximately inversely proportional to ϵ^2 and hence n^4.

Further evidence for the dependence of activation energy on refractive index is furnished by measurements of BUSCH *et alii* (1948) on barium titanate. In the neighbourhood of the Curie point (120°C) the refractive index of barium titanate shows a significant increase, while measurements of the resistance–temperature relation show that the activation energy undergoes a corresponding decrease in the same temperature region.

It is concluded therefore, that for the more refractive photoconductive *compounds*, there is some theoretical basis and experimental evidence for an approximate relation between the 'threshold' wavelength and refractive index, namely $n^4/\lambda_c = 77$. This theory has been used to indicate what compounds, as yet untried, should give photoconductivity at longer wavelengths in the infra-red (Moss, 1950).

9.2. TEMPERATURE VARIATION OF THE THRESHOLD WAVELENGTH

Since the threshold wavelength depends on the refractive index of the material, it is reasonable to suggest that the shift of the threshold to longer wavelengths on cooling, as observed for PbS, PbTe *etc* corresponds to a temperature variation of the refractive index. Unfortunately there seem to be no published data on the temperature variation of the refractive index for highly refractive materials. However, a rough estimate may be made theoretically. The Lorentz–Lorenz formula for the optical dielectric constant is:

$$(\epsilon - 1)/(\epsilon + 2) = C\mathcal{N}\alpha \qquad \ldots.(58)$$

where $\mathcal{N}$ is the number of molecules/vol, α the polarizability of the ions, and C is a constant. Differentiating,

$$\frac{\mathrm{d}\epsilon}{\mathrm{d}T} = \frac{1}{3}(\epsilon - 1)\,(\epsilon + 2)\,\frac{1}{\mathcal{N}}\,\frac{\mathrm{d}\mathcal{N}}{\mathrm{d}T}$$

and putting $$\frac{1}{3\mathcal{N}}\frac{\mathrm{d}\mathcal{N}}{\mathrm{d}T} = -\frac{1}{3V}\frac{\mathrm{d}V}{\mathrm{d}T} = \beta$$

—the linear expansion coefficient, we have

$$\frac{\mathrm{d}\epsilon}{\mathrm{d}T} = -(\epsilon^2 + \epsilon - 3)\beta = -\epsilon^2\beta \qquad \ldots.(59)$$

with an error of not more than 6 per cent for $\epsilon > 2{\cdot}6$.

This relation shows that there will be an increase in ϵ and hence in λ with decreasing temperature. Up to the time of writing the only materials measured which give an increase of threshold wavelength on cooling are the PbS, PbSe, PbTe series, whereas for other materials on which data are available *i.e.* Sb_2S_3 (COBLENTZ, 1920) and ZnS (MOGLICH and ROMPE, 1942) there is a slight decrease of wavelength on cooling.

That any increase on cooling would be expected to be small for these latter materials follows from the fact that a large value of $d\epsilon/dT$ necessitates both high refractive index and high expansion coefficient. These conditions are fulfilled for PbS, for which $\epsilon = (3{\cdot}9)^2$ and $\beta = 20 \times 10^{-6}$ giving $d\epsilon/dT = -46 \times 10^{-4}$. For Sb_2S_3 however, although the refractive index is high, namely 2·9, β is only $1{\cdot}5 \times 10^{-6}$, so that $d\epsilon/dT = 1{\cdot}1 \times 10^{-4}$. For ZnS, the variation of the photoconductive threshold with temperature has not been measured. However, it would be expected to behave similarly to CdS which shows a slight decrease of λ_c on cooling. Also the long-wave edge of the absorption band for ZnS decreases slightly in wavelength (from 0·335μ to 0·325μ) in a manner similar to that observed in CdS (MOGLICH and ROMPE, 1942). For ZnS, $n = 2{\cdot}36$ and $\beta = 6{\cdot}7 \times 10^{-6}$, giving $d\epsilon/dT = 2{\cdot}3 \times 10^{-4}$.

It is thus clear that while the effect of changing dielectric constant may be predominant in determining the temperature variation of the threshold wavelength for PbS, it will contribute little in the cases of Sb_2S_3 and ZnS. The fact that there is a small change in the opposite direction for these latter materials is presumably due to a secondary process operating in the reverse direction, which becomes predominant when the dielectric change is sufficiently small. Such a process is the broadening of the electron energy levels due to interaction with the thermally vibrating lattice, as discussed in the previous chapter.

The magnitude of the wavelength change expected may be evaluated for PbS. For the temperature interval 290° to 90°K, $\Delta\epsilon = \epsilon^2 \beta \Delta T = 0{\cdot}92$. Therefore $\lambda_{90}/\lambda_{290} = (1 + \Delta\epsilon/\epsilon)^2 = 1{\cdot}13$. This corresponds to a change from 3·0μ to 3·4μ. Although this is somewhat smaller than the observed values, it is of the right order, and shows that the theory predicts for PbS a large

increase of wavelength on cooling in contrast to the small changes of wavelength which are observed when the shift is in the opposite direction. For comparison with this figure, the limiting values for the shift for PbS observed by the author are: minimum 2·8μ to 3·4μ; maximum 2·9μ to 3·8μ.

The Lorentz–Lorenz formula for the dielectric constant is only an approximation, particularly for highly refractive materials, and a better check on the theory may be made by comparing the results for PbS and PbTe, so that any deficiencies in the above formula tend to be the same for both materials.

If E is the quantum energy corresponding to the threshold wavelength $\lambda_{\frac{1}{2}}$, then we have $E\epsilon^2 =$ constant. With equation 59 this gives

$$\frac{\mathrm{d}E}{\mathrm{d}T}E^{-\frac{1}{2}}\beta^{-1} = \text{constant} \qquad \ldots\ldots(60)$$

Values of this expression for PbS, PbSe and PbTe are given in *Table II* which shows the agreement to be satisfactory.

Table II

	$\lambda_{\frac{1}{2}}$ *at* 290°K	*Shift* 90°K—290°K	$\beta \times 10^{-6}$	$\frac{\mathrm{d}E}{\mathrm{d}T}E^{-\frac{1}{2}}\beta^{-1}$
PbS ..	2·8—2·9μ	0·6—0·9μ	20	30–38
PbSe ..	5·0μ	2·1μ	20	36
PbTe ..	3·6μ*	1·5μ	27†	33

* Moss (1948)—extrapolated to room temperature.
† Value measured by the author.

Measurements have also been carried out by the author on cadmium arsenide (see Moss, 1950), for which the value of $(\mathrm{d}E/\mathrm{d}T)E^{-\frac{1}{2}}\beta^{-1}$ is found to be 36, in good agreement with the above results for PbS and PbTe. It therefore appears that for materials which are photoconductive at long wavelengths, and for which the threshold wavelength increases on cooling, the shift can be largely explained by a temperature change of the refractive index.

9.3. APPLICATION TO INTRINSIC PHOTOCONDUCTIVITY IN THE ELEMENTS

In so far as photo-excitation of *impurity* centres is concerned, the above theory should apply to elements equally as well as to compounds, and this view is supported by the data already given (in § 9.2) for silicon, which show that the *thermal* activation energy of impurity centres is given quantitatively by the theory. However, few systematic measurements have yet been made on photoconductivity in impurity bands in the elements, and the primary interest lies in intrinsic photoconductivity.

No precise theory can yet be given to show that the intrinsic optical activation energy should be related to the refractive index, yet the data presented in the later sections show that there exists a general correlation between the threshold wavelength and the refractive index. Furthermore it would appear that for elements of the same crystal structure, the dependence on refractive index is similar to that found for compounds.

Some insight into this dependence of optical activation energy on refractive index may be obtained from study of the simple formula for refractive index obtained in § 3.3. Equation 17 gives $\epsilon - 1 = \mathcal{N}e^2/m\pi\nu_0^2$ where ν_0 is the frequency of the absorption maximum. Hence $h\nu_0 = U/n$ (where U is a constant) if ϵ is large. Thus the wavelength of the absorption maximum should increase with refractive index, though only linearly. However, the threshold wavelength and wavelength of maximum absorption differ greatly. For germanium, for example, the absorption maximum lies near $h\nu_0 = 3$eV, whereas the optical activation energy is only 0·73eV. If we assume a constant bandwidth ($2B$) for the absorption curve such that the energy at the threshold wavelength

$$h\nu_T = h\nu_0 - B = U/n - B \qquad \ldots\ldots(61)$$

then since B is comparable in magnitude to U/n, a small change in n will produce a large variation in $h\nu_T$. It will be shown in the later chapters that equation 61 is in reasonable agreement with the experimental data for the most highly refractive elements, and that U and B are then such that $h\nu_T$ varies roughly as the inverse fourth power of the refractive index.

10

EMISSION EFFECTS IN SEMICONDUCTORS

10.1. PHOTO-EMISSIVE MEASUREMENTS

Recent work on the external photo-effect has shown that considerable information about the energy levels of semiconductors can be obtained by this means. In particular it is possible to estimate the energy gap between the Fermi level and the top of the filled band. Hence if the sample measured is in the range of intrinsic conductivity, so that the Fermi level is midway between the full and conduction bands, then a value for the band separation, or activation energy, is obtained.

In the experiments, light of a single frequency ν is allowed to fall on the surface to be studied. The quanta of energy $h\nu$ are given up to electrons of various initial energies, and in consequence some of the electrons will be able to escape from the cathode. These emitted electrons will cover a range of energies, the distribution of which may be determined by measuring the photocurrent as the collector is biased progressively more negative, until the current finally ceases. The 'stopping potential' at which the current just ceases is found to be the same for all metallic cathodes, but is different for semiconductors. The reasons for this can be seen from consideration of the energy level diagrams for metals and semiconductors.

Figure 12 shows the distribution of energy states $N(E)$ for two typical metals of different work functions and an intrinsic semiconductor. In the case of the metals the occupied states (shown shaded) extend to energies as high as that of the Fermi level where they terminate more or less abruptly. Actually, of course, at any temperature above absolute zero some electrons have energies above the Fermi level, but since the effect only extends over an energy range of the order of kT,

it can be neglected at room temperature. The work functions ϕ_a and ϕ_b represent the energy required to remove an electron with an energy equal to that of the Fermi level from the metal into the vacuum.

The curves are drawn with the Fermi level coincident for all three materials because this is the equilibrium condition for the materials if they are placed in electrical contact with each other. The equilibrium can, of course, be established by electron flow in vacuum, without the materials being in actual physical contact.

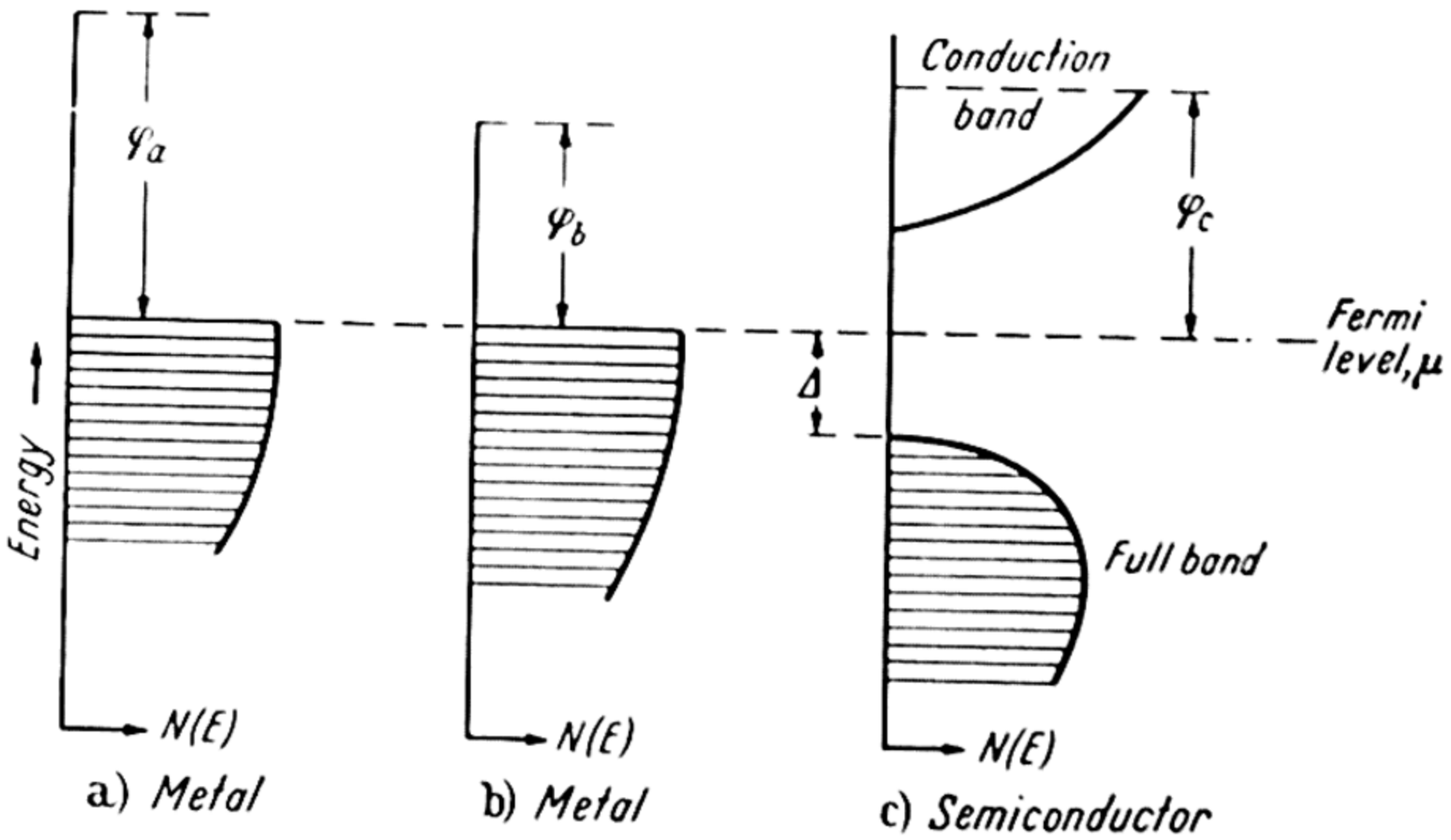

Figure 12. Distribution of energy states

Consider the case when metal a is the anode and metal b the cathode in a photocell. If a quantum $h\nu$ is absorbed by an electron which originally had energy E, then this electron will just be able to leave the metal if $h\nu + E = \mu + \phi_b$. Such an electron may not be collected by the anode however, because of the difference in work functions $\phi_a - \phi_b$ between anode and cathode. If an accelerating voltage V is applied between anode and cathode which is just sufficient to collect the electron then we have the condition

$$h\nu + E + eV - (\phi_a - \phi_b) = \mu + \phi_b$$

or

$$eV = \mu - E + \phi_a - h\nu \qquad \ldots\ldots(62)$$

Thus the minimum voltage for collection will occur for

photoelectrons which originate at the Fermi level and will be given by

$$eV_0 = -(h\nu - \phi_a) \qquad \ldots.(63)$$

The photocurrent will thus fall to zero for an applied voltage of V_0, which is therefore called the 'stopping potential'. It should be noted that equation 63 does not involve the work function of the emitter, so that V_0 is the same for all metallic emitters. All photoelectrons liberated from the cathode will be collected (giving saturation photocurrent) when the applied voltage $eV_s = \phi_a - \phi_b$.

For the semiconductor any photocurrent from the excitation of the few electrons in the conduction band can be ignored, and the photoelectrons considered to originate in the full band, the top of which is shown in *Figure 12 as* Δ below the Fermi level. For the semiconductor therefore, the stopping potential V_0' will occur for electrons originating at the top of the full band where $E = \mu - \Delta$, so that

$$eV_0' = -(h\nu - \phi_a - \Delta) = eV_0 + \Delta \qquad \ldots.(64)$$

The voltage for saturation photocurrent is again given by the contact potential difference, or $V_s' = \phi_a - \phi_c$.

The experiment thus consists essentially of determining the stopping potential with first a metallic emitter and then the semiconducting emitter. In practice APKER and his co-workers (1948) used a phototube of spherical symmetry, so that photoelectrons emitted in any direction would be subject to the same field. Several interchangeable emitters were mounted in the phototube together, being moved into position as required by tilting the (sealed-off) phototube. In order to determine the stopping potential precisely it is necessary to extrapolate the measured curves according to some theoretical law. For metals the theoretical relations are well established (see HUGHES and DUBRIDGE, 1932), but for semiconductors lack of definite knowledge of the form of the density of states function $N(E)$ at the top of the full band, and the transition probabilities, introduces some uncertainty into the interpretation of the measured values.

Apker *et alii* deduce that the energy distribution of the

emitted photoelectrons should be of the form

$$N(\nu, W) = q(\nu)W(h\nu - \phi_c - \Delta - W)^r \qquad \ldots.(65)$$

where W is the kinetic energy of the emitted electron, $q(\nu)$ is a slowly varying function of the frequency of the incident light, and r is a parameter determined by the form of $N(E)$ and the transition probability. The current–voltage characteristic will be given by the integral of this distribution function with respect to W between the limits of W and $W_{max} = h\nu - \phi_c - \Delta$. The resulting formula for the relative photocurrent is therefore of the form

$$i = q(\nu)(h\nu - \phi_c - \Delta)^{r+2} f(V) \qquad \ldots.(66)$$

where $f(V)$ is a function of the applied voltage only, to the power $r + 2$. Experimentally the variation with ν seems best fitted by a term $(h\nu - \phi_c - \Delta)^4$, giving $r = 2$ (in contrast to the case for a metal where the variation is as $(h\nu - \phi)^2$) while the variation with voltage indicates $r = 1$ to $1{\cdot}5$.

In spite of the uncertainty in the value of r, fairly definite values of Δ, the depth of the full band below the Fermi level have been obtained for boron, germanium, tellurium and arsenic, thus giving an additional means of estimating the activation energies.

10.2. LIGHT EMISSION PHENOMENA

It has recently been found experimentally that under suitable conditions light emission can be obtained from semiconductors. For silicon carbide, LEHOVEC *et alii* (1951) found that injection of carriers through p–n barriers produced a yellow light, although cases of blue light have also been reported. The effect is attributed to recombination of holes and electrons in the barrier region, so that the radiation would be expected to be roughly monochromatic with a wavelength appropriate to the optical activation energy.

The SiC specimens used were of unknown purity, and no definite correspondence was found, but it would seem that relatively pure p–n junctions, such as are obtainable in germanium for example, should emit monochromatic radiation appropriate to the intrinsic activation energy *i.e.* of wavelength approximately $1{\cdot}7\mu$.

PART II

EXPERIMENTAL METHODS AND RESULTS

INTRODUCTION

ALTHOUGH the first photoconductive material known was the element selenium (SMITH, 1873), until very recently little work had been carried out on photoconductivity in other elements. Up to the end of the recent war, only two other elements were investigated, namely sulphur (JOFFÉ, 1928; KURRELMEYER, 1927) and carbon—in the form of diamond (GUDDEN and POHL, 1923, 1924; ROBERTSON *et alii*, 1934; PANT, 1944). As the outcome of research work on crystal detectors for radar equipments, results for silicon were published soon after the end of the war (TEAL *et alii*, 1946).

On the basis of these rather meagre data, it was postulated by the author that all elements which were not metals, and which had a high refractive index (*i.e.* greater than about 2—this being Gudden and Pohl's criterion for photoconductivity in substances without artificially introduced impurities) would be photoconductive. *Table III* gives the part of the periodic table which covers the elements included in this statement. At this time many of the refractive indices were unknown, but general deductions from the reflectivities, and position in the periodic table, served to show that they should be high.

Table III

Be	B	C	N	O	
	Al	Si	P	S	Cl
	Ga	Ge	As	Se	Br
	In	Sn	Sb	Te	I
	Pb	Bi	Po	85	

Elements to the top right of the table are excluded by virtue of their low refractive indices. It may be remarked that none of them are solids at room temperature. Elements to the bottom left are metals—information on the radioactive elements

85 and polonium having been published by CORSON *et alii* (1940), and MAXWELL (1949) respectively. The elements in the '*b*' parts of the columns *i.e.* Ti, V, Cr, Mn and their congeners are all metals. The only one on which there was originally some doubt was Ti, but this has been dispelled by the work of MICHELS and WILFORD (1949).

There remains a total of no less than twelve elements which can exist in non-metallic forms and which it was therefore thought would be photoconductive. During the past five years, considerable experimental work has been carried out on all these listed elements, although for some of them which have been investigated by the author there is no published information as yet, except in the form of a dissertation*.

In Part II of this book, measurements on photoconductivity in ten of these elements are described. Regarding the remaining two, there is some doubt as to the interpretation of results obtained for antimony, so that the occurrence of photoconductivity in this material is not yet definitely established. For grey tin no data have so far been published on photoconductivity, but in view of the other properties of this element it is probably only a matter of overcoming the (considerable) experimental difficulties in order to demonstrate its occurrence. The original postulate has thus been largely confirmed.

In the following chapters details are given of the methods of measurement and data obtained for the twelve elements. In addition to the purely photoconductive effects, results are given for various electrical and optical properties which have been shown in Part I to influence the photoconductive processes.

The most important measurements described are:

i Variation of both dark and photocurrents with applied fields, and determination of specific resistance.

ii Relation between photocurrent and incident energy.

iii Spectral sensitivity measurements, from which optical activation energies are determined.

iv Resistance/temperature or Hall effect/temperature measurements, from which thermal activation energies and mobilities are deduced.

* Moss, Dissertation, Cambridge, 1950.

v Temperature and pressure dependence of activation energy.

vi Absorption constant.

vii Refractive index and dielectric constant.

viii Response times.

ix Behaviour as radiation detectors.

For those results which are as yet unpublished, particularly for boron, arsenic, phosphorus, tellurium and iodine, fuller details of the experimental conditions and techniques will be given than for results which have already been described in the literature and to which full references are provided.

11

BORON

11.1. GENERAL PROPERTIES

THERE is little information available on the properties of boron. The element normally occurs as a dark amorphous powder with a specific gravity of 2·34 (FORNSTECHER and RYSKEVIC, 1945). Thus from the atomic weight of 11, the number of atoms per cm^3 is $1{\cdot}3 \times 10^{23}$. In 'pure' crystalline form it is black and almost as hard as diamond (WEINTRAUB, 1909, 1911). Estimates for the melting point range from 2,200°C to 2,800°C.

The expansion coefficient is $8{\cdot}3 \times 10^{-6}$ (DUPUY and HACKSPILL, 1933), with no anomalies (indicating no phase changes) between 20°C and 750°C. X-ray measurements have been performed on crystalline boron (VON NARAY-SZABO, 1936), lattice parameters being quoted as $a = 12{\cdot}55$ Å, $c = 10{\cdot}18$ Å. However WYCKOFF (1948) states that the crystal structure of boron is still in doubt.

There has been considerable disagreement about the electrical properties of boron, but the data presented in this chapter confirm that it is a semiconductor and photoconductor.

11.2. PROPERTIES OF EVAPORATED FILMS

Preparation

Great difficulty was encountered in the evaporation of boron to form sensitive layers. Some of the factors contributing to the difficulties are:

a Vapour pressure of boron is low.

b Melting point high, ~ 2,300°C, so that it is not possible to get good thermal contact between the boron and a heater below this temperature.

c Only amorphous boron readily available. This cannot be heated in a wire basket for example.

Dewar flask type cells were used (see *Figure 13*a), and initial attempts were made to evaporate the powdered boron from

conical tungsten heaters, using commercial ' pure ' boron. In order to get the powder in a suitable form to stay in the tungsten baskets it was compressed into pellets. It was found necessary to raise the temperature of the heater to a brilliant white heat before any evaporation took place. The films formed were invariably of low resistance, with metallic resistance–temperature properties, and it was concluded that some of the tungsten had evaporated. It was apparent that the boron was much cooler than the tungsten during the evaporation, the temperature of the boron probably not exceeding 1,500°C. By winding the tungsten helix very closely and then painting the inside of it with *Aquadag* to increase the efficiency of heating of the boron, some films showing semiconducting properties were obtained, but none of these were photosensitive.

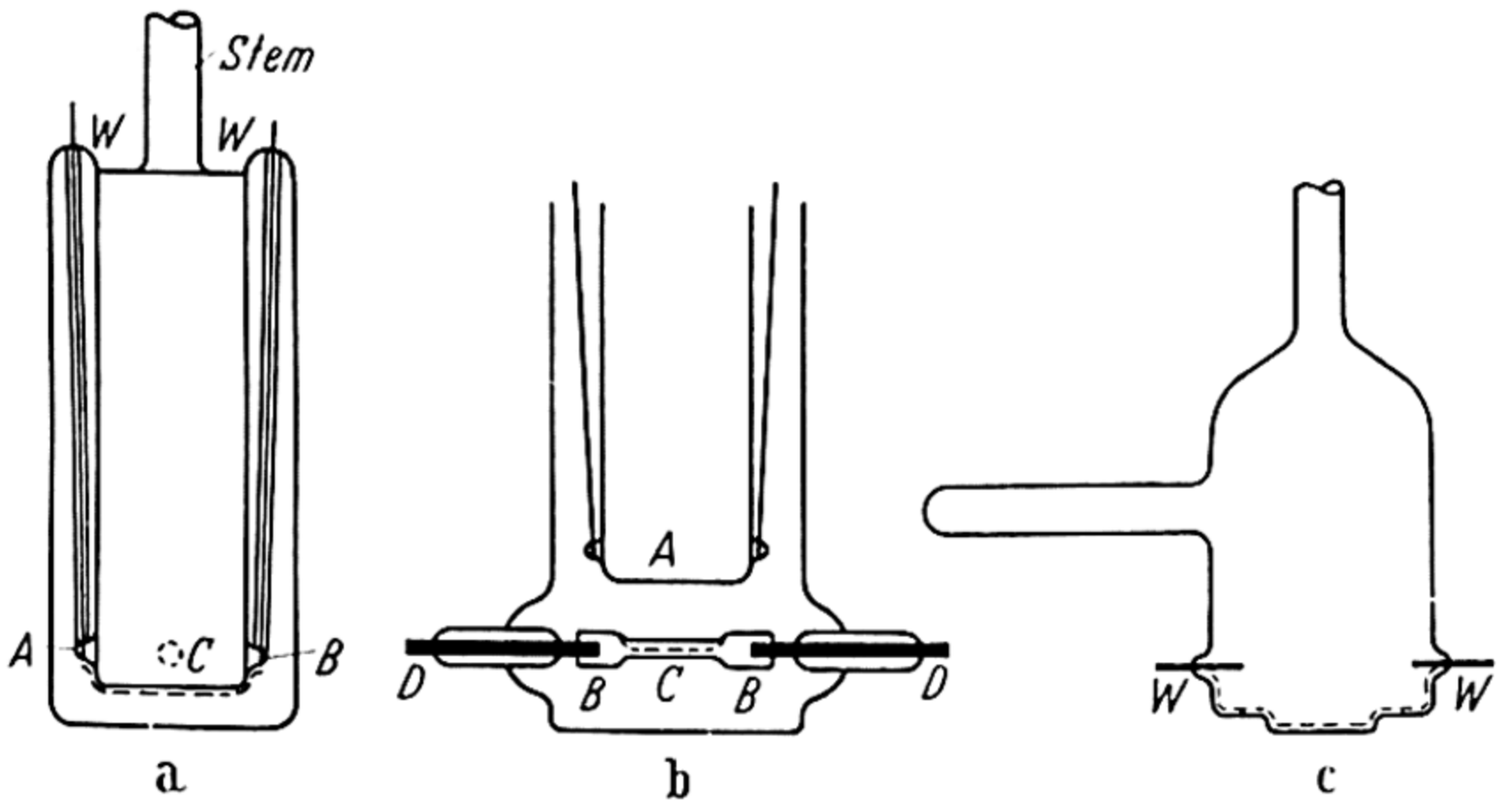

Figure 13. Designs of experimental cells

The next method of evaporation tried was by self-heating of the boron so that the desired temperature could be obtained without trouble from evaporating tungsten. The boron was compressed into rods about 1 cm long and 2 mm diameter. One of these rods was then mounted in a Dewar flask by means of graphite caps which were drilled on one side to be a close fit on the boron rod and on the other side to fit heavy tungsten electrodes sealed through the walls of the flask. A mica screen was placed inside the cell to prevent evaporation of boron on to the front window. This could be moved by tilting the cell to allow optical measurements to be made.

After evacuating the cell heating of the rod was attempted. The oven surrounding the cell was first raised to 500°C, to increase the conductivity of the boron, and then electrical heating applied. After some initial sparking the rod was raised to a fairly steady orange heat, but as the power input was increased a number of hot spots appeared on the rod and it soon became open circuited. A little evaporation had occurred, there being a thin brown film over part of the cell. The layer resistance was very high ($\sim 10^7\Omega$ at 100°C) and after cooling to room temperature it was not possible to detect either d.c. or a.c. photoconductivity. Subsequent attempts gave the same results, *i.e.* slight evaporation of boron, but no useful layers.

The final method tried was evaporation from an electrically heated graphite boat. A miniature boat was made, and mounted in the cell as shown in *Figure 13*b, beneath the layer electrodes at *A*. The boat had a central diameter of 2 mm and was hollowed out at *C* to leave a thin shell where the maximum heating was required. The ends of the boat were drilled to fit tightly on tungsten rod electrodes (*D D*) sealed through the cell walls. This system proved to be successful, and several photosensitive layers were made by its use. Lengthy outgassing of the carbon boat and its boron contents was required before it was possible to keep the boat at ~ 1,500°C without much rise in the pressure in the vacuum system. Much of the outgassing was probably due to liberation of oxygen, of which as much as 25 per cent may be present in amorphous boron according to KAHLENBERG (1925).

For the evaporation, the boat was kept at ~ 2,500°C for periods of a few seconds to a minute. This was sufficient to produce layers that were practically opaque to visible radiation. The resistances of the layers produced were usually in the range 50 to 150 kΩ, for electrodes 1 cm wide spaced 1 mm apart. It was found that the more prolonged the outgassing treatment, and the higher the temperatures at which it was carried out, the higher was the layer resistance and the greater the photosensitivity. Also the sensitivity was generally improved by keeping the electrode surface at a fairly high temperature during the evaporation to prevent the condensa-

tion of metallic impurities which are commonly present in boron, particularly magnesium. This metal does not condense at temperatures $> 400°C$. Use of much higher temperatures than this gave very 'noisy' layers, possibly as a result of contact noise caused by differential contraction between layer and substrate on cooling.

Measurements were carried out on four cells made in this manner. The sensitivity of the cells was low under both d.c. and a.c. conditions. For d.c. the conductivity change was ~1 per cent when a 100 W lamp was placed close to the cell *i.e.* a radiant intensity of $\sim 1/4$ W/cm^2 on the layer. Under a.c. conditions the limiting sensitivity, defined as the energy incident on the sensitive area of the cell required to produce a signal equal to the r.m.s. noise from the layer with an amplifier bandwidth of 1 c/s, varied from 10^{-5} W to 3×10^{-7} W for an operating frequency of 85 c/s. These measurements were made with monochromatic radiation at the wavelength of maximum sensitivity. Owing to these low sensitivities, it was necessary to use a very narrow band amplifier to obtain adequate signal/noise ratios to carry out measurements of the spectral distribution of sensitivity. The procedure adopted was to use a homodyne system *i.e.* an a.c. amplifier followed by a mixer circuit where the amplifier output and a reference voltage beat together to give a zero-frequency beat, or in other words, a d.c. output. To ensure that the reference frequency was identical with the frequency of the amplifier output, it was derived from the same chopper disc as that used to interrupt the radiation incident on the layer. This method of generating the reference voltage has the advantage that the speed of the chopping disc is not critical. However, the measurements were normally made at the same frequency, 85 c/s.

Tests were made to show that this frequency was not too great for the response times of the cells by observing that the signals from the cells did not decrease as the frequency was increased to 85 c/s. As no decrease as great as 10 per cent was observed for any of the cells, the response time must be much less than the duration of the pulses of radiation *i.e.* 6×10^{-3} sec, and probably $\tau < 2 \times 10^{-3}$ sec.

Measurements of Spectral Sensitivity

Measurements on four of the cells were carried out, using a lithium fluoride prism monochromator. The energy from the monochromator was calibrated by a radiation thermopile.

Cell A— The resistance of this cell, which had electrodes 6 mm wide, 0·6 mm apart, was 50,000 Ω at room temperature. The layer had about 10 per cent transmission for visible radiation, so that the thickness was probably about $\frac{1}{2}$ μ.

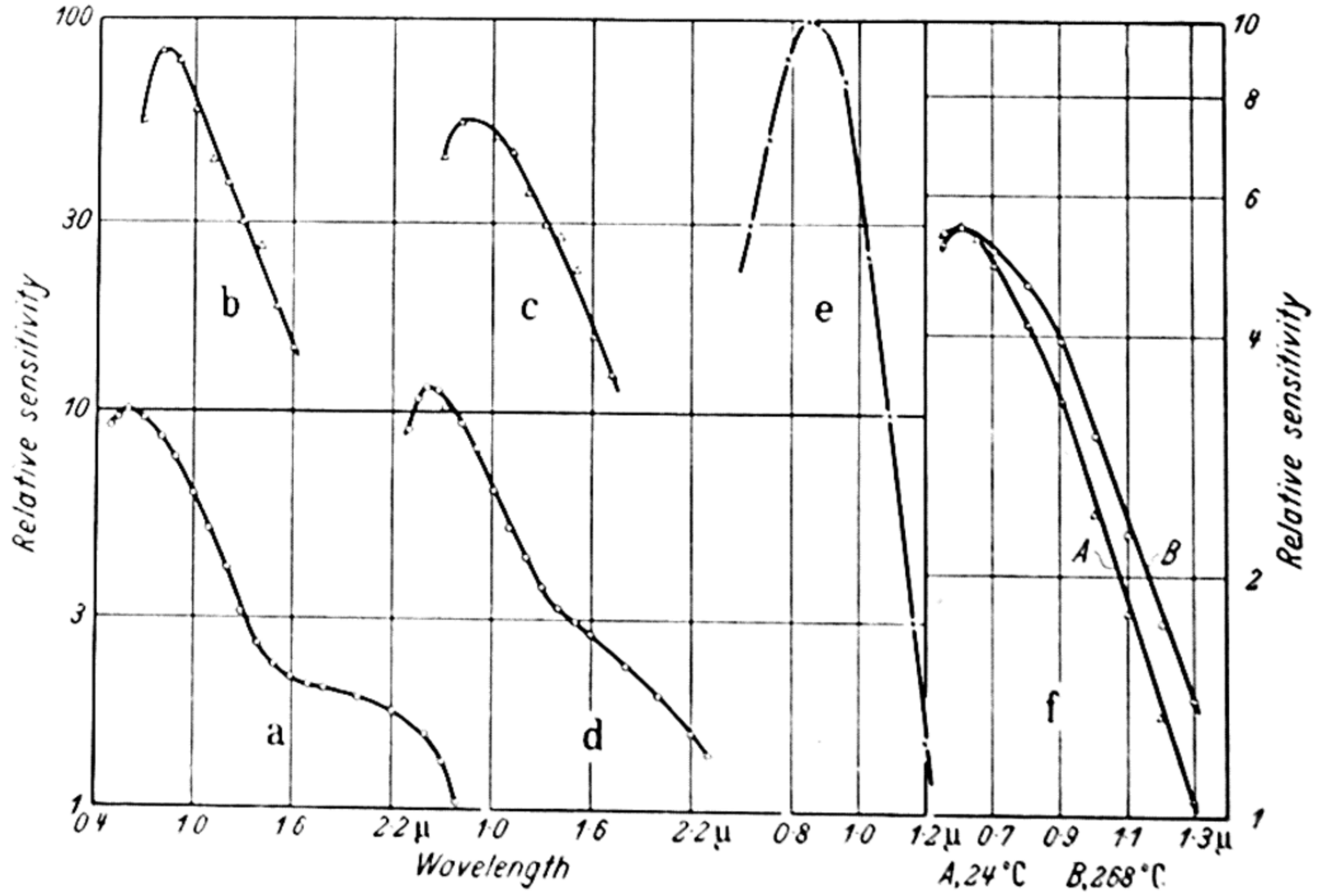

Figure 14. Spectral sensitivity curves for boron

The results are plotted on a logarithmic scale in *Figure 14*a as the ratio of (cell response)/(incident power) over the wavelength range 0·5 to 2·6 μ. Maximum sensitivity is seen to occur near 0·6 μ, after which the sensitivity falls steadily with increasing wavelength up to 1·6 μ. At longer wavelengths there is a second band of photosensitivity. For the main band of sensitivity $\lambda_1 = 1{\cdot}12\,\mu$, while for the secondary band $\lambda_1 = 2{\cdot}6\,\mu$.

Cell B— This cell had a thicker layer, probably ~ 1 μ thick, and gave a resistance of 75 kΩ for the same electrode dimensions as cell *A*. The cell was very noisy when current was passed through it, but it was possible to obtain spectral

sensitivity measurements over the restricted wavelength range of 0·7 μ to 1·6 μ. The results are shown in *Figure 14*b. Only the main band of sensitivity appears, with its maximum at 0·8 μ, the sensitivity falling approximately exponentially with wavelength for $\lambda > 0{\cdot}9\ \mu$. The threshold wavelength lies at $\lambda_{\frac{1}{2}} = 1{\cdot}2\ \mu$.

Cell C— This layer had a higher resistance (140 kΩ) than cells *A* and *B*, although it was totally opaque and therefore presumably thicker.

Spectral sensitivity measurements were possible from 0·7 to 1·7 μ. As seen from *Figure 14*c, $\lambda_{\frac{1}{2}} = 1{\cdot}2\ \mu$. This cell was opened to the air and remeasured. No significant change in the spectral sensitivity curve was observed, but the cell became noisier.

Cell D— For this cell the electrode surface was at 450°C during the deposition, in contrast to the previous cells where the substrate was not heated. The resulting layer was the most sensitive of those produced by evaporation, giving signal = noise in 1 c/s bandwidth for an incident energy of 3×10^{-7} W at 0·6 μ. With this higher sensitivity it was possible to carry out more measurements than had been possible on the other cells.

Spectral sensitivity measurements covered the range 0·5 μ to 2·6 μ. At the latter wavelength the absorption in the glass window of the cell was beginning to be important. The curve plotted in *Figure 14*d shows that for the main band of sensitivity $\lambda_{\frac{1}{2}} = 1{\cdot}05\ \mu$. The secondary band of sensitivity is not well defined, but it is estimated that $\lambda_{\frac{1}{2}} \sim 2{\cdot}8\ \mu$.

Field and Energy Dependence of Photocurrent

For cell *D* measurements of dark current and a.c. photocurrent were made for various applied voltages. The results proved that the layer obeyed Ohm's law for voltages between 1 and 100 V *i.e.* 14 to 1,400 V/cm. The layer resistance was 95 kΩ, which for a layer $6 \times 0{\cdot}7$ mm² and an assumed thickness of 1 μ, indicates a specific resistance of 80 Ωcm. The dependence of the a.c. signal from the layer on the applied field was also linear for the same range of fields.

The variation of a.c. photocurrent with incident radiation

was observed for intensities up to 1/5 W/cm². To prevent heating of the layer, the electrode surface was water-cooled. The measurements shown in curve *A* of *Figure 15* lie well on a straight line, showing that the response is linear at least up to a power of 9×10^{-3} W on the layer.

When these measurements were completed, cell *D* was opened to the air and the sign of the thermoelectric power observed. This showed the layer to be a hole conductor.

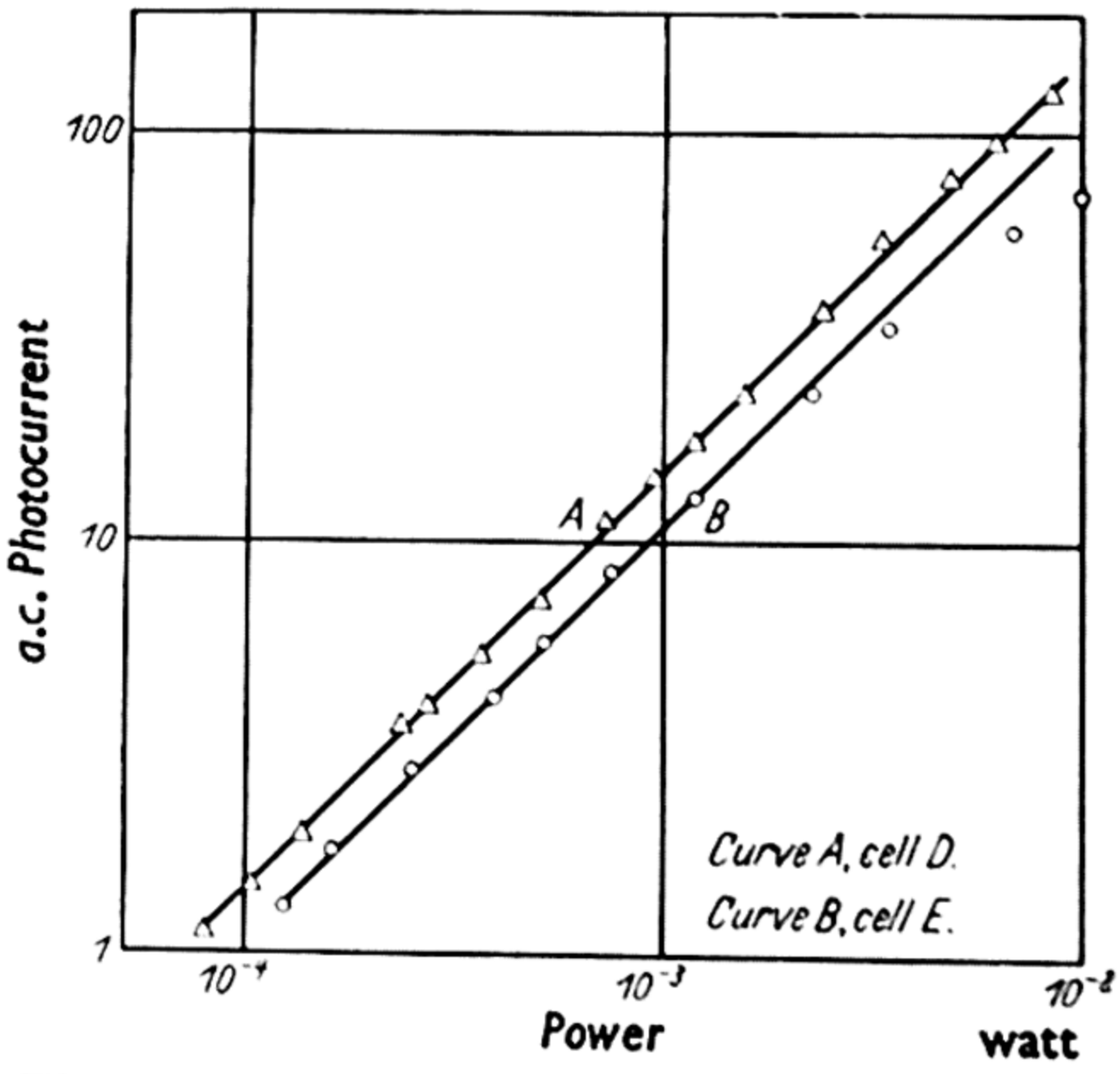

Figure 15. Variation of a.c. photocurrent with incident power for boron films

II.3. LAYERS MADE BY PYROLYTIC DEPOSITION

After the measurements on evaporated films were completed, a series of layers were made by a new method, namely by the thermal decomposition of a boron hydride gas to give a deposit of boron. Boron forms a series of hydrides (of which the lower members are gases at ordinary temperatures), which all possess the property of decomposing into boron and hydrogen at temperatures above 500°C (EMELÉUS and BELL, 1948). These boron hydrides are not readily available, but small quantities of diborane (B_2H_6) of a high degree of purity were obtained from a chemical research laboratory*. The gas was prepared, stored and transported under vacuum conditions.

* Kindly provided by F. G. A. Stone, Cambridge University Chemical Laboratory.

Dewar flask type cells were used as before, with arrangements to pass the diborane into the cell as required. About 10 to 20 cm^3 B_2H_6 (at s.t.p.) were required to form a typical layer. After outgassing the cell a small quantity of Wood's metal was put in the inner part of the Dewar and heated electrically to 550°C. With the electrode surface at this temperature the cell was sealed off from the vacuum system, and the diborane admitted. The gas decomposed in a few seconds and formed a film of boron on the heated portion of the cell.

As the cell was allowed to cool (after removing the Wood's metal), the layer resistance increased steadily to reach about 80 MΩ at room temperature. This is a factor of 1,000 greater than the average evaporated cells, thus indicating much greater purity of the layer. After pumping away the hydrogen formed by the decomposition, the cell was sealed off from the vacuum system. Several cells made in this manner showed similar behaviour, and all gave fairly good sensitivity, compared with the evaporated layers.

Measurements of the dependence of the dark current and a.c. photocurrent with applied field were carried out on one cell (cell *E*), direct proportionality being found in both cases throughout a range of applied fields of 30 to 3,000 V/cm. The a.c. photocurrent was measured as a function of radiant intensity for this cell, the results being shown as curve *B* in *Figure 15*. The relationship is seen to be linear for the lower intensities, but the signal increases less rapidly than the power at high levels. The curve deviates 10 per cent from linear at an incident power of approximately 3×10^{-3} W. The signal obtained with this power was not exceeded in the spectral sensitivity measurements, in order to ensure linearity of cell response.

Measurements of Spectral Sensitivity and Spectral Shift

These measurements were made on four cells, under the same experimental conditions as for the evaporated layers.

Cell E— The spectral sensitivity curve for this cell was similar to that of *Figure 14*, curve a, with a maximum at 0·6 μ and $\lambda_1 = 0{\cdot}97$ μ. The secondary band of sensitivity, which

was much smaller than for cell *A* (only ~ 5 per cent of the main band) had $\lambda_{\frac{1}{2}} \simeq 2{\cdot}6\ \mu$.

Cell F— This layer was not so sensitive as cell *E* and it was impossible to observe the secondary band of photosensitivity. The maximum was at $0{\cdot}7\ \mu$—with an exponential fall of 10 : 1 in sensitivity between $0{\cdot}9\ \mu$ and $1{\cdot}6\ \mu$—and $\lambda_{\frac{1}{2}} = 1{\cdot}04\ \mu$.

Cell G— Again only the main band of sensitivity was observed. The impurity band, if present, must have been < 10 per cent of the main band. The peak wavelength was $0{\cdot}7\ \mu$ and $\lambda_{\frac{1}{2}} = 1{\cdot}13\ \mu$.

Cell H— This cell was very noisy, but it was possible to plot the main band of sensitivity over a range of $0{\cdot}7\ \mu$ to $1{\cdot}7\ \mu$, which gave $\lambda_{\frac{1}{2}} = 1{\cdot}23\ \mu$.

A measurement of the spectral shift with temperature was undertaken on cell *E* as this was the most sensitive one made. The cell was set up on the spectrometer, and the inner cavity of the Dewar filled with glycerine. An electrical heater and a thermometer were immersed in the glycerine, the heater being decoupled by suitable condensers to eliminate electrical interference which was otherwise picked up on the high resistance cell.

Measurements were taken at 268°C—the temperature being kept constant to within 1°C throughout the measurements—and the cell then allowed to cool and a second set of measurements performed at 24°C. The two spectral sensitivity curves thus obtained are plotted in *Figure 14*f. The threshold values found are:

$$24°\text{C},\ \lambda_{\frac{1}{2}} = 0{\cdot}97\ \mu$$
$$268°\text{C},\ \lambda_{\frac{1}{2}} = 1{\cdot}04\ \mu$$

Hence the spectral shift is $0{\cdot}07\ \mu$ for 244°C, or $\mathrm{d}E/\mathrm{d}T = -\ 3{\cdot}5 \times 10^{-4}$eV/°C. The experimental conditions, and well-defined shape of the curves render the determination of the $\lambda_{\frac{1}{2}}$ values fairly precise; and the shift probably lies between 3×10^{-4} and 4×10^{-4}eV/°C.

Resistance/Temperature Measurements

For these experiments the outside of the cell was lagged with asbestos wool, and Wood's metal used as a heating bath in the inner part of the cell. The Wood's metal was heated electrically,

and temperatures were read by a mercury thermometer whose range extended to 550°C. Readings were taken on heating, the temperature being allowed to stabilize before each reading.

Cell E— For this cell the resistance was found to change by a factor of 10^4 between 20°C and 550°C. The results which are shown by the dotted line on the customary semi-log plot in *Figure 17*, fall on two straight lines. For the high temperature region the slope corresponds to a thermal activation energy of 0·98 eV. From the graph the resistivity at 700°K is 20 Ωcm, estimating the layer thickness to be $\frac{1}{2}\ \mu$*. Putting

$$\sigma = \sigma_0 \exp(-0{\cdot}98/2kT)$$

we obtain $\sigma_0 \simeq 200$. This magnitude indicates that the conductivity is intrinsic and that the mobility is about 50 cm $sec^{-1}/V\ cm^{-1}$ at room temperature.

It may be noted that there was little permanent change produced by heating the layer to 550°C. Check points taken on cooling led to an activation energy 0·97 eV. For the low temperature region, the slope gives an activation energy of 0·59 eV.

Cell F— This cell was measured over the temperature range 30°C to 480°C. The points again lie close to two straight lines on the semi-log plot, from the slopes of which the activation energies are 0·90 eV and 0·61 eV.

Cell H— For this cell the points lay on one straight line for temperatures of 150°C to 400°C, the slope of the line giving an activation energy of 1·0 eV.

Reflectivity Measurements

Although the boron layers were not optically flat, it was decided that valuable information about the optical properties of boron might be obtained by measurements of the reflectivity of the layers. Cell *E* was selected as having the best surface. In consequence of the layer not being flat, a very diffuse image resulted from the reflection, the area being about $10 \times 7\ mm^2$ with the optical arrangement used. The image was received on a large area lead sulphide cell detector, and although care was taken to use an image as nearly as possible the same size

* See next section on reflectivity measurements.

and on the same part of the cell both with and without the boron layer in the beam, absolute values of the reflectivity cannot be very accurate.

The results obtained are shown in *Figure 16* where two interference fringes may be seen. There are reflection maxima at 5,500 and 9,500 cm^{-1}, and minima at 7,000 and 4,000 cm^{-1}.

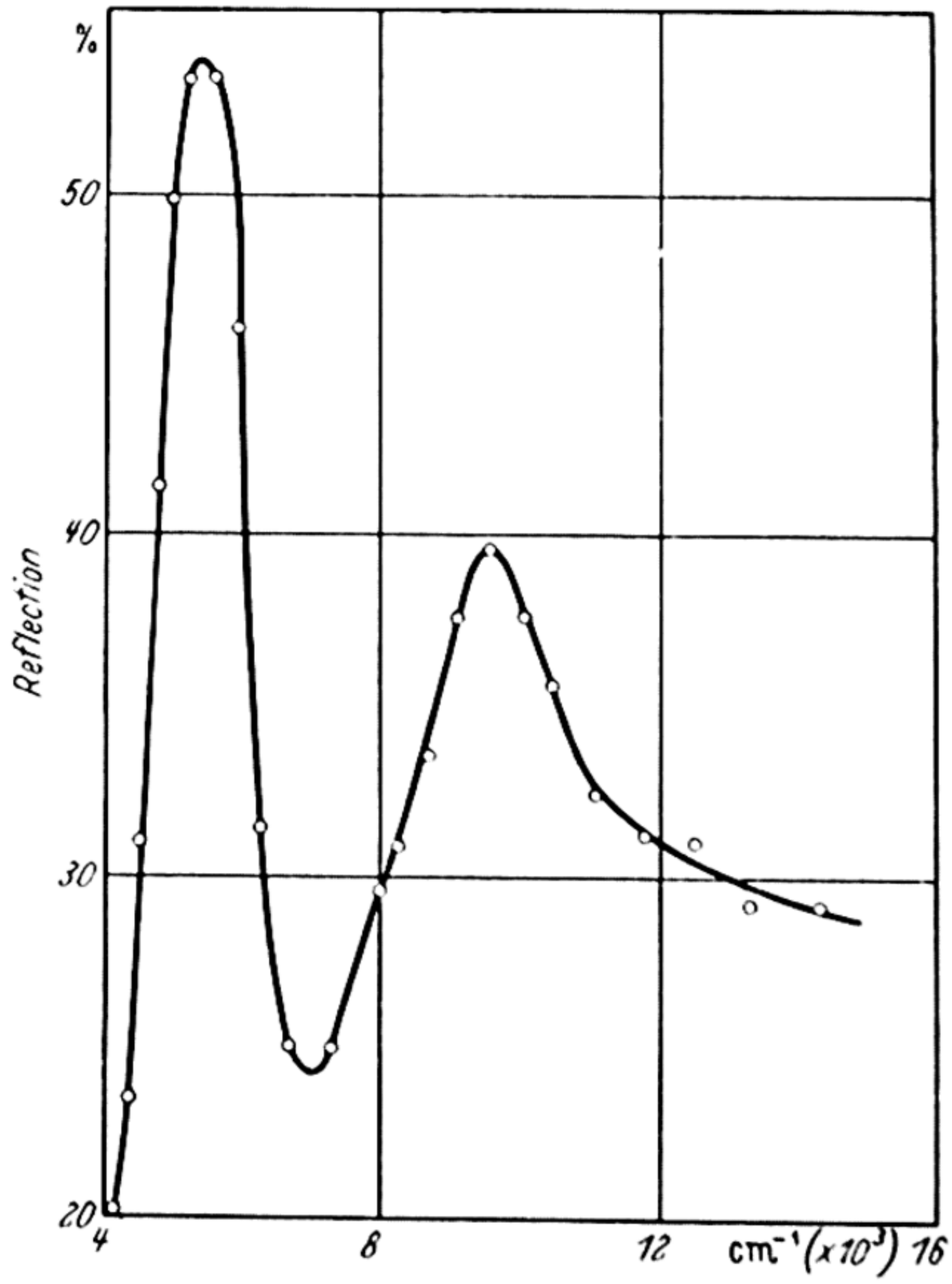

Figure 16. Reflection of boron film

From these figures the average fringe separation is 3,500 cm^{-1}, so that the refractive index is given by $2nd = 1/3{,}500 = 2{\cdot}9\ \mu$, where d is the film thickness.* It was not possible to measure the thickness, so the value of the refractive index could not be obtained directly from this value of $2nd$. However, estimates were made from the values of the reflectivity.

At short wavelengths, where the absorption is high enough to suppress interference fringes, the reflectivity is ~ 29 per cent so that with $(n-1)^2/(n+1)^2 = 0{\cdot}29$, $n \simeq 3{\cdot}3$. With $2nd = 2{\cdot}9\ \mu$ this gives $d \simeq 0{\cdot}5\ \mu$. This value of thickness

* See appendix on interference theory.

cannot be seriously in error and is therefore used in the resistivity calculations of the previous section.

From the interference theory the reflected amplitude at maximum is $2r/(1 + r^2)$, the reflecting power being the square of this. From the curve of *Figure 16* the maximum reflectivity is 54 per cent, and hence $r = 0{\cdot}42$. Now $r^2 = (n - 1)^2/(n + 1)^2$, therefore $n = 2{\cdot}5$. This is a lower limit to n as the maximum reflectivity only equals the above expression when there is no absorption *i.e.* when the minimum reflectivity is zero. With a transmission factor of a for each traversal of the film we have:

$$\text{minimum reflection} = \frac{r(1 - a^2)}{1 - a^2r^2} = (0{\cdot}2)^{\frac{1}{2}}$$

$$\text{maximum reflection} = \frac{r(1 + a^2)}{1 + a^2r^2} = (0{\cdot}54)^{\frac{1}{2}}$$

From these equations $n \simeq 4$. Taking the average of these values of n, we may conclude that the refractive index is somewhat greater than 3.

From the variation in amplitude of the fringes it is clear that the absorption is increasing rapidly with wave number over the range of measurements, being low at 2 μ and high at 0·8 μ relative to an absorption constant of $10^4 cm^{-1}$.

II.4. PROPERTIES OF BULK BORON

The most thorough investigation of the properties of pure solid boron is that of WEINTRAUB (1909, 1913). After establishing that previous methods of producing boron could give as much as 15 per cent of oxygen and 5 per cent of magnesium in the material, this worker devised a new method of preparation and succeeded in producing fused boron of purity at least 99·8 per cent. The residual 0·2 per cent represented the possible errors of the analysis, so that the actual purity might well have been much greater. The electrical properties of the material indicate much less impurity than 0·2 per cent.

The method of production was to reduce high purity boron trichloride by oxygen-free hydrogen using a high voltage electric arc. Copper was found to be the most satisfactory material for the arc electrodes, as its affinity for boron is very low. The boron was deposited partly as powder and partly

as fused beads which grew on the electrodes. These beads were extremely hard—almost as hard as diamond—and showed conchoidal fracture. It was on these fused samples that measurements of electrical characteristics were carried out.

Conductivity

At 23°C Weintraub found the specific resistance to be $1{\cdot}7 \times 10^6 \Omega$cm, falling to about 1 Ωcm at 1,000°C. Measurements on two samples when heated above room temperature

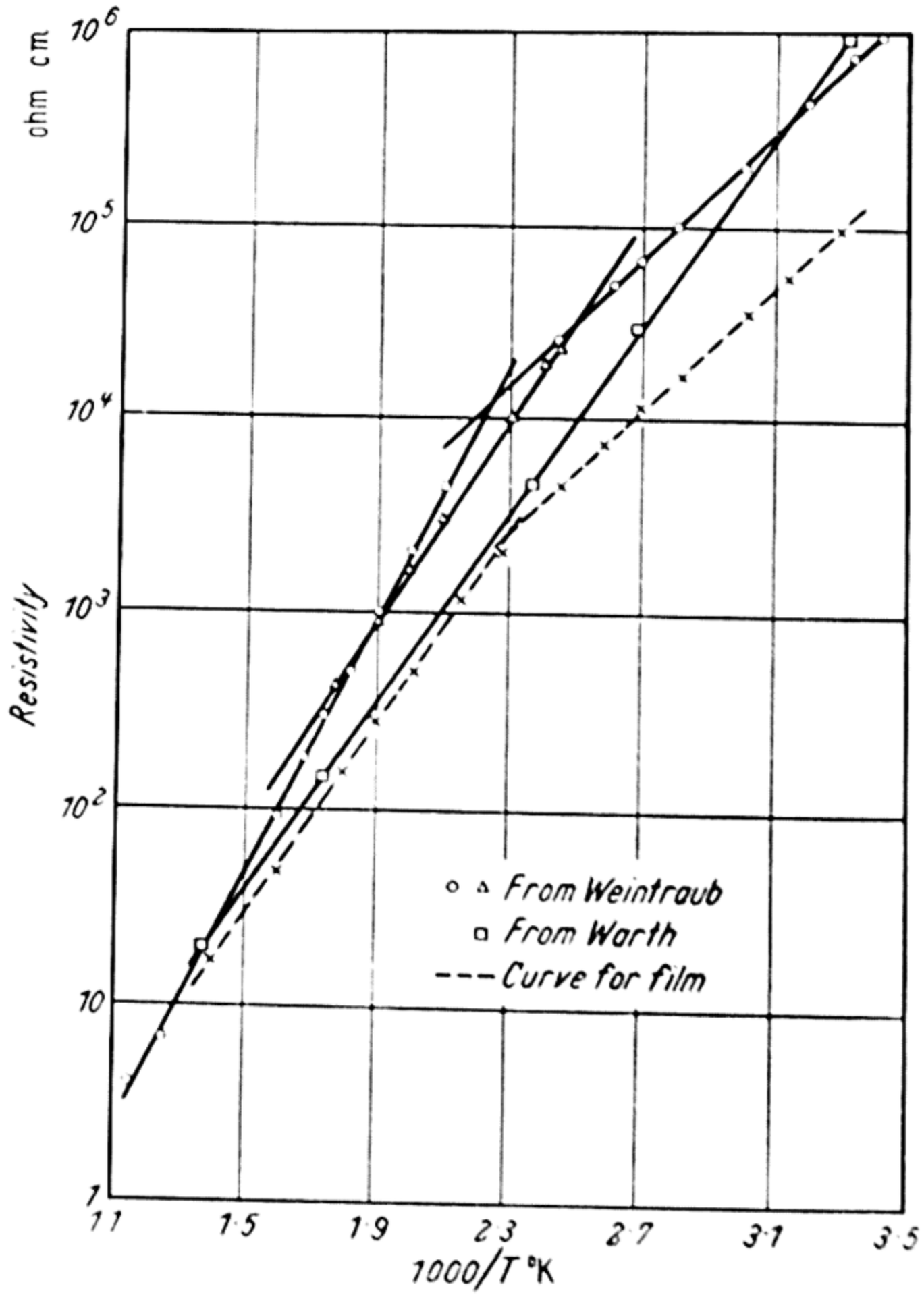

Figure 17. Boron resistivity

are shown plotted as log(resistance) against reciprocal temperature in *Figure 17*. The slopes of the two curves in the high temperature region give thermal activation energies of 1·25 eV and 1·05 eV.

Assuming that the conductivity is intrinsic in the high temperature region, we may estimate the activation energy

from the relation $\sigma = \sigma_0 \exp(-E/2kT)$, where $\sigma_0 \simeq 4 \times$ mobility at room temperature. For the two curves the specific resistances are $10^4 \Omega$cm at 465°C and 445°C, giving a mean of 455°C. Hence taking $\sigma_0 \simeq 1{,}000$, gives $E \simeq 1{\cdot}25$ eV. This figure is sufficiently near to those obtained from the slopes of the curves to confirm that the conductivity is indeed intrinsic at the higher temperatures used for the measurements.

Other measurements of the conductivity of bulk samples of boron have been carried out by WARTH (1923, 1925)—who used the same method of preparation as Weintraub—and by FREYMANN and STIEBER (1934). Warth's results, which are also plotted in *Figure 17*, are seen to give a single straight line for all temperatures above 300°K. The activation energy given by the slope is $E = 0{\cdot}98$ eV. The conductivity continues to rise with increasing temperature to at least 1,800°C, where it is several hundred $\Omega^{-1}\text{cm}^{-1}$.

At 30°C Freymann and Stieber found the resistivity to be $2{\cdot}1 \times 10^6 \Omega$cm, in reasonable agreement with Warth's value of $0{\cdot}9 \times 10^6 \Omega$cm. Assuming intrinsic conductivity (with $\sigma_0 \simeq 1{,}000$) gives values of activation energy of 1·12 and 1·08 eV. The resistivity is sufficiently large to make this estimate fairly accurate. For example, an error of 5 : 1 in the assumed value of σ_0 would only change the calculated energy by 8 per cent.

An estimate of mobility is best made from the value of conductivity at high temperatures. At 725°K Warth and Weintraub's figures coincide at $\rho = 20\,\Omega$cm. With the activation energies as given by the slopes we have $\sigma_0 \sim 120$ and 1,000 in the two cases, indicating mobilities ~ 30 and 250 $\text{cm}^2/\text{V sec}$.

Some of the more recent measurements on boron show only small dependence of resistance on temperature. HENNINGER (1937) found this to be the case, and LAUBENGAYER *et alii* (1943) maintained that the resistivity changed by $< 100 : 1$ between 20°C and 600°C. However, in the latter paper, although the boron (which was made by deposition on a hot tungsten wire) was claimed as 'pure', it is admitted that it may have been only 99 per cent pure. An impurity concentration of 1 per cent is of course extremely large where electrical properties are concerned. WEINTRAUB (1913) in fact observed

that the addition of 1 per cent of carbon reduced the specific resistance of his boron by a million times at room temperature, and at the same time the high temperature coefficient of resistance disappeared.

A FIAT* review states that the resistance varies rapidly with temperature in the 300 to 400°C region, the conductivity doubling for every 19°C rise in temperature. With $\sigma = \sigma_0 \exp(-E/2kT)$, then for a ratio of 2 : 1 in σ, $E = 1{\cdot}4\, kT_1T_2 \div (T_1 - T_2)$. With $T_1 - T_2 = 19$°C, this gives $E \sim 1$ eV.

Estimates of the thermal activation energy obtained from the slopes of the log(resistance)–reciprocal temperature curves thus range from 0·98 to 1·25 eV. Estimates for the gap width from the absolute conductivity fall in the same range *i.e.* 1·1 eV with a tolerance of about ± 10 per cent.

For the impurity activation energy, values of 0·65 to 0·7 eV are obtained from the lower temperature parts of Weintraub's curves. An estimate of the density of impurity centres may be made from equation 7 *i.e.* $n^2 = N\Upsilon \exp(-\Delta E/kT)$. From curve *A* of *Figure 17* $\sigma = 10^{-6}$ at 300°K, so that $n \sim 10^{11}$ carriers/cm^3. With an average value of $\Delta E = 0{\cdot}68$ eV, we find the density of centres $N \sim 10^{15}$/cm^3, which indicates a high degree of purity.

Photoconductivity

A set of measurements of photoconductivity in crystalline boron has been given by FREYMANN and STIEBER (1934). Using a sample 5 mm long and 1·5 mm diameter they were able to measure the d.c. photocurrent over the spectral range 0·6 to 1·2 μ. Their results, shown in *Figure 14*e give a maximum at 0·85 μ, and a threshold wavelength $\lambda_1 = 0{\cdot}98$ μ. This value falls within the range already obtained from measurements on films.

11.5. SUMMARY AND DISCUSSION

Photoconductivity has now been observed in boron layers, formed either by evaporation or by decomposition of diborane, and in crystalline samples. For the layers the measurements were made at 85 c/s, so that only rapid photo-effects were

* Review of German war-time science.

involved. Both dark and photocurrents were found to be proportional to the applied field over a wide range, and the a.c. photocurrent was proportional to the incident power provided this did not exceed 1/20 W/cm^2.

Measurement of the reflectivity indicates that the refractive index of boron is somewhat greater than 3. Values of activation energy are available from both photoconductive measurements and resistance–temperature measurements on layers and bulk samples. The energies (in eV) are summarized in *Table IV*.

Table IV

	Sample	*Optical Energy*	*Thermal Energy*	*Specific Resistance*
Layers	*Cell A*	1·1	—	1·1
	Cell B	1·03	—	
	Cell C	1·03	—	
	Cell D	1·18	—	
	Cell E	1·27	0·98	
	Cell F	1·18	0·90	
	Cell G	1·07	—	
	Cell H	1·0	1·0	
Bulk Samples	*Freymann and Stieber*	1·26	—	1·12
	Warth	—	0·98	1·08
	Weintraub	—	1·25 / 1·05	1·25
	FIAT review ..	—	~1·0	

The magnitude of the conductivity at high temperatures, and the similarity of the activation energies obtained by a variety of methods on widely differing samples, establishes that the conductivity and photoconductivity are *intrinsic*. The average values of the intrinsic activation energy are :

i optically 1·12 eV ;

ii thermally 1·03 eV, with an overall average of 1·08 eV.

The temperature dependence of the energy gap was found by measuring the shift of the photoconductive spectral sensitivity curve. The value obtained was $dE/dT = -3{\cdot}5(\pm 0{\cdot}5) \times 10^{-4}$eV/°C. The shift is thus of the same sign as for the diamond–germanium series. For the impurity activation

energy, values between 0·45 and 0·7 eV are given by either optical or thermal methods, with no significant difference between results for layers and bulk samples.

An independent estimate of the width of the forbidden zone in boron is obtained from the photo-emissive measurements of Apker *et alii* (1948). These workers used thick films deposited by pyrolysis of diborane on to tantalum substrates at 700°C. From the results it was not possible to determine uniquely the value of the index r in equation 65 and 66, the fit of the data being equally good with $r = 1$ or $r = 2$. For the former, the energy separation of the full band and Fermi level was found to be $\Delta \simeq 0{\cdot}5$ eV, and for the latter, $\Delta \simeq 0{\cdot}25$ eV. The former value would thus indicate an intrinsic activation energy of 1 eV, assuming the samples to be pure enough to be in the range of intrinsic conductivity, with the Fermi level midway between the full and conduction bands. Actually Apker *et alii* reported that the layers were *p*-type as judged by thermoelectric power measurements. As values of impurity activation energy obtained for *p*-type films by other measurements range from 0·45 to 0·7 eV, the corresponding value of Δ would be 0·22 to 0·35 eV. The results of Apker *et alii* are thus in agreement with the energy values found by other methods, and give support to the conclusion that boron is a semiconductor with an intrinsic activation energy of approximately 1·1 eV.

12

DIAMOND

12.1. GENERAL PROPERTIES

Carbon appears in the allotropic forms of graphite, diamond, and as amorphous powders. Only diamond of these forms has been reported as showing photoconductivity, and only this allotrope will be dealt with at present.

Diamond crystallizes so that each carbon atom has four nearest neighbours arranged tetrahedrally about it. The interatomic distance is 1·54 Å and the lattice constant $a = 3{\cdot}560$ Å. The crystals are colourless, indicating that absorption occurs only in the ultra-violet. Diamond is normally classed as an insulator, the specific resistance at room temperature being in the neighbourhood of $10^{14}\ \Omega$ cm.

Kimball (1935) has carried out a quantum-mechanical zone treatment of diamond, and thus derived the form of the energy bands depicted in *Figure 1*. His results show that diamond should be an insulator (as the four valence electrons per atom are just sufficient to fill the lower band) with a large energy gap between the full and conduction bands*. As no method of making diamonds artificially has yet been established, all the measurements described relate to natural crystals.

12.2. PHOTOCONDUCTIVITY

Photoconductivity of diamond, when irradiated by wavelengths in the near ultra-violet region of the spectrum, has been observed by several workers, including Gudden and Pohl (1923), Robertson *et alii* (1934), and Pant (1944). Robertson *et alii* found that not all diamonds were photoconductive, but only those of type *II i.e.* the type which is most transparent both in the ultra-violet and infra-red regions of the spectrum. Rectification effects in photoconducting diamonds have been observed by Curl and Danielson (1952).

* Similar results have been obtained more recently by Hall (1952).

Gudden and Pohl found that at low voltages the photocurrent increased in proportion to the applied voltage, but that saturation of the photocurrent was obtained with about 1,500 volts applied to a crystal 1 mm thick. As shown in *Figure* 5b, their results agree well with the theoretical formula of equation 22. Taking the experimental values from the graph the equation becomes

$$\frac{Q}{V} = 2{\cdot}5 \times 10^{-12} \left(1 - \frac{V}{2V_m}\right)$$

where $V_m = 1{,}570$ V

Now
$$\frac{V}{V_m} = \frac{d}{h} = \frac{b\tau F}{h} = \frac{b\tau V}{h^2}$$

$$\therefore b\tau = \frac{Vh^2}{V_m}.$$

In the example given the electrode separation was $h = 1{\cdot}02$ mm^2, and hence $b\tau = 6{\cdot}6 \times 10^{-6}$ cm^2/V. A value for the product of the mobility of the current carriers and their life-time is thus obtained.

More recently the behaviour of currents produced by bombardment have been studied by McKay (1948 and 1950) with respect to their voltage dependence. He finds the results to be well fitted by a somewhat more elaborate formula for the photocurrent given by Hecht (1932). The formula—which applies for electrons produced near one electrode, not uniformly as in equation 22—is $i/i_0 = d/h\{1 - \exp(-h/d)\}$. As $d/h = V/V_0$, this expression may be written as

$$i/i_0 = V/V_0\{1 - \exp(V_0/V)\}.$$

It has the same general shape as equation 22. From the values of d/h obtained from McKay's curves the product of the mobility and life-time of the carriers can again be computed. The values obtained are $b\tau = 8{\cdot}3 \times 10^{-6}$ cm^2/V for electrons and $4{\cdot}6 \times 10^{-6}$ cm^2/V for positive holes, the values being sensibly independent of the applied voltage between 5 and 14 kV. The values thus agree closely with that calculated from Gudden and Pohl's work.

The mobility and time constant terms cannot be separated by this type of measurement alone, but with independent

estimates of b as given later, these values may be used to estimate τ. By the use of pulse techniques, PEARLSTEIN and SUTTON (1950) have measured the response time for diamond directly, obtaining the value 9×10^{-9} sec (within ± 10 per cent). The effect of space charge on photocurrents in diamond has been discussed by NEWTON (1949), and compared with McKay's measurements.

GUDDEN and POHL (1923) found that by illuminating a diamond with red light at the same time as the ultra-violet illumination was applied, approximately double the photocurrent was obtained. The red light alone had no photoconductive effect, and hence its action was interpreted as freeing the positive holes produced by the primary photoeffect, these being otherwise relatively immobile. Alternatively, if the red light was applied *after* the u.v. had been switched off, the quantity of electricity passing between the electrodes was almost exactly equal to that which passed during the u.v. irradiation. Typical figures obtained were:

U.V. alone	*Subsequent red light*
$3{\cdot}75 \times 10^{-10}$ coulomb	$3{\cdot}63 \times 10^{-10}$ coulomb
$3{\cdot}38 \times 10^{-10}$	$3{\cdot}38 \times 10^{-10}$
$2{\cdot}00 \times 10^{-10}$	$2{\cdot}03 \times 10^{-10}$

PANT (1944) however, found that in general the extra current due to the red light was only 40 to 60 per cent of the original photocurrent.

GUDDEN and POHL (1923) showed that under favourable conditions the quantum efficiency in diamond was unity *i.e.* each *absorbed* quantum of radiation produced one photoelectron. The accuracy of the results has already been indicated in §4.1. These workers had shown previously (1920) that the photocurrent was proportional to the incident light intensity for all wavelengths between 0·254 and 0·436 μ. The linear relation holds both for saturation currents and also for currents at low field strengths.

Temperature Variation of Photocurrent

The variation of photocurrent with temperature was observed from room temperature to 380°C by LENZ (1927). As shown

in *Figure 18* (curve *A*) there was little change below 190°C, while from 190°C to 380°C the photocurrent increased by 5·5 : 1, the increase being approximately linear with temperature. MENDELSSOHN and DEMBER (1940) carried out measurements at higher temperatures, and as shown in *Figure 18* (curve *B*) they found an increase of about 1,000 : 1 in photocurrent as the temperature was raised from 400°C to 700°C.

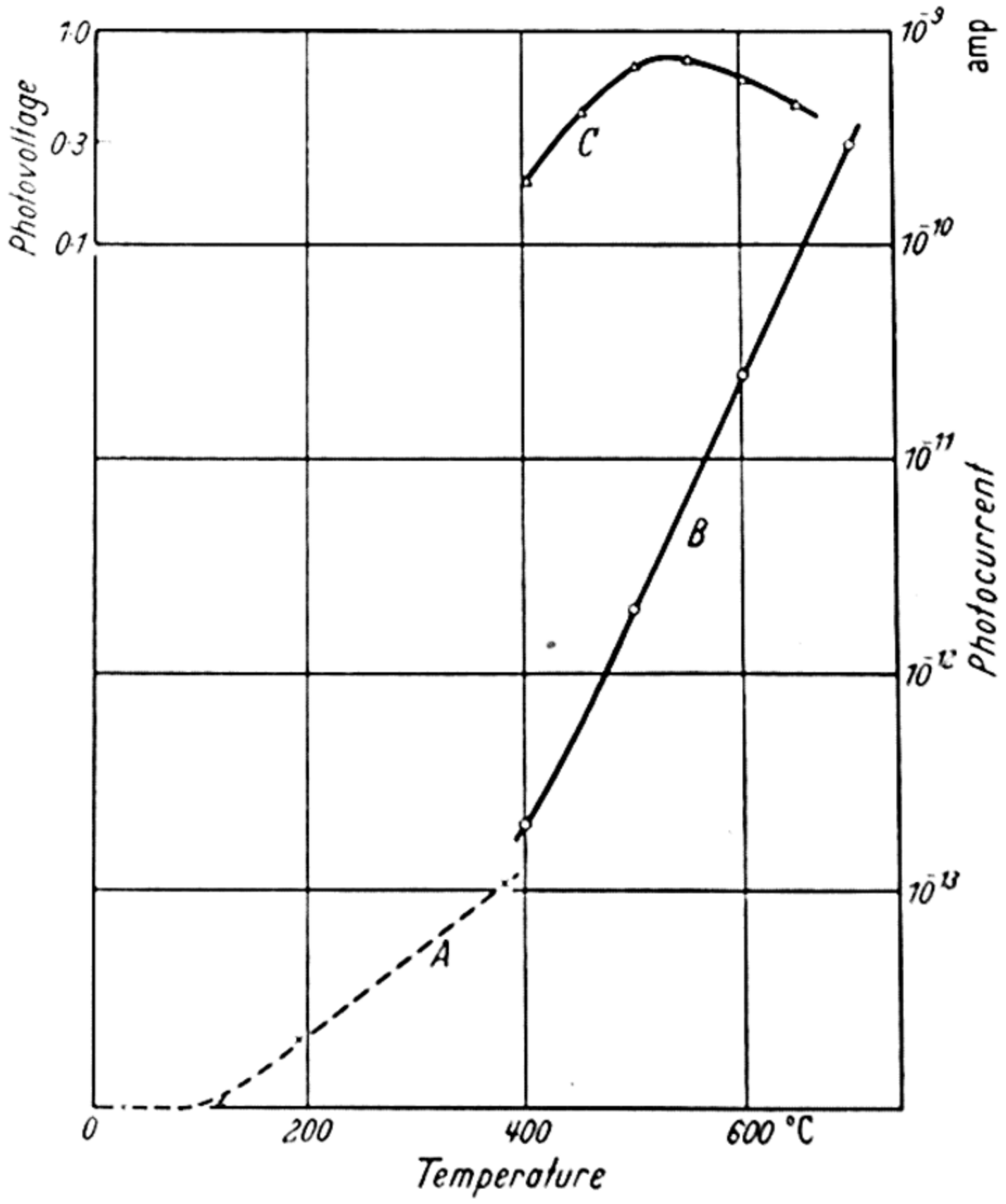

Figure 18. Photocurrent–temperature for diamond
Photocurrent: curve A, from LENZ *(arbitrary scale) curve B, from* MENDELSSOHN *and* DEMBER
Photovoltage: curve C, from MENDELSSOHN *and* DEMBER

The photocurrent increased approximately exponentially with temperature, a relation which has previously been observed for various compounds.

Also shown in *Figure 18* (curve *C*) is the temperature variation of the photovoltage observed by Mendelssohn and Dember.

At the optimum temperature, the photovoltage reaches the remarkably high value of three-quarters of a volt. ROBERTSON *et alii* (1934) measured the current generated without an applied voltage—which would be expected to behave in a similar manner to the photovoltaic effect—and found that it reached a maximum in the neighbourhood of — 40°C. For the photoconductive effect however, these workers found the optimum temperature to be 250°C, falling rapidly as the temperature was further increased.

12.3. SPECTRAL DISTRIBUTION OF SENSITIVITY

The spectral sensitivity curve of photocurrent against incident energy is found to have a peak in the region 2,250 to 2,300 Å. Results obtained by ROBERTSON *et alii* (1934) for two diamonds are plotted in *Figure 19* on a semilogarithmic scale. It will be

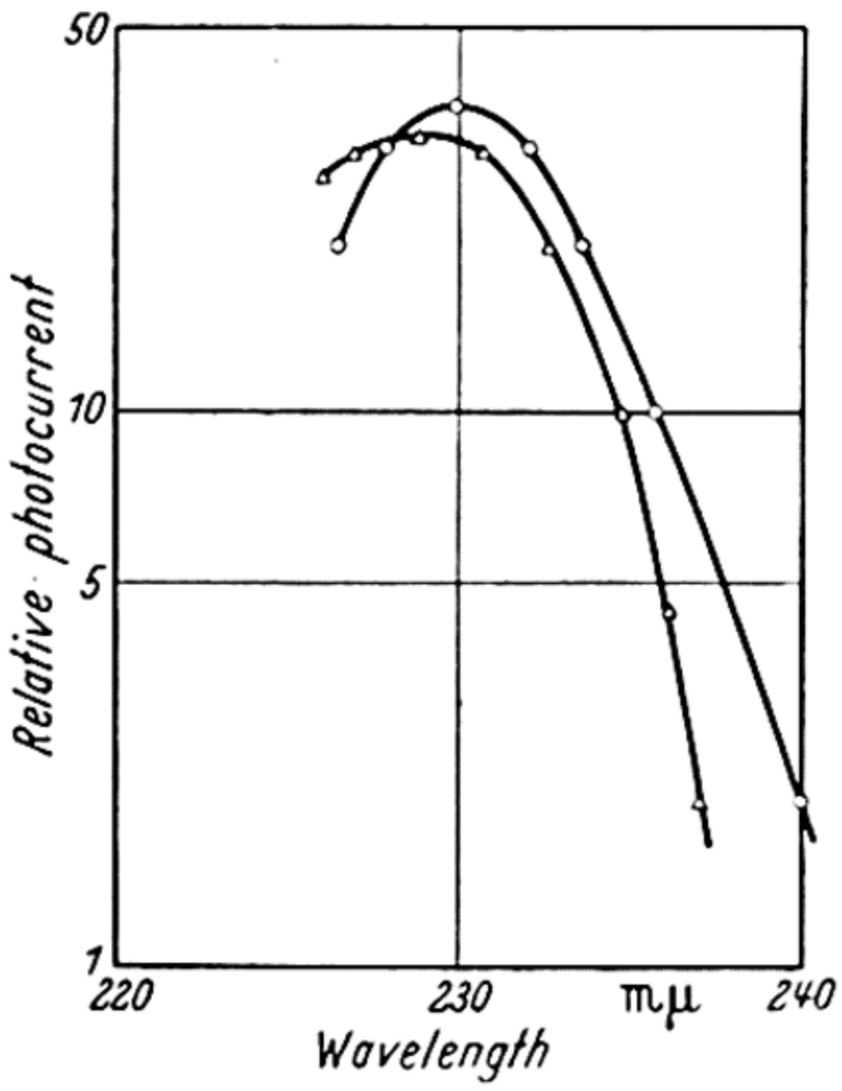

Figure 19. Photoconductivity in diamond (from ROBERTSON *et alii)*

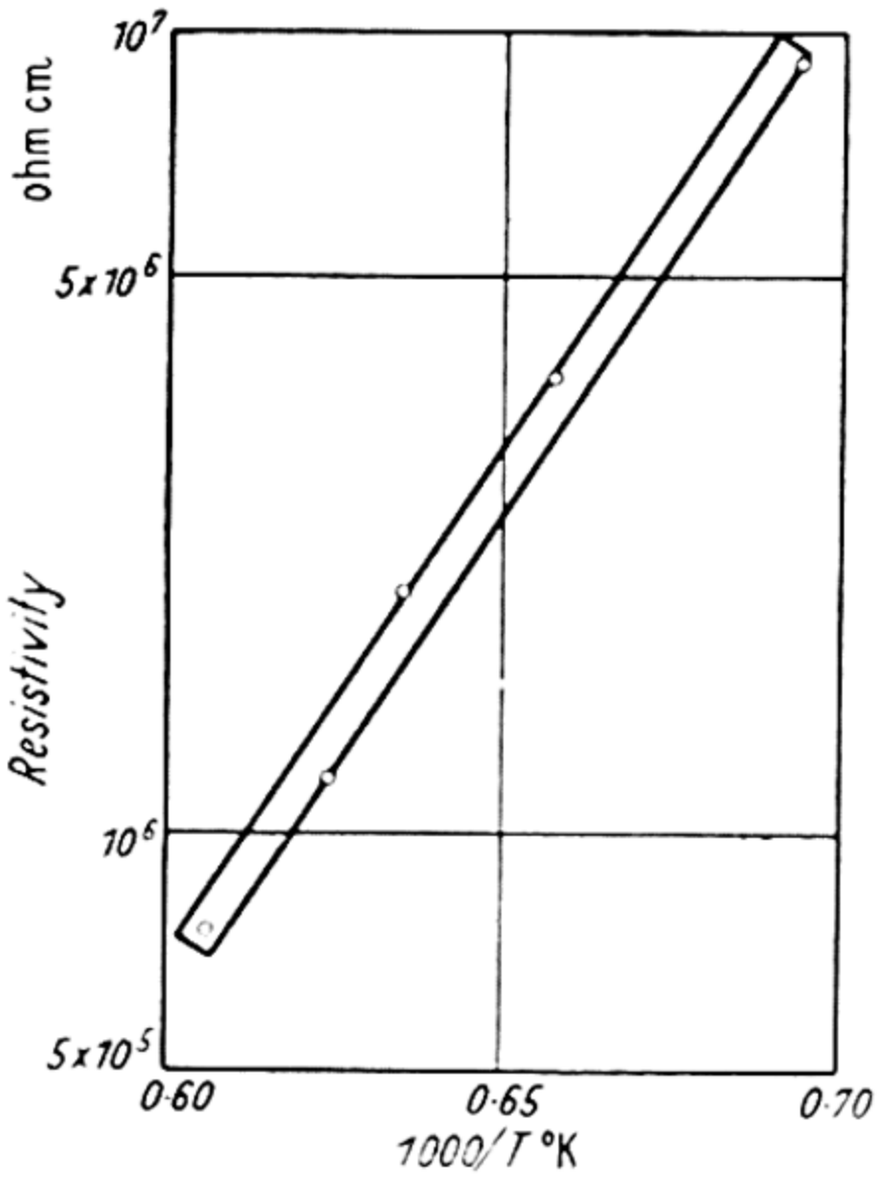

Figure 20. Diamond resistivity (from WARTENBERG)

seen that both curves show peaks near 2,300 Å, and fall rapidly for $\lambda >$ 2,320 Å. From these two curves, the photocurrent is half its maximum value at $\lambda_{\frac{1}{2}} = 0{\cdot}233\ \mu$ and $0{\cdot}234\ \mu$. For two other diamonds measured by these workers the threshold wavelengths are $\lambda_{\frac{1}{2}} = 0{\cdot}231$ and $0{\cdot}226\ \mu$. From a curve given by GUDDEN and POHL (1923) the value is

$\lambda_1 = 0{\cdot}235\ \mu$. A spectral sensitivity curve has also been given by LENZ (1927) from which it is found that $\lambda_1 = 0{\cdot}243\ \mu$. Hence, taking the mean of these six values, we have $\lambda_1 = 0{\cdot}233\ \mu$ and therefore the average optical activation energy is 5·3 eV.

Spectral sensitivity measurements have been carried out on the photovoltaic effect by MENDELSSOHN and DEMBER (1940), who find that the sensitivity is still rising at the short wavelength limit of their measurements—namely 2,300 Å. No definite value can thus be obtained for the threshold wavelength from their work though the indications are that $0{\cdot}23\ \mu > \lambda_1 > 0{\cdot}22\ \mu$.

12.4. CONDUCTIVITY AND HALL EFFECT

In spite of the fact that the activation energy deduced from the optical measurements is over 5 eV, it is still possible to excite appreciable numbers of electrons into the conduction band by thermal means since diamond may be heated to high temperatures without permanent physical changes occurring. Also of course, no electrolytic conductivity takes place even at these high temperatures, as the material is non-polar.

Conductivity measurements were carried out over the rather restricted temperature range of 1,170°C to 1,380°C by WARTENBERG (1912). On plotting his results as log (resistance) against reciprocal temperature, the graph of *Figure 20* is obtained. There is considerable scatter of the points, but they may be confined within a fairly narrow zone between parallel straight lines as shown. The mean slope of this zone is 2·6 eV, indicating that the thermal activation energy is approximately 5·2 eV. Taking the limits of error as set by the slopes of the two diagonals of the rectangular zone we find for the energy gap $E = 5{\cdot}2 \pm 0{\cdot}3$ eV. This value is very near to that found for the optical activation energy.

LENZ (1925) investigated the Hall effect in photoconducting diamonds. The mere fact that a Hall effect was present confirmed that the current was electronic and not electrolytic in character. He found the Hall voltage to be proportional to the magnetic field, and to the electric field up to 5,000 V/cm. He calculated the mean velocity of the electrons in a 4,000 V/cm

field to be $3{\cdot}4 \times 10^6$ cm sec^{-1}, which indicates a mobility of 800 cm sec^{-1}/V cm^{-1}.

In recent Hall effect measurements (again using photocurrent) KLICK and MAURER (1949 and 1951) find the mobility of the electrons to be 900 cm sec^{-1}/V cm^{-1} at room temperature, with comparatively negligible mobility for the holes. The mobility was found to follow a $T^{-3/2}$ law as predicted by SEITZ (1948), although disagreeing with the absolute value calculated by Seitz, which is $\sim$ 150 cm sec^{-1}/V cm^{-1}*. Taking the average value of the mobility as 850 cm^2/V sec, we can estimate the lifetime of the carriers from McKay's value of $b_e\tau = 8{\cdot}3 \times 10^{-6}$ as given in §12.2. We find $\tau = 10^{-8}$ sec, in very good agreement with the value of 9×10^{-9} sec found directly by PEARLSTEIN and SUTTON (1950).

We may also use this value of the mobility in conjunction with the specific conductivity to estimate the activation energy from the formula $\sigma = \sigma_0 e^{-E/2kT}$, where σ_0 is taken as 4 $\times$ mobility at room temperature. From *Figure 20*, $\sigma = 10^{-7}\Omega^{-1}$ cm^{-1} at 1,440°K and hence a mobility of 850 cm sec^{-1}/V cm^{-1} gives $E = 5{\cdot}8$ eV. This last method is clearly not an accurate one for estimating the activation energy, but it nevertheless gives a value in rough agreement with that found by other methods, and thereby indicates that at these temperatures the conductivity is probably intrinsic.

In the lower temperature region of 400 to 700°C, Mendelssohn and Dember found that the dark conductivity could be represented by an exponential function of reciprocal temperature. From these results they were therefore able to calculate an impurity activation energy, which lay in the range 1·45 to 1·75 eV.

From measurements of the thermal release of trapped electrons, MCKAY (1950) concluded that the traps were roughly 0·3 eV below the conduction band. Such a value would be in fair agreement with the theoretical energy for a hydrogen-like system with a dielectric constant equal to that of diamond *i.e.* 5.7. As shown in §9.1 the energy should then be $13{\cdot}5/(5{\cdot}7)^2 = 0{\cdot}4$ eV.

* AHEARN (1951) has pointed out that inhomogeneities in the samples measured can give rise to errors in the experimental values of mobility.

One further method of obtaining the width of the energy gap in diamond has been used, namely bombardment measurements with high energy electrons. By knowing the energy of the incident electrons, and counting the number of conduction electrons produced per incident electron, the average energy given up to excite one conduction electron is found. CHYNOWETH (1951) found this energy to be about 7 eV*. From data quoted by MCKAY (1951) for other materials, it is clear that a loss of approximately 2 eV (per conduction electron) to the lattice is generally found, so that when this is allowed for, a value of activation energy in good agreement with the values already quoted is obtained.

12.5. OPTICAL PROPERTIES

Refractive Index

Measurements have been carried out by several observers in the visible and ultra-violet spectral regions, with good agreement between them. Typical values from WALTER (1891) are:

Wavelength	0·397μ	0·486μ	0·589μ	0·759μ
Refractive Index	2·4648	2·4354	2·4173	2·4024

If these results are plotted according to the dispersion formula of equation 19 *i.e.* as $1/(n^2 - 1)$ against $1/\lambda^2$, the points are found to lie on a straight line. Extrapolating to $\lambda = \infty$, gives the value for the zero frequency refractive index $n_0 = 2{\cdot}38$, and $n_0^2 = 5{\cdot}67$. From MARTENS' (1902) results $n_0^2 = 5.666$, and the same value is given by PETER's (1923) measurements. This figure is thus established to a high degree of accuracy. For the dielectric constant at low frequencies WHITEHEAD and HACKETT (1939) give $5{\cdot}68 \pm 0{\cdot}03$, and BHAGAVANTAM (1948) 5·70. Maxwell's relation $n^2 = \epsilon$ is thus accurately obeyed, the possible discrepancy being less than 1 per cent.

Absorption

Clear, type *II* diamonds are transparent for wavelengths down to about 2,300 Å (ROBERTSON *et alii*, 1934). The absorption constant has been measured by PETER (1923) with the following values:

* A somewhat higher value has been given by FREEMAN, and VAN DER VELDEN (1952).

Wavelength (microns),	0·405	0·313	0·257	0·231	0·226
Absorption Constant (cm^{-1}),	0·12	0·36	0·72	6·78	14·8

The absorption constant is thus rising rapidly in the region of the threshold wavelength for the photoconductive effect (*i.e.* $\sim 0{\cdot}23\mu$). The dispersion of the refractive index indicates that the peak of the main absorption band lies at much shorter wavelengths than this. Hence maximum photoconductivity occurs on the long wavelength edge of the main absorption band.

Diamonds exhibit several absorption bands in the infra-red region of the spectrum, but they are of very small intensity. Type *II* diamonds absorb only at 3 μ and 4·1 to 4·8 μ (ROBERTSON *et alii*, 1934), the most intense band being the one at 4·8 μ (*i.e.* ~ 0·4 eV) where the absorption constant is of the order of 1 mm^{-1}. Apart from these bands there is no absorption for wavelengths up to 20 μ according to REINKOBER (1911)*. In view of the good agreement between the square of the refractive index and the dielectric constant, no intense absorption bands would be expected in the infra-red.

12.6. TEMPERATURE DEPENDENCE OF ACTIVATION ENERGY

Photoconductivity and Absorption Measurements

No thorough measurements of the spectral shift of photoconductivity have been published for diamond. Results by Lenz indicate that the spectral shift is roughly 20 Å between room temperature and liquid air temperature, which would correspond to $dE/dT = -2 \times 10^{-4}$ eV/°C. This figure is liable to be in error by ± 50 per cent.

Extensive measurements of the shift of the absorption edge with temperature were made by ROBERTSON *et alii* (1934), using photographic methods to measure the transmitted light. For a type *II* diamond they found a shift from 2,355Å to 2,393 Å for the temperature range 17°C to 314°C *i.e.* wavelength increasing with rising temperature. This shift corresponds to an average energy change of

$$dE/dT = -2{\cdot}7 \times 10^{-4} \text{ eV/°C.}$$

* The transmission at 108 μ is given as 45 per cent in Smithsonian Tables.

At lower temperatures the shift was found to be somewhat smaller, being 144 cm^{-1} for the temperature interval 17°C to 130°C, or $dE/dT = -1{\cdot}6 \times 10^{-4}$ eV/°C.

Change of Refractive Index

It will be shown later, when the data on activation energies are reviewed, that for the series diamond, silicon, germanium, the energy is approximately inversely proportional to the fourth power of the refractive index. Hence we may write $E = Cn^{-4}$, where C is a constant, giving

$$\frac{1}{E}\frac{dE}{dT} = -\frac{4}{n}\frac{dn}{dT}$$

From SELLA (see MELLOR, 1924), the refractive index changes with temperature between 22°C and 93°C such that the average value of $(1/n)dn/dT = 7{\cdot}7 \times 10^{-6}$. Hence from this theory we would expect $dE/dT = -0{\cdot}31E \times 10^{-4}$, which with $E = 5{\cdot}3$ eV gives $-1{\cdot}65 \times 10^{-4}$ eV/°C.

Thus over similar temperature ranges (*i.e.* room temperature to 100°C) the theoretical and experimental figures for the shift of activation energy agree well in sign and magnitude. It should be pointed out that the precise agreement is fortuitous, as the measurements of absorption shift for this small temperature range may well be in error by 10 per cent. Furthermore, measurements of change of refractive index by RAMACHANDRAN (1947) are considerably less than those above, the mean value for the temperature range 20°C to 130°C being $dn/dT = 13 \times 10^{-6}$ compared with Sella's value of 18×10^{-6}. Ramachandran's measurements extend to 400°C, so that the change in refractive index may be compared with the absorption shift over the full temperature range covered by the absorption data *i.e.* 17° to 314°C. From the refractive index $(4E/n)dn/dT = -1{\cdot}8 \times 10^{-4}$ eV/°C. This is still of the right order, but is too small by a factor of 1·5 : 1 to account for the full absorption shift for this temperature range.

Calculations from Mobilities

From equations 56 and 57 the variation of the energy gap may be related to the mobilities. From equation 57,

assuming the effective mass to be the free elcctron mass, $bC^2T^{3/2} = 7{\cdot}2 \times 10^{-5}\, Mu^2/\omega$ when b is in cm²/V sec and C in eV. According to SHOCKLEY and BARDEEN (1950), $Mu^2/\omega = 10{\cdot}8 \times 10^{+12}$ c.g.s. units as deduced from compressibility data. Hence $bC^2 = 16 \times 10^4$. Thus with $b_e = 900$ cm²/V sec, $C_e = 13$ eV. For holes there are no reliable mobility data, but Shockley and Bardeen estimate $C_h \sim 45$ eV, so that $C_e + C_h \sim 58$ eV.

For the temperature range 28°C to 105°C KRISHNAN (1946) measured the volume expansion by an x-ray method and found $(1/V)\mathrm{d}V/\mathrm{d}T = 4{\cdot}36 \times 10^{-6}$. Hence for this temperature range we have $\mathrm{d}E/\mathrm{d}T \sim -1{\cdot}7 \times 10^{-4}$ eV/°C. This value is again close to the measured absorption shift for the same temperature range. The data available to calculate the shift due to broadening of the allowed bands are unsatisfactory due to the uncertainty in C_h, which is now squared in equation 55. The magnitude of the effect may well be of the same order as the lattice dilatation effect given above. The theory of the temperature shift in diamond, and the uncertainties in the data used, are discussed by MUTO and OYAMA (1951).

It is interesting to note that the refractive index decreases with increasing pressure (RAMACHANDRAN, 1947, also RAMACHANDRAN and RADHAKRISHNAN, 1952), thus showing that n decreases as the lattice contracts. From the calculations of the band structure of diamond by Kimball (see *Figure 1*) it is clear that the energy gap increases as the lattice contracts. Thus the changes in n and E with compression are in the right directions to satisfy the relation $E \propto n^{-4}$.

12.7. SUMMARY AND CONCLUSIONS

Diamond is normally a good insulator, but becomes conducting at high temperatures, or when irradiated by ultra-violet radiation or bombarded by high energy electrons. From spectral sensitivity measurements, the optical activation energy is found to be 5·3 eV. Resistance–temperature measurements yield an energy value of $5{\cdot}2 \pm 0{\cdot}3$ eV. There is thus good agreement between the thermal and optical activation energies. A value of 850 cm²/V sec is found for the mobility of electrons in diamond at room temperature, increasing to 2,500 cm²/V sec

at liquid air temperatures. The mobility of the positive holes appears to be much less.

The life-time of the current carriers is only about 10^{-8} sec, the same value being obtained by different experimental methods. For 10^{16} trapping centres per cm^3 as estimated by CHYNOWETH (1951) this would correspond to a recombination probability $B \sim 10^{-8}$ cm^3/sec. Measurements of the temperature variation of the absorption edge show that the energy gap decreases with rising temperature with $dE/dT = -1{\cdot}6 \times 10^{-4}$ eV/°C between room temperature and 130°C. This value is close to that predicted from the temperature variation of the refractive index, although there is some scatter in the various measurements reported for this latter quantity.

The dielectric constant and the square of the refractive index extrapolated to long wavelengths agree to within 1 per cent, the value being $n_0^2 = 5{\cdot}67$.

13

SILICON

13.1. GENERAL PROPERTIES

Silicon crystallizes in the diamond lattice, with a lattice constant of 5·43 Å (the inter-atomic distance being 2·35 Å) and $5{\cdot}2 \times 10^{22}$ atoms/cm^3. It has a high melting point, 1,420°C.

Relatively pure silicon, with an impurity content of one or two parts per 1,000, can be made by reduction of silicon tetrachloride with zinc. This material can then be further purified by melting *in vacuo* and re-crystallizing. In view of the high melting point, crucibles of beryllia or quartz are used, in conjunction with an alundum furnace. By slowly cooling the molten silicon down to room temperature good quality single crystals can be obtained. In order to obtain crystals with prescribed impurity contents, the requisite small quantities are added to the melt. By addition of boron or aluminium, *p*-type crystals can be made, whilst phosphorus or antimony are commonly used to give *n*-type material.

The band structure has been worked out by Mullaney (1944), using the Wigner-Seitz method. The results obtained resemble those found previously for diamond, which are shown in *Figure 1*.

Although there was little reliable information on either the electrical or optical properties of silicon until recently, much research on this element has now been carried out—largely on single crystals of known purity. Some of the properties of silicon have been reviewed by Boltaks (1950).

13.2. PHOTOCONDUCTIVITY

Photoconductivity in silicon layers has been investigated by Teal *et alii* (1946). The films were made by pyrolitic deposition from silicon tetrachloride vapour on to quartz or ceramic surfaces. Photosensitive films of a few microns thickness were obtained when a mixture of the vapour and hydrogen was

passed over such a surface at 1,000 to 1,250°C. The magnitude of the photoeffect was such that the layer conductivity increased by 10 to 20 times per lumen.

The photocurrent was found to be proportional to the intensity of illumination over the range of intensities employed *i.e.* ~ 12 : 1. When the cells were illuminated with interrupted radiation, the dark current, average photocurrent and peak photocurrent were all proportional to the applied electric field up to 250 V/cm. Above this field strength the currents increased less than proportionally. The response times of the cells were ~ 200 μsec, the response to radiation chopped at 720 c/s being about 60 per cent of the low frequency value. Heating the layers to red heat in air did not impair the room temperature photosensitivity, which was little affected by background illumination.

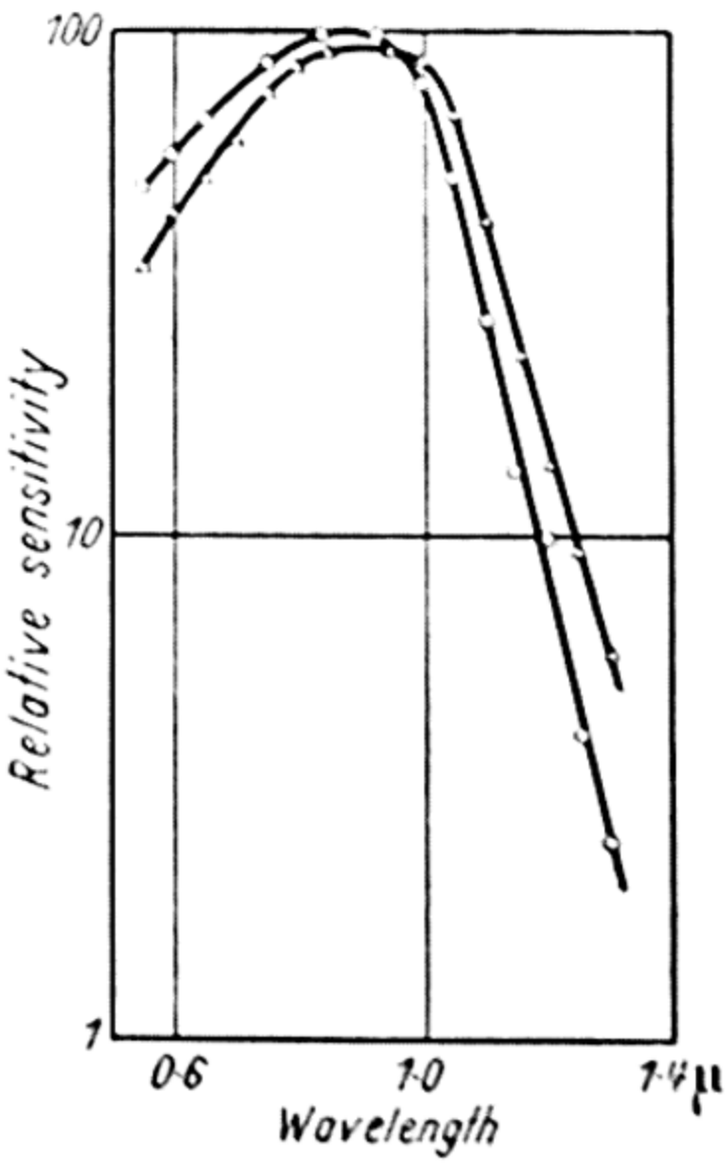

Figure 21. Photoconductivity in silicon (from TEAL *et alii)*

It is reported that both photoconductive and photovoltaic effects have been observed in single crystals (see TORREY and WHITMER, 1948), and that photoeffects have been observed in silicon *p–n* junctions (see PEARSON and BARDEEN, 1949), but no detailed measurements have yet been published.

13.3. SPECTRAL SENSITIVITY

Results given by Teal *et alii* have been plotted in *Figure 21*, using a logarithmic scale to show more clearly the form of the

fall in sensitivity as the wavelength increases. It will be seen that the maximum sensitivity lies in the infra-red region near 0·9 μ; and that at wavelengths greater than 1·0 μ the points fit fairly well on straight lines, indicating exponential falls of sensitivity with wavelength, as is found for most of the elements. The threshold wavelengths lie at $\lambda_1 = 1{\cdot}05\ \mu$ and 1·10 μ for the two curves. Hence the optical activation energy is 1·12 to 1·18 eV.

13.4. CONDUCTIVITY AND HALL EFFECT MEASUREMENTS

Extensive measurements on single crystals, of both Hall effect and conductivity, over a wide temperature range have been reported by PEARSON and BARDEEN (1949). For samples of highest purity the resistance was ~ 30 Ωcm at room temperature. This was reduced by a factor of 10^5 by the addition of 1 per cent of boron. A resistance of 30 Ωcm would correspond to an impurity content of about 1 part in 10^7. The purest samples were in the range of intrinsic conductivity above ~ 600°K, but with even 0·01 per cent of boron present it was necessary to exceed 1,000°K before the intrinsic conductivity became comparable with the impurity conductivity.

By suitable additions both *p*-type and *n*-type crystals could be made. Phosphorus, for example, formed donor centres (the phosphorus atom having one more valence electron than silicon), while boron, having one less electron than silicon, gave acceptor centres. On studying the variation of lattice constant as the amount of boron impurity was increased, it was found that the lattice contracted. If the boron atoms were taking up interstitial positions, the lattice of course would expand. It was therefore concluded that the boron (whose atomic radius is less than that of silicon) was entering the lattice substitutionally.

From the slopes of the Hall effect and conductivity temperature curves in the high temperature (intrinsic conductivity) region, these workers found the thermal activation energy to be 1·12 eV. *Figure 22* shows some measurements of resistivity by PEARSON (1947). Both pure and impure samples have the same conductivity at high temperatures (although differing

by 500 : 1 near room temperature), so that they must then be in the range of intrinsic conductivity. For the pure sample the experimental points lie on a straight line over a wide range of resistivities. The slope of the line gives an activation energy of 1·2 eV. Values of 1·12 eV and 1·14 eV were obtained by TEAL *et alii* (1946) for pyrolytically deposited films, the purest of which had a specific conductivity of only $2 \times 10^{-5}\Omega^{-1}\text{cm}^{-1}$ at 30°C. The thermal and optical activation energies are thus almost identical.

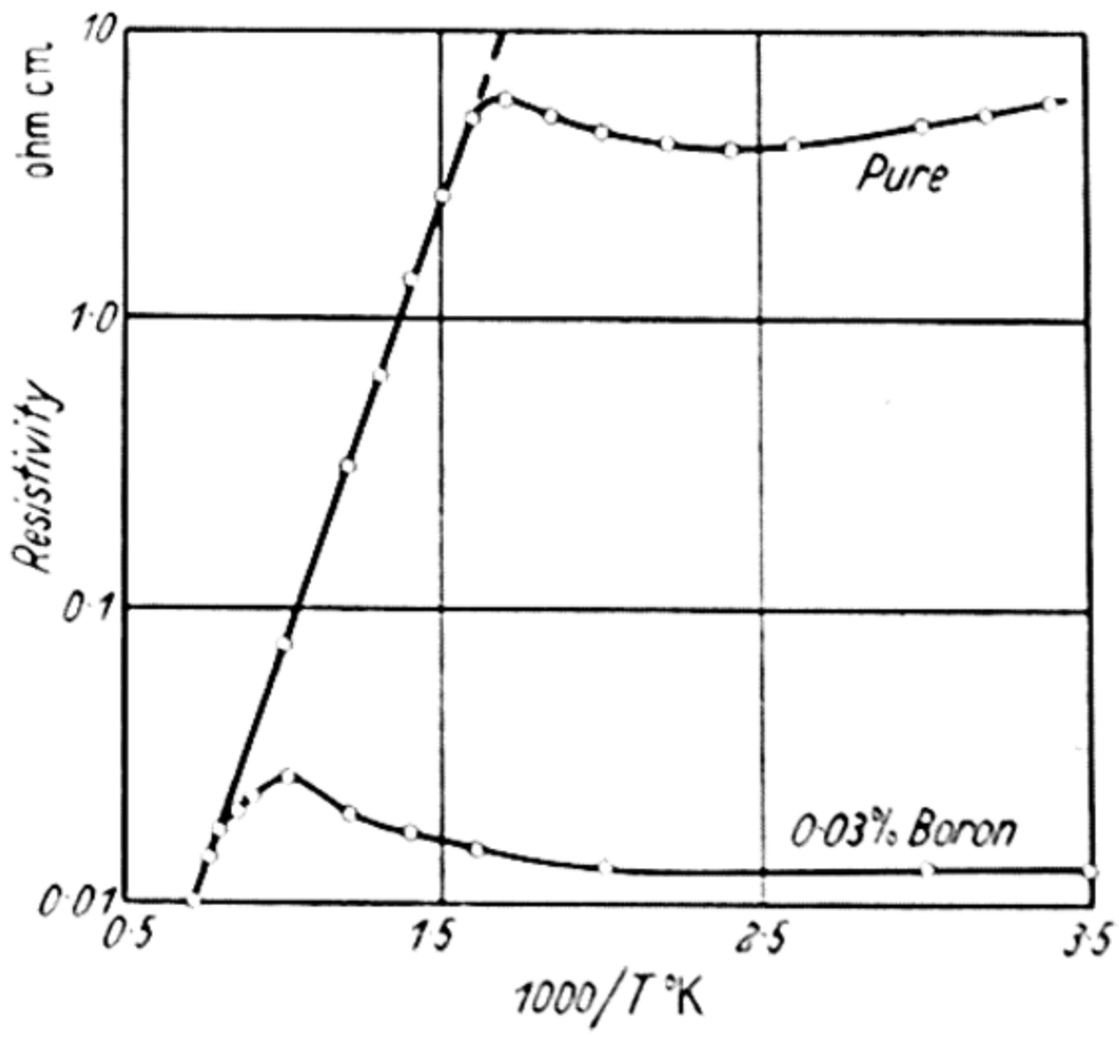

Figure 22. Silicon resistivity (from PEARSON)

From the Hall effect measurements of PEARSON and BARDEEN (1949) the mobility of the conduction electrons was 300 cm $\text{sec}^{-1}/\text{V cm}^{-1}$ at 300°C, and was found to follow a $T^{-3/2}$ law for temperatures higher than this (where lattice scattering was predominant), in accordance with the theory of SEITZ (1948). At lower temperatures, scattering by both ionized and neutral impurity centres becomes important. The mobility of the positive holes was $\frac{1}{3}$ that of the electrons*.

For the temperature range 100 to 1,000°K Pearson and Bardeen found no discontinuities as reported in the early measurements of KOENIGSBERGER and SCHILLING (1910). This is in accord with the results of SCHULZE (1930) who, from dilatometer studies, concluded that there were no phase transformations below 1,000°C.

* HAYNES and WESTPHAL (1952) now give $b_e = 1{,}200$, $b_h \sim 250$ for drift mobilities in silicon crystals.

The thermal activation energy found for boron impurity centres was 0·08 eV, when the density of centres was so dilute that there was no interaction between them. This may be compared with the theoretical energy value obtained from the Bohr formula for a hydrogen atom, scaled down to allow for the high dielectric constant of the bulk silicon. We have $\Delta E = 13{\cdot}5/\epsilon^2$ eV, which with $\epsilon = 12$ gives $\Delta E = 0{\cdot}09$ eV, so that the experimental and theoretical values are in close agreement. The activation energy decreased as the impurity concentration increased, the decrease from the value at high dilution being roughly proportional to the cube root of the density of impurity centres, and hence to the average linear separation of the impurity atoms. Measurements on the effect of impurities on the resistance of silicon have also been reported by STOCKMAN (1950).

Photoconductivity arising from the impurity levels in silicon has not so far been reported, although data have been published on the absorption properties of donor and acceptor centres by BURSTEIN *et alii* (1951). For energies near 0·05 eV (*i.e.* at wavelengths $\sim 20\,\mu$) the absorption cross-section for the centres is found to be $3 \times 10^{-15}\text{cm}^2$. For comparison the area of a circle of radius $\epsilon \times$ Bohr radius $= 7$ Å (see § 9.1) would be $3{\cdot}7 \times 10^{-15}\text{cm}^2$.

13.5. OPTICAL PROPERTIES

Refractive Index

Precise measurements of the refractive index have recently been carried out in the infra-red region (where high purity silicon is transparent), using thin prisms of the material (BRIGGS, 1950). The results obtained are:

Wavelength	1·1μ	1·6μ	2·0μ	2·6μ
Refractive Index	3·553	3·480	3·458	3·443

From these figures the refractive index extrapolated to long wavelengths is $n_0 = 3{\cdot}43$ and hence the dielectric constant is $n_0^2 = 11{\cdot}8$. Briggs' values are somewhat lower than those previously obtained by INGERSOLL (1910) from reflection measurements with polarized light. According to PFESTORF (1926) the index reaches a maximum value of 4·6 at a

wavelength $\sim 0{\cdot}4\ \mu$, and then falls rapidly with decreasing wavelength.

Transmission and reflection measurements

Silicon absorbs strongly in the visible region of the spectrum, but very pure samples become transparent at wavelengths a little greater than 1 μ, even for a thickness of several mm (Fan and Becker, 1950; Hass and Scott, 1950; Cotton, 1950; see also Becker *et alii*, 1952). Measurements of the transmission of single crystals showed a maximum near $1{\cdot}2\ \mu$. The minimum value of the absorption constant depends on the resistivity of the sample as follows:

$\rho =$	$0{\cdot}014\,\Omega$cm	$0{\cdot}07\,\Omega$cm	$0{\cdot}5\,\Omega$cm	$30\,\Omega$cm
$K =$	$60\,\text{cm}^{-1}$	$12\,\text{cm}^{-1}$	$0{\cdot}3\,\text{cm}^{-1}$	$0{\cdot}01\,\text{cm}^{-1}$

The last figure is obtained from measurements by Briggs (1950) on what is perhaps the purest silicon so far produced*. The absorption constant is seen to decrease somewhat more rapidly than the conductivity decreases.

For wavelengths below $1{\cdot}2\ \mu$ the absorption constant rises very rapidly, increasing from $0{\cdot}01\ \text{cm}^{-1}$ at $1{\cdot}2\ \mu$ to 100cm^{-1} at $1{\cdot}0\ \mu$ for the purest material. The latter wavelength is the shortest at which direct measurements of the absorption in single crystals have been carried out. From Pfestorf's reflection measurements of the optical constants, there is a single absorption band in the range $0{\cdot}2\mu$ to $1{\cdot}0\mu$ with a maximum absorption constant $> 10^6\text{cm}^{-1}$. Such a high value shows that this must be the main lattice absorption. *Figure 23* shows the absorption plotted over the wavelength range $0{\cdot}25\ \mu$ to $10\ \mu$, the absorption constant ranging over 8 decades for this spectral region.

It is not possible to determine a specific absorption edge from this curve, but the absorption constant is changing most rapidly in the neighbourhood of $1{\cdot}1\ \mu$. We may thus take the absorption edge as corresponding to a quantum energy of approximately 1·1 eV, which agrees with the values found for the activation energy by other means. The imaginary part of

* Silicon with resistivity as high as 10,000 Ω cm has however been prepared by neutron bombardment (Lark-Horovitz, 1951).

the dielectric constant is plotted in *Figure 23* as a broken line, from which maximum absorption is seen to occur at a wavelength of 0·36 μ.

As given in § 3.3, it should be possible to calculate the value of the low frequency refractive index from the absorption curve, if this is known for all frequencies, the relation being

$$n_0^2 - 1 = -\int^{\infty} \frac{4nk}{\pi\nu}\,\mathrm{d}\nu = \int_0^{\infty} \frac{4nk}{\pi\lambda}\,\mathrm{d}\lambda$$

The curve of $4nk/\pi\lambda$ is readily derived from *Figure 23*, and with little error it may be extrapolated to zero wavelength and the

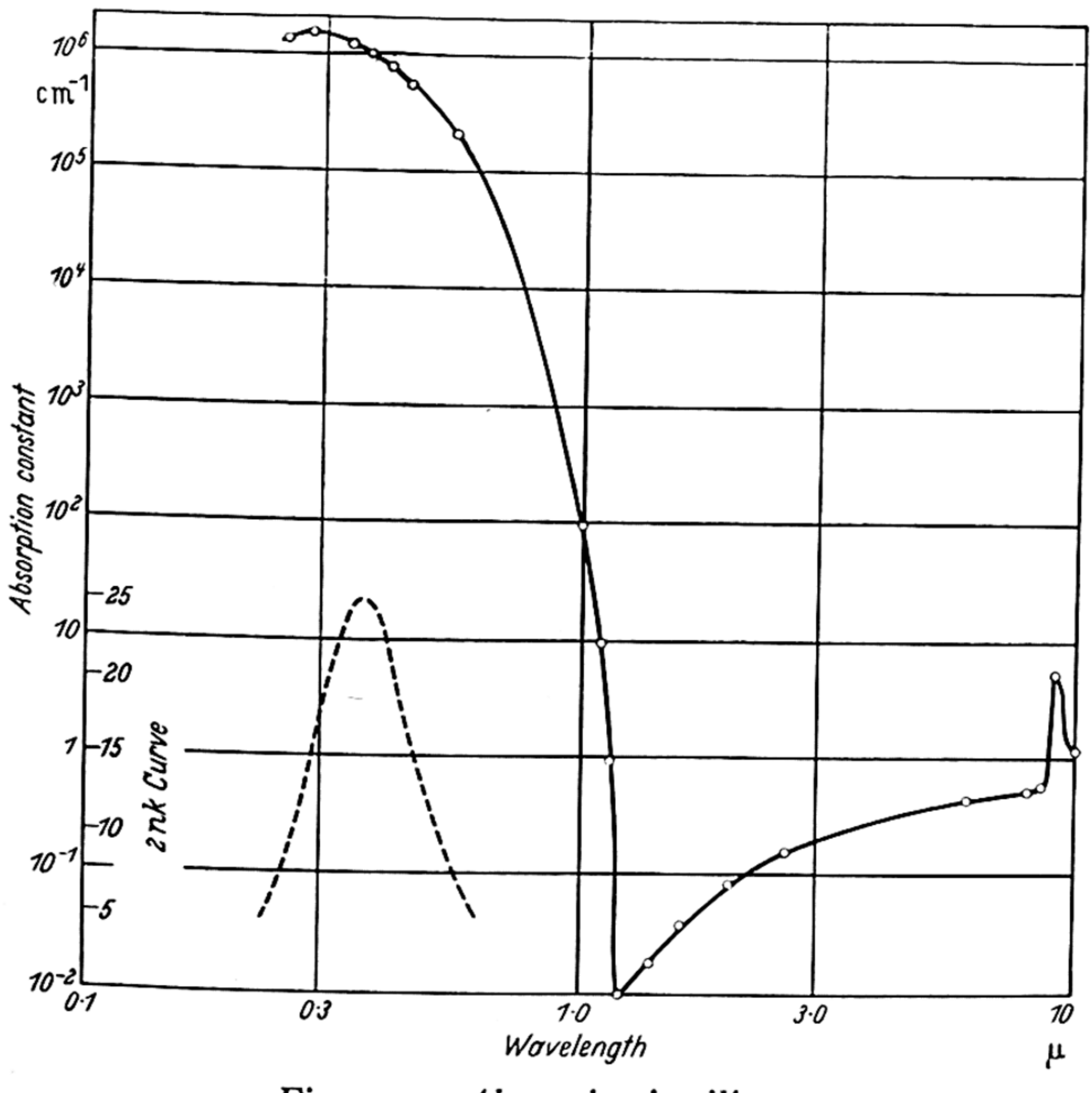

Figure 23. Absorption in silicon

integration carried out graphically. The value obtained is $n_0^2 - 1 = 10{\cdot}5$, therefore $n_0^2 = 11{\cdot}5$. This figure is remarkably near to the experimental value obtained for the square of the refractive index at low frequencies. Silicon is one of the very

few materials for which the optical properties have been measured in sufficient detail for this relation to be applied. The good agreement obtained shows that no important absorption bands exist in parts of the spectrum where measurements have not yet been made.

As shown by *Figure 23*, very pure silicon gives good transmission for wavelengths of at least 10 μ, except for a small absorption band (of intensity about 5 cm^{-1}) which always seems to occur near 9 μ. In view of its good transmission and high refractive index, silicon has been suggested as a useful optical material for the infra-red. TREUTING (1951) has given design data for silicon–germanium achromatic lenses.

For less pure samples the absorption at long wavelengths increases linearly with the concentration of holes in *p*-type samples, according to BRIGGS (1950). The absorption increases approximately as λ^2 in accordance with the theoretical dependence given by equation 14, but the absolute magnitude is about ten times as great as the theory indicates. A more rigorous treatment of the theory outlined by FAN and BECKER (1951) does little to improve the agreement, and the origin of the discrepancy is not yet known.

Measurements at very long wavelengths have been made recently by LORD (1952) who finds good transmission from 20 to 40 μ. Several small absorption bands are observed however, between 12 μ and 20 μ. The strongest of these bands, where $K \sim 17\ cm^{-1}$, lies at 16·5 μ. This wavelength corresponds to an energy of 0·075 eV, which is very close to the value found for the thermal activation energy of *p*-type impurity centres.

13.6. TEMPERATURE DEPENDENCE OF ACTIVATION ENERGY

Measurements by BECKER and FAN (1949) show that the position of the absorption edge is temperature dependent, moving to longer wavelengths as the temperature is raised. For wavelengths where the absorption constant is 80 cm^{-1} their curves give:

77°K	195°K	295°K	493°K
0·938μ	0·978μ	1·025μ	1·094μ

i.e. a shift of 0·156 μ for 416°C, or $4{\cdot}5 \times 10^{-4}$eV/°C. The value obtained from curves by FAN and BECKER (1950) is somewhat less, namely $3{\cdot}5 \times 10^{-4}$eV/°C. This lower value is considered by FAN and BECKER (1951) to be more reliable.

From measurements of conductivity and Hall effect in the range of intrinsic conductivity, PEARSON and BARDEEN (1949) conclude that the energy gap decreases with temperature to the extent of 3×10^{-4}eV/°C. According to BARDEEN and SHOCKLEY (1950), measurements of the spectral shift of photoconductivity in a *p–n* junction show an energy change from 1·1 eV at 77°K to 1·0 eV at 297°K *i.e.* about $4{\cdot}5 \times 10^{-4}$eV/°C. Thus these different methods all give values in the range $4(\pm 1) \times 10^{-4}$eV/°C for the temperature dependence of the energy gap.

Calculations by MULLANEY (1944) on the shapes of the energy bands indicate that there should be a fractional change of energy gap of ~ 10 times the dilatation. Taking the cubical expansion coefficient $\sim 10^{-5}$*, this would give a shift $\sim 1 \times 10^{-4}$eV/°C. Estimates by HOLMES (1949) of the width of the forbidden zone for various internuclear spacings leads to a similar value. The effect of dilatation on the conductivity of silicon has been investigated experimentally by BRIDGMAN (1951), but no definite information about the energy shift has been obtained from the data as yet.

Using the theory of BARDEEN and SHOCKLEY (1950) for the energy shift with dilatation, we find from equation 57 that $C_e = 9{\cdot}8$ and $C_h = 17$ for the mobility values used by Bardeen and Shockley, *i.e.* $b_e = 300$ and $b_h = 100$. With $\beta = 4{\cdot}15 \times 10^{-6}$ equation 56 gives $(\mathrm{d}E/\mathrm{d}T)_2 = -2{\cdot}2 \times 10^{-4}$eV/°C. Using the higher (drift) mobility values of $b_e = 1200$, $b_h = 250$ reduces the shift to $-1{\cdot}3 \times 10^{-4}$ eV/°C. Bardeen and Shockley point out that whereas the free electron mass (m) is probably a good approximation for m_h, there is evidence that $m/m_e \sim 1{\cdot}5$, so that a better estimate of the shift would be $(\mathrm{d}E/\mathrm{d}T)_2 = -1{\cdot}6 \times 10^{-4}$eV/°C. The contribution arising from broadening of the allowed levels given by equation 55 is

* Accurate x-ray measurements of the linear expansion coefficient have now been made by STRAUMARIS and AKA (1952) who find $\beta = 4{\cdot}15 \times 10^{-6}$ and hence the cubical coefficient is $12{\cdot}5 \times 10^{-6}$.

$(\mathrm{d}E/\mathrm{d}T)_1 = -3{\cdot}5 \times 10^{-4}$eV/°C, with the parameters used by FAN (1950 and 1951). However FAN and BECKER (1951) point out that this value should be halved because the silicon lattice has two atoms per unit cell. The calculated value is further reduced when the drift mobilities are used, being $(\mathrm{d}E/\mathrm{d}T)_1 = -0{\cdot}9 \times 10^{-4}$eV/°C for $m/m_e = 1{\cdot}5$. The total calculated shift is therefore $-2{\cdot}5 \times 10^{-4}$eV/°C. In view of the uncertainty in the values of some of the parameters used, this value may be considered to be in good agreement with the experimental observations.

13.7. SUMMARY AND CONCLUSIONS

The purest silicon at present available is an intrinsic semiconductor above 300°C; the conductivity at lower temperatures resulting from either donor or acceptor impurity centres. The energy gap between the full and conduction bands is 1·12 to 1·2 eV from thermal measurements and 1·12 to 1·18 eV from photoconductivity measurements. There is thus very close agreement between the optical and thermal activation energies.

Measurements of temperature dependence of absorption, of spectral sensitivity of p–n junctions, and Hall effect measurements, all indicate a shift of this activation energy of $\mathrm{d}E/\mathrm{d}T = -4(\pm 1) \times 10^{-4}$eV/°C. This value is in accord with theoretical expectations. BRIGGS (1950) has observed that the refractive index of silicon *increases* with temperature. This is the direction of change indicated by the relation $E \propto n^{-4}$ which is discussed in §§ 9.3 and 23.4*.

High purity silicon is transparent to wavelengths $> 1{\cdot}2\,\mu$ in thicknesses of 1 cm or more. At long wavelengths the measured refractive index is 3·43, in agreement with the value calculated from the absorption data.

* Application of the simple theory of §3.3 (equation 17) shows that the refractive index is roughly proportional to the wavelength of peak absorption. Assuming that the absorption peak shifts to the same extent as the absorption edge (*i.e.* from 3·5 eV at room temperature to 3·6 eV at 77°K), then the refractive index at 77°K should be approximately 3·34. The calculated increase in n^{-4} due to this cooling is thus $\sim$ 10 per cent, which compares well with the observed increase in E.

14

GERMANIUM

14.1. GENERAL PROPERTIES

GERMANIUM crystallizes in the diamond lattice with a lattice constant $a = 5{\cdot}647$Å, and having $4{\cdot}5 \times 10^{22}$ atoms/cm^2. No transitions have been observed between 20°K and 1,100°K, the latter temperature being not far below the melting point of 985°C.

A great deal of experimental work has been carried out on germanium during the last ten years, and more is now known about its properties than about those of any other semiconductor.

14.2. PREPARATION

Much of the success in the investigation of the properties of germanium has resulted from the preparation of extremely high purity material, and from the production of single crystals with known amounts of impurity.

Two methods of obtaining pure germanium have been used commercially. The first is analogous to that described for production of silicon, namely the reduction of the tetrachloride by zinc vapour. Silica reactors are used at temperatures between the boiling point of zinc and the melting point of germanium. Any excess zinc is removed by hydrochloric acid before final purification by vacuum melting. The second method is to reduce germanium oxide with hydrogen, again using silica furnaces. Samples with specific resistances as high as 1 to 10 Ω cm* may be obtained by this process.

Either of these methods is normally followed by purification by melting in a good vacuum, generally as part of the process of growing single crystals, with repeated crystallizations if

* 1 Ωcm material corresponds to roughly one impurity atom per 10^7 germanium atoms.

necessary. Various methods of cutting, polishing or etching specimens are used depending on the type of measurement to be carried out. Germanium wafers have been ground as thin as 0·05 mm, and filaments only 0·2 × 0·2 mm², several mm in length, have been cut from single crystals.

Either *p*-type or *n*-type germanium samples can be prepared by adding controlled amounts of impurities to the germanium melt before crystallization. Metals of group III of the periodic table produce *p*-type samples, gallium being generally used. For *n*-type samples, elements of group V, particularly antimony, are used. One interesting application of antimony as an impurity agent has been the use of the radio-active isotope of mass 124 as a tracer. Geiger counter measurements can then reveal the distribution of the antimony throughout the ingots and crystals. Furthermore the method can be applied quantitatively to determine the impurity concentration even when it is as low as one atom per hundred million germanium atoms. Conventional methods of chemical analysis would of course be quite inadequate to deal with such small concentrations. It has been shown by PEARSON, STUTHERS and THEUERER (1950) that in samples with Sb^{124} impurity, the number of conduction electrons found by Hall effect measurements equals the number of antimony atoms found from counter measurements within the accuracy of the experiments. Thus (at normal temperatures) each atom of antimony provides one free electron. Curves showing the distribution of Sb^{124} impurities in typical melts have been given by LARK-HOROVITZ (1949).

It is possible to convert one conductivity type into the other in a variety of ways. For example, *n*-type germanium, if of good purity initially (*i.e.* ~ 5Ω cm) can be converted to *p*-type by heating to 850° to 900°C for a few hours and then quenching. FULLER, THEUERER and VAN ROOSBROECK (1952) showed that the equilibrium concentration of thermally produced acceptor centres varies exponentially with reciprocal temperature from 2×10^{16} per cm³ at 900°C to 3×10^{14} per cm³ at 600°C. DE SORBO and DUNLAP (1951) quenched in oil, whereas THEUERER and SCAFF (1951) used air quenching. Prolonged heating to 450°C converts the *p*-type back into *n*-type.

Extensive measurements of the effects of bombardment by high energy electrons, alpha particles and neutrons have been carried out by Lark-Horovitz and his co-workers (see LARK-HOROVITZ, 1951, and JOHNSON and LARK-HOROVITZ, 1951). They found that slow neutron bombardment gave *p*-type material. The neutrons cause actual transmutations of the germanium atoms into either gallium or arsenic, about three of the former being formed for each of the latter, so that the positive holes resulting from the gallium atoms predominate in spite of the higher mobility of the conduction electrons from the arsenic atoms. Fast electrons and α-particles were also found to convert *n*-type germanium into *p*-type.

By the use of sharply defined beams of charged particles it is possible to produce localized *p*-*n* junctions in single crystals of germanium. A method of growing single crystals with internal *p*-*n* junctions has been described by TEAL *et alii* (1951). These workers used a ' pulling technique ' to form their single crystals *i.e.* a rod bearing a crystal fragment is allowed to make contact with the surface of the molten germanium and then slowly withdrawn. The germanium solidifies as it is withdrawn from the melt, and by suitably controlling the temperatures and rate of pulling, rods several inches long, which are single crystals, may be obtained. The *p*-*n* junction is produced by simply changing the constitution of the melt half-way through the pulling process by adding the relevant impurity agent. Starting with a *p*-type melt for example, addition of the appropriate amount of antimony will give the *p*-*n* junction. By a logical extension of the technique, *p*-*n*-*p* transistors are made with a thin layer of *n*-type between two thick *p*-type sections, by the addition of sufficient gallium to convert the melt back to *p*-type as soon as the required thickness of *n*-layer has crystallized.

14.3. PHOTO-EFFECTS

A variety of photo-effects have now been observed in germanium, including photoconductivity, photovoltaic effects at both *p*-*n* junctions and at metal contacts, and photo-transistor action.

Photoconductivity

Measurements of photoconductivity in germanium have been described by BECKER (1949) whose results for the spectral sensitivity of germanium have been replotted on a logarithmic scale in *Figure 24*. It will be seen that the sensitivity extends from the visible region to 2 μ, being about 1 per cent of its maximum at this latter wavelength. The fall in sensitivity at long wavelengths is approximately exponential. From the curve we find $\lambda_{\frac{1}{2}} = 1{\cdot}72\ \mu$, equivalent to an optical activation energy of 0·72 eV. It will be seen that there is little fall in sensitivity at the shortest wavelengths measured although as

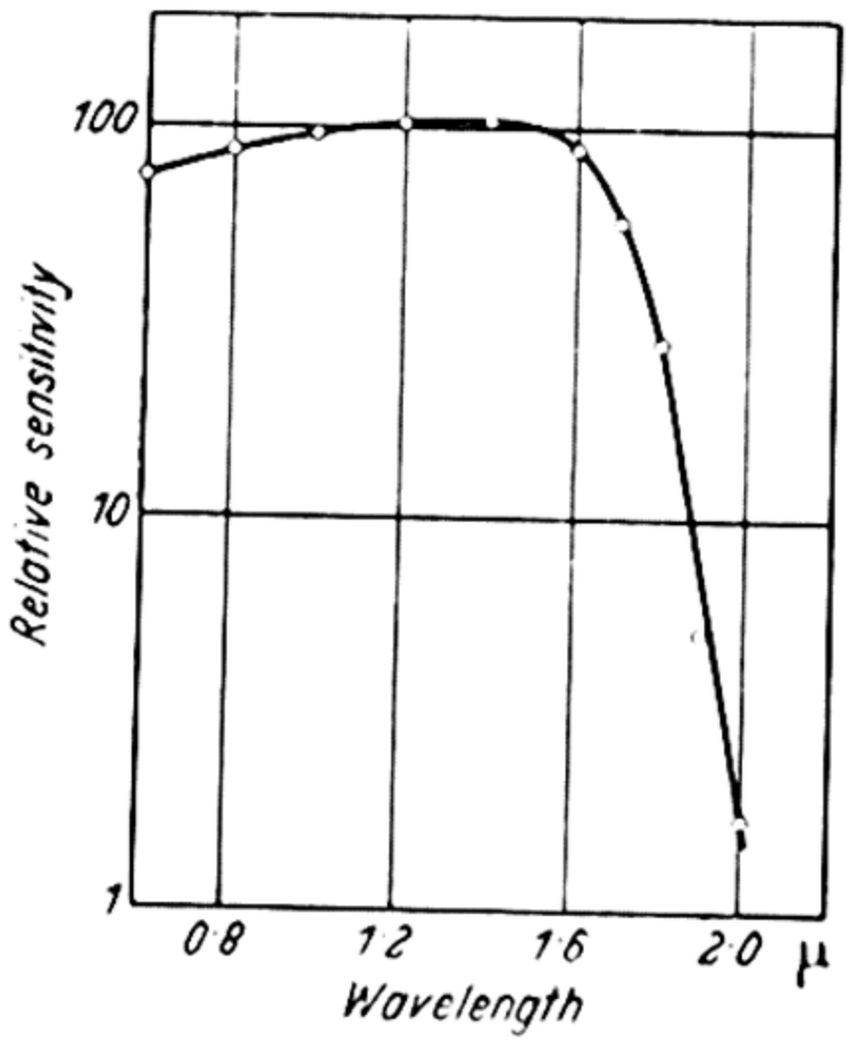

Figure 24. Germanium photoconductivity (from BECKER)

shown by *Figure 4* the absorption constant at 0·6 μ exceeds $10^5\ cm^{-1}$. This supports the theory of §6.5 that the high diffusion constant of germanium is important in preventing a fall in sensitivity due to high recombination rates when the radiation is absorbed in a thin surface layer. SHIVE (1949) has also described a photoconductive cell of germanium where the spectral sensitivity was said to peak near 1·5 μ and fall rapidly for wavelengths greater than 1·6 μ. These results are clearly similar to those shown in *Figure 24*.

GOUCHER (1950) has measured the quantum efficiency for photoconductivity in single crystals of *n*-type germanium. Long rectangular specimens of uniform cross-sectional area and conductivity had part of their surface irradiated by monochromatic light of known wavelength. The number of incident

quanta was determined by use of a calibrated thermopile, and the number of absorbed quanta calculated therefrom by subtracting reflection and transmission losses. Care was taken to illuminate only the central part of the filament, sections greater in length than the mean range of the photo-electrons and photo-holes being un-illuminated, and to ensure that the conductivity of the illuminated portion was not increased sufficiently to produce any appreciable distortion of the field along the specimen. From the measured photoconductivity, knowledge of the specimen geometry and applied field, with values of mobilities determined by separated drift velocity experiments, the number of electron-hole pairs generated by the light could be calculated. For the range 1 μ to the threshold wavelength it was found that within the accuracy of the experiment ($\sim$ 10 per cent) each absorbed quantum produced one photo-electron and one photo-hole, thus establishing the principle of quantum equivalence for this material.

The lifetime of the holes in the above specimen was 67 μ sec. As the material was *n*-type with a known resistivity, it is possible to calculate the recombination coefficient. Sample resistivity $= 5\ \Omega\,\mathrm{cm} = 1/(n_e e b_e)$. Hence with $b_e = 3{,}600$ $n_e = 3{\cdot}5 \times 10^{14}/\mathrm{cm}^3$. Hence $\tau_p = 1/Bn_e$ (see §6.1) gives $B = 4 \times 10^{-11}\,\mathrm{cm}^3\,\mathrm{sec}^{-1}$. This value is an upper limit to B, as surface recombination effects have been ignored.

Photovoltaic Effects

Measurements on single crystal *p-n* junctions made by α-particle bombardment (see LARK-HOROVITZ, BLEULER, DAVIS and TENDAM, 1948, or LARK-HOROVITZ, 1951) have been carried out by BECKER and FAN (1949) and FAN and BECKER (1950). The photovoltage under effectively open-circuit conditions was obtained by using an amplifier with an input resistance high compared with the barrier resistance. Measurements with increasing input resistance showed that the photovoltage increased steadily at first, but finally reached a saturation value. At liquid-air temperatures, $10^9\ \Omega$ impedance was required to satisfy this condition. The photovoltage was measured over a range of intensities of $5 \times 10^5 : 1$, the

increase being linear over the two lowest decades of intensity. Above this level the voltage increased progressively less rapidly than the intensity. As shown by *Figure 11* the results can be represented by the theoretical equation 52, $V_p = V_0 \log (1 + SQ)$ over the whole range of intensities.

Working in the region of linear response the spectral sensitivity curves were measured at various temperatures. At room temperature the results were similar to those shown in *Figure 24* although the fall at shorter wavelengths was somewhat greater. From Fan and Becker's published curves the threshold wavelengths are :

Temperature (°K)	100	210	293
$\lambda_{\frac{1}{2}}(\mu)$	1·63	1·68	1·78

Of these values the last is probably not so accurate as those at lower temperatures as the sensitivity was very low at 293°K. Taking the 210°K point as representative, the optical activation energy is 0·73 eV, in close agreement with the photoconductive value.

The response time and sensitivity were also measured for the above temperatures, with the following results :

Temperature (°K)	100	210	293
Response Time (μsec)	1500	130	<12
Sensitivity (*relative photovoltage*)	$2{\cdot}5 \times 10^5$	7×10^3	30

Both response time and sensitivity thus increase markedly on cooling. In the range of linear response equation 52 reduces to $eV_p = kTSQ = kTQ\tau/n_{\min}$ where $n_{\min}$ is the density of minority carriers. As $n_{\min}$ will decrease on cooling, the sensitivity should increase more rapidly than the response time, as is seen to be the case from the above figures. No change in τ with wavelength occurred in the range 0·9 to 1·8 μ.

Photo-effects at a *p-n* junction have also been studied by GOUCHER *et alii* (1951) who measured the variation in photo-response as a function of the distance of the light spot from the junction. The results showed an exponential decrease with displacement on either side of the junction. With allowance for the finite width of the light spot used, the distances for a decrease to 1/e can be found. The theoretical diffusion lengths in the material can be calculated from the diffusion constants

and time constants, the required relation being $L = (D\tau)^{\frac{1}{2}}$ where $D = bkT/e$. The experimentally observed and calculated lengths were:

	τ	D	$(D\tau)^{\frac{1}{2}}$	*Expt*
n region	56μsec	43	0·5mm	0·55mm
p region	52μsec	90	0·7mm	0·75mm

The agreement is seen to be very good, showing that the effective range of the photoelectrons and photoholes in the absence of an applied field can be determined accurately from simple diffusion considerations.

Longer response times than the above have been observed in very pure germanium samples. TEAL *et alii* (1951) report values in excess of 600 μ sec at room temperature for their purest specimens. Taking these to be of resistivity $\sim 20\ \Omega$ cm, the recombination constant becomes $B \simeq 10^{-11}\ \text{cm}^3\ \text{sec}^{-1}$. This value is in accord with the estimate given by SHOCKLEY (1950) of $10^{-18}\ \text{cm}^2$ for the capture cross-section.

PIETENPOL (1951) has measured the sensitivity of a *p-n* junction, and found the quantum efficiency to be approximately unity. The responsivity is very high, it being possible to produce 100 V of signal across a 1 MΩ load with 1/100 lumen of radiation from a source at 2,900°K. The current sensitivity (in μ amp) for this source temperature was:

Applied Volts	*Dark*	0·03 lm	0·06 lm
80	~10	340	700
2	≪10	310	620

ROTHLEIN (1951) has pointed out that surface *p-n* barriers give high photovoltaic response, and that the sensitivity on a signal–noise basis is also good. For the spectral sensitivity, results similar to those of BECKER and FAN (1950) were obtained.

Two types of photoeffect described as 'photodiode' and 'photopeak' have been found by BENZER (1946–7) at metal–germanium contacts. The behaviour is thought to be primarily determined by surface barriers in the material rather than the actual metal–semiconductor junction. The photodiode is so

called because the current through the junction saturates easily in the easy flow direction, the current–voltage curve for the rectifier being reminiscent of a temperature-limited diode. This saturation current is found to be markedly light sensitive, the change in current being linear with illuminating intensity. Typical currents obtained with a unit biased at 2 volts are:

Dark	0·3	0·6	0·9 lm/cm²
2·8	5·6	8·4	11·4 m amp

The quantum efficiency is $\sim 0{\cdot}9$ and the response time 10^{-5} sec. Spectral sensitivity measurements show a maximum at $1{\cdot}3\,\mu$ with rapidly falling sensitivity near $1{\cdot}6\,\mu$. The saturation current varies exponentially with reciprocal temperature, giving an activation energy $E = 0{\cdot}7$ to $0{\cdot}8$ eV.

The photopeak effect occurs at junctions where the voltage which can be maintained in the forward direction is sharply peaked *i.e.* as the forward current is increased the voltage across the junction first increases and then decreases. The latter part of the characteristic therefore corresponds to a negative resistance. The value of the peak voltage is usually 1 to 2 V, although as much as 25 V occurs occasionally. The peak voltage decreases on illumination, the decrease being linear at low intensities. For a sensitive junction $\frac{1}{2}$ lm/cm² is sufficient to remove the voltage peak almost entirely. Rothlein and Stahl (1950) and Stahl (1951) have suggested utilizing this device as a photoswitch or trigger photocell. If the cell is set with a positive bias somewhat below the peak voltage, the current passing will be very small. On illumination such that the peak voltage falls below the steady bias, the unit will be driven into the negative resistance region of the characteristic, and the current will increase until limited by external circuit resistances. Currents large enough to operate relays can easily be obtained in this condition. The rectifying property of the junction may be utilized to obtain the bias from an a.c. supply, in which case the unit is automatically restored to its operating condition when the illumination is removed.

Benzer (1949) has tried to correlate the sensitivity of photovoltaic junctions with the maximum back-voltage which the

unit can withstand. Over a range of > 1,000 : 1, he found the photovoltaic short-circuit current to increase roughly as the cube of the maximum back voltage.

The Phototransistor

The amplifying properties of the transistor can be combined with the photosensitive properties of germanium to give a phototransistor (SHOCKLEY, 1950, SHOCKLEY, SPARKS and TEAL, 1951). In an *n-p-n* transistor for example, the photohole current produced in one of the *n* regions (near the *p-n* boundary) will be amplified so that the collector current is as much as a hundred times greater than the current corresponding to one photohole for each incident radiation quantum*. In similar measurements MCKAY (1951) has found an effective quantum efficiency of 60. SHIVE (1950–51) has described the construction and properties of a coaxial phototransistor. This consists of a germanium wafer which is concave on one surface, the central thickness being about 3×10^{-3} inch. On one side of this thin central part a pointed electrode makes contact. The sensitive area of the device is opposite this electrode on the other side of the wafer, its diameter being $\sim 8 \times 10^{-3}$ inch. The sensitivity of the unit is 70 m amp/lm, the response time being such that there is little loss in signal with light modulated at 200 kc/s. The spectral response curve is similar to that of *Figure 24*.

14.4. CONDUCTIVITY AND HALL EFFECT

The first reliable measurements of the temperature dependence of resistivity of germanium were carried out by BIDWELL (1922). These results received little attention at the time because there was no theory of semiconduction to use in interpreting them. However, when plotted in the now customary manner of log (resistance) against reciprocal temperature, the results fall on a straight line over most of the temperature range as shown by *Figure 25*. From the slope of this line we find the

* SHOCKLEY, SPARKS and TEAL (1951) give the apparent quantum efficiency as $\eta = 1 + L\sigma_e/l\sigma_h$ where L is the diffusion distance for holes in the n region and e is the length of the p region. Now $L^2 = D\tau$, where $D = kTb_h/e$ and $\tau = 1/Bn_e$. Since $n_e = \sigma_e/eb_e$, then $\eta = 1 + 0{\cdot}05(\sigma_e)^{\frac{1}{2}}/\sigma_h l$ for $B = 10^{-11}$ as found above. Hence $\sigma_e = 100$, $\sigma_h = 1$ and $l = \frac{1}{2}$ mm gives $\eta = 100$.

thermal activation energy to be 0·75 eV. At 550°C the value of the resistance from the graph is 1·0 Ω, which, from the dimensions of the specimen used, represents a specific conductivity of 11·2 $\Omega^{-1}\,cm^{-1}$. Putting $\sigma = \sigma_0 \exp(-E/2kT)$ we find $\sigma_0 = 3 \times 10^4\,\Omega^{-1}\,cm^{-1}$. This value emphasizes the very high mobilities found in germanium, and at the same time indicates that the conductivity must be intrinsic.

Measurements by BARDEEN and BRATTAIN (1949) give almost identical results, namely an activation energy $E = 0{\cdot}75$ eV and $\sigma_0 = 3{\cdot}3 \times 10^4\,\Omega^{-1}\,cm^{-1}$, while LARK-HOROVITZ *et alii* (1946) give $E = 0{\cdot}76$ eV, and JOHNSON and FAN (1950) find $E = 0{\cdot}73$ eV. Results given by LARK-

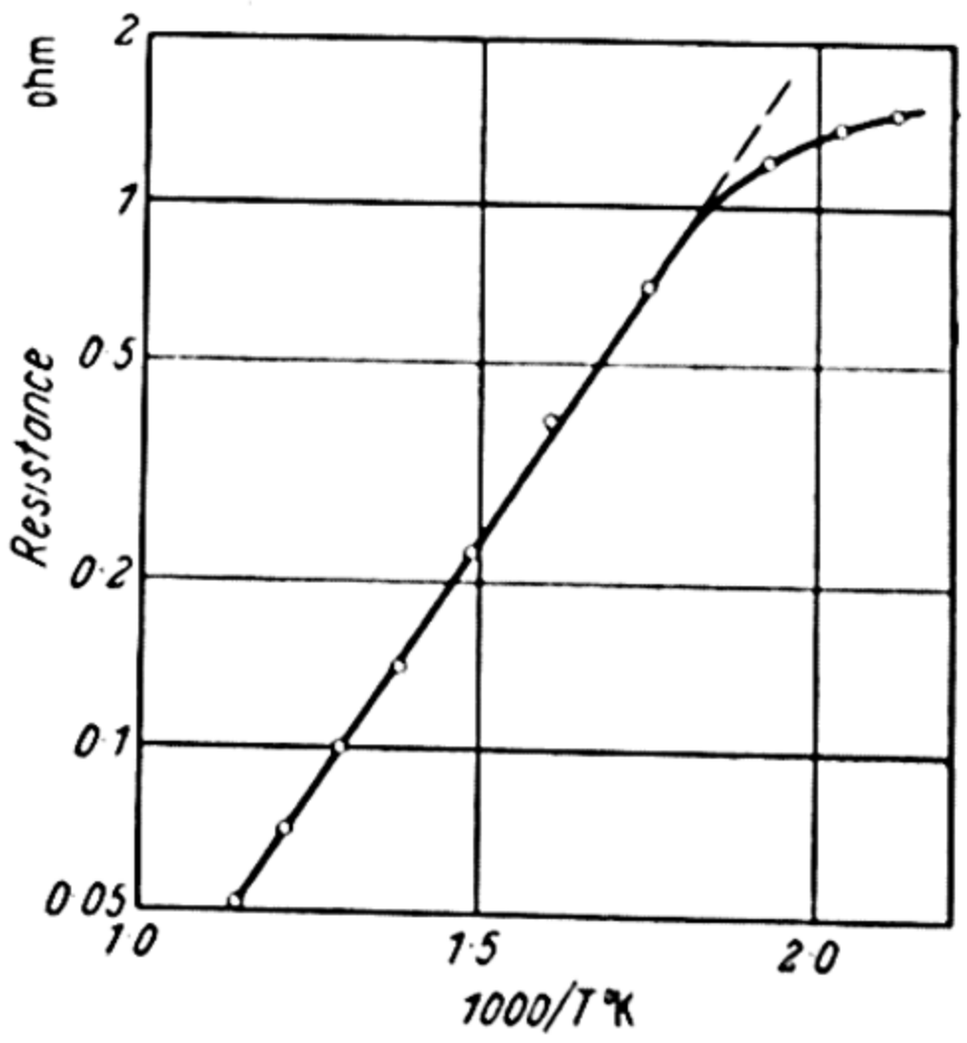

Figure 25. Germanium resistance (*from* BIDWELL)

HOROVITZ (1949) show that the purest samples of germanium are in the intrinsic range for temperatures above about 70°C, the slope of the log (resistance) — $1/T$ curve between this temperature and 650°C giving an activation energy of 0·75 eV. The room temperature resistivity of germanium with and without various concentrations of antimony impurity was :

'*Pure*'	$2{\cdot}5 \times 10^{-7}$	2×10^{-6}	10^{-5} *atoms* Sb/*atom* Ge
5	0·2	0·03	0·008 Ωcm.

DUNLAP (1950) has measured conductivities and Hall constants for high purity germanium crystals, mainly of *p*-type.

Samples were prepared by melting *in vacuo* and then annealing until the characteristics did not change on further annealing. The potential distribution along the samples was found to be linear over lengths of 1 cm or more, thus establishing the homogeneity of the material. The purest specimen had a resistivity of 20 Ω cm, with a density of conducting holes of only $10^{14}/cm^3$. Variation of conductivity with temperature in the intrinsic range corresponded to activation energies of 0·74 eV and 0·755 eV, a similar value resulting from the Hall effect measurements.

For one *p*-type specimen where the Hall coefficient at low temperatures indicated an impurity concentration of $1{\cdot}8 \times 10^{14}/cm^3$, the Hall coefficient reversed sign (*i.e.* passed through zero) at 344°K. A value for the activation energy may be obtained from this data by use of the formula for Hall coefficient given in Chapter 2. The required condition is given by equating the expression for the Hall coefficient in equation 5 to zero *i.e.* $n_e b_e^2 = n_h b_h^2$. If n_i is the density of intrinsic electrons and holes, then $n_i(b_e^2/b_h^2 - 1) = 1{\cdot}8 \times 10^{14}$. Current estimates for the mobility ratio in germanium lie in the range 1·5 : 1 to 2 : 1, so we may take $b_e^2/b_h^2 \sim 3$. Hence $n_i = 9 \times 10^{13}$ at 344°K. Putting $n_i = \Upsilon \exp(-E/2kT)$ where Υ (given by equation 2) has the value $3{\cdot}9 \times 10^{19}$, gives $E = 0{\cdot}75$ eV. From these various values the average thermal activation energy is 0·74 eV.

By extrapolating his intrinsic resistivity values to room temperature, Dunlap estimates the resistivity of ideally pure germanium to be ~ 70 Ω cm at 25°C. As the temperature is raised the conductivity increases until just below the melting point the resistivity is only 800×10^{-6} Ω cm, *i.e.* less than ten times that of bismuth or mercury.

Impurity Conductivity

Below room temperature all samples of germanium exhibit impurity conductivity. Measurements of Hall effect or conductivity by a number of workers all show very low values of activation energy. For temperatures above that of liquid air, Pearson and Shockley (1947) found 0·007 eV. For a similar temperature range Putley (1949) obtained values of 0·03

to 0·038 eV. Between 30°K and 78°K De Sorbo and Dunlap (1951) obtained a considerably higher figure, namely 0·12 eV, and 0·003 eV for temperatures < 30°K. Gerritsen (1949) extended the measurements down to 1·6°K, finding the activation energy to be 0·0055 eV. Hung and Gleissman (1950) found that for their purest samples the activation energy was approximately 0·01 eV, with lower energies for the more impure crystals. Shockley (1950) takes the value to be 0·04 eV. Dunlap (1952) gives 0·003 eV for indium impurity, and 0·03 eV for zinc, for the temperature range 14 to 50°K.

There is thus a wide variation in the reported values. The lowest figures may well result from reduction in the activation energy by interaction between impurity centres, as discussed previously for silicon, and as found experimentally by Hung and Gleissman. Also the high value of 0·12 eV found by De Sorbo and Dunlap is thought to be due to lattice defects, not simple substitutional impurities. The activation energy for this latter type of centre therefore probably lies in the range 0·01 eV to 0·04 eV. For comparison with these figures, the Rydberg energy for the hydrogen atom scaled down in proportion to the square of the dielectric constant is $13{\cdot}5/(16)^2 = 0{\cdot}05$ eV, assuming the effective mass to be that of a free electron.

Even these small activation energies give large variations in resistance at low enough temperatures. For example, Hung and Gleissman (1950) found the resistivity of their purest specimen to be $3 \times 10^7\ \Omega$ cm at 6°K, while Friedberg (1951) has shown that germanium with $\sim 10^{17}$ impurities per cm^3 or iridium makes an accurate resistance thermometer for temperatures between 2 and 4°K.

Mobility

Various different methods of measuring the mobilities of both electrons and positive holes in germanium have now been used. Most results have been deduced from Hall effect and conductivity measurements. Early values given by Bardeen and Brattain (1949), which were $\sim$ 1,000 cm^2/V sec, have been exceeded by a considerable factor since purer crystals

have been obtainable. For their most recent Hall effect values, HAYNES and SHOCKLEY (1951) give $b_e = 2{,}600$ (± 300), $b_h = 1{,}700$ ($+ 500 - 100$) although DUNLAP (1950) finds mobilities up to $b_e = 3{,}200$ and $b_h = 2{,}300$. DUNLAP (1951) also observed some variation of the Hall coefficient with magnetic field, and interpreted this as a dependence of mobility on magnetic field. RINGER and WELKER (1948) investigated *n*-type samples with copper impurities (giving 10^{15} to 10^{22} conduction electrons/cm^3) and found $b_e \simeq 2{,}000$ for the purest crystals.

PEARSON, STRUTHERS and THEUERER (1950) obtained a value for mobility purely from the conductivity of specimens containing radio-active antimony. The impurity concentration was found by Gieger counter measurements, and with the assumption of one conduction electron per antimony atom, the value $b_e \simeq 3{,}000$ was obtained.

Drift mobilities have been measured on germanium filaments for both electrons and holes by SHOCKLEY *et alii* (1949) and HAYNES and SHOCKLEY (1951). They found $b_e = 3{,}600$ and $b_h = 1{,}700$. These latter results are quoted with a tolerance of only ± 5 per cent (for transit distances ~ 1 cm and times of 20 to 60 μ sec), so that they are probably the most accurate values available. Also, drift velocity mobilities are subject to less doubt in their interpretation than Hall effect mobilities. A less direct estimate of hole mobility of $b_h = 1{,}600$ is given by MOORE and HERMAN (1951) from bombardment measurements on metal–germanium contacts.

Extensive studies of the magneto-resistance effect in oriented single crystals of germanium have been reported by PEARSON and SUHL (1951). From the theory of magneto-resistance given by equation 4 the mobility is proportional to $(\Delta\rho/\rho)^{\frac{1}{2}}H^{-1}$ when the magnetic field H is perpendicular to the current, so that this quantity should be invariant with field. At 300°K this was found to be so for fields $\gtrsim 3{,}000$ G. The mobility figures obtained were $b_e \sim 5{,}000$ and $b_h \sim 5{,}800$. Thus although the mobility for electrons is only some 30 per cent above that found by drift measurements, the hole mobility is three times too big relative to the drift mobility. Similar values *i.e.* up to 5,400 were obtained by ESTERMANN and FONER (1950). Pearson and Suhl consider that this discrepancy

is probably caused by non-spherical energy surfaces as discussed by SHOCKLEY (1950).

A limiting value for the sum of the mobilities can be found from photoconductivity measurements. In barrier free conditions where there are no secondary photocurrents the quantum efficiency (η) cannot exceed unity, so that by assuming $\eta = 1$ a minimum value for $b_e + b_h$ is obtained. From GOUCHER's (1950) results $b_e + b_h \not< 5{,}300 \pm 10$ per cent. For vacuum evacuated germanium films, which are always p-type, the mobility is only 1 to 50 cm^2/V sec (THORNHILL and LARK-HOROVITZ, 1951). These various mobility values are summarized in *Table V*:

Table V

	Hall	*Drift*	*Conductivity*	*Magneto-res.*	*Films*	*Photoconductivity*
b_e	2,300–3,200	3,600 ± 200	3,400 ± 400	~5,000	—	Sum $\not<$ 5,300 ± 500
b_h	1,600–2,300	1,700 ± 100	—	~5,800	1–50	

The mobility increases greatly on cooling, values up to 10^5 cm^2/V sec being obtained at liquid helium temperatures. According to the measurements of PEARSON and SUHL (1951), BARDEEN and BRATTAIN (1949) and TORREY and WHITMER (1948), the mobility has a $T^{-3/2}$ temperature dependence, in accordance with theoretical expectations.

In high electric fields germanium no longer obeys Ohm's law due to a falling-off in mobility. RYDER (1951) finds ohmic behaviour only up to 600 V/cm at room temperature, and to 200 V/cm at liquid air temperature. At fields $> 10^4$ V/cm the current saturates at a value which indicates that the electrons have a constant drift velocity $\sim 10^7$ cm/sec. As this is the thermal velocity appropriate to a free electron with kinetic energy of kT, the inference is that the random path followed by the electron in field-free conditions has been 'straightened out' by the high field, so that the electron travels only in the direction of the field, and its drift velocity therefore approaches its actual speed.

14.5. TEMPERATURE DEPENDENCE OF ACTIVATION ENERGY

There are now several ways in which the shift of activation energy with temperature has been measured:

1 Spectral sensitivity curves— From the photovoltaic results of BECKER and FAN (1950) there is a shift between 100°K and 210°K of 0·023 eV, and between 210°K and 293°K of 0·041 eV. These figures, of which the first seems more reliable, correspond to $dE/dT = -2 \times 10^{-4}$ eV/°C, and -5×10^{-4} eV/°C. BARDEEN and SHOCKLEY (1950) quote results deduced from photoconductive measurements in *p-n* junctions as giving approximately the same shift as for silicon, namely $\sim 4 \times 10^{-4}$ eV/°C.

2 Absolute conductivity measurements— Assuming a linear variation of activation energy *i.e.* $E = E_0 + \gamma T$, the normal expression for conductivity becomes $\sigma = \sigma_0 e^{-\gamma/2k} e^{-E/2kT}$. Hence by comparing the observed conductivity with the theoretical value of σ_0, the value of γ can be found. Using the data of BARDEEN and BRATTAIN (1949), $\exp(-\gamma/2k) = 3{\cdot}6$ and hence $\gamma = -2{\cdot}2 \times 10^{-4}$ eV/°C, whilst JOHNSON and FAN (1950) give $\gamma = -1{\cdot}1 \times 10^{-4}$ eV/°C.

3 Change of resistance with pressure— An estimate of the contribution from the lattice dilatation alone may be obtained from this measurement. Putting $r = r_0 \exp(E/2kT)$ we have $dr/r dp = 1/2kT$. The compressibility $c = dV/V dp$, and the coefficient of volume expansion $3\beta = dV/V dT$, so that $(dE/dT)_2 = (dr/r dp)(3\beta/c)\ 2kT$. From measurements by MILLER and TAYLOR (1949) the resistance increase with pressure was such that $dr/r dp = 4 \times 10^{-5}$/atm at 408°K. With $c = 1{\cdot}24 \times 10^{-6}$ (BRIDGMAN, 1949), and $3\beta = 23 \times 10^{-6}$* $(dE/dT)_2 = -0{\cdot}5 \times 10^{-4}$ eV/°C. A later result by TAYLOR (1950) is $dr/r dp = 10^{-4}$/atm at ~ 300°K and therefore $(dE/dT)_2 = -0{\cdot}9 \times 10^{-4}$ eV/°C. Resistance-pressure measurements on a *p-n* junction have been reported by HALL *et alii* (1951). The junction measured was found to obey the theoretical rectifier formula $I/I_0 = \exp(eV/kT) - 1$ accurately,

* A more accurate value has recently been obtained by STRAUMARIS and AKA (1952) by an x-ray method, namely $\beta = 5{\cdot}9 \times 10^{-6}$.

and the pressure dependence was such that $\Delta I_0/I_0 = -1{\cdot}25$ per cent for 1,000 lb/in^2. As shown in § 8.2, I_{10} is proportional to exp $(-E/kT)$ so that $(\Delta I_0/I_0)/(\Delta V/V) = -(\Delta E/kT)/(\Delta V/V)$. Hence $\Delta E/(\Delta V/V) = -4{\cdot}5$ eV or $(\mathrm{d}E/\mathrm{d}T)_2 = -10^{-4}$ eV/°C.

4 Shift of absorption edge— No specific figures have been published for this measurement, but BARDEEN and SHOCKLEY (1950) state that it is about the same as for silicon *i.e.* $\sim 4 \times 10^{-4}$ eV/°C, while FAN (1950) states $-4{\cdot}6 \times 10^{-4}$ eV/°C.

There is thus considerable scatter in the experimental values for the energy shift with temperature, average values being approximately $(\mathrm{d}E/\mathrm{d}T)_2 = -1 \times 10^{-6}$, and $(\mathrm{d}E/\mathrm{d}T)_1 + (\mathrm{d}E/\mathrm{d}T)_2 = -3 \times 10^{-4}$ eV/°C. For comparison with these figures, the calculated shift with dilatation deduced from equation 56 is given by SHOCKLEY and BARDEEN (1950) as $(\mathrm{d}E/\mathrm{d}T)_2 = -0{\cdot}95 \times 10^{-4}$, in good agreement with the experimental value. From equation 55 FAN (1950) calculates $(\mathrm{d}E/\mathrm{d}T)_1 = -0{\cdot}25 \times 10^{-4}$, giving a theoretical total of $-1{\cdot}2 \times 10^{-4}$ eV/°C, which is considerably less than the average experimental value. That this discrepancy may be the fault of inadequate experimental data on effective masses, sound velocities and mobilities rather than the theory, has been emphasized by MUTO and OYAMA (1951). FAN and BECKER (1951) have pointed out that taking m/m_e and m/m_h to be ~ 3 would increase both the calculated shift and the value obtained from the absolute conductivity to $\sim -4 \times 10^{-4}$eV/°C, and thus remove the discrepancies.

It is of interest to estimate on the basis of the above data what the energy shift would be if germanium were compressed until its lattice constant equalled that of silicon. We have $V\mathrm{d}E/\mathrm{d}V = \mathrm{d}r/r\mathrm{d}p \,.\, 2kT/c$, which gives $\Delta E = 4\Delta V/V$ eV. From the lattice constants for silicon and germanium, $\Delta V/V = 11{\cdot}7$ per cent, so that $\Delta E \simeq 0{\cdot}47$ eV. The activation energy of germanium would thus be increased from 0·74 eV to 1·2 eV by this process, and would have a value near to that actually found for silicon. It therefore appears from these rough considerations that if germanium could be compressed to have the same atomic spacing as silicon, its electrical properties would become very similar to those of silicon. From the above

compressibility data, the estimated pressure required would be of the order of 10^5 atmospheres. Such pressures have been attained recently by Bridgman in some of his experiments.

14.6. OPTICAL PROPERTIES

Refractive Index

Precise measurements have been made by BRIGGS (1950) in the infra-red region, using thin prisms of high purity germanium. The results obtained are:

Wavelength (μ)	1·8	2·0	2·2	2·4	2·6
Refractive Index	4·143	4·116	4·092	4·078	4·068

If these results are plotted on the basis of the dispersion formula, which may for simplicity be taken as equation 19, the points are found to lie well on a straight line. Extrapolating to zero frequency gives $n_0 = 4{\cdot}00$, so that the dielectric constant is 16·0. These values are some 6 per cent lower than those previously found by BRATTAIN and BRIGGS (1949) by interference measurements on thin films, although the form of the dispersion curve is approximately the same. It is of interest to note that LARK-HOROVITZ (1942–45) had earlier estimated that the dielectric constant equalled 16, from considerations of the effect of impurity scattering on the mobility. PEARSON *et alii* (1952) find from capacity measurements on *p-n* junctions that $\epsilon = 16{\cdot}1$.

Accurate measurements of reflectivity have been carried out by LARK-HOROVITZ and MEISSNER (1949) at long wavelengths where the germanium is known to be transparent. For the purest material, the value was constant at 37·2 per cent from 8·7 μ to 30 μ. From the Fresnel formula $(n-1)/(n+2) = (0{\cdot}372)^{\frac{1}{2}}$, $n = 4{\cdot}1$. Briggs states that the refractive index *increases* with *rising* temperature, which is the direction which would be expected from the relation $E \propto n^{-4}$ discussed in §9.3.

Absorption Data

Transmission measurements have been carried out on samples of high purity germanium by BECKER and FAN (1949), specimens up to 1·5 cm thick being used. For material of specific resistance 5 Ω cm, the absorption constant lies below 0·1 cm^{-1} over the range 2 μ to 9 μ. This value increases by 10 : 1 for

0·015 Ω cm material. As shown by *Figure 4*, the absorption rises rapidly in the region of 1·7 μ, the threshold wavelength for photoconductivity. Between 1·9 μ and 1·6 μ, the absorption constant rises from $< 1\ cm^{-1}$ to $100\ cm^{-1}$. This range of wavelengths includes the λ_i wavelength found from spectral sensitivity curves.

From measurements on thin films (BRATTAIN and BRIGGS, 1949) the absorption is found to increase at shorter wavelengths, until at 0·6 μ, where there is a maximum in the *nk* curve, the absorption constant is in the region of $10^6\ cm^{-1}$. This is of magnitude to indicate a main lattice absorption, and hence the maximum of the photoconductive effect occurs on the long wavelength edge of the main absorption band. In the region 4 to 12 μ the absorption increases roughly as the square of the wavelength, as expected from theoretical considerations (equation 15), although there is some discrepancy in the absolute magnitude of the absorption. According to BARDEEN (1950) this discrepancy is mostly eliminated if second order transitions are considered *i.e.* transitions where a carrier absorbs a photon and simultaneously absorbs or emits a phonon. Transmission measurements by LORD (1952) show that for the wavelength range 12 to 40 μ, the main absorption band is at $330\ cm^{-1}$, where the absorption constant is $\sim 20\ cm^{-1}$. This wavenumber corresponds to an energy of 0·04 eV, which is in the range of impurity activation energies estimated by thermal measurements.

14.7. SUMMARY AND CONCLUSIONS

At temperatures slightly above room temperature, germanium may be made sufficiently pure to be an intrinsic semiconductor. The width of the forbidden zone as determined by thermal measurements (Hall effect or conductivity) is 0·74 eV.

Both photoconductive and photovoltaic effects have been observed in germanium, the wavelengths of the maxima lying on the long wavelength edge of the main lattice absorption band. From the λ_i values, the optical activation energy is found to be 0·72 to 0·73 eV. There is thus no significant difference in the thermal and optical activation energies for

this material. The energy gap decreases with rising temperature to the extent of $\sim 3 \times 10^{-4}$ eV/°C.

The current carriers have very high mobilities in germanium; values $\sim 3{,}500$ cm sec^{-1}/V cm^{-1} being obtained for electrons, and about half this figure for positive holes. The refractive index is high, the value at long wavelengths, where germanium is highly transparent, being 4·0.

The remarkable properties of germanium which have been discovered but recently, have already been utilized in a variety of ways—mainly for experimental purposes up to the present—of which the following may be mentioned:

i Resistance thermometer at liquid helium temperatures.
ii Magnetic field measurement by Hall effect.
iii Diode detectors and mixers.
iv Transistor amplifiers and oscillators.
v Surge limiter and stabilizer using Zener currents.
vi Optical filter, with cut-off $\sim 1{\cdot}6\ \mu$.
vii Photoconductive and photovoltaic cells, or phototransistors.
viii Photo-triggering device.
ix Counter for α particles.
x Conducting transparent electrode for wavelengths $> 1{\cdot}6\ \mu$.
xi Lenses for infra-red use of very small f number.
xii Delay line for short electrical pulses.
xiii Possible source of monochromatic radiation at $1{\cdot}6\ \mu$.

15

GREY TIN

15.1. GENERAL PROPERTIES

TIN occurs in two allotropic forms. The normal metallic, β form, is stable above 13°C, but if cooled below this temperature it is slowly converted into the grey, α form. Grey tin crystallizes in the diamond lattice with a lattice constant $a = 6{\cdot}49$ Å (BROWNLEE, 1950), from which the calculated density is $5{\cdot}76$ g/cm^3. Little reliable information was available on the electrical properties until measurements were described at the 1950 Reading Conference on Semiconductors. It had previously been established by SHARWIN (1945) that grey tin was not a super-conductor in contrast to the metallic form, and PAULING (1948) had shown that metallic bonding would not be expected in grey tin. BLUM and GORYUNOVA (1950) had also concluded that it was a semiconductor.

Photoconductivity has not so far been reported for grey tin, but in view of the close resemblance between its electrical properties and those of silicon and germanium, it is confidently expected that it will prove to be photoconductive.

15.2. PREPARATION OF GREY TIN

In order to transform pure β-tin into α-tin, it is kept at a low temperature for a matter of days to months. The maximum rate of transition occurs near — 25°C. It has been shown by BUSCH *et alii* (1950 and 1951) that the rate of transition can be increased by the addition of small amounts of aluminium, the optimum concentration being approximately 0·1 per cent. These workers used *Specpure* tin ($\sim$ 0·005 per cent impurity) with and without known additions of aluminium. The tin was rolled into thin strips at a temperature of — 40°C and then stored in high vacuum at — 25°C for the period required to convert it to the α form. The progress of the transition was studied by x-ray photographs.

15.3. ELECTRICAL CONDUCTIVITY AND HALL EFFECT

So far it has not been possible to produce crystals of grey tin, and normally it can only be obtained in powder form. Furthermore it is not possible to compress the powder into pellets or rods because under pressure it reverts to the metallic form. Busch and his co-workers therefore adopted the procedure of measuring the conductivity by observing the increased damping of a tuned circuit when a core of the grey tin powder was

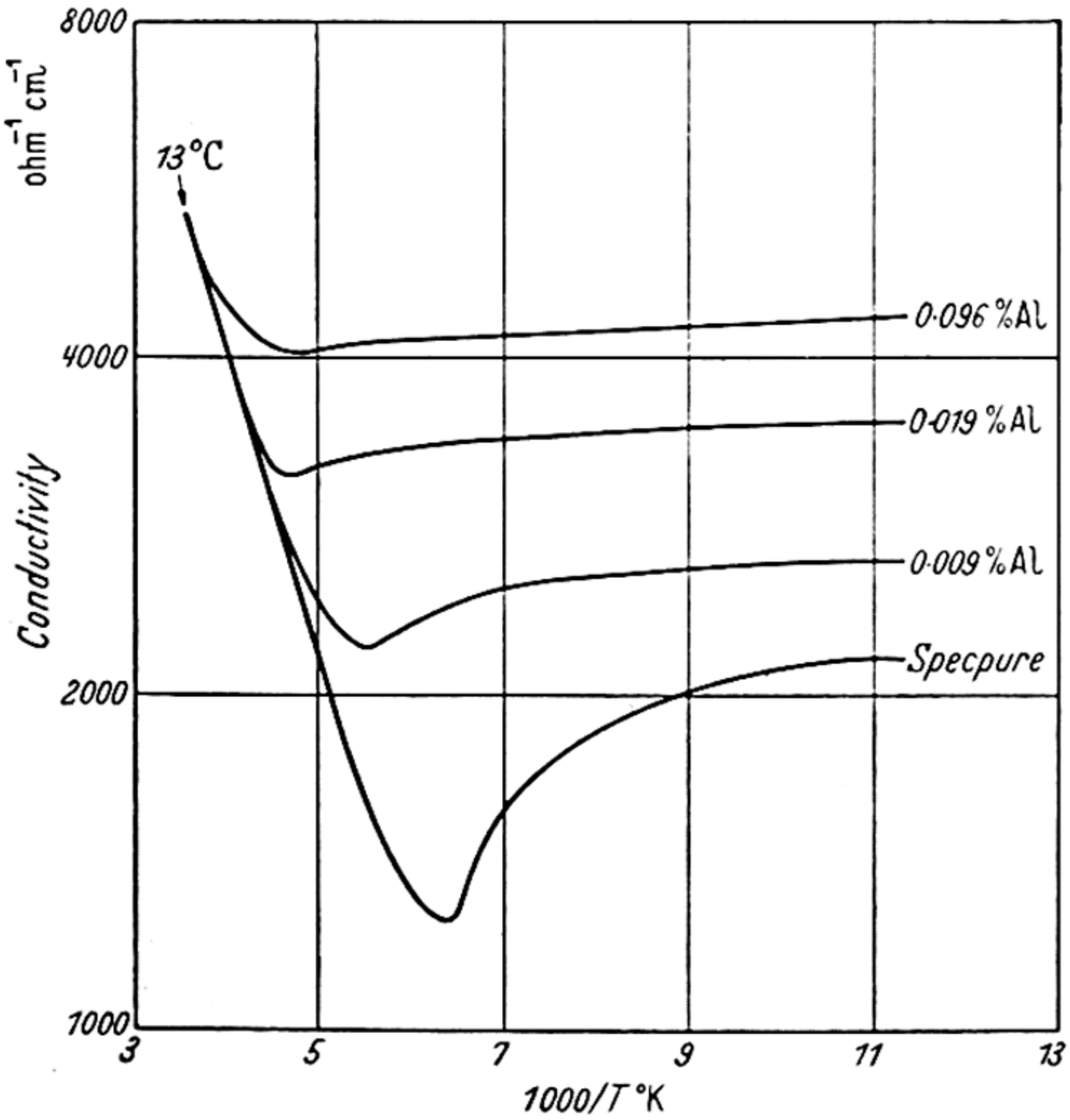

Figure 26. Conductivity of grey tin (Reproduced by kind permission of G. Busch *and his co-workers)*

placed inside the coil. Frequencies of 1 to 50 Mc/s were used for the measurements. In order to calibrate the system, the sample was finally allowed to revert to metallic tin and the damping again measured. If the Q factors for the tuned circuit alone, with β-tin, and with α-tin cores are Q_0, Q_β and Q_α respectively, it may readily be shown that $\sigma_\alpha/\sigma_\beta = (Q_0 - Q_\alpha)/(Q_0 - Q_\beta)$.

The results obtained for the conductivity from liquid air

temperatures to the transition temperature at 13°C are shown in *Figure 26*. At the highest temperatures the conductivities for all samples lie on the same curve, so that the common curve must be that for intrinsic conductivity. For the *Specpure* tin intrinsic conductivity extends down to about — 100°C. From the slope of the curve the intrinsic activation energy is found to be approximately 0·1 eV. The fact that this value is so small explains why intrinsic conductivity can be observed at such very low temperatures. The absolute value of conductivity at 0°C is estimated as 5,000 $\Omega^{-1}cm^{-1}$.

KENDALL (1950) estimates the conductivity to be 2,500 $\Omega^{-1}cm^{-1}$ at 0°C from d.c. measurements on bulk samples. This worker transformed a large mass of *Specpure* tin into the grey form, and succeeded in finding small lumps which could be measured by pressing electrodes against them. The range of intrinsic conductivity was found to extend down to about — 150°C, and from the slope of the log σ — $1/T$ curve the activation energy was again found to be very close to 0·1 eV. As the estimation of absolute conductivity is difficult by either method, the discrepancy of 2:1 is not surprising.

Hall Effect Measurements

To measure the Hall effect, BUSCH *et alii* used the same powdered material pressed lightly into a rectangular insulating box fitted with suitable probes and current electrodes. The contacts were found to be ohmic over the range of currents used, and the chief inaccuracy in the results was due to the difficulty of estimating the current density through the sample. The pure material was found to be an electron conductor throughout, whilst alloys with 0·05 per cent aluminium (or more) were hole conductors. For low concentrations of aluminium, the Hall voltage reversed in sign, showing that although at low temperatures the conductivity was mainly caused by positive holes, at the higher temperatures there was a sufficient number of intrinsic electrons for their higher mobility to dominate the Hall coefficient*.

* For a sample with a low temperature Hall constant of 1·8, the sign reversal occurred at 190°K. This data can be used to estimate the activation energy as in §14.4. Taking $(b_e/b_h)^2 \simeq 3$, the calculated energy is close to 0·1 eV.

The density of conduction electrons was very high, the *Specpure* material having $10^{17}/cm^3$ at 100°K, and almost $10^{20}/cm^3$ at the transition temperature. There is thus considerable degeneracy at these higher temperatures.

Mobility

In view of the possible errors in the values of conductivity and Hall constant, Busch and his co-workers found it more accurate to determine the mobility by measurement of the magneto-resistance effect. To calculate the mobility it is only required to know the *fractional* change of resistance caused by the magnetic field, the absolute resistance being unimportant.

Very high resistance changes were observed, an increase of as much as 3 : 1 occurring in a field of 20,000 G at liquid air temperatures. The fractional resistance change $\Delta\rho/\rho$ was found to be proportional to the square of the magnetic field at low field strengths in accord with theoretical expectations. Equation 4 was used to calculate the mobilities except that the numerical factor of 0·38 was replaced by the older theoretical figure of 0·27. The values obtained ranged from 3,000 cm^2/V sec at the transition temperature to 30,000 cm^2/V sec at 100°K. The simple $T^{-3/2}$ temperature dependence found for silicon and germanium does not seem to be obeyed by grey tin.

Magnetic Susceptibility

Busch and Mooser (1951) have measured the contribution of the free carriers to the magnetic susceptibility. A logarithmic plot of the susceptibility (which is proportional to the carrier concentration) as a function of the reciprocal temperature gives a straight line for the range 100°K to the transition temperature. From the slope the activation energy is found to be 0·1 eV.

15.4. CONCLUSIONS

It is now established that grey tin is an intrinsic semi-conductor above 150°K for the highest purity obtainable. The activation energy has the very low value of 0·1 eV. Figures for the absolute conductivity and for the mobility are subject to

inaccuracies because it has not yet been possible to prepare single crystals.

Photoconductivity has not so far been observed in grey tin, largely because of the experimental difficulties in the production of suitable specimens—efforts to make evaporated films being unsuccessful. The most hopeful method of detecting a photo-effect would seem to be the investigation of metal–semiconductor contacts of the type used for silicon and germanium photodiodes. As a result of the very high concentrations of intrinsic carriers in grey tin even at temperatures as low as that of liquid air, it will probably be necessary to work at liquid hydrogen temperatures to obtain appreciable photo-effects.

It is presumed that under suitable conditions, grey tin would exhibit photoconductivity with a threshold wavelength in the region of 12 μ.

16

PHOSPHORUS

16.1. GENERAL PROPERTIES

THERE is still considerable speculation as to how many of the forms in which phosphorus appears are true allotropic forms. The majority of workers favour reducing the number to three, namely:

1 White or ' Yellow ' Phosphorus
2 Red or Violet Phosphorus
3 Black Phosphorus

Of these, the first is the ordinary so-called yellow phosphorus which melts at 44°C. In the purest state, and if kept in a dark room in absence of oxygen, this form is quite colourless (WOLF and RISTAU, 1925). The yellow colour rapidly appears on exposure to light or x-rays, or on heating. According to BRIDGMAN (1914 and 1916) yellow phosphorus itself consists of α and β modifications, with a transition temperature of −77°C under a pressure of 11,000 Kg/cm^2, the β form being hexagonal while the ordinary, α form is cubic. SUGAWARA *et alii* (1949) report that the β form is birefringent, and the α form isotropic.

Yellow phosphorus may be converted to the red form by heating in the absence of air. Various workers quote different amounts of heating, but 24 hours at 240°C seems a fair average, and the change is said to proceed fairly rapidly at 280°C. When the reaction has gone to completion the product is violet phosphorus—samples of varying degrees of redness consisting of various mixtures of yellow and violet phosphorus. It is difficult to obtain pure red or violet phosphorus without any of the yellow form present.

Black phosphorus was produced by Bridgman by heating yellow phosphorus to 200°C under a pressure of 13,000 Kg/cm^2. This allotrope is semi-metallic in nature.

The only measurements given in the literature for the conductivity of white phosphorus are those by FOUSSEREAU

(1883–5), who found a specific resistance of 10^{11} Ωcm at 11°C, and 3×10^{10}/ Ωcm at 34°C. No conductivity measurements for red phosphorus have been published, and there is no recorded information on photoconductivity in any of the allotropic forms.

Measurements are now described on the conductivity of both white and red phosphorus, and of photoconductivity in the latter.

16.2. EXPERIMENTAL DETAILS OF CONDUCTIVITY AND PHOTOCONDUCTIVITY MEASUREMENTS

The main experimental interest was in red phosphorus, as this has the higher refractive index (see RETGERS, 1893) and should be photoconductive at longer wavelengths. This means a lower activation energy, which might therefore be more easily determined from resistance–temperature measurements. Since white phosphorus melts at 44°C, and must have a high activation energy, as it only absorbs in the ultra-violet, it would be extremely difficult to measure it in the range of intrinsic conductivity. Also red or violet phosphorus is the form corresponding to the grey photoconductive form of arsenic (see for example PARTINGTON, 1949), so that when comparing these two to see the effect of position in the periodic table, it is the red form of phosphorus which should be considered. In the experiments performed, no photoconductivity was ever found in ordinary white or yellow phosphorus. Irradiation by powerful ultra-violet sources was not tried, so it is still possible that yellow phosphorus would be photoconductive under these conditions.

Phosphorus is a difficult material to deal with experimentally for the following reasons:

a Yellow phosphorus, which is the usual starting material, burns spontaneously in air, so that it is difficult to seal it into a cell and evacuate before much oxidation occurs. When baking to convert to the red form, it is necessary to heat above the boiling point in order to operate at an efficient transition temperature, and as phosphorus vapour ignites spontaneously on contact with air at this temperature, the risk of explosion has to be contended with.

b Yellow phosphorus has such a high vapour pressure that it is not possible to outgas at much above room temperature. Usually a temperature just above the melting point was used (*i.e.* $\sim 50°C$). Even prolonged pumping at room temperature is not possible, since in a good vacuum, a cubic centimetre of yellow phosphorus can be pumped away in a few hours.

c The isolation of allotropic forms is difficult.

d Both yellow and red phosphorus are near insulators, which increases the difficulties of carrying out electrical measurements. In order to plot spectral sensitivity curves it was often necessary to measure photocurrents little greater than 10^{-13} amp.

Because of the low conductivity of phosphorus, a high impedance current amplifier was used for measurements on the various experimental cells. This consisted of two valves designed to have very low grid currents, used in a balanced cathode follower circuit. The amplifier had a current gain of 3×10^4, so that when a sensitive galvanometer was used on the output, currents down to 10^{-13} amp could be measured. Voltages in the region 200 to 400 V were generally applied to the cells, so that measurements could be made of resistances $> 10^{15}\,\Omega$. The use of insulation was avoided wherever possible, paraffin wax being used when necessary. The apparatus—including cell and batteries—was screened, and a heater was provided inside the screening box to keep the surfaces dry.

For photoconductivity measurements, the cells were mounted with the sensitive layer near a hole in the wall of the screening box, through which radiation could be directed on to the layer. The hole was covered by a glass plate to prevent draughts affecting the layer temperature, and by copper gauze, since the cell, being of such a high impedance, was very sensitive to electrostatic pick-up. The galvanometers used had fairly rapid response times, and measurements of photoconductivity were made as quickly as possible in order to minimise thermal drifts.

Cells were normally made in *Pyrex* envelopes fitted with tungsten electrodes which were glassed over a length of one or two inches external to the cell wall, to give better insulation. These leads were waxed after preparing the layers to reduce surface leakage currents.

16.3. RESISTIVITY OF YELLOW PHOSPHORUS

Cell 1

The first cell was designed to measure the specific resistance of yellow or white phosphorus. It was fitted with two circular nickel electrodes of 2·3 cm diameter and 1·4 mm separation. The phosphorus was outgassed at 50°C, and after sealing-off the cell from the vacuum system the liquid phosphorus was allowed to run between the plates and solidify. At 17°C, the layer resistance was $2{\cdot}3 \times 10^{13}\,\Omega$, giving a resistivity $\rho = 7 \times 10^{14}\Omega$cm. This is considered to be a representative value for the specific resistance of yellow (*i.e.* almost colourless) phosphorus.

The only previous measurements which appear in the literature are those of FOUSSEREAU (1883 and 1885), who found a specific resistance of $8{\cdot}4 \times 10^{10}\,\Omega$ at 15°C. Foussereau's measurement was not made *in vacuo*, and it is thus likely that the value of resistance he found is much too low. Vacuum distillation of phosphorus to make it completely colourless might give an even higher resistivity than that found above.

16.4. PHOTOCONDUCTIVITY IN RED PHOSPHORUS

Cell 2

Attempts were now made to form layers of yellow phosphorus, and convert them to red phosphorus by baking at temperatures near the boiling point *i.e.* 280°C. A layer of yellow phosphorus ~ 1 mm thick was formed *in vacuo* in a cell as illustrated in *Figure 13*c. This was then baked in the sealed-off state for 1 hour at 300°C. This procedure gave a layer of a definite red colour.

The layer dimensions were 9 mm wide, 1·1 mm between electrodes, and 1 mm thick, so that the measured resistance of $5 \times 10^{13}\,\Omega$ indicated a resistivity of $4 \times 10^{13}\,\Omega$cm. The layer showed considerable photosensitivity, the resistance falling by 20 times under the illumination from a 100 W lamp at a distance of 50 cm *i.e.* about 300 μW total radiation falling on the layer. The sensitivity to a.c. illumination at 80 c/s was very poor (possibly due in part to the fact that the amplifier used was not suitable for use with such high impedance cells), and only d.c. measurements were carried out.

Spectral sensitivity— Although the photocurrents were very small, it was possible to plot spectral sensitivity curves for the cell over the wavelength range 0·38 to 1·2 μ, using a rock-salt prism monochromator. Readings were taken zero–signal–zero as quickly as possible to minimize changes due to thermal effects which were apparent in the long wavelength region where there was high energy falling on the cell but little photoconductivity. The results are plotted as the ratio (photocurrent)/(incident intensity) in *Figure 27*a. It will be seen that the sensitivity falls by almost one thousand times between the wavelength of maximum sensitivity at 0·4μ, and 1·1μ.

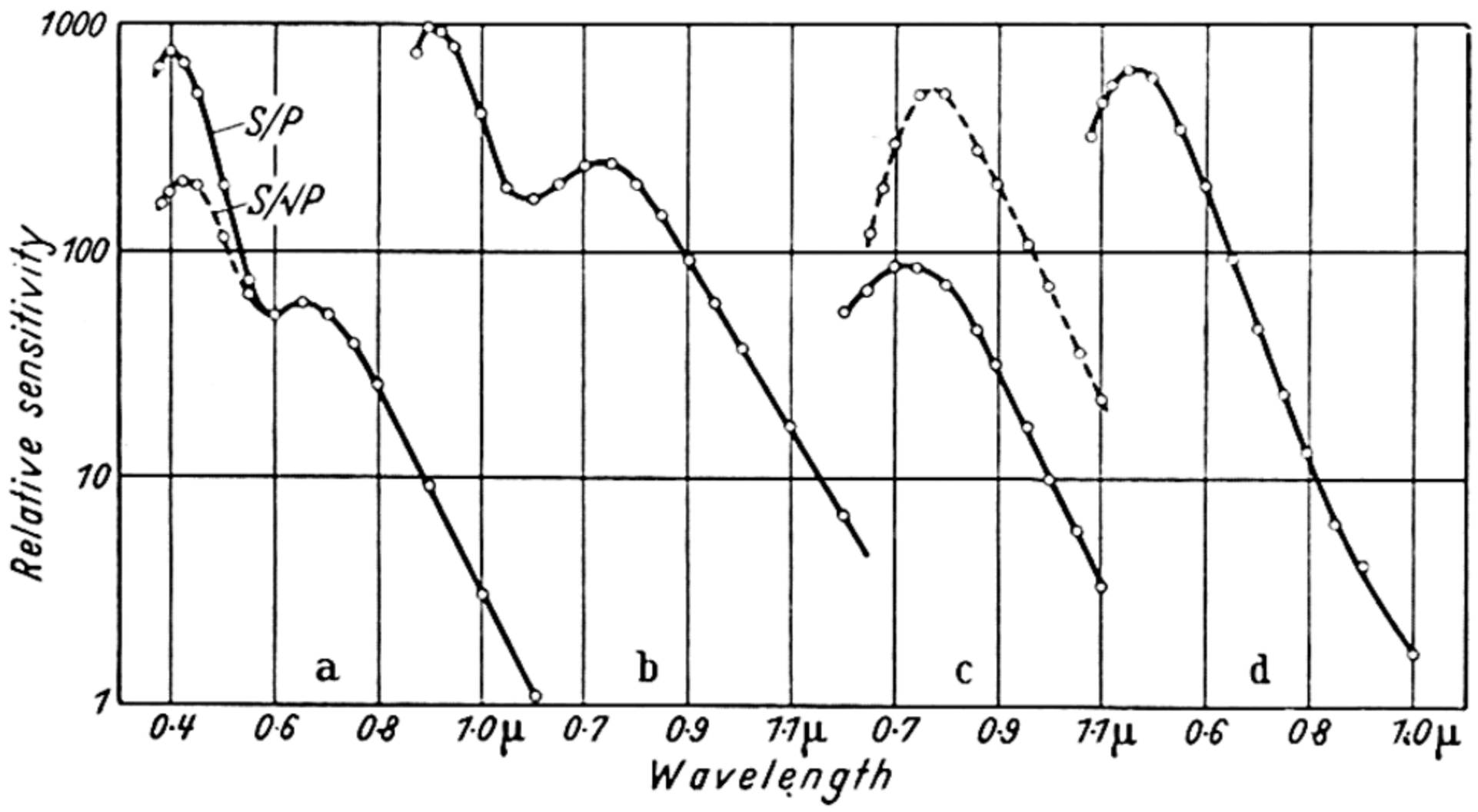

Figure 27. Spectral sensitivity curves for phosphorus

Two bands of sensitivity are clearly indicated, and both have approximately exponential falls on the long wavelength side. The wavelengths of half maximum sensitivity are $\lambda_{\frac{1}{2}} = 0{\cdot}48\,\mu$ and $0{\cdot}79\,\mu$, the corresponding energy figures being 2·6 and 1·56 eV. It would seem probable that the $0{\cdot}79\,\mu$ band arises from the red phosphorus, while the $0{\cdot}48\,\mu$ band is perhaps due to the yellow form.

Photocurrent–intensity measurements— The photocurrent was measured as a function of the radiation incident on the layer. A tungsten lamp operating at its normal temperature of approximately 2,500°C, was used as the source. The results obtained

are plotted on logarithmic scales in *Figure 28*, curve *A*. It will be seen that the points lie on a straight line of slope 0·68; so that Signal ∝ (Power)$^{0\cdot68}$. According to the simple recombination theory of § 6.1, the relation should be Signal ∝ Power at low energy levels, and Signal ∝ (Power)$^{\frac{1}{2}}$ at high levels, with an appropriate transition region between the two.

Further measurements were carried out using a sodium discharge lamp, to see whether the simple recombination relations would hold with monochromatic light. The results are shown in curve *B* of *Figure 28*. The graph is a straight line of slope very close to unity, thus showing that in this case the simple linear relation is obeyed. Presumably the relation

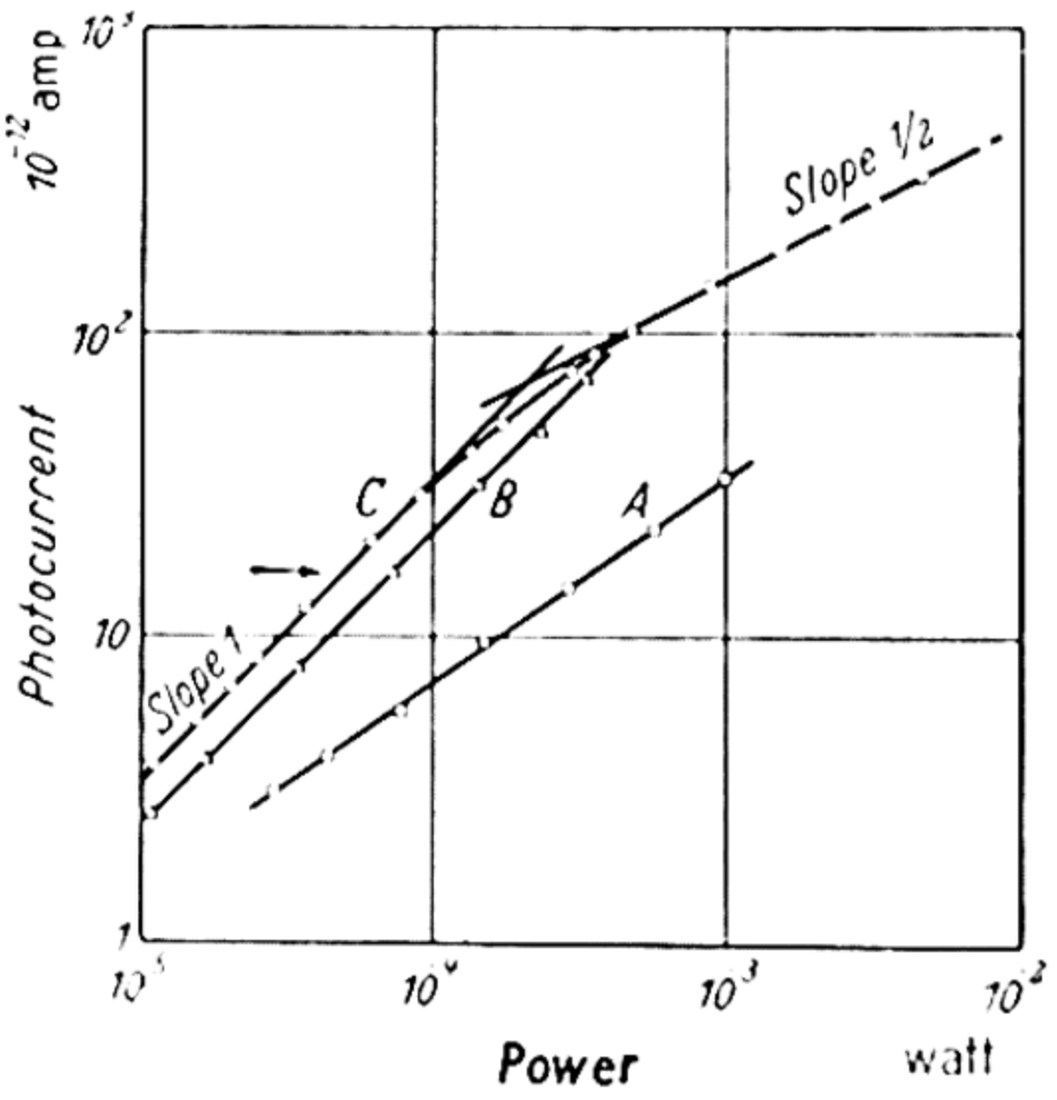

Figure 28. Intensity dependence of photocurrent in phosphorus

would become a (Power)$^{\frac{1}{2}}$ law at sufficiently intense illumination, but there was no sign of this occurring within the range of intensities which could be used. On extrapolation to lower powers the two curves would intersect at a level of 0·5 μW. For powers of this order a linear signal–intensity law would be expected even with the tungsten lamp source, but the sensitivity of the cell was inadequate to carry out measurements at such low levels.

From the experiment using the sodium light, it is clear that the cell response is linear with intensity up to at least 100 μW incident on the layer. The response would be expected to follow a linear law at wavelengths longer than 0·589 μ, as the absorption constant for the material should decrease with

increasing wavelength, and the *density* of photoelectrons in the layer should therefore decrease. At shorter wavelengths however, the absorption constant would be expected to rise, giving a high density of photoelectrons in a thin surface layer. In view of the theory of Chapter 6, this would lead to a (Power)$^{\frac{1}{2}}$ law at much lower powers.

Hence the spectral sensitivity curve of *Figure 27*a is effectively an equal-intensity spectral sensitivity curve for long wavelengths, but for short wavelengths it would be preferable to plot (photocurrent)/(Power)$^{\frac{1}{2}}$. This curve is shown dotted in *Figure 27*a. It will be observed that although this procedure alters the peak sensitivity considerably, it merely increases $\lambda_{\frac{1}{2}}$ from 0·48 to 0·51. As the (Power)$^{\frac{1}{2}}$ law may only apply at wavelengths $\ll 0{\cdot}589\ \mu$, the true equal-energy curve will lie somewhere between the two shown, so that $0{\cdot}51\ \mu > \lambda_{\frac{1}{2}} > 0{\cdot}48\ \mu$.

This cell was baked for a further four hours at 300°C. The resulting layer was a very deep red colour—almost black—and showed greater photoconductivity. The resistance of the cell at 18°C corresponded to a specific resistance of $9 \times 10^{12}\ \Omega$ *i.e.* about a quarter of its previous value. This would indicate that a greater proportion of the material had now been converted to red phosphorus, as confirmed by the colour of the layer. The photosensitivity was such that 56 μW radiation from the sodium lamp incident on the layer gave a photocurrent of 3×10^{-11} amp with 2,700 V/cm field. This is equivalent to a transfer of one electron fully across the layer per 10^6 incident quanta.

The spectral sensitivity curve was measured again, with the results shown in *Figure 27*b. The two bands of sensitivity have become more clearly separated, there being a marked dip between them in the region of 0·6 μ. The threshold wavelengths are found to be $\lambda_{\frac{1}{2}} = 0{\cdot}49$ and 0·86 μ, so that there is some shift to longer wavelengths of the long wavelength band, presumably due to the greater proportion of red phosphorus present.

The cell was baked for a further six hours at 300°C, and the spectral sensitivity measurements repeated. There was little change in the results, the new $\lambda_{\frac{1}{2}}$ values being 0·86 μ and 0·50 μ.

Cell 3

This cell was again of the type shown in *Figure 13*c. A layer of yellow phosphorus was formed initially. Its resistance was $6 \times 10^{14}\,\Omega$ for electrodes $9 \times 1{\cdot}2\ \text{mm}^2$ and layer thickness 1·5 mm, corresponding to a resistivity of $6 \times 10^{14}\,\Omega\text{cm}$. The cell was baked for 30 minutes at 310°C, after which the layer was a dark red colour. The spectral sensitivity curve had a maximum at 0·43 μ, where the sensitivity was 1,000 times greater than at 1·1 μ. The $\lambda_{\frac{1}{2}}$ values were 0·50 μ and 0·83 μ.

Cell 4

A layer of yellow phosphorus was formed as before, and converted to a deep red colour by baking for five hours at 315°C. The resistance of the layer was $3{\cdot}1 \times 10^{11}\,\Omega$ in the dark, and about half this when illuminated by a 100 W lamp held near to the layer.

Spectral sensitivity measurements could only be extended over the wavelength range 0·6 to 1·1 μ, the results being shown in *Figure 27*c. Only the long wavelength band of sensitivity therefore appears. However, had the sensitivity increased with decreasing wavelength as in earlier cells it would have been possible to extend the measurements to shorter wavelengths. We may therefore conclude that the short wavelength band of sensitivity is absent in this cell—or at least of relatively low intensity. From the curve we find $\lambda_{\frac{1}{2}} = 0{\cdot}85\ \mu$.

Photocurrent–intensity relation— The results obtained for the intensity dependence of the photocurrent, using a tungsten lamp source, are shown in *Figure 28*, curve *C*. This is the most rational signal–power curve obtained with any of the phosphorus cells, as it shows clearly a region of photocurrent proportional to radiant energy at low levels, and photocurrent proportional to (Power)$^{\frac{1}{2}}$ at high levels. The reason for this simplified behaviour is presumably the fact that only the long wavelength band of photoconductivity is present in this cell.

The arrow in *Figure 28* indicates the maximum photocurrent from the cell in the spectral sensitivity measurements, under the same conditions of temperature and applied voltage. As this is well within the linear range, the spectral sensitivity curve plotted can be taken as an equal-intensity curve. These

measurements add support to the suggestion made previously, that at wavelengths greater than that of sodium light the cell response would be linear for the range of energies used in the spectral sensitivity measurements.

This cell was given a further baking of four hours at 315°C, and spectral sensitivity measurements repeated. The results are given by the broken curve in *Figure 27*c. Again only the one band of sensitivity appears, with the slightly greater threshold wavelength of $\lambda_{\frac{1}{2}} = 0{\cdot}89\ \mu$.

Cell 5

This cell was made by evaporation of violet phosphorus from a tungsten heater, in a cell blank as shown in *Figure 13*a. It had previously been found impossible to evaporate violet phosphorus at temperatures below the softening point of Pyrex. Accordingly a small quartz crucible was made to hold the phosphorus, the crucible fitting closely into the tungsten heater. The cell and phosphorus were outgassed for some hours at 250°C. This baking should also have removed any white phosphorus still present in the violet. In order to prevent the deposition of any white phosphorus that might be formed during the evaporation, the whole cell was maintained at 250°C, and pumped continuously throughout the evaporation. A clear yellow layer was formed. To verify that this was not due to the ordinary yellow-white phosphorus, the cell was baked at 320°C (*i.e.* well above the white phosphorus boiling point) for 40 minutes. No perceptible change resulted.

The cell was photosensitive. At 25°C the dark resistance was $2{\cdot}5 \times 10^{12}\ \Omega$, and when illuminated by a 100 W lamp held close to the cell it fell to $5{\cdot}5 \times 10^{11}\ \Omega$. Using a sensitive galvanometer in conjunction with the current amplifier it was possible to plot the spectral sensitivity curve over a wide range of sensitivity, as shown by *Figure 27*d. For this cell only one band of sensitivity appears, the sensitivity falling roughly exponentially for $\lambda > 0{\cdot}5\ \mu$. The threshold wavelength $\lambda_{\frac{1}{2}} = 0{\cdot}55$.

Measurements of the dependence of the d.c. photocurrent on the incident energy were carried out using a tungsten lamp as source. The resulting points lay on a line of slope 0·66 on a log–log plot for photocurrents between 5×10^{-11} amp and

10^{-9} amp. For the same range of photocurrents using a sodium lamp however, the points lay on a line of slope unity over almost the whole range.

16.5. RESISTANCE–TEMPERATURE MEASUREMENTS

Cell 5

As this cell was stable at relatively high temperatures, it was possible to measure the resistance variation over several decades. Measurements, which were taken over the range 40°C to 160°C, were quite repeatable.

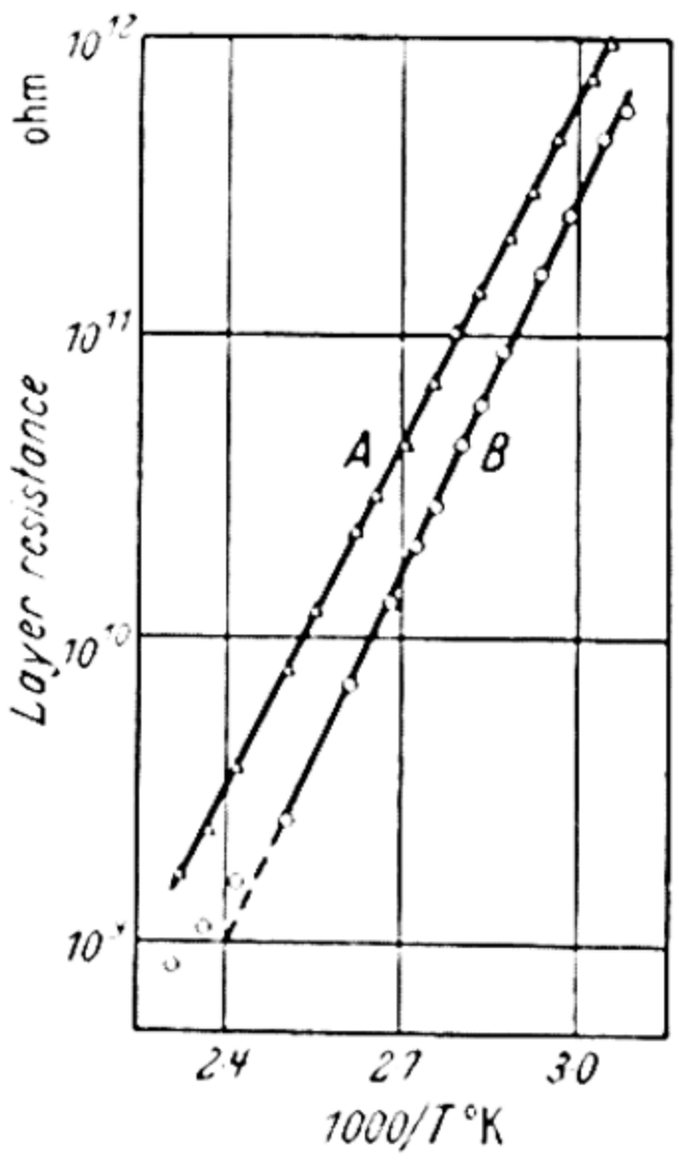

Figure 29. Resistance of red phosphorus

The results are plotted in *Figure 29* (curve *A*), from which it may be seen that the points fall on a straight line over the whole range. The slope of the line indicates an activation energy of 1·5 eV. This is equivalent to the quantum energy at a wavelength of 0·83 μ, which is near to the threshold wavelengths found for the ' red ' phosphorus band of sensitivity in earlier cells. The band does not appear in the spectral sensitivity curve of this cell, possibly because the concentration of levels with this activation energy is low compared with those of 2·2 eV (0·55 μ), so that the effect is not observed in the photoconductivity. However, even 1 per cent of levels of 1·5 eV would control the resistance–temperature curve for all temperatures up to about 1,700°C. Hence it would seem that both

optical and thermal measurements ascribe an activation energy of approximately 1·5 eV to the red phosphorus.

After the above measurements had been completed, the cell was baked for a further 24 hours at 280°C. No appreciable change in the layer occurred, so that the material must be quite stable at this temperature.

Cell 6

This cell was again of the Dewar flask type. The layer was formed by evaporating violet phosphorus electrically, the cell being maintained at 270°C during the evaporation. A clear yellow film was again formed. The layer showed little sensitivity, and no photoconductive measurements were attempted, but measurements were carried out on the temperature dependence of the resistance.

The results obtained are shown in *Figure 29*, curve *B*, from which it will be seen that the plotted points lie on a straight line over a range of resistance of more than 100 : 1. The slope of the line is 0·8 eV, indicating a thermal activation energy of 1·6 eV. At 52°C, the lowest temperature point plotted, the resistance of the layer was $5{\cdot}7 \times 10^{11}\,\Omega$. With the thickness assumed to be 10 μ, this gives $\rho = 2{\cdot}3 \times 10^{9}\,\Omega$cm. Thus taking $\sigma \sim 10^{3} \exp(-E/2kT)$ gives $E = 1{\cdot}58$ eV, which is in agreement with the value obtained from the slope.

Cell 2

Over a small temperature range, resistance measurements gave an activation energy of 1·55 eV for this cell.

16.6. TRANSMISSION MEASUREMENTS

Bulk Sample

The first set of transmission measurements were carried out on a sample of red phosphorus taken from cell 2 after the other measurements had been completed. The material was ground down to a thickness of 0·3 mm, and lightly polished. Initially measurements were carried out using chopped radiation and a PbS cell as detector. This system gave good results at relatively long wavelengths, but when measuring the intense absorption found in the near visible region, trouble was encountered due to

scatter of long wavelength radiation in the spectrometer. By using water filters to cut out radiation of wavelength $> 1{\cdot}3\ \mu$, reasonable results could be obtained down to about $0{\cdot}9\ \mu$. To carry the measurements to shorter wavelengths, a photocell of the Cs–Ag–O type was used as detector. Results were then obtained down to $0{\cdot}7\ \mu$, where the absorption approached $10^5 : 1$.

The results are shown in *Figure 30*, where the curve *A* is drawn between the two sets of points measured with the two types of detector. At $0{\cdot}9\ \mu$ the absorption deduced from the PbS cell results will be too small due to scatter of long wavelength radiation when the sample is in position, and similarly the absorption deduced from the photocell measurements will be too great as a result of scatter of short wavelength light with the sample out.

The absorption value found in the $2\ \mu$ region is $\sim 5 : 1$, but this includes reflection losses at both surfaces of the sample. This result is in accord with the observations of COBLENTZ (1908) that there is little absorption between $1\ \mu$ and $8\ \mu$. At $0{\cdot}7\ \mu$ the absorption constant is $400\ \text{cm}^{-1}$, which is still far below the normal values for the centre of a main lattice absorption band.

Measurements on an Evaporated Layer

This layer was of the yellow type obtained by evaporation of violet phosphorus on to a hot substrate. It was stable at 300°C. As the layer was much thinner than the plate previously measured, results were obtained at shorter wavelengths. A Cs–Ag–O photocell was used for the range $0{\cdot}54\ \mu$ to $1{\cdot}1\ \mu$. However, at shorter wavelengths, scatter was again introducing inaccuracies, and accordingly a Cs–Sb photocell was used for the region $0{\cdot}48$ to $0{\cdot}6\ \mu$. The measured absorption is shown in *Figure 30*, curve *B*.

There are signs of two absorption bands. The main band lies beyond the short wave limit of measurements, while a slight hump in the $0{\cdot}8\ \mu$ region indicates the presence of a second band. These two bands are presumably related to the two bands of photoconductivity. The thickness of the film was determined by weighing, the value obtained being approximately $3\ \mu$. Hence at $0{\cdot}48\ \mu$, $K = 2 \times 10^4\ \text{cm}^{-1}$.

16.7. REFRACTIVE INDEX AND DIELECTRIC CONSTANT

Yellow Phosphorus

The refractive index of yellow phosphorus is > 2, which is the criterion for photoconductivity. Precise measurements of

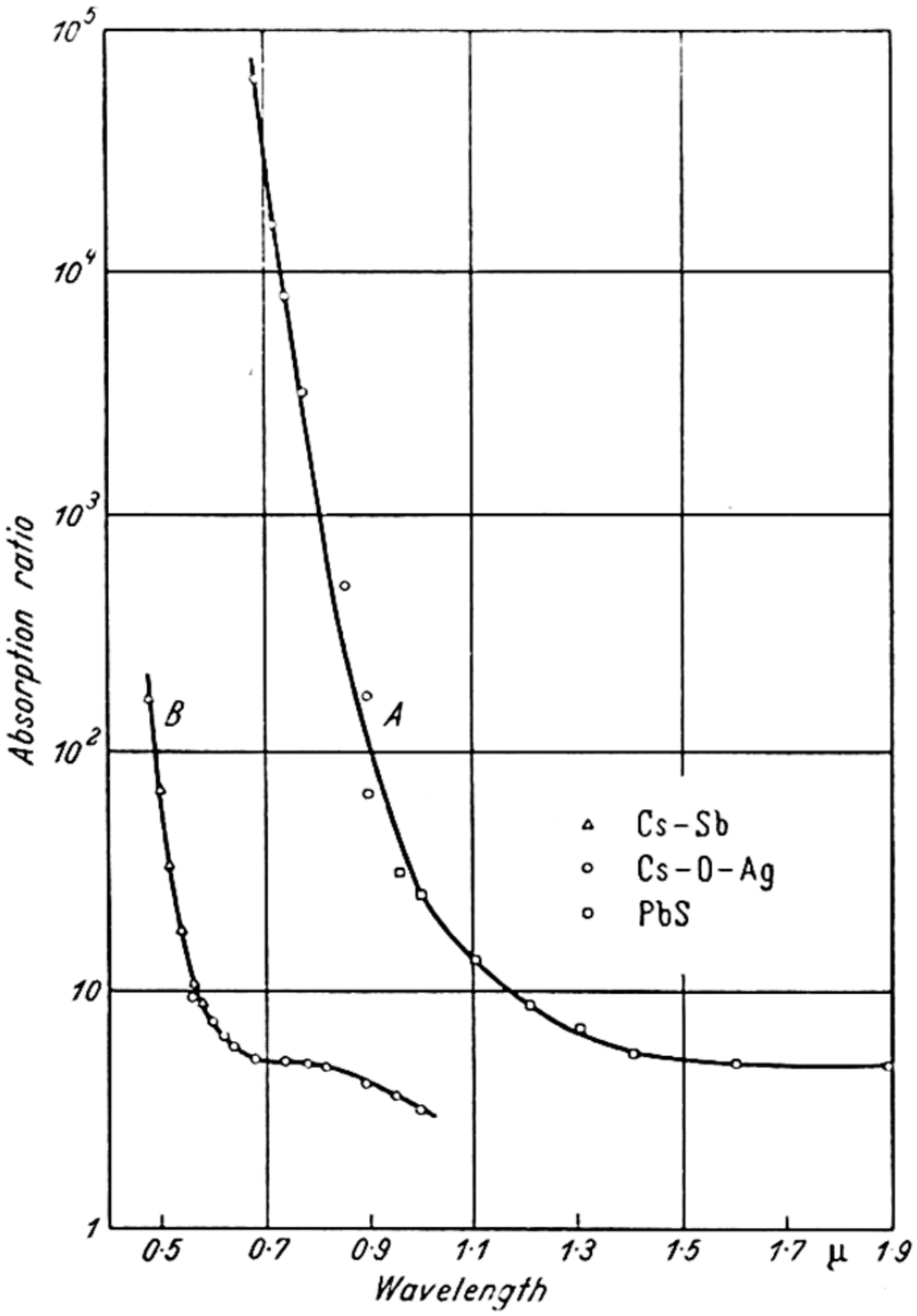

Figure 30. Phosphorus absorption: A, 0·3 mm plate; B, 3 μ film

the refractive index were carried out by DAMIEN (1881), the results obtained being given in *Table VI.*

Table VI

		0·4342μ	0·4844μ	0·6566μ	*Density*
Solid	29·2°C	2·19885	2·15831	2·09300	1·8244
	34·7°C	2·19748	2·15766	2·09154	1·8209
	37·5°C	2·19462	2·15388	2·08873	1·8191
Liquid	37·5°C	2·15634	2·11675	2·05370	1·7616

Plotting the values at 29·2°C according to equation 19 the three points are found to lie on a straight line, and by extrapolating to $\lambda = \infty$ it is found that $n_0^2 = 4{\cdot}094$. This value should equal the dielectric constant for low frequency fields, since the material is non-polar. According to SCHLUNDT (1904) the value of the dielectric constant is 4·1, so that this element provides an excellent check on Maxwell's theory.

The measurements of variation of index with temperature are the most comprehensive in the literature for a non-polar material with $n > 2$, and it is instructive to see if the material obeys the LORENTZ-LORENZ formula: $(n^2-1)/(n^2+2) \propto$ density. Differentiating gives $\delta n = \{(n^2+2)(n^2-1)/6ng\}\ \delta g$, where g = density.

The observed change in refractive index at 0·656 μ is 0·0043 for the 29·2°C to 37·5°C range, compared with the calculated value of 0·0050, so the agreement is fairly good. For the much greater change of density on melting, the refractive index change is calculated to be 0·055. This is considerably larger than the observed change of 0·035.

Red Phosphorus

The dielectric constant was measured at radio frequencies, using a small condenser made from a piece of the bulk red phosphorus from cell 2. The material was ground down to 0·27 mm thickness, and to a rectangular shape of area 17·7 mm². *Aquadag* electrodes were painted over both surfaces and the capacity measured at frequencies of 100 kc/s and 400 kc/s by use of the tuned circuit and calibrated condenser in a standard Q meter. The capacity at both frequencies was found to be 3·9 $\mu\mu$F. Hence $\epsilon = 6{\cdot}7$.

As the Maxwell relation $n_0^2 = \epsilon$ is found to be correct for yellow phosphorus, and should in fact hold for all monatomic solids, it is justifiable to put $n_0^2 = 6{\cdot}7$ for red phosphorus, giving $n_0 = 2{\cdot}6$.

16.8. SUMMARY AND CONCLUSIONS

Photoconductivity

Photoconductivity has now been observed in red phosphorus, but not in ordinary yellow phosphorus. The photocurrents

are small; in the region of 10^{-13} to 10^{-9} amp. Two bands of photoconductivity appear, possibly pertaining to two allotropic forms. One band has its peak in the blue region, the other in the very near infra-red region of the spectrum. For the short wavelength band, the measured $\lambda_{\frac{1}{2}}$ values are 0·48 μ, 0·49 μ, 0·50 μ, 0·50 μ and 0·55 μ, giving an average of 0·50 μ or 2·47 eV. The values found for the threshold wavelength for the red phosphorus band of sensitivity are, 0·79 μ, 0·86 μ, 0·86 μ, 0·83 μ, 0·85 μ and 0·89 μ, giving an average of 0·85 μ or 1·45 eV.

The relation between the energy falling on the cell and photocurrent produced, though at first appearing complicated was found to be explicable on the basis of the recombination theory of photo-response. In particular, with monochromatic sodium light, all cells gave a linear response at low light levels, and some cells gave a (Power)$^{\frac{1}{2}}$ law at high levels. These simple laws were also obeyed by one cell with a white light source, this cell being unique in that it showed only the long wavelength band of photoconductivity. We may thus conclude that for $\lambda \geqslant 0{\cdot}589$ μ where the absorption is not very intense, linear response occurs for not too large intensities; while in the short wavelength, high absorption region, a square root relation holds. For a white light source the result will in general be a compromise between the two. It may readily be verified that on a log–log plot of the simple function $P + \sqrt{P}$ the points lie very close to a straight line of slope 0·67 for $1 > P > 0{\cdot}05$, *i.e.* just the slope observed in many of the experiments with white light sources.

Resistivity and Resistance–Temperature Measurements

The specific resistance of yellow phosphorus was found to be $7 \times 10^{14}\ \Omega$cm. If we assume that this represents an intrinsic semiconductor, then we may put $\sigma = A\, e^{-E/2kT}$, where A is $\sim 10^3$ for average mobilities. Hence $E = 2{\cdot}1$ eV. Thus the activation energy of yellow phosphorus must be at least 2·1 eV —probably considerably more, depending on the extent to which the resistivity is determined by impurities. If we assume the measured conductivity is due to the presence of small amounts of red phosphorus with an activation energy of

$\sim 1{\cdot}5$ eV, then the formula would give $A \simeq 10^{-2}$. Comparison with the normal value of A would indicate about one part in 10^5 of red phosphorus present in the yellow phosphorus. The only value of specific resistance occurring in the literature is $10^{11}\,\Omega$cm (FOUSSEREAU, 1883) which must therefore be regarded as far too low.

It was found possible to perform resistance–temperature measurements on three samples of red phosphorus. The following activation energies were deduced: 1·51 eV, 1·55 eV and 1·6 eV, with average = 1·55 eV. Thus the optically and thermally determined activation energies lie in the same range, there being a discrepancy of < 7 per cent in the average values, and we may therefore conclude that for red phosphorus the activation energy lies near to 1·5 eV.

Optical Properties

Transmission measurements show that for evaporated layers the peak of the main absorption band lies below 0·54 μ, the limit of the measurements at 0·48 μ giving an absorption coefficient of $2 \times 10^4 \text{cm}^{-1}$. The presence of a second absorption band in the 0·8 μ region is indicated. There is little absorption in red phosphorus for $\lambda > 2\ \mu$.

For yellow phosphorus the dielectric constant and the square of the refractive index are both very close to 4·1. For red phosphorus the dielectric constant was found to be 6·7, so that assuming that $\epsilon = n_0^2$ for this material also, we have $n_0 = 2{\cdot}6$.

Allotropic Forms

With ordinary pale yellow phosphorus, no photoconductivity was found. Since this form may be prepared in the colourless state, it is clear that it can have no absorption bands in the visible, and hence photoconductivity can only occur in the ultra-violet. The yellow coloration may be produced by heat or light, indicating that it is an allotropic form.

Baking turns the layer dark red, almost black. It is suggested that the two bands of photoconductivity observed are due to two allotropic forms, the 0·85 μ band being clearly due to the red phosphorus. The short wavelength band may be due to

the yellow form which appears in the otherwise colourless phosphorus.

The presence of a new form of phosphorus is strongly indicated by the measurements on cells 5 and 6, where yellow layers were found to be stable at 320°C in a good vacuum. This allotrope is presumably formed to a small extent by light from colourless phosphorus (but not to a sufficient degree to give photoconductivity), and to a much greater extent by heating to 250 or 300°C. Most of the samples on which measurements were made would therefore consist of a mixture of red phosphorus and this yellow form, so that the measured value of the dielectric constant for example, would apply to a mixture of the two.

17

ARSENIC

17.1. GENERAL PROPERTIES

ARSENIC occurs in several allotropic forms, of which the most stable form is the metallic one. This form occurs as rhombohedral crystals which are isomorphous with metallic antimony and bismuth. Grey arsenic, which is the form of interest in the present work, may be formed by evaporation of metallic arsenic, providing the condensation is performed not much above room temperature. It is stable at moderate temperatures, but is converted into the metallic form by heating to about 300°C (MELLOR, 1929). It has a specific gravity of 4·64 compared with 5·72 for the metallic variety. The relations between the allotropic forms of phosphorus, arsenic, and antimony have been discussed by KREBS (1951). Grey arsenic is considered to be isomorphous with red phosphorus and 'black' antimony. Arsenic can be readily evaporated *in vacuo*, the metallic form having a vapour pressure of 6 mm Hg at 400°C (VALLANCE, 1938).

Few data are available on the physical properties of grey arsenic. There is doubt about its precise crystal form. There is little published information on optical properties, and photoconductivity has not previously been reported.

Regarding the electrical conductivity, APKER and TAFT (1949) quote the resistivity as $\sim 10^7\,\Omega$cm. FRANK (1912, see MELLOR, 1929) observed that the conductivity increased rapidly with temperature in the neighbourhood of 200°C. Comprehensive measurements have now been carried out on both conductivity and photoconductivity in arsenic layers, and on the temperature dependence of these. The refractive index and optical absorption have also been measured.

17.2. EXPERIMENTAL DETAILS

All measurements were carried out on layers evaporated *in vacuo* on to glass substrates. Arsenic evaporates readily *in vacuo*

at temperatures much above 300°C. However the material was found to be peculiar in that it required a much lower *condensation* temperature than that at which it evaporated. It was found quite impossible to distil the material in an oven (in a continuously pumped cell) using local cooling by an air blast. Use of a Dewar flask type of cell with either air or water cooling of the inner part produced negligible condensation. After formation however, layers were found to be quite stable up to temperatures of 250°C or more. Dewar flask type cells (as shown in *Figure 13*a) were used throughout, various techniques being employed to obtain the layers described.

17.3. PHOTOCONDUCTIVITY MEASUREMENTS

Cell 1

After outgassing the cell and the arsenic at 250°C, the material was evaporated by a blow torch on to the end of the inner part of the flask which was cooled by ice-water. Much of the material was lost, but some condensed on the electrode surface. The layer so formed had a grey, matt appearance, and showed a tendency to crack.

The cell showed some photoconductivity, a decrease in resistance of 10 per cent occurring when a 100 W lamp was held near the cell. The resistance of the layer was very high at room temperature, being 750 MΩ for electrodes 30 mm wide and 0·6 mm separation. These values indicate a specific resistance $> 10^6$ Ωcm. When used under a.c. conditions the cell was found to be very noisy. With radiation interrupted at 80 c/s, using an amplifier of 16 c/s bandwidth, it was found that 160 μW of radiation from a tungsten lamp were required to give signal = noise.

Frequency response— The a.c. output from the cell was measured as a function of the chopping frequency, using a wide band amplifier and oscilloscope to observe the signals. It was found that the signal amplitude fell to half its low frequency value at an interruption frequency of 560 c/s. Consideration of the resulting waveforms shows that when the amplitude is half maximum, the duration of the square pulses of radiation are $1{\cdot}45\,\tau$, where τ is the response time. Hence $\tau = 600$ μsec.

Spectral sensitivity— The measurements were carried out on a rock-salt monochromator. As a result of the extremely low sensitivity of the layer very wide slits had to be used to obtain adequate signal to noise ratios, and hence the resolution of the instrument was poor, particularly as the dispersion of rock-salt is relatively low. However a rough spectral sensitivity curve was obtained, as shown in *Figure 31*a*.

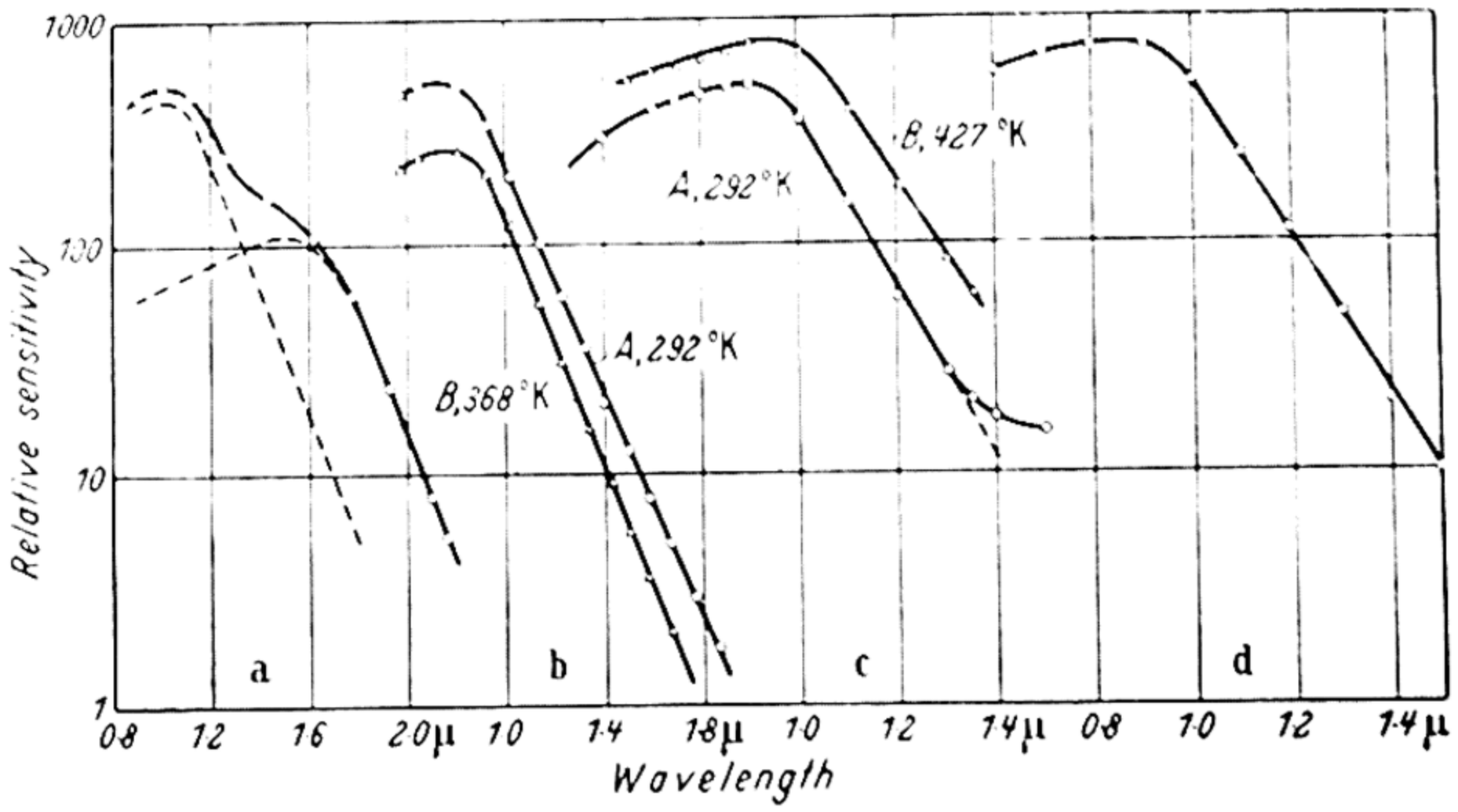

Figure 31. Spectral sensitivity curves for arsenic

Two bands of sensitivity are apparent. In order to find the optical activation energies, it is advisable to separate the observed results into the two component bands of sensitivity as shown by the broken lines. These curves were derived on the assumptions that both bands have the same exponential fall, and that at short wavelengths the second band will show roughly constant quantum efficiency.

The threshold wavelengths are found to be $\lambda_1 \simeq 1{\cdot}2\ \mu$ for the main band, and $1{\cdot}8\ \mu$ for the secondary band. Due to the poor resolution used ($\sim 0{\cdot}3\ \mu$) the measured curve will be displaced towards long wavelengths, and the λ_1 values somewhat too large. However the figures serve to show roughly the magnitudes of the activation energies.

Cell 2

This layer was made by evaporating arsenic from a tungsten spiral, after lengthy outgassing of the cell at 280°C under a

* A similar curve has already been published by the author (Moss 1949).

good vacuum. The evaporation was carried out quite rapidly with the electrode surface at the temperature of iced water. The layer so produced was of much better appearance than in cell 1, being free from cracking and having a smooth surface with metallic sheen.

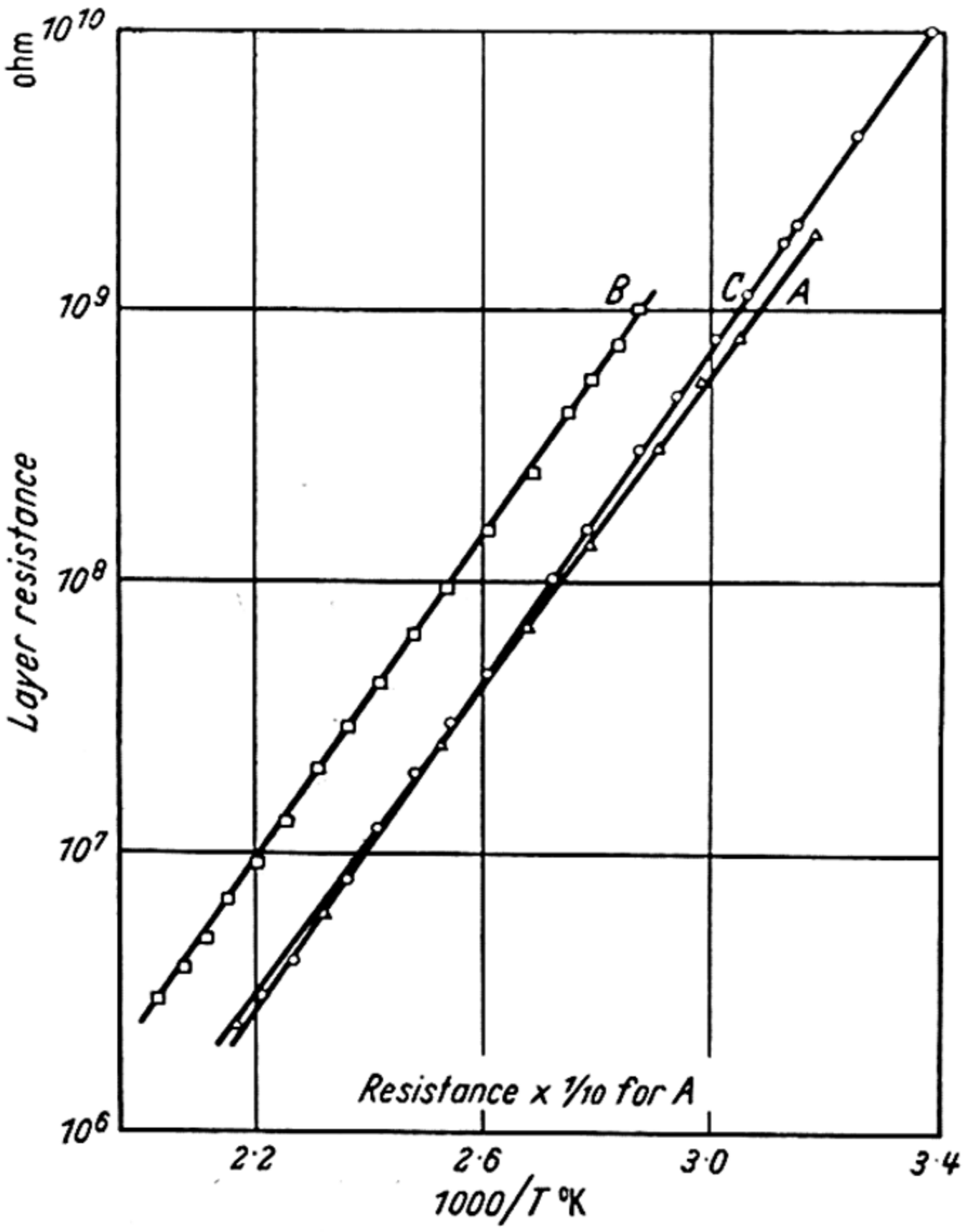

Figure 32. Resistance of arsenic

The resistance at room temperature was about 2,000 MΩ, and the layer showed good photosensitivity. The resistance dropped by a factor of 2·5 with 10^{-2} W of radiation from a tungsten watt lamp falling on the layer. The actual photocurrent produced was 4×10^{-8} amp with a field of 2,400 V/cm. The quantum efficiency must thus be very low, this current being equivalent to $\sim 10^{-5}$ electrons passing between the electrodes per incident quantum.

The sensitivity of the cell was such that signal = noise in 1 c/s bandwidth at 80 c/s was obtained with an incident power of 3×10^{-8} W of monochromatic radiation of wavelength 0·8 μ.

Dependence of photocurrent on field and intensity— The relation between the alternating signal voltage produced across the layer and the steady electric field applied to the cell was investigated, the results being shown in *Figure 33*, curve *A*. The signal is seen to be linear with applied voltage > 100 volts.

The dependence of the a.c. photocurrent on the incident intensity is shown by curve *B* of *Figure 33*. It will be seen that the points lie on a straight line and that therefore the response is linear with intensity.

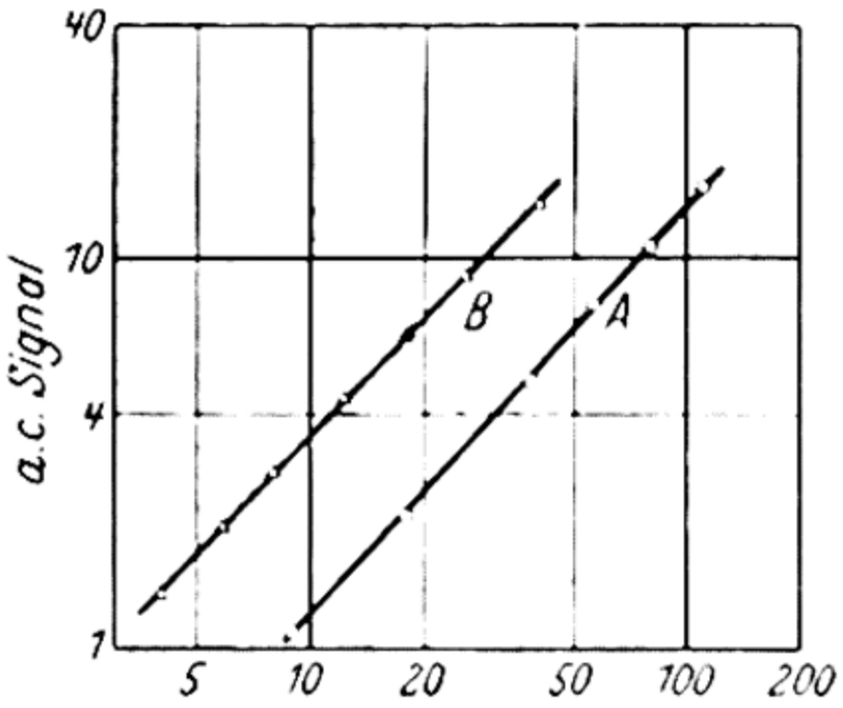

Figure 33. Photo-response in arsenic (Horizontal scales: A, volts; B, 10^{-4} watts)

Spectral sensitivity measurements— Measurements of the spectral distribution of sensitivity were made using a lithium fluoride prism monochromator, with radiation chopped at 80 c/s. As a result of the higher sensitivity of the cell and the better dispersion of the lithium fluoride, measurements of much greater accuracy than those obtained with cell 1 were possible. The results with the layer at room temperature, for the range 0.·55 μ to 2 μ, are shown in curve *A* of *Figure 31*b.

The maximum power falling on the cell at any wavelength was 300 μW. Since the data obtained in the signal–intensity measurements show the relation to be linear up to at least 5,000 μW, the curve of signal per unit power is effectively an equal-intensity spectral sensitivity curve. It will be seen that the maximum lies in the 0·75 μ region, and that for $\lambda > 0{\cdot}9\ \mu$ the sensitivity falls exponentially over a range of 500 : 1 in sensitivity. The sensitivity falls to half maximum at $\lambda_{\frac{1}{2}} \simeq 1\ \mu$. Only the one band of sensitivity appears.

To find out if this material showed any temperature dependence of the spectral sensitivity, the measurements were repeated at a higher temperature. Water inside the cell was

maintained at 95°C by an electric heater, the conditions of measurement being otherwise unchanged. The results obtained, as shown by *Figure 31*b, curve B, are similar to those obtained at room temperature*. As read from the curves, the threshold wavelengths are

$$292°\text{K} \quad \lambda_{\frac{1}{2}} = 0{\cdot}97\ \mu$$
$$368°\text{K} \quad \lambda_{\frac{1}{2}} = 1{\cdot}00\ \mu$$

Thus for the temperature rise of 76°C, there is an indicated shift to longer wavelengths of 0·03 μ. This shift is so small that the percentage accuracy is poor, but it serves to show the magnitude of the effect. In terms of energy, the shift is $\mathrm{d}E/\mathrm{d}T \sim -5 \times 10^{-4}$eV/°C.

Cell 3

In order to overcome the difficulty of losing the arsenic on evaporation, it was decided to try the effect of evaporation in a sealed-off cell, where the arsenic would perforce have to condense on the coolest part of the cell. The cell was outgassed briefly and sealed off whilst still hot. The inner part of the cell was then cooled quickly and the arsenic evaporated by a blow-torch flame. The resulting layer was of relatively low resistance *i.e.* $\sim 10^8\ \Omega$.

Spectral sensitivity curve— The spectral distribution of sensitivity was measured using the LiF prism monochromator. The results were similar to those obtained for cell 1, two bands of sensitivity appearing. As the long wavelength band did not occur in cell 2, its presence is attributed to impurities. The conditions of manufacture of this cell were such as to lead one to expect a relatively impure layer since there would inevitably be some liberation of gas on heating the cell during the evaporation, and as the cell was sealed off this gas would not be pumped away. Analysing the results into two bands of sensitivity, as in *Figure 31*a, gives $\lambda_{\frac{1}{2}} \sim 1{\cdot}08$ and 1·7 μ.

Cell 4

For this cell a successful method of distilling the arsenic (without sealing off the cell) was evolved. A cell blank of the

* The absolute sensitivities are not to the same scale for curves *A* and *B*.

Dewar flask type was fitted with an additional tube surrounding the base of the cell. After an initial outgassing of the cell and contents, liquid nitrogen was poured into this outer tube, and the arsenic evaporated by a blow-torch flame. The material condensed on the cold area with little loss. This condensate was outgassed (with the pressure $\sim 5 \times 10^{-7}$ mm Hg) at as high a temperature as possible without it evaporating, and was then distilled on to the front window of the cell. For this operation the window was cooled by a jet of liquid nitrogen while the cell was heated in the oven. After further baking, the layer was finally distilled on to the liquid nitrogen cooled electrode surface by a blow-torch flame. A mirror-like film, of high resistance and good photosensitivity was obtained.

Spectral sensitivity— The resulting spectral sensitivity curve for the layer at room temperature is shown in *Figure 31*c, curve *A*. The impurity band of photoconductivity is hardly apparent, its presence being indicated only at the longest wavelengths. For the main band of sensitivity $\lambda_i = 1{\cdot}04\ \mu$.

The measurements were repeated with the layer at a temperature of 154°C, produced by electrically heating glycerol inside the cell, the other measuring conditions remaining unchanged. The results are shown on curve *B* of *Figure 31*c (on 1/10 scale). From the λ_i values at the two temperatures, it is found that there is a shift of 0·06 μ to longer wavelengths for this temperature rise of 135°C. The conditions of measurement were good, and the shift is probably not in error by more than $\pm$ 0·01 μ. Hence $dE/dT = -5 \times 10^{-4}$ eV/°C ($\pm$ 15 per cent).

Signal–temperature relation— The variation of the a.c. photocurrent for the temperature range — 78°C to 144°C was investigated, using monochromatic radiation at 1·0 μ to produce the signal. Within this temperature range the cell resistance was always $> 10^7\ \Omega$, and thus high compared with the load impedance of 1·5 MΩ. The results are shown in *Figure 34*, from which it will be seen that the sensitivity *decreases* with decreasing temperature. Below 30°C, the graph is a straight line, indicating an exponential variation of signal with temperature.

From a study of the spectral sensitivity curves, the spectral

shift which would occur over this temperature range would not account for a variation in signal of more than 2 : 1 over the whole range; so the main cause of the effect must be sought elsewhere.

Cell 5

This cell was made in the same manner as cell 4. The layer resistance was $9 \times 10^9\,\Omega$ at 21°C, decreasing to $6{\cdot}5 \times 10^9\,\Omega$ under the illumination of a 100 W lamp. The spectral sensitivity was measured, using the lithium fluoride prism

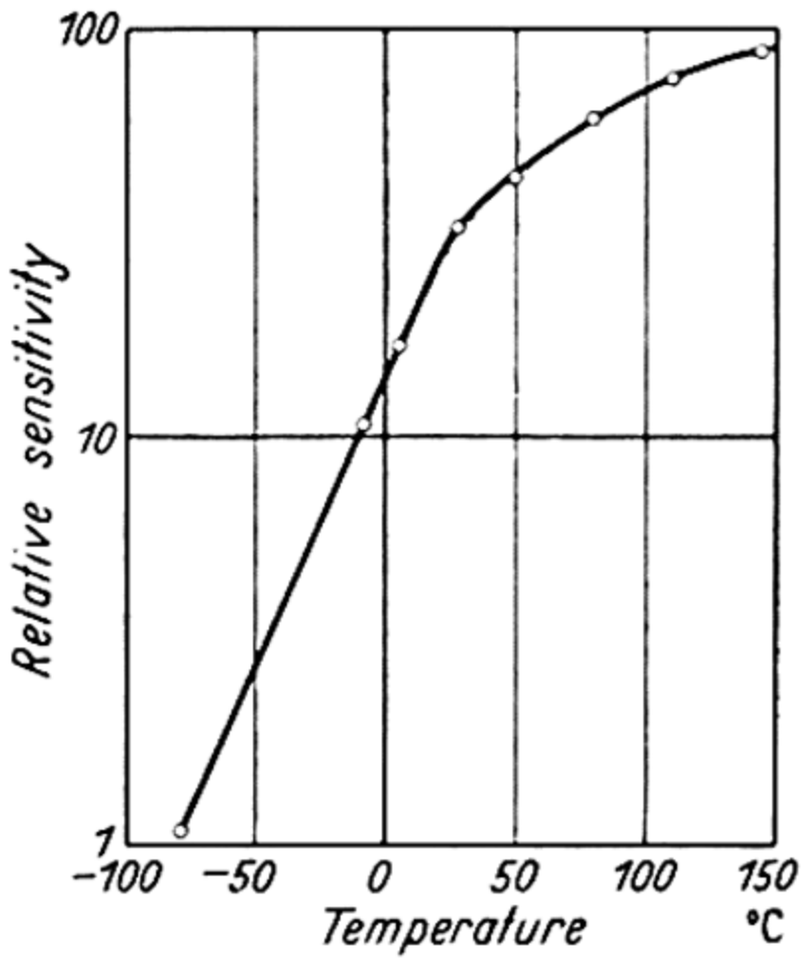

Figure 34. Temperature variation of photosensitivity of arsenic

monochromator. The results, plotted in *Figure 31*d show no indication of an impurity band, the sensitivity falling exponentially to the limit of measurements. The threshold wavelength is $\lambda_{\frac{1}{2}} = 1{\cdot}04\,\mu$.

17.4. RESISTANCE–TEMPERATURE MEASUREMENTS

Cell 1

The layer temperature was varied by the electrical heating of glycerine in the inner part of the cell. Repeatable values of resistance were obtained up to 240°C, at higher temperatures the resistance started to fluctuate—possibly as a result of evaporation of the layer. The curve of log (resistance) against reciprocal temperature is shown in *Figure 32*, curve *A*. For temperatures of 40°C to 200°C the points are well fitted by a straight line of slope 0·57 eV—corresponding to an activation energy of 1·14 eV. At the lower temperature limit of the

measurements *i.e.* 40°C the layer resistance is 185 MΩ. Assuming a layer thickness ~ 1 μ the resistivity $\rho \sim 10^6$ Ωcm.

Putting $\sigma = \sigma_0 \exp(-E/2kT)$ we may find the value of σ_0 preferably from measurements at high temperatures. At 463°K the resistivity of ~ 1,200 Ωcm, with $E = 1{\cdot}14$ as found from the slope, gives $\sigma_0 \sim 1{,}300\ \Omega^{-1}\text{cm}^{-1}$. This high value indicates intrinsic conductivity.

Cell 2

As before, the measurement was made by heating glycerine inside the cell. The results are shown in *Figure 32*, curve *B*. The points fall accurately on a straight line over the whole temperature range. The slope of the line is 0·60 eV, so that $E = 1{\cdot}20$ eV.

At the lower temperature end of the range, *i.e.* 75°C, the cell resistance was $1{\cdot}0 \times 10^9\ \Omega$. The electrodes were $6 \times 1\ \text{mm}^2$. From the weight of arsenic used, and the layer area, the thickness would be approximately 1 μ. Hence $\rho = 6 \times 10^5$ Ωcm at 75°C.

Cell 4

Measurements were taken between room temperature and 180°C. The results are shown by curve *C* of *Figure 32*. The points lie on a straight line for the whole range of 3,000 : 1 in resistance. From the slope we find the activation energy is 1·21 eV.

At the lower temperature end of the graph the layer resistance is $10^{10}\ \Omega$ at 22°C. The electrodes were $8 \times 0{\cdot}6\ \text{mm}^2$, and as described later (in §17.5) the thickness of this film was found to be 0·28 μ. Hence the resistivity is 4×10^6 Ωcm at 22°C—the conductivity being *intrinsic* at this temperature. Using this value in the formula $\sigma \simeq 10^3 e^{-E/2kT}$ gives $E = 1{\cdot}14$ eV. Alternatively at the high temperature end of the range, where $\rho = 1{,}500\ \Omega\text{cm}$ at 179°C, use of the formula $\sigma = \sigma_0 e^{-E/2kT}$, with $E = 1{\cdot}2$ eV (as found from the optical and thermal measurements) gives $\sigma_0 = 260$. The relation $\sigma_0 = 4 \times$ (mobility) leads to a mobility of approximately 65 cm $\text{sec}^{-1}/\text{V cm}^{-1}$ at room temperature.

17.5. OPTICAL MEASUREMENTS

Attempts were made to prepare a layer of arsenic on a plate of artificial sapphire in order to carry out measurements of the refractive index by observing interference fringes in the infra-red region where the material becomes transparent. Great difficulty was encountered in producing a film on the sapphire plate. The method finally adopted was to distil the arsenic *in vacuo* in the manner used for cells 4 and 5, and then seal off the tube containing the plate. Rapid heating of the whole evaporation tube by a blow torch caused the arsenic to condense on the sapphire, as (due to the poor heat conduction) this remained relatively cold.

Refractive Index

The refractive index was found by measurement of interference fringes. Using a rock-salt prism monochromator, fringes were observed in reflection between 3 μ and 8 μ. The recording system of this spectrometer was arranged to be linear in wave-numbers.

Runs were made with and without the sample in, and the positions of the maxima and minima read off directly from the records. The values found were:

Reflection minima, 1,720, 2,530 and 3,290 cm^{-1}
Reflection maxima, 1,300, 2,120 and 2,900 cm^{-1}

Hence the average frequency separation of maxima and minima is 398 cm^{-1}. Thus (see Appendix) $4nd = 1/398$ cm, or $2nd = 12{\cdot}5\ \mu$.

The thickness of the film was determined by weighing, using a semi-micro balance. The weight of the film was $1{\cdot}61 \pm 0{\cdot}005$ mg, and the area 2·083 cm^2. The density of bulk grey arsenic given by MELLOR (1929) is 4·64 gm/cm^3. For an evaporated film it will be somewhat less, probably within $4{\cdot}5 \pm 2$ per cent. Using this latter value, we find the film thickness to be $1{\cdot}72\ \mu$.

From the approximate value of $2nd$ just given, the actual numbers of the fringes can be found. Use of the relation $2nd = N\lambda$ then gives the results of *Table VII*. The main source

of error in these measurements is certainly in the estimation of the density of the film; the other errors should not total more than 1 per cent. From these results we may conclude that at long wavelengths, the refractive index is very near to $n_0 = 3{\cdot}35$, or the dielectric constant equals 11·3.

Table VII

N	cm^{-1}	λ	$2nd$	n
1·5	1,300	7·7μ	11·55	3·36
2	1,720	5·82	11·64	3·39
2·5	2,120	4·72	11·80	3·43
3	2,530	3·95	11·85	3·45
3·5	2,900	3·45	12·07	3·50
4	3,290	3·04	12·16	3·53

The only measurement of refractive index of arsenic quoted in the literature gives $n = 3{\cdot}6$ in the 0·6 μ to 0·7 μ region (*Landolt–Bornstein Tables*, 1927). As the original article could not be obtained, it is not known how the measurements were performed, and it is not even known what allotropic form of arsenic was used.

Reflection measurements were also carried out on the layer of cell 4 after the outer part of the Dewar flask had been removed. A lithium fluoride prism monochromator was used with a lead sulphide cell detector of large area. This was advisable as the electrode surface of the cell on which the layer was deposited was not absolutely flat, so that a blurred image resulted from the reflection. For comparison purposes, an unpolished aluminium plate (which gave similar defocusing of the image) was used. Plotting the reflection ratio gave a curve with several well-defined interference fringes, with the following values of maxima and minima :

Reflection minima at 5,050, 9,300 cm^{-1}.
Reflection maxima at 7,300, 11,300 cm^{-1}.

The frequency separations between maxima and minima are thus $\delta f = 2{,}250$, 2,000 and 2,000 cm^{-1}.

Using the long wavelength value of δf in order to be clear of the dispersion region, we find $2nd = 2{\cdot}22\ \mu$. Putting in the integral values of N in the formula $2nd = N\lambda$ gives the results of *Table VIII*. From the previous measurements, the value of the refractive index at $2\ \mu$ is near to 3·6. Hence the thickness of the film is $d = 0{\cdot}28\ \mu$. This is the value used in the earlier

Table VIII

N	cm^{-1}	λ	$2nd$	n
1	5,050	1·99μ	1·99μ	3·6
1·5	7,300	1·37	2·06	3·71
2	9,300	1·08	2·16	3·89
2·5	11,300	0·89	2·22	4·00

section to calculate the specific resistance, and it is used here to calculate the last column of *Table VIII*. The table shows that there is considerable dispersion in the region 1 μ.

Absorption

The transmission of the layer on the sapphire plate was measured using a lithium fluoride prism monochromator, and a lead sulphide cell detector. The results are shown in *Figure 35*, curve *A*. The transmission fell to less than 0·1 per cent at 0·9 μ, while in the 2 μ region ~ 50 per cent transmission was obtained. As a large area detector was used, any possible distortion in the sapphire plate would have little effect on the signal, and so the insertion loss should result entirely from reflection and absorption. The measurements of refractive index show that the reflection at the arsenic surface should be ~ 30 per cent, at the sapphire surface 8 per cent, and at the arsenic–sapphire surface ~ 12 per cent. The actual absorption in the film is therefore probably < 5 per cent at 2 μ.

As the thickness of the film was found to be 1·72 μ, then the absorption constant $K = 4 \times 10^4 cm^{-1}$ at 0·93 μ, and $\sim 120\ cm^{-1}$ at 2 μ.

Using the same experimental arrangement as above, the transmission of the layer from cell 4 was measured. The results are shown in *Figure 35*, curve *B*. At the minimum wavelength

of 0·65 μ the absorption was ~ 200 : 1, corresponding to an absorption constant $K = 2 \times 10^5 \text{cm}^{-1}$. This high value shows that the absorption is due to the main lattice. A comparison of the absorption curve with the photoconductive curve shows that the peak of photoconductivity occurs on the long wavelength edge of the main absorption band.

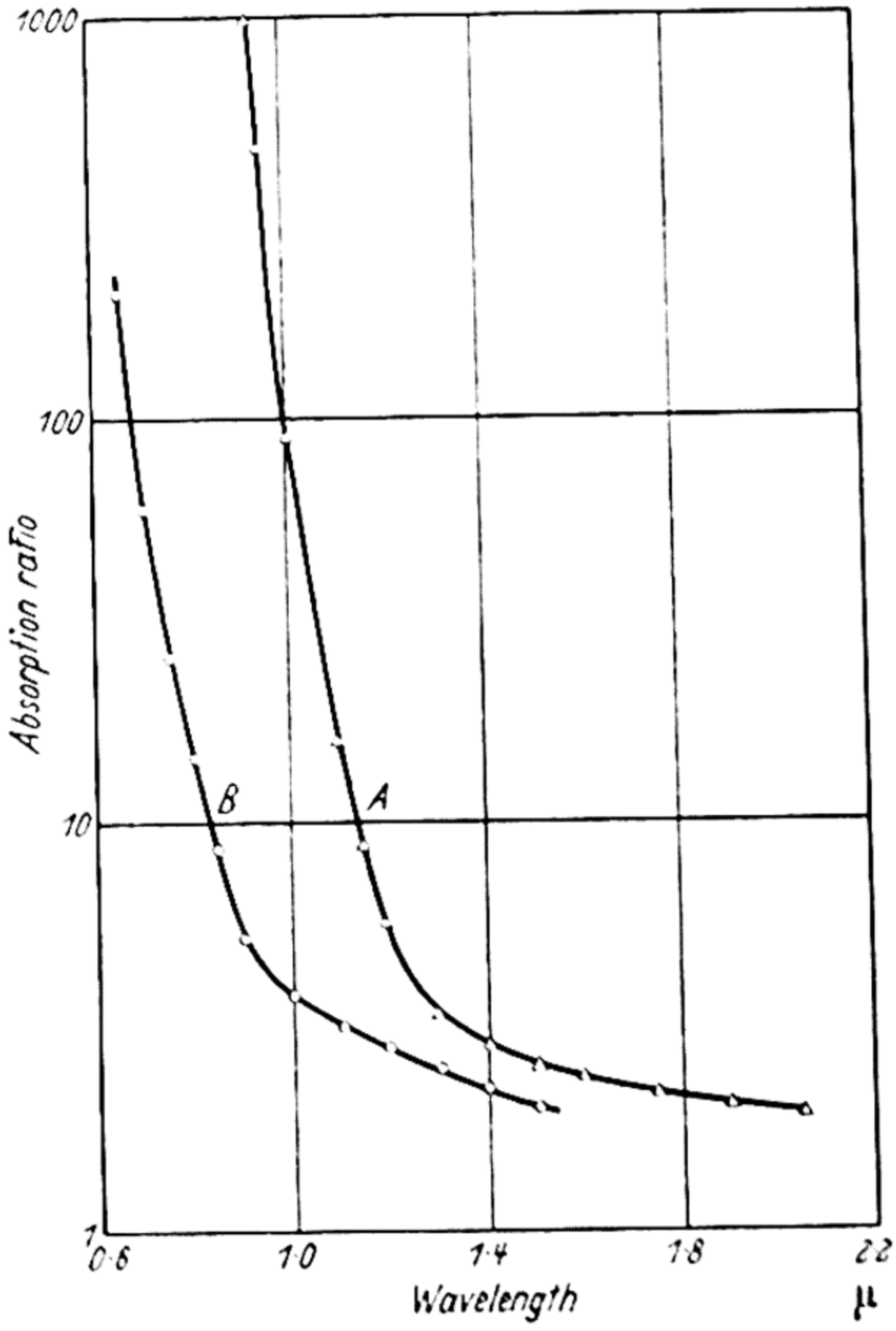

Figure 35. Absorption in arsenic: A, 1·72 μ ; B, 0·28 μ thick.

17.6. SUMMARY AND DISCUSSION

Photoconductivity

The presence of photoconductivity has been established in evaporated layers of grey arsenic. The a.c. photocurrents were found to be proportional to the applied field (at least up to 1,000 V/cm) and also to the intensity of radiation incident on

the layer. The a.c. sensitivity decreased by 100 : 1 on cooling from 150°C to — 80°C. Limiting sensitivities were found to lie in the range 3×10^{-8} to 3×10^{-5} W for radiation of 1 μ wavelength. The response time of one cell was observed to be 600 μ sec.

Specific Resistance and Mobility

The resistivity was found to be $4 \times 10^{6}\,\Omega$cm at 22°C, the conductivity being *intrinsic*. The mobility of the current carriers is ~ 60 cm sec^{-1}/V cm^{-1}.

Optical Measurements

Transmission measurements showed that at 0·65 μ, the absorption constant $K > 10^{5}$cm^{-1}, indicating a main lattice absorption. At longer wavelengths than this the absorption fell rapidly, until at 2 μ, $K \sim 100$ cm^{-1}.

The refractive index at long wavelengths was found to be 3·35, rising considerably in the region of 1·0 μ.

Activation Energies

From spectral sensitivity measurements on three cells which showed negligible signs of impurities, the threshold wavelengths were determined as $\lambda_{\frac{1}{2}} = 1{\cdot}0$, 1·04 and 1·04 μ. Hence the optical activation energy = 1·19 to 1·23 eV. From resistance-temperature measurements on three cells we find the thermal activation energy to be 1·14 to 1·21 eV. From the resistivity of cell 4, an estimate of 1·14 eV is obtained. There is thus very close agreement between the optical and thermal activation energies.

Work by Apker and Taft (1949, see also Becker, 1949) on the photoelectric properties of arsenic films furnishes an independent method of estimating the width of the energy gap. They find that the gap between the Fermi level and the top of the full band is 0·5 to 0·55 eV. It has been shown in the above resistance–temperature measurements that it is possible to prepare layers sufficiently pure for them to be in the range of intrinsic conductivity at room temperature. Assuming Apker and Taft's layers to be of comparable purity, then the Fermi level must be approximately midway between the full and

conduction bands, and the activation energy $\sim$ 1 or 1·1 eV. This is further confirmation of the magnitude of the activation energy, and that it is indeed the width of the forbidden zone. We may thus conclude that grey arsenic is an intrinsic semiconductor at room temperature, with an activation energy of 1·2 eV.

From the temperature shift of the spectral sensitivity curves it is found that the above energy value decreases by 5×10^{-4} eV per °C rise in temperature. This shift is in the same direction as for all other elements on which measurements have now been made, with the exception of tellurium.

In some cells an impurity band of photoconductivity was observed, with threshold wavelengths near 1·8 μ, giving an impurity activation energy $\sim$ 0·7 eV.

18

ANTIMONY

18.1. GENERAL PROPERTIES

LITTLE INFORMATION is available concerning allotropic modifications of antimony, with the exception of the normal, metallic form. The existence of 'black' and 'explosive' antimony has been suggested. The part of the periodic table shown in the Introduction to Part II of this volume shows that the elements on either side of antimony, namely tellurium and grey tin, are semiconductors. To preserve an ordered progression in this table therefore requires the existence of a semiconducting form of antimony. Furthermore, the activation energies are found to decrease progressively on passing from right to left of the table (see Chapter 23), so that the activation energy of antimony would be expected to lie between that of tellurium (0·37 eV) and grey tin (0·1 eV). Semiconducting antimony might therefore be expected to be photoconductive at long wavelengths. Measurements are now described on layers of antimony which show semiconducting properties, and which are sensitive to radiation.

18.2. PREPARATION OF LAYERS

By analogy with the method used to produce grey arsenic, the layers were made by distilling high purity antimony *in vacuo* on to cooled substrates. It was found necessary to cool the substrate with liquid air or solid carbon dioxide in order to obtain satisfactory layers.

The layers were found to be stable only if kept at temperatures well below 0°C. If allowed to warm to 0°C the material rapidly reverted to the metallic form. To prevent this happening, cells were stored in solid carbon dioxide. About twenty sensitive layers were made in all. Measurements are described on a few of these.

Initially layers were prepared in cell blanks of the type shown in *Figure 13*a, using 'bubble' windows of very thin

glass. Layers of thickness $\sim 1\ \mu$ were found to have resistances $\sim 10^5\ \Omega$ at liquid-air temperatures.

18.3. RESISTANCE–TEMPERATURE MEASUREMENT

In order to avoid warming the layer above the transition temperature, the following procedure was adopted. The cell, which had been kept at 195°K, had mercury cooled to — 30°C poured into the inner part of the Dewar. A thermo-junction was placed in the mercury which was then cooled with liquid nitrogen. Measurements were made as the layer warmed slowly towards room temperature. The results for cell 1 are shown in *Figure 36*, the readings being repeatable over the given range of temperatures.

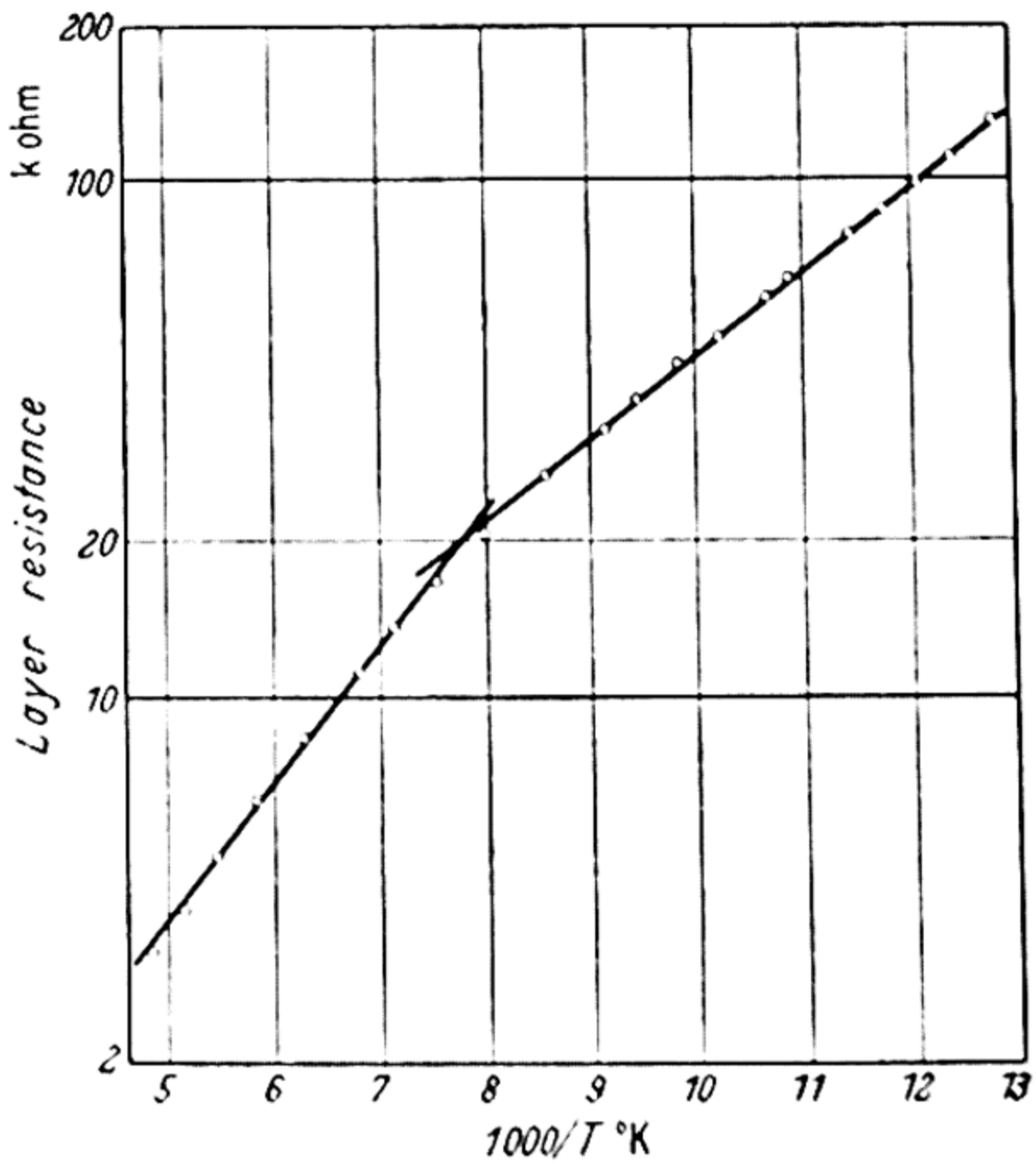

Figure 36. Resistance of antimony

The points do not all fall on a straight line, but two lines may be drawn through the points to obtain an estimate of the activation energy. The straightest part of the curve occurs at low temperatures and gives an activation energy of 0·07 eV. The high temperature line gives 0·11 eV. These energy values would correspond to a photoconductive threshold wavelength of 11 to 17 μ.

At 200°K the layer resistance was 3,800 Ω. Estimating the thickness as $\frac{1}{2}\ \mu$, the specific resistance would be 2Ω cm. Hence from $\sigma = \sigma_0 \exp(-E/2kT)$, we find $\sigma_0 = 10\ \Omega^{-1}\ \text{cm}^{-1}$, taking E as 0·1 eV. This figure implies a mobility of 2 to 3 cm $\text{sec}^{-1}/\text{V cm}^{-1}$, which is not an unreasonable value for a film.

18.4. EFFECT OF RADIATION

Cell 1

The conductivity of this cell was found to be sensitive to radiation, and its spectral sensitivity curve was measured using radiation chopped at 33 c/s. The sensitivity was found to be roughly constant from 1 to 4 μ, with a sharp rise in the region of 5 μ.

The response time of the layer was measured using a mechanically produced square pulse of radiation, and it was found that the signal rose to 1−1/e of its full value in 2×10^{-3} sec. The sensitivity decreased by 130 : 1 on warming the layer from 90°K to 195°K, using the same current through the layer in each case. For the same temperature range the resistance fell by 58 : 1.

Cell 2

This cell was made in a soda-glass envelope, with a window of periclase (*i.e.* MgO) sealed directly to the soda glass. Considerable difficulty was experienced in obtaining good layers in soda-glass cells, because if the final evaporation was carried out too slowly the layer backing became overheated, whereas if the cell blank was heated too quickly it was likely to crack.

The cell showed reasonable sensitivity, and it was possible to measure the spectral sensitivity curve up to a wavelength of 9·6 μ, at which point the absorption of the periclase window became serious. The resulting curve (for a layer temperature of 77°K) is shown in *Figure 37*, curve *A*, the results being corrected for the measured loss in the periclase window.

It will be seen that the sensitivity falls slowly with increasing wavelength to a minimum at about 4 μ, after which it rises rapidly until at 8 μ it has increased by some 22 : 1. From 8 μ onwards the sensitivity did not vary within the limits of measurement.

Cell 3

Attempts were made now to produce a cell with a window capable of transmitting to longer wavelengths, using *KRS 5* plates sealed on by vacuum wax. As this mode of sealing prevented any heating of the cell, the material had to be evaporated from an electrical heater built into the cell. The antimony was placed in a small silica crucible in a tungsten helix and evaporated on to an electrode surface cooled by solid carbon dioxide.

Some resistance measurements were made, the following values being obtained: 77°K, 410 kΩ; 90°K, 210 kΩ; 195°K, 12 kΩ. It was found possible to allow the layer to warm until the resistance was 3kΩ, and it would still return to the value of 410 kΩ on recooling with liquid nitrogen. If the activation energy is calculated from the above figures (on the assumption that the log (resistance)–reciprocal temperature curve is linear between the measured points) the values obtained are:

195°K to 90°K, $E = 0{\cdot}085$ eV
90°K to 77°K, $E = 0{\cdot}06$ eV.

As the two values do not differ greatly, the resistance–temperature graph cannot be very curved, and the above values should be a fair approximation to the actual activation energy.

The response time was measured using a pulsed neon lamp as source. The values obtained were:

77°K, 720 μsec
90°K, 720 μsec
195°K, 550 μsec

The sensitivity of this cell was not very high, but with care it was possible to make spectral sensitivity measurements at wavelengths up to 11 μ, the results being shown by curve *B*, of *Figure 37*. A marked rise in sensitivity again occurs in the 5 to 9 μ region—the increase being 37 : 1. There was no significant change of sensitivity in the 9 to 11 μ region.

Cell 4

This cell was the most sensitive one made with a *KRS 5* window. For this reason careful measurements of the spectral

sensitivity were made at the longest possible wavelengths. The cell was found to be more sensitive (on a signal/noise basis) at 195°K than at liquid-air temperatures, and accordingly the measurements were carried out using solid carbon dioxide as coolant.

The results are shown in *Figure 37*, curve *C*. The usual sharp rise in sensitivity is observed between 4 μ and 9 μ. For wavelengths greater than 9 μ the sensitivity is practically constant, although it is possible that there is a significant fall

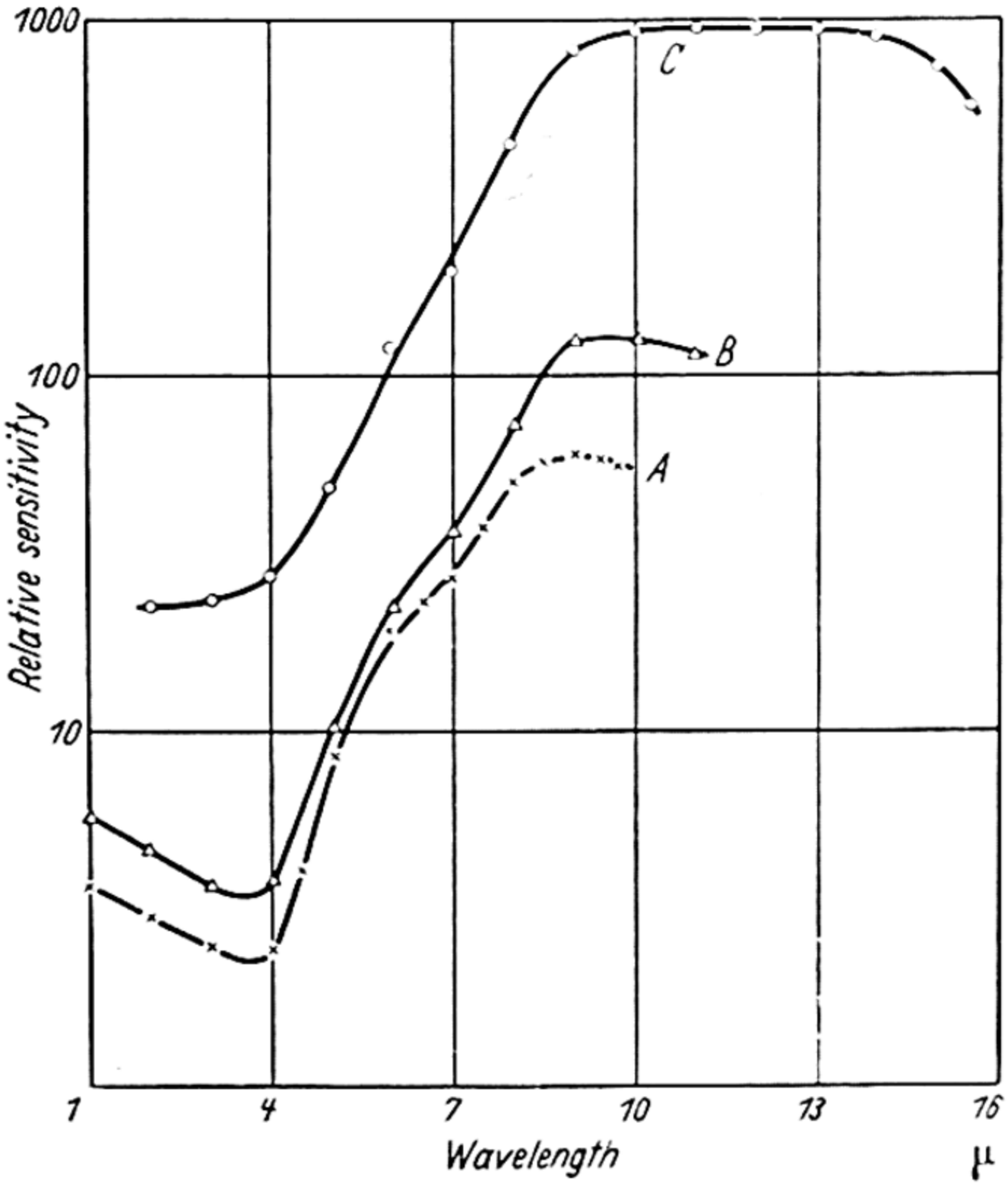

Figure 37. Spectral sensitivity curves for cooled antimony layers

at the longest wavelengths. If this fall *is* significant, it would indicate $\lambda_{\frac{1}{2}} \sim 16$ μ. In this wavelength region the rocksalt prism monochromator used was becoming inefficient and it would be necessary to use other prisms to extend the measurements to longer wavelengths.

The response times of this layer were found to be:

195°K, 900 μsec
90°K, 520 μsec
77°K, 400 μsec

The sensitivity was such that signal = noise in 1 c/s bandwidth was obtained with an incident energy of 2×10^{-7} W from a 200°C source.

18.5. OPTICAL PROPERTIES

SUHRMANN and BERNDT (1940) found that antimony layers condensed at liquid air temperatures had reflection coefficients different from the normal metallic coefficients, and that the reflection changed irreversibly on warming to about 270°K. The reflection coefficients at 0·6 μ at an angle of incidence of 71° (for light parallel and perpendicular to the plane of incidence) were found to be 15 per cent and 80 per cent before warming*, and 38 per cent and 90 per cent after warming.

18.6. SUMMARY AND CONCLUSIONS

Semiconducting layers sensitive to radiation have been produced. The main point to be decided in the measurement of response of the layers to radiation is whether they are acting as photoconductors or as bolometers. From the sensitivities obtained either mechanism would be feasible. Also response times of 10^{-3} sec are quite appropriate to thin layer backed bolometers. In general the response time of a photoconductive layer would increase on cooling, while a bolometer time constant would decrease. The two sets of results obtained go in opposite directions, so no definite conclusion can be drawn from them.

The spectral sensitivity curves obtained give the most interesting information on the properties of the layers. The most marked feature is the rise in sensitivity of some 30 or 40 times as the wavelength is increased from 4 μ to 9 μ. Presumably a corresponding absorption band is implied, either of an electronic nature giving rise to photoconductivity, or of a molecular nature resulting in a bolometric effect. Beyond 9 μ the spectral sensitivity curves are substantially flat, although in the case of the longest wavelength measurements there is an

* Analysis of this data by D. G. AVERY gives $n = 1{\cdot}5$, $K = 3{\cdot}3 \times 10^5$ at 0·4 μ and $n = 4$, $K = 5{\cdot}6 \times 10^5$ cm^{-1} at 0·6 μ.

indication of a fall-off in sensitivity, but it is doubtful if the measurements are sufficiently accurate to be significant.

Estimates of the activation energy obtained from resistance-temperature data lie in the range 0·06 to 0·11 eV, which would correspond to a wavelength of 11 to 18 μ. Suhrmann and Berndt estimated the activation energy to be 0·055 eV to 0·18 eV. The spectral sensitivity curves show that the threshold wavelength cannot be less than 16 μ, which would therefore not be inconsistent with the resistance–temperature measurements.

The existence of a non-metallic form of antimony is established, the estimated values of activation energy ranging from 0·06 to 0·18 eV. It has not been possible to observe a threshold wavelength in the spectral sensitivity curve, and at present it cannot be decided whether the sensitivity to radiation is a photoconductive or a bolometric effect.

19

SULPHUR

19.1. GENERAL PROPERTIES

The ordinary (α) form of crystalline sulphur is of rhombic, octahedral form. The crystal structure is built up of puckered rings of S_8 molecules, the spacing between atoms being 2·05 Å. The relation of sulphur to oxygen, selenium and tellurium has been discussed by von Hippel (1948). This writer points out that as a consequence of the ring structure, positive holes should not be mobile. At ordinary temperatures sulphur is one of the best insulators known.

19.2. PHOTOCONDUCTIVITY

Photoconductivity has been observed by Pigulewsky (1912) and by Joffé (1928), the latter finding an increase of conductivity of as much as a million times on illumination. Measurements of the variation of photocurrents with applied field and intensity have been made by Kurrelmeyer (1927). The currents observed, which were exceedingly small (the resistivity being $> 10^{18}\ \Omega$ cm in the dark), were measured by a string electrometer. The photocurrent was found to be directly proportional to the applied field from 20 to 15,000 V/cm and proportional to the light intensity over a 100 : 1 range. The photocurrents were found to reach full value in a time less than the response time of the electrometer *i.e.* $< 0{\cdot}1$ sec. In *Figure 38*, curve *A*, Kurrelmeyer's spectral sensitivity measurements have been plotted on a semi-log scale. The shape is similar to that found for many other materials, having a long wavelength fall-off that is roughly exponential. The $\lambda_{\frac{1}{2}}$ value is 0·51 μ. Kurrelmeyer had to use very wide slits on his monochromator in order to get measurable photocurrents, the effective bandwidths being 15 mμ at short wavelengths, and 80 mμ at long wavelengths. These wide slits would have the effect of making the tail of the curve lie at too long wave-

lengths, so that the true value of $\lambda_{\frac{1}{2}}$ should be somewhat less than 0·51 μ, probably 0·49 or 0·50 μ. Hence the corresponding activation energy is 2·5 eV.

Spectral measurements have also been carried out by TARTAKOVSKY and REKALOVA (1940). The results obtained by these workers for a specimen 5 mm thick are shown in curves *B* and *C* of *Figure 38*. Curve *C*, taken at room temperature has $\lambda_{\frac{1}{2}} = 0{\cdot}54\ \mu$, corresponding to an activation energy of 2·3 eV.

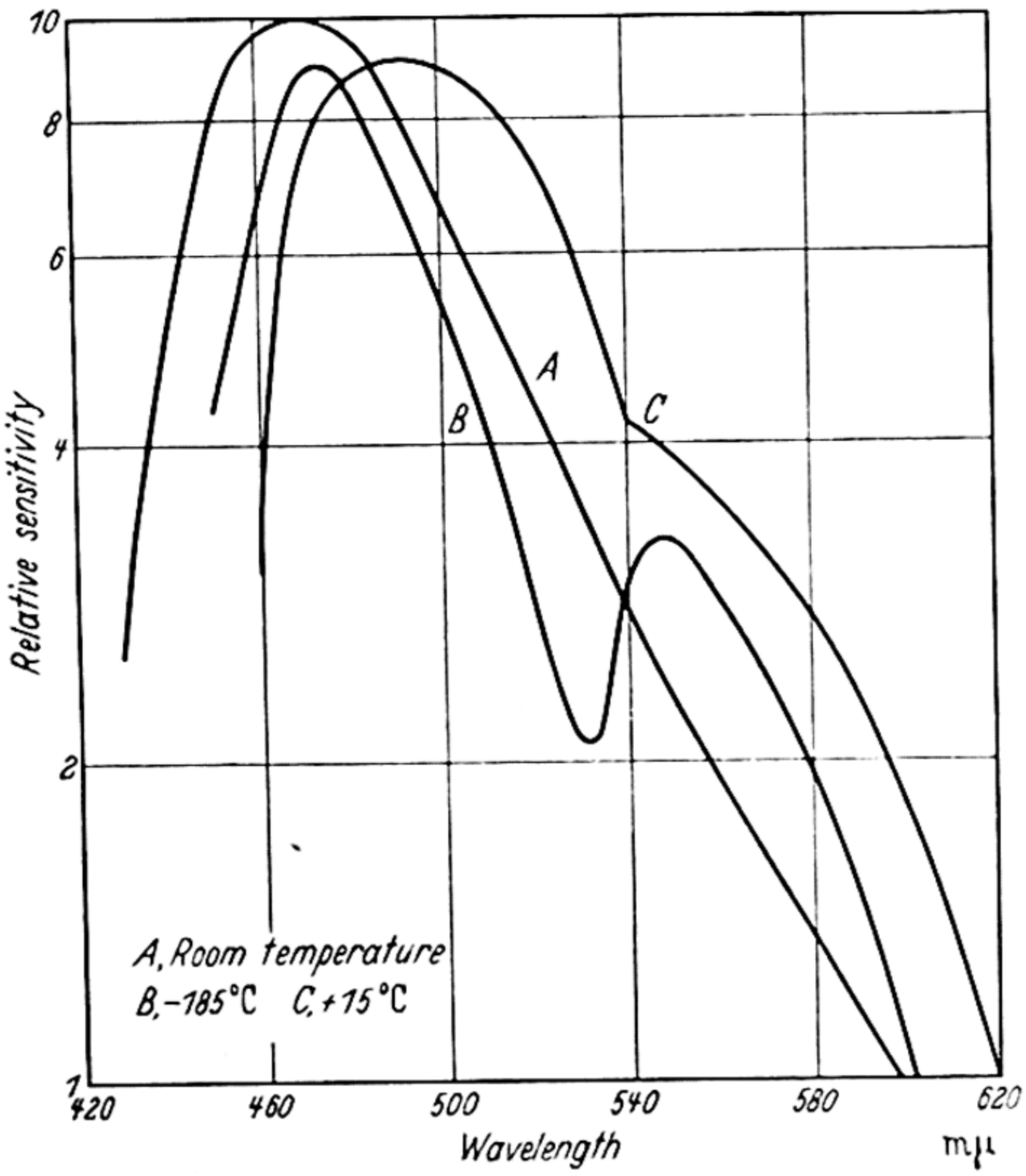

Figure 38. Spectral sensitivity of sulphur (from TARTAKOVSKY *and* KURRELMEYER)

A similar value has also been given by KOLOMIETS and RYVKIN (1947). The average energy value obtained from photoconductivity measurements is therefore 2·4 eV approximately.

TARTAKOVSKY and REKALOVA (1940) obtained curve *B* of *Figure 38* for the spectral distribution of sensitivity at liquid-air temperature. The threshold wavelength is seen to move to shorter wavelengths on cooling, the shift being 30 mμ. Hence

the energy change is $dE/dT = -7{\cdot}5 \times 10^{-4}$ eV/°C. According to FUKUDA (1921), the absorption edge for a sample 0·3 mm thick moves from 408 mμ at 0°C to 458 mμ at 200°C. This represents an energy shift, $dE/dT = -16 \times 10^{-4}$ eV/°C. This very high value of the spectral shift is probably related to the high thermal expansion of sulphur. The volume expansion coefficient is 224×10^{-6}, so that for the above temperature rise of 200°C, the lattice dilatation is 4 per cent. The discrepancy between the two values for the shift may be partly due to the fact that the dilatation will be greater for 200° of heating than for 200° of cooling.

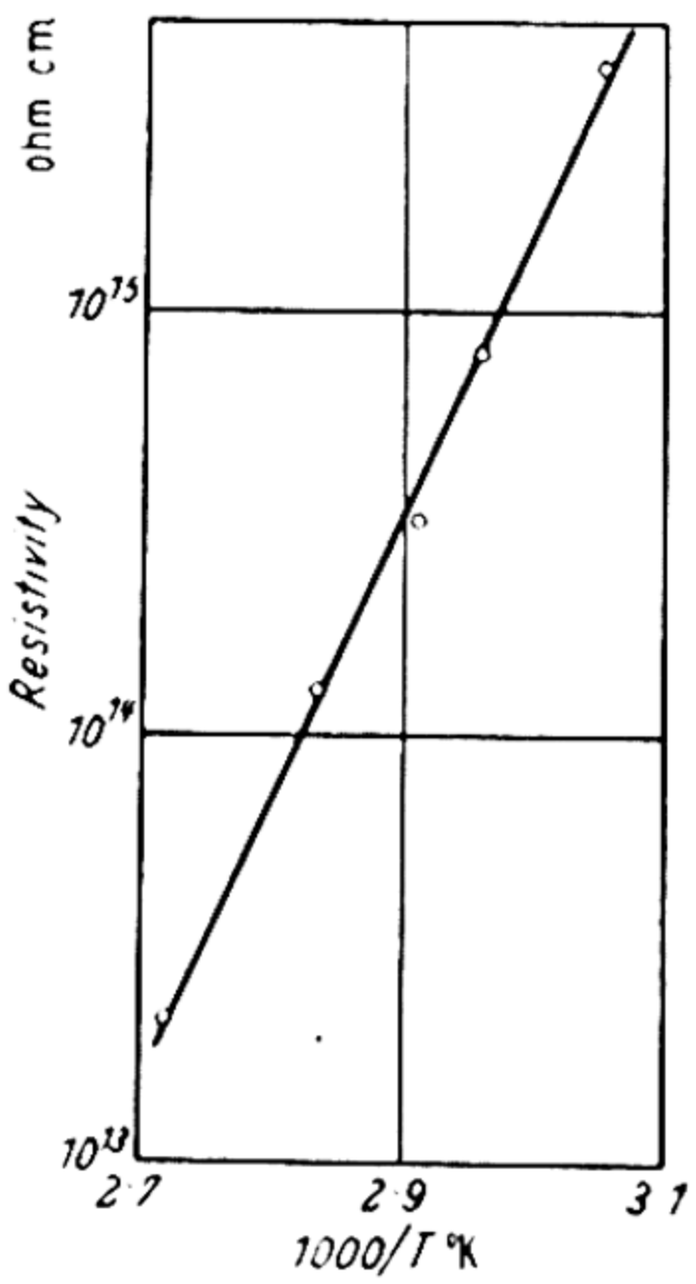

Figure 39. Sulphur resistivity (from FOUSSEREAU)

19.3. RESISTANCE MEASUREMENTS

The most comprehensive measurements of the variation of resistance with temperature are those of FOUSSEREAU (1885). On plotting the values quoted by him as log (resistance) against reciprocal temperature, the graph of *Figure 39* is obtained. Considering the difficulty of the measurements, the points lie fairly near to a straight line. The slope is 1·3 eV, so that thermal activation energy is 2·6 eV.

Measurements by NEUMANN (1927), performed *in vacuo*, give the resistivity of crystalline sulphur as $2 \times 10^{18} - 2 \times 10^{19}\,\Omega$ cm at 19°C. Using a mean value of $5 \times 10^{18}\,\Omega$ cm in the

formula $\sigma = \sigma_0 \exp(-E/2kT)$ gives $E = 2{\cdot}5$ eV for $\sigma_0 \sim 10^3$. It may be noted than an error of 10 : 1 in the assumed value of σ_0 will only change E by 0·1 eV.

19.4. OPTICAL PROPERTIES

For normal α-sulphur, the refractive indices for the three crystal directions given by SCHRAUF (1890) are shown in *Table IX*. If these results are plotted according to the dispersion

Table IX

Wavelength Å	*Refractive Indices*		
3969	2·32967	2·11721	2·01704
5270	2·25875	2·05443	1·96425
5893	2·24052	2·03832	1·95047
6869	2·22145	2·02098	1·93651

formula of equation 19 they are found to lie on a straight line. Extrapolating to zero frequency gives the following values for the refractive index: $n_0^2 = 4{\cdot}74,\ 3{\cdot}93,\ 3{\cdot}62$. Measurements have also been made by SCHMIDT (see MELLOR, 1930) from whose curves the refractive indices at infinite wavelength are estimated as 2·18, 1·99, 1·92; so that $n_0^2 = 4{\cdot}75,\ 3{\cdot}95,\ 3{\cdot}7$.

Now accurate measurements of the dielectric constant of crystalline sulphur have been made by BOLTZMANN (1874) who found for the three crystal directions: $\epsilon = 4{\cdot}77,\ 3{\cdot}97,\ 3{\cdot}81$. These values are thus very close to the values found from the extrapolated refractive indices—those for the first two crystal directions agreeing within 1 per cent. Thus sulphur obeys Maxwell's law $n_0^2 = \epsilon$ to a high degree of accuracy; so that the thermal and optical activation energies would be expected to be the same.

SCHRAUF (1890) has also measured the temperature variation of the refractive index, finding a decrease of 0·25 per cent on heating from 8°C to 30°C. This change is of the opposite sign to that which would be expected from the sign of the energy shift with temperature.

In the infra-red region of the spectrum, sulphur is transparent up to a wavelength of 120 μ, except for a small absorption band near 40 to 50 μ, where the absorption constant reaches 30 cm^{-1}*.

19.5. SUMMARY AND CONCLUSIONS

From measurements of photoconductivity and resistivity in sulphur the following estimations of the activation energy are obtained:

i optically, 2·4 eV;
ii resistance–temperature, 2·6 eV;
iii specific resistance, 2·5 eV.

The values are sufficiently close—especially in view of the difficulties involved in carrying out measurements on such a high resistance material—for it to be concluded that there is no significant difference between the optical and thermal activation energies, the mean value being 2·5 eV.

Putting $\sigma = \sigma_0 e^{-E/2kT}$, using Foussereau's value of resistivity at 375°K and the above value of E, gives $\sigma_0 \sim 5{,}000\ \Omega^{-1}\ cm^{-1}$. This figure cannot be expected to be very accurate, but nevertheless its high value is a strong indication that the conductivity is intrinsic.

Thus sulphur, although one of the best known insulators, may be described as a 'semiconductor' with an intrinsic activation energy of 2·5 eV. From Neumann's results, it appears that the purest crystals are in (or near) the intrinsic range of conductivity at room temperature, with a specific conductivity $\sim 10^{-19}\ \Omega^{-1}\ cm^{-1}$. With $E = 2{\cdot}5$ eV, the density of conduction electrons at 20°C will be $\sim 2{\cdot}5 \times 10^{19}\ e^{-2{\cdot}5/2kT}$ or $\sim 6 \times 10^{-3}$; *i.e.* there is only about one conduction electron per 150 cm^3 of crystal.

* See *Smithsonian Physical Tables* Washington, 1933.

20

SELENIUM

20.1. GENERAL PROPERTIES

SELENIUM occurs in three allotropic forms, all of which show photoconductive effects, namely:

1 Amorphous or vitreous selenium.

2 Crystalline red selenium.

3 Crystalline grey selenium, or hexagonal, metallic selenium.

The red crystalline (mono-clinic) form consists of Se_8 rings, while the hexagonal form is made up of long parallel chains of selenium atoms.

A vast amount of experimental work has been carried out on the photoconductivity of grey selenium, whereas little has been done with the other varieties. However, the results for these are more susceptible to interpretation, and will be considered first.

20.2. AMORPHOUS SELENIUM

According to VON HIPPEL (1948) both amorphous and liquid selenium have a random chain structure, with a few ring molecules present. The density is 4·26 (BARNARD, 1930). Layers of this type of selenium can be produced by vacuum evaporation, or by rapid solidification of molten selenium. It converts to the metallic form on heating, the speed of transformation being greatly affected by the additions of impurities (KREBS, 1951). Amorphous selenium is a near insulator, and was for a long time regarded as not photoconductive. It is only in the past year or two that measurements on photoconductivity have been reported.

Resistance Measurements on Amorphous Selenium

The resistivity of films ($\sim$ 0·1 mm thick) of amorphous selenium at room temperature was found by NASLEDOV and MALYSHEF (1946) to be $\sim 10^{12}\,\Omega\,\text{cm}$. A similar value has

been quoted by WEIMER (1950). No measurements of the temperature dependence of the resistance appear in the literature, but the following results have been obtained by the present author.

A cell of the type shown in *Figure 13*a was used, the electrode system consisting of a narrow gap in a graphite layer, of dimensions $50 \times 0{\cdot}1$ mm^2. *Specpure* selenium was distilled repeatedly in a good vacuum before depositing on the electrode surface. At 19°C the resistance was found to be $8{\cdot}7 \times 10^{11}\,\Omega$. Estimating the layer thickness as 10 μ from the amount of selenium used, the resistivity $\rho \sim 5 \times 10^{11}\,\Omega$ cm. Glycerol was placed in the inner part of the cell and heated electrically to 60°C—previous measurements having shown that at this temperature there was negligible change in properties as a result of conversion to the metallic form. However temperatures not much higher than this produced irreversible resistance changes.

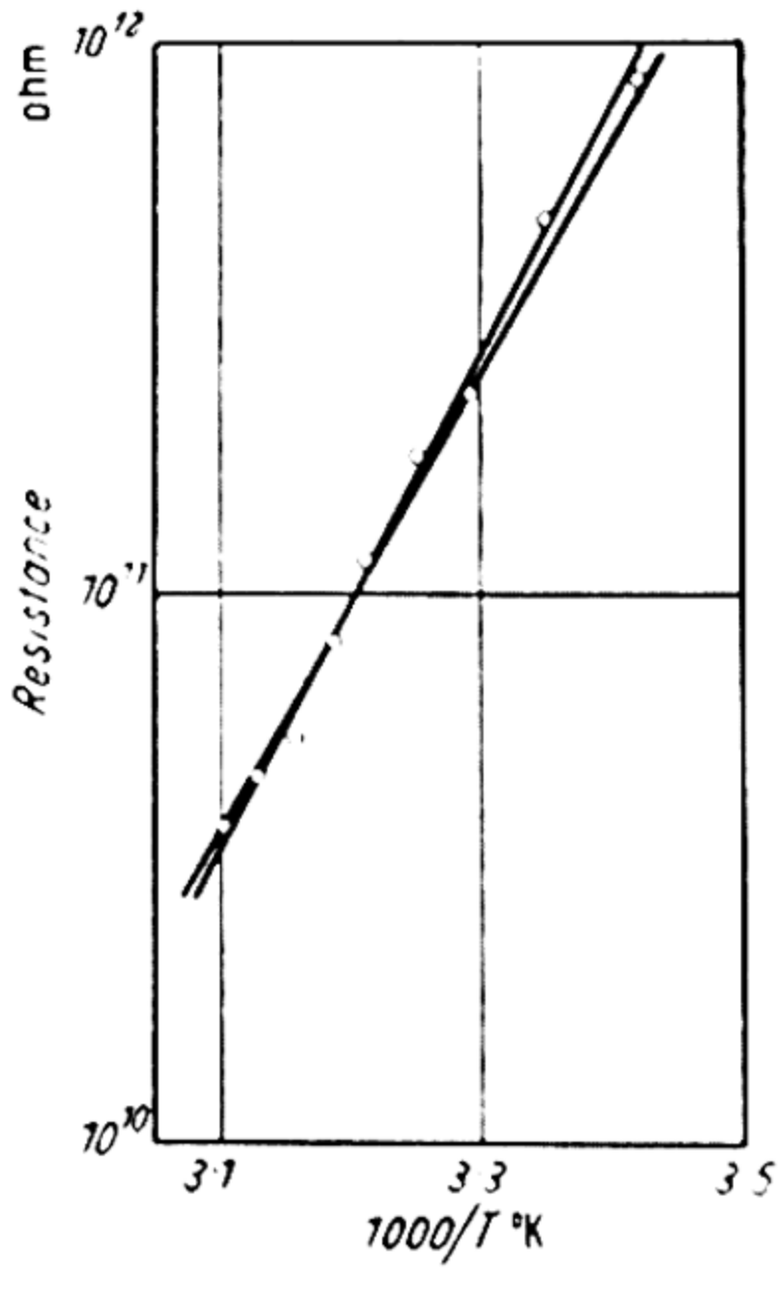

Figure 40. Resistance of amorphous selenium

The resistance values obtained are shown by a log (resistance)–reciprocal temperature plot in *Figure 40*. To give an idea of the tolerance caused by the scatter of the points, two lines, of slopes 0·85 and 0·90 eV have been drawn. From the distribution of the points about these lines it seems reasonable to conclude that the activation energy is approximately 1·7 eV.

From the resistivity of $5 \times 10^{11}\,\Omega$ cm at 19°C, the formula $\sigma = \sigma_0 \exp(-E/2kT)$ gives $E = 1{\cdot}7$ eV if σ_0 is taken $\sim 10^3$ as usual. As this value is near to that found from the slope, the conductivity must be of intrinsic magnitude. It should be noted however that from the low values of mobility reported for selenium, σ_0 may be much less than this.

Photoconductivity in Amorphous Selenium

The cell described above was photosensitive, and spectral sensitivity measurements were carried out on it. A rock-salt prism monochromator was used, the d.c. photocurrent being measured under steady illumination. An electronic current amplifier and galvanometer were used to observe the currents, readings being taken as rapidly as the galvanometer response time ($\sim$ 1 sec) would permit.

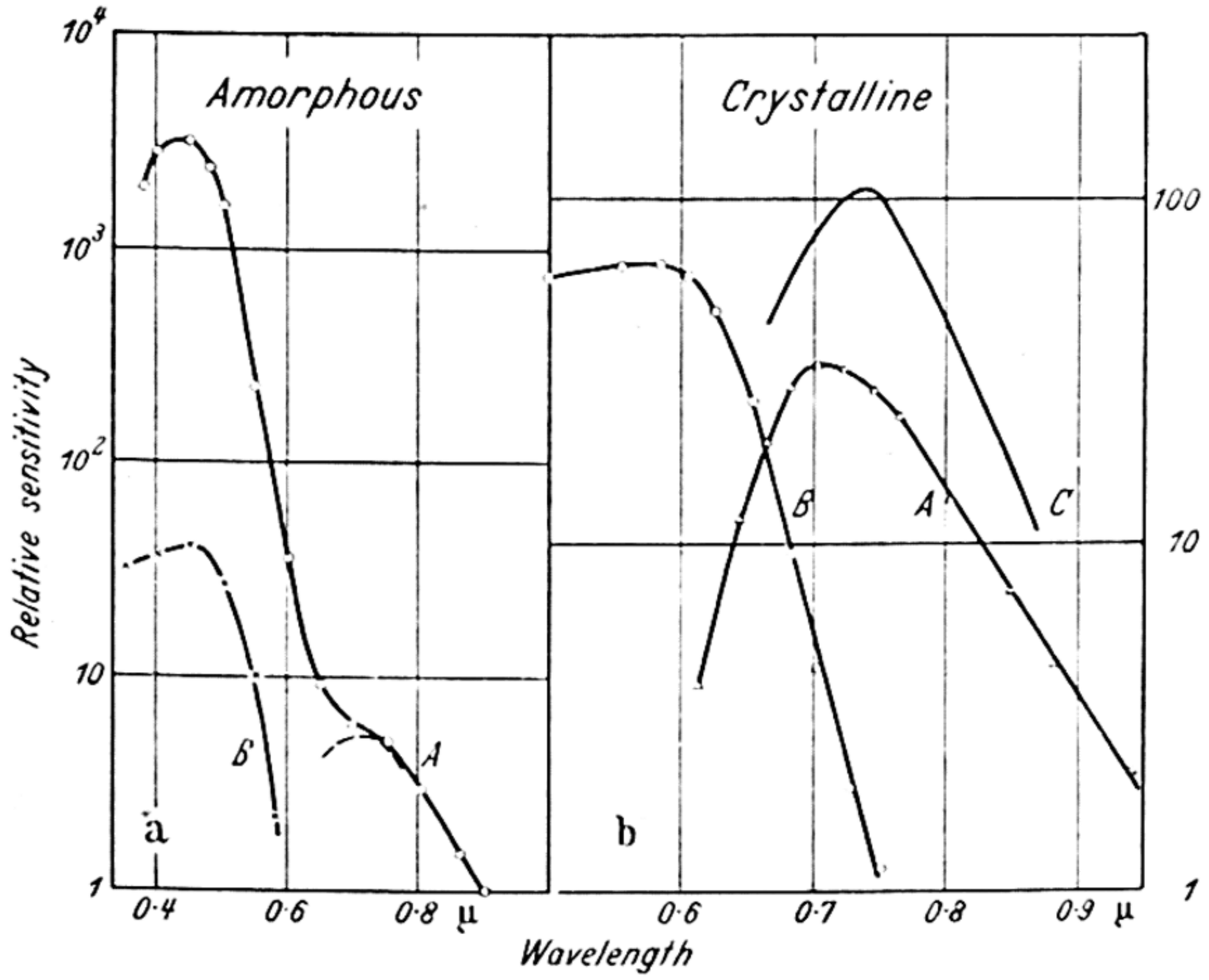

Figure 41. Spectral sensitivity curves for selenium

The results obtained are shown in *Figure 41* a curve *A*. It will be seen that the main band of photoconductivity appears at very short wavelengths—the maximum lying near 0·44 μ, and the threshold at $\lambda_{\frac{1}{2}} = 0{\cdot}50\,\mu$. At wavelengths beyond 0·5 μ, the sensitivity falls rapidly in an exponential manner over a range of 200 : 1. At still longer wavelengths a second band of

sensitivity appears. Subtraction of the extrapolated edge of the main band serves to isolate this band, as shown by the broken curve. This long wavelength band, which occurs at a similar wavelength and has similar shape to the band measured by GUDDEN and POHL (1925) in monoclinic selenium, has $\lambda_{\frac{1}{2}} \simeq 0{\cdot}8\ \mu$.

These measurements have been largely confirmed by recent results by WEIMER (1950) which give spectral sensitivity curves for films of red selenium. These results show a maximum at $0{\cdot}45\ \mu$, and $\lambda_{\frac{1}{2}} = 0{\cdot}5\ \mu$; but as the measurements extend only over a range of about 10 : 1 in sensitivity, there is no sign of the long wavelength band shown in curve *A* of *Figure 41*a.

More detailed measurements have been published by WEIMER and DANFORTH-COPE (1951). 'Sandwich' layers 5 to $10\ \mu$ thick were used, illumination being through a transparent electrode of a special form of conducting glass. The photoconductivity was observed by scanning the layer with an electron beam. The photocurrent was found to be carried mainly by positive holes, currents passing through the film when the thickness was several times as great as the penetration depth of the radiation. The mean range of the holes was found to be 10^{-3} cm in a field of 5×10^4 V/cm, compared with $\sim 10^{-4}$ cm for electrons in the same field. Similar values for the range of holes and electrons have previously been observed by PENSAK (1950) in measurements on bombardment currents in selenium layers.

Response times were found to be $< 50\ \mu$ sec, this being the limit of the measurements. At low levels of illumination the photocurrent was proportional to the illuminating intensity. At high levels, saturation occurred. At 20°C, photocurrents of $1\ \mu$ amp/cm^2 were obtained with 30 V applied to the layer, this current density falling by $\sim 15 : 1$ on cooling to 0°C.

For the pure material, quantum efficiencies of unity were obtained over the wavelength range 3,200 to 4,600 Å, but no values > 1 were observed. For layers with added impurities however, quantum efficiencies $\gg 1$ were found, together with the typical long response times associated with secondary photo-effects. Measurements of the spectral sensitivity

obtained by these workers have been plotted as curve *B* of *Figure 41*a. From the curve $\lambda_{\frac{1}{2}} = 0{\cdot}51\ \mu$, in good agreement with the figure given earlier.

GILLEO (1951) has also reported photoconductivity in films of red amorphous selenium. The films were prepared by vacuum deposition on to quartz plates. Measurements of the spectral sensitivity were carried out with radiation interrupted at 60 c/s, using a high impedance, narrow band amplifier. For a thin layer ($0{\cdot}57\ \mu$) at 22°C, the relative sensitivity was found to fall rapidly with increasing wavelength, becoming immeasurable at 5600 Å. At − 172°C this limiting wavelength was reduced to 5000 Å. As the measurements did not cover the maxima of sensitivity, precise $\lambda_{\frac{1}{2}}$ values cannot be obtained from the curves. However, an estimate of the spectral shift is given by the results above, namely 600 Å for 194°C temperature change. Hence $dE/dT \simeq -13 \times 10^{-4}$eV/°C.

Absorption in Amorphous Selenium

GILLEO (1951) has carried out extensive absorption measurements over a wide range of temperature, using evaporated films of thickness $0{\cdot}03\ \mu$ to $98\ \mu$. The thickness was determined by weighing. A quartz prism double monochromator was used, the resolution of wavelength and accuracy being such that the position of the absorption edge (at a given optical density) could be located within ± 10 Å.

The results obtained for the absorption constant for the wavelength range $0{\cdot}22\ \mu$ to $0{\cdot}7\ \mu$ are shown in *Figure 42*. The absorption is seen to reach a maximum at about $0{\cdot}26\ \mu$, the value then being $5{\cdot}4 \times 10^5\ \text{cm}^{-1}$. This magnitude shows that the absorption is in the main lattice. SOEZIMA (1949) also found that maximum absorption occurred near $0{\cdot}3\ \mu$ for films of unspecified thickness. At wavelengths $> 0{\cdot}55\ \mu$ the absorption falls rapidly. Also shown in *Figure 42* are some values derived from a transmission curve given by GEBBIE and SAKER (1951). These measurements, which were taken on a layer (1·62 mm thick) formed by the rapid cooling of molten selenium, show that $K \sim 1\ \text{cm}^{-1}$ at $0{\cdot}9\ \mu$, with even smaller values occurring at longer wavelengths. The observed values of K thus cover a range of $10^6 : 1$.

Becker and Schaper (1944) have also carried out transmission measurements on amorphous layers. For films 0·2 μ to 22 μ thick their values of absorption constant range from 2×10^3 cm^{-1} at 0·65 μ to $6{\cdot}4 \times 10^4$ cm^{-1} at 0·55 μ, the shortest wavelength measured. For this spectral region the results thus confirm those of Gilleo. Dowd (1951) measured amorphous films over the range 0·35 to 0·7 μ. As shown by *Figure 42* his results again lie very near to those of Gilleo, so

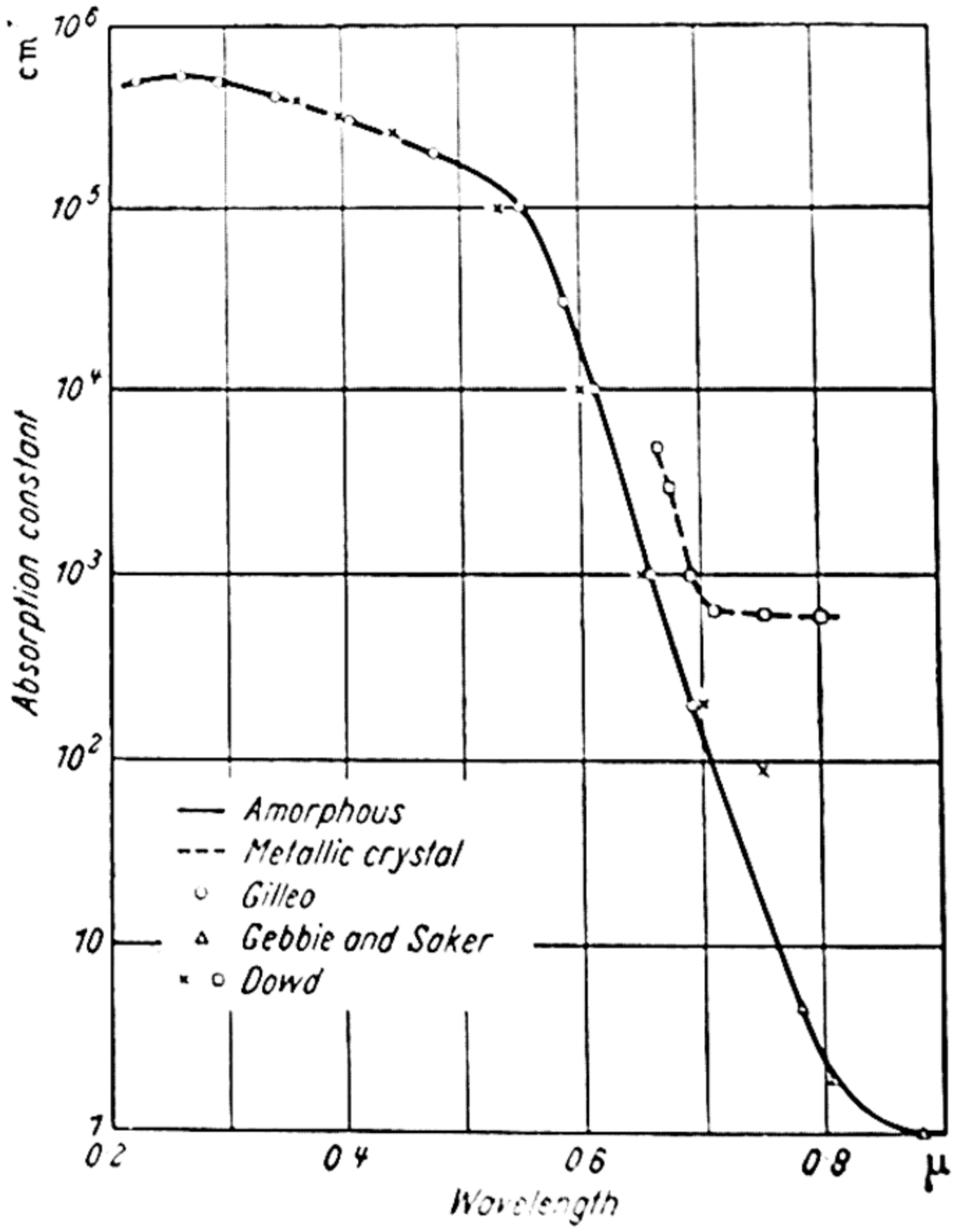

Figure 42. Absorption in selenium

that this part of the absorption curve can be regarded as well established. The absorption falls relatively slowly, so that the edge is not well defined. In germanium for example, K decreases by 100 : 1 per 0·1 eV, whereas for selenium the same fall requires 0·3 eV. Also the rate of fall is roughly constant from 0·55 to 0·8 μ. Nevertheless, Gilleo interprets his results as locating the absorption edge near 2·5 eV, and points

out that the Se–Se bond strength of 57 k cal/mole corresponds to approximately this energy.

Becker and Schaper measured the temperature shift of the absorption edge for the range ± 150°C. For a layer 0·45 μ thick the wavelengths for 30 per cent transmission were:

− 150	− 60	+ 20	+ 90	+ 150°C
570	583	593	601	608 mμ

Hence for the whole range of temperature the average energy shift is $dE/dT = -4{\cdot}6 \times 10^{-4}$ eV/°C.

Gilleo measured the absorption in a layer of thickness 98 μ between room temperature and liquid air temperature. The wavelengths for an absorption constant of 700 cm^{-1} were:

298	262	228	199	163	125	86°K
657	646	637	629	620	613	607 mμ

The average shift for this temperature range is therefore $dE/dT = -7{\cdot}5 \times 10^{-4}$ eV/°C.

Monch (1939) measured the shift of the absorption edge of selenium layers formed by rapid cooling of the melt. The wavelength for a given absorption level was found to decrease from 670 mμ at + 50°C to 600 mμ at − 200°C. The corresponding energy shift is therefore $dE/dT = -8{\cdot}8 \times 10^{-4}$ eV/°C. These values of dE/dT determined from the absorption shift should be more reliable than the rough estimate obtained from the photoconductivity data, the mean value being $dE/dT = -7 \times 10^{-4}$ eV/°C.

20.3. MONOCLINIC RED SELENIUM

This variety of selenium, which has a density of 4·46 gm/cm^3, may be prepared by crystallization from solutions in carbon disulphide. The crystals are stable at room temperature, but convert to the metallic form if heated above 100°C.

The material is a near insulator. According to von Hippel (1948) the current should be carried primarily by electrons, the positive holes being immobile as they belong to closed ring molecules.

Conductivity and Photoconductivity of Monoclinic Form

Gudden and Pohl (Gudden, 1928) carried out an investigation of the primary photocurrent in this form of selenium. From

various curves published by these workers, it appears that at room temperature the resistivity $\rho \sim 10^{15}\,\Omega$ cm. Use of the formula for intrinsic conductivity $\sigma = \sigma_0 \exp(-E/2kT)$, with $\sigma_0 \sim 1{,}000$ as is commonly observed, gives $E = 2{\cdot}1$ eV. However, present estimates of mobility in selenium are < 1 cm sec^{-1}/V cm, so that $\sigma_0 \sim 1$. This would reduce the estimated value of E to $1{\cdot}7$ eV.

Gudden and Pohl found that the photocurrent was directly proportional to the applied field for the range of measurements used *i.e.* up to 4,000 V/cm. Photocurrents were of the order 10^{-13} to 10^{-11} amp. Furthermore the current was strictly proportional to the incident intensity, for powers up to 10^{-4} W/cm^2. It was found necessary to use short illumination times (*i.e.* ~ 1 sec) to ensure that the rate of charge transfer across the crystal was constant. The spectral distribution of sensitivity is shown in *Figure 41*b, curve A. The peak sensitivity lies at $0{\cdot}7\,\mu$ *i.e.* at much longer wavelengths than for the amorphous films. The threshold wavelength of $\lambda_t = 0{\cdot}78\,\mu$ gives an optical activation energy of $1{\cdot}6$ eV. On illuminating the crystal in a direction at right angles to that used above, a similar curve was obtained, but shifted slightly (by $0{\cdot}02\,\mu$) to shorter wavelengths.

20.4. HEXAGONAL METALLIC SELENIUM

The grey form of selenium is referred to as the metallic type because its conductivity is some 10^{10} times greater than the monoclinic form. However its conductivity is still a factor of 10^{10} below that of a good metal, being $\sim 10^5\,\Omega$ cm at room temperature. This is the form of selenium which is used in practical selenium photocells, and for this reason it was for a long time the only form in which there was much experimental interest. It has a density of $4{\cdot}8$ g/cm^3, and lattice constants $a = 4{\cdot}355$, $c/a = 1{\cdot}365$ (Straumaris, 1940). The lattice is built up of long spiral chains of atoms, with homopolar binding between adjacent atoms of the chains, and van der Waals forces between the chains. It is a highly anisotropic material, as shown by the fact that the thermal expansion coefficients are of opposite signs for the different crystal

directions. Perpendicular to the c axis $\mathrm{d}L/L\mathrm{d}T = 74 \times 10^{-6}$, and parallel $\mathrm{d}L/L\mathrm{d}T = -18 \times 10^{-6}$.

Conductivity in Metallic Selenium

MULLER (1938) measured the conductivity of small needle-shaped crystals and obtained $\rho \simeq 10^5\ \Omega$ cm at room temperature. SCHWEICKERT (1950) found that by the addition of small quantities of halogens the resistivity could be raised to $10^7\ \Omega$ cm. HENISCH and SAKER (1952) found an increase in resistivity on adding mercury, but AFANASEV (1950) found the conductivity increased if sulphur (up to 5 per cent) was added. The effects of small amounts of antimony and tellurium have been investigated by KOZLOUSKI and NASLEDOV (1943).

Marked anisotry in the conductivity is shown by the results of DE BOER (1947) who gives the resistivities parallel ($\|$) and perpendicular ($\perp$) to the c axis as 2 to $5 \times 10^4\ \Omega$ cm and $2 \times 10^6\ \Omega$ cm respectively. The conductivity is thus greater *along* the chains of atoms. More extensive measurements have been carried out by HENKELS (1949–50), who found the conductivity to be less anisotropic than given by de Boer. At room temperature Henkels found $\|\ c$ axis, $\rho = 1$ to $2 \times 10^5\ \Omega$ cm, and $\perp\ c$ axis, $\rho = 5 \times 10^5\ \Omega$ cm. The conductivity was found to increase on heating, the plot of log (resistance) against reciprocal temperature being fairly linear between room temperature and the melting point. The activation energy was 0·3 eV. No intrinsic conductivity is apparent, in fact measurements of thermoelectric power indicate that the carrier concentration (of positive holes) *decreases* on heating. Typical concentrations are $2 \times 10^{14}/\mathrm{cm}^3$ at 315°K and $4 \times 10^{13}/\mathrm{cm}^3$ at 480°K for highly purified samples. The thermoelectric power is not anisotropic, so that the anisotropy in the conductivity must lie in the mobility. Typical values found by Henkels are:

T	50°C	100°C	190°C
n	1·5	1·0	$0{\cdot}6 \times 10^{14}/\mathrm{cm}^3$
$b\|\|c$	0·4	1·0	5 cm sec^{-1}/V cm^{-1}
$b\perp c$	0·1	0·3	1 cm sec^{-1}/V cm^{-1}

DE BOER (1947) also found an activation energy of 0·3 eV $\perp$

to the c axis, but only for temperatures $< 70°C$. At higher temperatures he found an energy of 1·6 eV.

Singularly few Hall constant measurements have been reported for selenium. ECKART and KITTEL (1941) found a mobility ~ 1 cm^2/V sec at room temperature. The only measurements over a range of temperatures are those by PLESSNER (1951), who found it impossible to obtain reliable results by conventional d.c. methods, and adopted a method in which the magnetic field was alternating at 80 c/s. Direct current was passed through the specimen (as this was found to give lower noise than alternating current) and the 80 c/s Hall voltage amplified in a narrow band amplifier, and rectified in a phase sensitive detector. The sign of the Hall effect confirmed that the carriers were positive holes, and that the concentration did indeed decrease with rising temperature. The figures obtained were:

T	460	357	294°K
σ	1·3	0·5	$0{\cdot}27 \times 10^{-5}\Omega^{-1}\text{cm}^{-1}$
n	0·8	0·7	$1{\cdot}1 \times 10^{14}/\text{cm}^3$
b	1·0	0·4	0·2 cm sec^{-1}/V cm^{-1}

Over the temperature range 250°K to 500°K the conductivity for both crystal directions obeyed an exp $(-E/2kT)$ law with $E = 0{\cdot}26$ eV. The ratio $\sigma_{\parallel}/\sigma_{\perp}$ was 10 : 1.

Plessner concludes from these results that the conductivity is largely determined by internal barriers within the crystals, a conclusion which is supported by the non-ohmic behaviour of the crystals for field strengths of only a few V/cm. BILLIG (1952) postulates that these barriers are formed by gaps between the ends of long chains of atoms, the carriers having high mobility within any individual chain. The same reasoning would explain the low conductivity perpendicular to the chains relative to that along the chains. This worker also points out that while the spacing of atoms along the chain is quite definite, the spacing between chains is to some extent dependent on the previous treatment. This is presumably the explanation of the range of values (3 to 100) reported for $\sigma_{\parallel}/\sigma_{\perp}$.

An extension of this idea would attribute the insulating properties of red selenium to the fact that in this form the

chains are closed into rings of only 8 atoms, so that the distance which an electron might travel freely would be strictly limited.

Photoconductivity in Metallic Selenium

Since photoconductivity was first reported in selenium almost 60 years ago (SMITH, 1873) a vast amount of research and development work has been carried out on cells made of this allotropic form. Most of the work has been on layers which have been given various baking or annealing treatments by the workers concerned, but there is also considerable data for single crystals.

Spectral Sensitivity Measurements on Metallic Selenium

Many spectral sensitivity curves have been presented by SIEG and BROWN (1914, see also HUGHES and DUBRIDGE, 1932, or BARNARD, 1930). These results (of which a typical set are shown by curve *C* of *Figure 41*b) are for single crystals grown from the vapour. They show peaks in the range 0·7 to 0·8 μ, with $\lambda_{\frac{1}{2}}$ values between 0·76 and 0·83 μ. Measurements by the same workers (BROWN and SIEG, 1914) for various commercial and experimental selenium cells show similar curves, with $\lambda_{\frac{1}{2}}$ values in the range 0·76 to 0·84 μ.

Both sets of curves show evidence of an additional maximum at short wavelengths for some of the samples measured. This maximum would perhaps correspond with the band of sensitivity found in evaporated amorphous layers, as shown by *Figure 41*a. For evaporated layers of metallic selenium $\sim \frac{1}{2}$ μ thick, GILLEO (1951) found $\lambda_{\frac{1}{2}} = 0{\cdot}7$ μ.

Spectral sensitivity curves for the photovoltaic effect in various barrier layer cells are given by ZWORYKIN and RAMBERG (1949). The curves are all very similar, the maxima lying between 0·55 and 0·60 μ, and $\lambda_{\frac{1}{2}} = 0{\cdot}63$ to 0·65 μ. These curves resemble that obtained by ECKART and SCHMIDT (1941) which is shown in *Figure 41*b, curve *B*. The sensitivity falls rapidly at long wavelengths, being only 1 per cent of the maximum at 0·75 μ. The fall is more gradual at short wavelengths, and 10 to 50 per cent sensitivity is retained at 0·35 μ.

SIEG and BROWN (1914) measured spectral sensitivity curves for crystals when they were irradiated along three mutually

perpendicular axes. The values of λ_2 were found to vary over the range 0·78 to 0·83 μ for the three directions. This effect may explain much of the scatter in the λ_2 values which have been reported for crystals of unknown orientation, or layers of crystal aggregates.

PUTSEIKO (1949) measured the spectral sensitivity by an a.c. method, putting the selenium between the plates of a condenser. He found two peaks at 0·55 μ and 0·73 μ, with λ_2 values of 0·64 μ and 0·79 μ. These two figures agree well with those obtained for barrier layer cells and photoconductive cells respectively, as though the condenser method represented a combination of the two types of cell.

Observations by RIES (1918) and ELLIOT (1915) show that the maximum of the spectral sensitivity curve shifts to shorter wavelengths on cooling, and to longer wavelengths on warming. The former gives a shift of 0·04 μ for 72°C, and the latter 0·07 μ for 210°C. These values give $dE/dT = -4{\cdot}5 \pm 1 \times 10^{-4}$ eV/°C. This value is rather less than that found from the shift of the absorption edge.

The addition of small amounts of tellurium to selenium is found to increase the sensitivity in the neighbourhood of 0·9 μ, while cadmium gives a secondary band of photovoltaic sensitivity at 0·7 μ (GORLICH, 1948 and 1951).

Photocurrent–Intensity Relation

Different observers have found different laws for the relation between photocurrent and intensity of the incident radiation. GUDDEN and POHL (1925) found a linear relation at fairly low powers, whereas other workers have found a (Power)$^{\frac{1}{2}}$ law (BERNDT, 1904; MINCHIN, 1908). Complicated laws, including laws with fractional and decimal indices, have also been quoted.

Much confusion occurs through workers using unresolved light, by not carrying the measurements over a sufficiently large range of intensities, and by use of cells of non-linear current–voltage characteristics. Also errors are introduced by use of load resistors comparable with the cell resistance, such that both cell current and applied voltage vary during the measurements. Further errors may be introduced by heating of the layers by the radiation.

For monochromatic radiation at fairly low intensities, using crystals where the current was proportional to the applied voltage, and with constant voltage across the crystal, Gudden and Pohl found a definite proportionality between photocurrent and energy. This is as would be expected on the photo-response theory of § 6.1. Fournier d'Able (1913) found both linear and (Power)$^{\frac{1}{2}}$ laws. Pfund (1912) found that there was a linear relation when red light was used, but that with short wavelength light—violet to yellow—a (Power)$^{\frac{1}{2}}$ law resulted. Similar results were obtained by Brown and Sieg (1914). The explanation is presumably the same as suggested for the results on phosphorus, namely that, whereas the red light is only weakly absorbed and thus produces photoelectrons throughout the material, the short wavelengths will be absorbed in a thin surface layer, where there will therefore be a high density of photoelectrons. The rate of recombination will thus increase and lead to a (Power)$^{\frac{1}{2}}$ law. For sufficiently small intensities of course, the response should be linear even at short wavelengths.

As already discussed in Chapter 8, the response of photovoltaic cells is a logarithmic function of the intensity of irradiation. Photovoltages as high as 0·5 V (with quantum efficiencies $\sim$ 70 per cent) have been reported by Preston (1950) for cells using layers of cadmium oxide as the transparent, conducting electrode. Keck (1946) gives the limiting sensitivity of a selenium cell as $\sim 10^{-7}$ W/cm^2 for a 2,400°K tungsten source, with a quantum efficiency of 30 per cent at 0·55 μ.

Response Time

Selenium photoconductive cells show pronounced time lag effects. In some cases five minutes may be required to reach 90 per cent of the final photocurrent, with a similar recovery time after removal of the radiation. With chopped radiation the response therefore falls rapidly with increasing frequency. However for frequencies of 1 to 3 kc/s the response is practically constant (Zworykin and Ramberg, 1949). The slow effects are no doubt caused by secondary photocurrents, while the sensitivity remaining at the high frequencies results from the

primary photo-effect. The increase in response time when secondary photocurrents occur has been clearly demonstrated for amorphous films.

For barrier-layer photovoltaic cells, the frequency response is determined mainly by the high capacity of the barrier layer. For typical cells the response falls to half its low frequency value at 5 to 10 kc/s.

Absorption in Metallic Selenium

Transmission measurements have been carried out on single crystals by Dowd (1951), who used crystals only 10^{-3} to 10^{-2} cm thick, formed by evaporation. The absorption increased rapidly as the wavelength was reduced below 0·7 μ, whilst at longer wavelengths it was practically constant. The results are shown by the broken line of *Figure 42*. For wavelengths below 0·7 μ the absorption constant is about five times greater than for amorphous selenium. At longer wavelengths the absorption remains constant at ~ 600 cm^{-1}. This absorption must be due to the free carriers present in metallic selenium, which are absent in the near insulating amorphous form. By comparison with germanium and silicon this absorption is very high. With a carrier concentration $\sim 10^{14}$/cm^3 (as is found for pure selenium), the absorption constant for germanium or silicon would be $\sim 0{\cdot}1$ cm^{-1}. As shown by equation 15, the absorption produced by free carriers is inversely proportional to the (mobility)^2. As the measured mobility in selenium is $\sim 10^4$ times less than in germanium this factor would more than explain the difference in absorption constants.

Gilleo (1951) studied the absorption of selenium layers before and after transformation from the amorphous type to the metallic type. He found that the wavelength for a given absorption level was increased from 500 to 600 mμ (or 560 to 680 mμ for a different absorption level) *i.e.* a decrease of 0·4 eV in the quantum energy.

For the metallic form, a secondary peak was found in the absorption spectrum at 520 mμ. In the region of 0·6 μ the absorption edge moved to shorter wavelengths by 30 mμ on cooling from 360°K to 74°K, corresponding to an energy shift of $dE/dT = -4 \times 10^{-4}$ eV/°C. This value is close to that found

from the shift in spectral sensitivity curves. Reflection measurements of the absorption index of single crystals by SIEG (1922) and WELD (1922) show two maxima for both crystal directions. One maximum lies at $\lambda < 0{\cdot}45\ \mu$, and the other (secondary) maximum at $0{\cdot}65\ \mu$.

20.5. LIQUID SELENIUM

The properties of liquid selenium are of importance because the chain structure thought to exist in the liquid state is similar to that which occurs in amorphous selenium. It is therefore of interest to find that the conductivity of liquid selenium increases very rapidly with temperature. HENKELS (1950b) has carried out extensive measurements on very pure selenium, and finds an activation energy from the conductivity temperature curves of 2·3 eV, in substantial agreement with earlier results by PELABON (1921). LIZELL (1952) finds the conductivity to be $1{\cdot}26 \times 10^{-4}\ \Omega^{-1}\,\mathrm{cm}^{-1}$ at 480°C, with an activation energy of 2·28 eV. This worker also confirmed that the d.c. conductivity equalled that at 1 Mc/s provided low applied fields were used. These energies are near to that of the Se–Se bond (57 k cal/mole) and to the optical activation energy found from photoconductive measurements on amorphous selenium.

20.6. REFRACTIVE INDEX AND DIELECTRIC CONSTANT

There is much conflicting data on the refractive index of selenium, particularly amongst the measurements performed on single crystals. Some results for single crystals are summarized in *Table X*, where the two values given refer to two crystal directions. From these results, one can only

Table X

Observer	0·4 μ		0·5 μ		0·6 μ		0·67 μ	
Sieg (1922) ..			5·0	3·2	5·2	3·8	5·0	4·0
Miller (1925) ..	3·7	3·2	3·4	3·4				
Skinner (1917) ..	4·4	2·8	4·1	2·8	4·1	3·0	4·0	3·1
Weld (1922) ..			5·0	3·2	5·2	3·8	4·9	3·9

say that the two refractive indices are roughly 4 to 5 for electric vector parallel to the crystal axis, and 3 to 4 when perpendicular. These measurements were all made by reflection of polarized light in a spectral region where the selenium is absorbing strongly. Furthermore, EDMUNDS (1904) has shown that the results obtained by these methods are very susceptible to the state of the surface of the selenium. None of the above results show any signs of fitting a normal dispersion curve. For these reasons it is felt that not much reliance can be placed on these measurements.

Accurate measurements were made by WOOD (1902) of the refractive index of a thin prism. This was made by casting molten selenium between flat plates, so that presumably the material would be in the vitreous or amorphous state. Results obtained over the whole visible spectrum are shown in *Figure 43*.

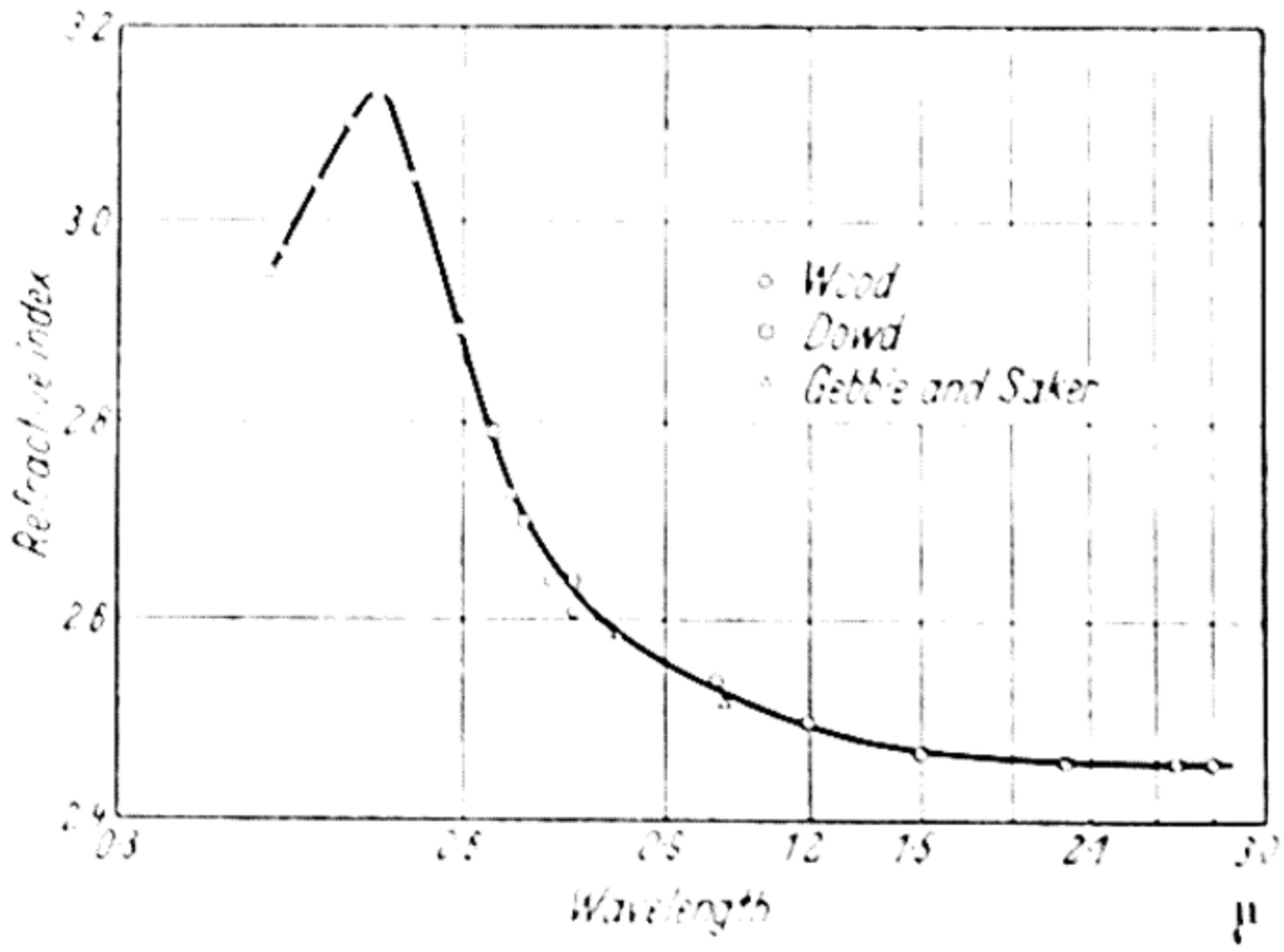

Figure 43. Refractive index of selenium

A maximum value of $n = 3{\cdot}13$ is obtained at $0{\cdot}5\ \mu$, the index falling rapidly at shorter wavelengths as the main absorption band is entered (see *Figure 42*). At the red end of the visible region the index has fallen to $\sim 2{\cdot}6$. GEBBIE and SAKER (1951) have recently extended the measurements into the near infra-red by using an image-converter tube to measure the angle of minimum deviation of their prism. DOWD (1951) has further extended the measurements to $2{\cdot}7\ \mu$ with the aid of a lead sulphide detector. As may be seen from *Figure 43* there is little

dispersion beyond 1·5 μ, the constant value of the index being $n_0 = 2{\cdot}46$. At still longer wavelengths COBLENTZ (1908) gives the reflectivity as 18·5 per cent which corresponds to $n \simeq 2{\cdot}5$.

From the refractive index value of 2·46, the dielectric constant would be expected to be near 6·05. Measured values by SCHMIDT (1903) and VONWILLER (1907) are 6·6 and 6·13, while TAMMAN (1931) gives 6·31 at 16°C. GEBBIE and KIELY (1952) quote a recent (unpublished) measurement by Clark as giving $6{\cdot}3 \pm 0{\cdot}1$ at frequencies < 40 Mc/s, while at a frequency of 10^{10} c/s they themselves find $5{\cdot}97 \pm 0{\cdot}04$ for amorphous selenium. It may be noted that the dielectric constant of liquid selenium differs little from that of the amorphous solid, the value given by WESELOWSKI (1938) being $\epsilon = 6{\cdot}07$. The values for the dielectric constant, and (refractive index)^2 agree well for the amorphous material, if we take the value of ϵ at 10^{10} c/s. There seems to be a significant difference between the values at 10^{10} c/s and 10^7 c/s, indicating appreciable absorption in this range. For crystalline selenium precise measurements of ϵ in different crystal directions, and of n in the infra-red on prisms cut from single crystals would be required to provide an accurate check of the validity of the relation $n_0{}^2 = \epsilon$.

From the data of MEIER (1910), the maximum in the imaginary part of the optical dielectric constant occurs near 0·34 μ. Using this value in the simple formula of equation 17 would give a calculated dielectric constant of ~ 5. More accurate agreement with the measured value might be obtained if fuller absorption data were available, so that the area under the absorption curve could be integrated in the manner shown to give good results for silicon.

TAMMAN (1931) found the dielectric constant varied linearly with temperature from 6·31 at 16°C to 6·34 at 29°C. The decrease on cooling would lead one to expect a shift of the spectral sensitivity curve to shorter wavelengths if the $E \propto n^{-4}$ relation applies*. Such a shift is in fact observed. The change in ϵ is equivalent to a change in n^4 of $\sim 7 \times 10^{-4}$ per °C, so the expected change in activation energy would be $\sim 13 \times 10^{-4}$ eV/°C (at a wavelength of 0·7 μ). This is about

* Discussed in Chapter 9.

twice the observed shift, but in view of the extremely small range of measurement of ϵ, the agreement is reasonable.

20.7. SUMMARY AND DISCUSSION

Photoconductivity has been observed in all three forms of selenium. For both the amorphous and red crystalline varieties the photocurrent is proportional to the radiant power. For the metallic type both linear and (Power)$^{\frac{1}{2}}$ laws may be obtained, depending on the intensities and wavelengths used. The primary photocurrent has been shown to have a response time $< 50\ \mu$ sec in amorphous selenium, the long-time effects often found in selenium cells being attributed to secondary photocurrents. Both photocurrents (in amorphous Se) and dark currents (in metallic Se) are carried mainly by positive holes, the mobilities in the latter case being $\sim 0{\cdot}2$ cm sec^{-1}/V cm^{-1} at room temperature.

Regarding the difference in conductivity of the various forms, VON HIPPEL (1948) has suggested that the low conductivity of the red crystalline variety results from the fact that the positive holes belong to ring molecules and are thus immobile, whereas in the metallic form charge transfer can take place along the semi-infinite chains of atoms. BILLIG (1952) has suggested that the positive holes arise from acceptor centres produced by structural defects, possibly associated with the terminations of the chains.

Activation Energies

Activation energies estimated for the various forms cover the range 1·5 to 2·5 eV. For amorphous selenium, the activation energy found from photoconductive measurements is 2·5 eV. This agrees approximately with the wavelength at which the absorption constant begins to fall rapidly. Liquid selenium, which has a similar structure to amorphous selenium, shows a thermal activation energy of 2·3 eV. Furthermore the strength of the Se–Se bond is 2·5 eV. All these values thus agree fairly well, and indicate that for the random chain structure free current carriers can be produced either optically or thermally when an energy of approximately 2·4 eV is used to break an Se–Se bond.

Both metallic and red selenium crystals show activation energies in the range 1·5 to 1·65 eV as determined from photoconductivity measurements, the scatter being partly due to the random orientation of the anisotropic crystals. From photovoltaic measurements an activation energy of 1·9 eV is obtained. By resistance–temperature measurements on an amorphous film (which showed photoconductivity in the same spectral region as the crystalline forms, in addition to the short wavelength band) a thermal activation energy of approximately 1·7 eV was found.

The absorption curve has been shown to move to longer wavelengths when an amorphous layer is converted to a metallic one, a secondary absorption band being formed. It thus appears that as the short chains in amorphous selenium increase in length, and become ordered and parallel (as in the metallic modification) the activation energy falls by 0·5 to 1·0 eV.

Soft x-ray absorption measurements have been reported for selenium by GIVENS and SIEGMUND (1952). The absorption curve, which should be of the same form as the density of states function, shows a doublet on the absorption edge with a separation of only 0·7 eV. It is possible that this doublet represents structure in the conduction band, and that the two peaks correspond to the two peaks observed in the optical absorption curve.

21

TELLURIUM

21.1. GENERAL PROPERTIES

Recent x-ray investigations of tellurium layers *in vacuo*, from liquid air temperature up to the melting point, show that no change in the crystal structure occurs (Scanlon and Lark-Horovitz, 1947). High pressure measurements (Bridgman, 1938) also show that no phase change occurs up to a pressure of 30,000 kg/cm^2. It thus seems probable that tellurium exists in only one form.

The relation of tellurium to the other members of Group VI of the periodic table has been discussed by von Hippel (1948), who describes the lattice as made up of spiral chains of atoms, with interatomic spacing 2·86 Å. Tellurium crystals are highly anisotropic—for example the compressibility coefficients have *opposite* signs parallel and perpendicular to the main crystal axis (Gmelin, 1940). Tellurium boils at 1,390°C at atmospheric pressure, and the vapour pressure is quite high at moderate temperatures (0·5 mm Hg at 490°C), so that the material may readily be distilled *in vacuo*.

21.2. CONDUCTIVITY AND HALL EFFECT IN TELLURIUM

Bridgman (1938) gives the resistivities parallel and perpendicular to the crystal axis as $\rho_{\parallel} = 0{\cdot}056\ \Omega$cm and $\rho_{\perp} = 0{\cdot}15\ \Omega$cm. However, very small traces of impurities affect the conductivity, and with 99·99 per cent purity tellurium Cartwright and Haberfeld-Schwarz (1935) found $\rho = 0{\cdot}37$ to $0{\cdot}43\ \Omega$cm. With small additions of copper these workers obtained the following conductivities:

Cu *content*	0·1	0·2	0·6	1·5 per cent
Conductivity	8	16	30	100 Ω^{-1}cm^{-1}

The results were not sufficiently definite to decide whether the conductivity increased in proportion to the impurity

content, or to the square root thereof *i.e.* whether each impurity atom produced a free current carrier, or whether equation 7 applied. Small amounts of antimony had marked effects on the conductivity, 0·1 per cent giving $\sigma = 300\ \Omega^{-1}\text{cm}^{-1}$.

For polycrystalline specimens of extreme purity, BOTTOM (1949) obtained a resistivity of 0·6 Ωcm at 300°K. Further measurements by this worker established that this was *intrinsic* conductivity, the impurity conductivity at lower temperatures being approximately 10 times smaller.

WARBURTON (1927) and KRAUS and JOHNSON (1928) observed that the conductivity increased with rising temperature, with indications of a low value of activation energy. For the temperature range 10°C to 100°C, the results of CARTWRIGHT and HABERFELD-SCHWARZ (1935) show an activation energy of approximately 0·3 eV. With additions of 0·3 per cent of antimony or more, the material became semi-metallic, and the resistance *increased* with temperature. Measurements at very low temperatures have been reported by CHENTSOV (1948).

WOLD (1916) measured the Hall effect in bulk tellurium, his values indicating an activation energy $\sim$ 0·4 eV for the restricted temperature range 27 to 79°C. For layers evaporated *in vacuo*, SCANLON and LARK-HOROVITZ (1947) found $E = 0{\cdot}36$ eV, the Hall effect indicating that positive holes were the predominant current carriers. At low temperatures the impurity activation energy was 0·04 eV. BOTTOM (1948) gives $E = 0{\cdot}38$ eV. This worker found that the Hall constant showed a double reversal as soon as the purity reached a certain minimum value, being negative between -40°C and $+230$°C, and positive elsewhere. The anisotropy in resistance was found to be $\rho_\perp/\rho_{\parallel} = 1{\cdot}9 \pm {\cdot}1$, with no isotropy in the Hall constant. JOHNSON (1948) also gives $E = 0{\cdot}38$ eV, with a hole mobility given by $b_h = 2{\cdot}7 \times 10^6 T^{-3/2}$ *i.e.* $\sim 550\ \text{cm sec}^{-1}/\text{V cm}^{-1}$ at room temperature. The electron mobility was found to have approximately the same value.

The most recent and most extensive measurements published, are those by FUKUROI *et alii* (1949 and 1950). These workers used single crystals made from material which had been purified by repeated fractional distillations. For the final

material, spectroscopic examination showed the main impurity to be tin in proportions of 10^{-4} to 10^{-3} per cent *i.e.* a few parts per million. The tellurium was cast in glass tubes and crystallized by slow cooling. The glass was then dissolved by hydrofluoric acid to give cylindrical specimens 1 to 2 mm diameter and 20 mm long. Simultaneous measurements of conductivity, Hall effect, thermoelectric power, and magneto-resistance were made on these specimens for temperatures between 85°K and 600°K.

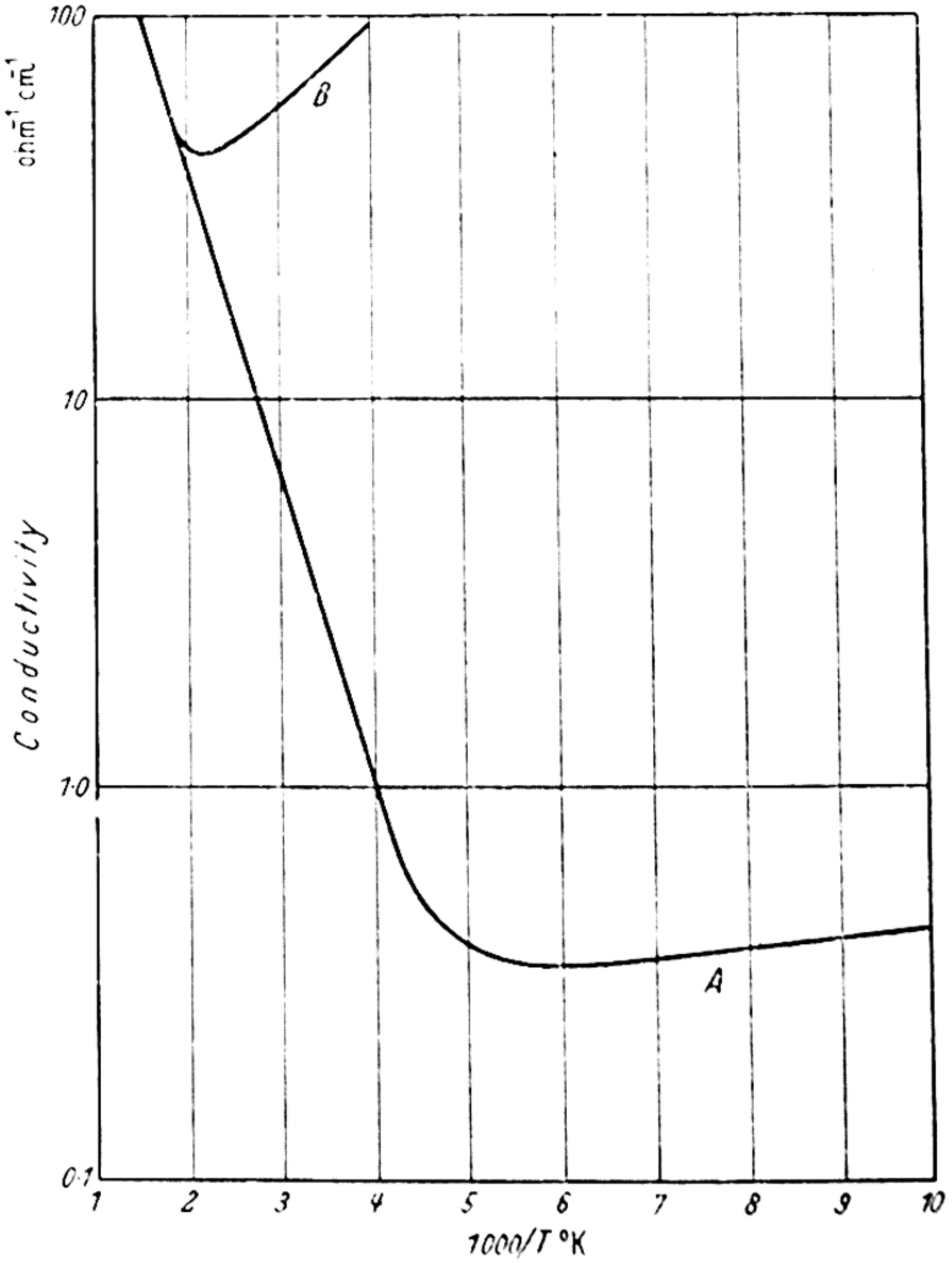

Figure 44. Conductivity of tellurium

The conductivity of one of the purest specimens over this temperature range is shown in curve *A* of *Figure 44*. It will be seen that below 200°K the resistivity is approximately constant at 2·5 Ωcm. At higher temperatures the conductivity rises

rapidly. For an impure specimen, the values of curve *B* are obtained*. Points for both specimens lie on the same line at high temperatures, thus establishing that this is the intrinsic line. From the slope of the line the activation energy is 0·34 eV.

Double reversal of the Hall constant was found for all pure specimens, the higher temperature change-over point being 240°C in close agreement with Bottom's value. The thermo-electric power also showed a double reversal of sign, although not at exactly the same temperatures as for the Hall effect change. The reversal of Hall constant is attributed to different temperature variation of the mobilities, b_h being $> b_e$ above 240°C, and $b_e > b_h$ at lower temperatures. The estimated mobility values are given in *Table XI*.

Table XI

T °C	μ_e $cm^2/V\ sec$	μ_h $cm^2/V\ sec$
0	1,850	1,350
27	1,650	1,100
127	1,000	610
200	570	450
240	400	400
320	260	320

It was established that both a.c. and d.c. Hall effect measurements gave substantially the same results.

The magneto-resistance effect was measured, and the value $\Delta\rho/\rho H^2 = 3 \times 10^{-10}$ obtained at room temperature. Using equation 4 this result indicates a mobility $\sim 2{,}500\ cm^2/V\ sec$ at room temperature and $\sim 1{,}000\ cm^2/V\ sec$ at 500°K.

From the mobility values given in *Table XI* and the intrinsic conductivity of $3\ \Omega^{-1}cm^{-1}$ (for the particular orientation of the crystal used) the carrier concentration is $n_e = n_h = 7 \times 10^{15}/cm^3$ at room temperature.

Resistance–temperature measurements have been carried out on evaporated films by Sakurai and Munesue (1952). These workers find that their results obey the expected exponential

* Results quoted by Putley, 1952.

law between room temperature and 500°K, provided allowance is made for a certain temperature independent residual resistance, the magnitude of which varies with heat treatment and deposition temperature. The value of activation energy is found to be 0·34 eV.

Tellurium is anomalous in that for certain temperature regions the mobility of holes can exceed that of electrons. Also the mobility varies for the different crystal directions, and the magneto–resistance effect shows unusual variations with temperature. All these effects emphasize the anisotropy of tellurium, and indicate that the simple theory of Hall effect, magneto–resistance effect, and the concepts of effective mass, must be applied with caution to this element.

21.3. PHOTOCONDUCTIVITY

Early attempts to observe photoconductivity in tellurium were unsuccessful, and the workers concluded that the element was not photosensitive (COBLENTZ, 1918; BROWN and MACMAHON, 1929). However extensive measurements have now been carried out on photoconductivity in tellurium layers, although the photoconductive effect is only of significance when the layers are cooled.

Experimental cells were made in Dewar flask type envelopes of the type illustrated in *Figure 13*a. The layers were formed by repeated distillation of *Specpure* tellurium with the cells evacuated to pressures $< 10^{-6}$mm Hg. Electrodes of graphite or platinum, painted on the end of the inner part of the Dewar flask, were used to make contact with the layers.

Cell 1

Graphite electrodes were used, of dimensions 8 mm × 2 mm gap. About 1 mg of *Specpure* tellurium was inserted in the cell, and after outgassing for some hours in a good vacuum, the material was evaporated on to the front window of the cell by heating the whole cell in the oven, whilst cooling the front window with an air blast. The material was later distilled over to the electrode surface (water-cooled) by an air–gas flame.

The area of film was approximately 2 cm^2, giving an

estimated layer thickness of $\frac{1}{2}$ to 1 μ. At room temperature the resistance was 2·7 kΩ. This figure indicates a specific resistance ~ 0·35 Ωcm. On cooling to 90°K the resistance increased by a factor of 5, falling by about 15 per cent on illumination with a 40 W lamp.

Spectral sensitivity— The spectral distribution of sensitivity was measured, using a lithium fluoride prism monochromator with radiation interrupted at 800 c/s, the layer being cooled by liquid oxygen. The resulting curve is shown in *Figure 45*a. The broken curve has been corrected for the absorption loss in the Pyrex window. This loss was measured at a later stage by breaking open the cell.

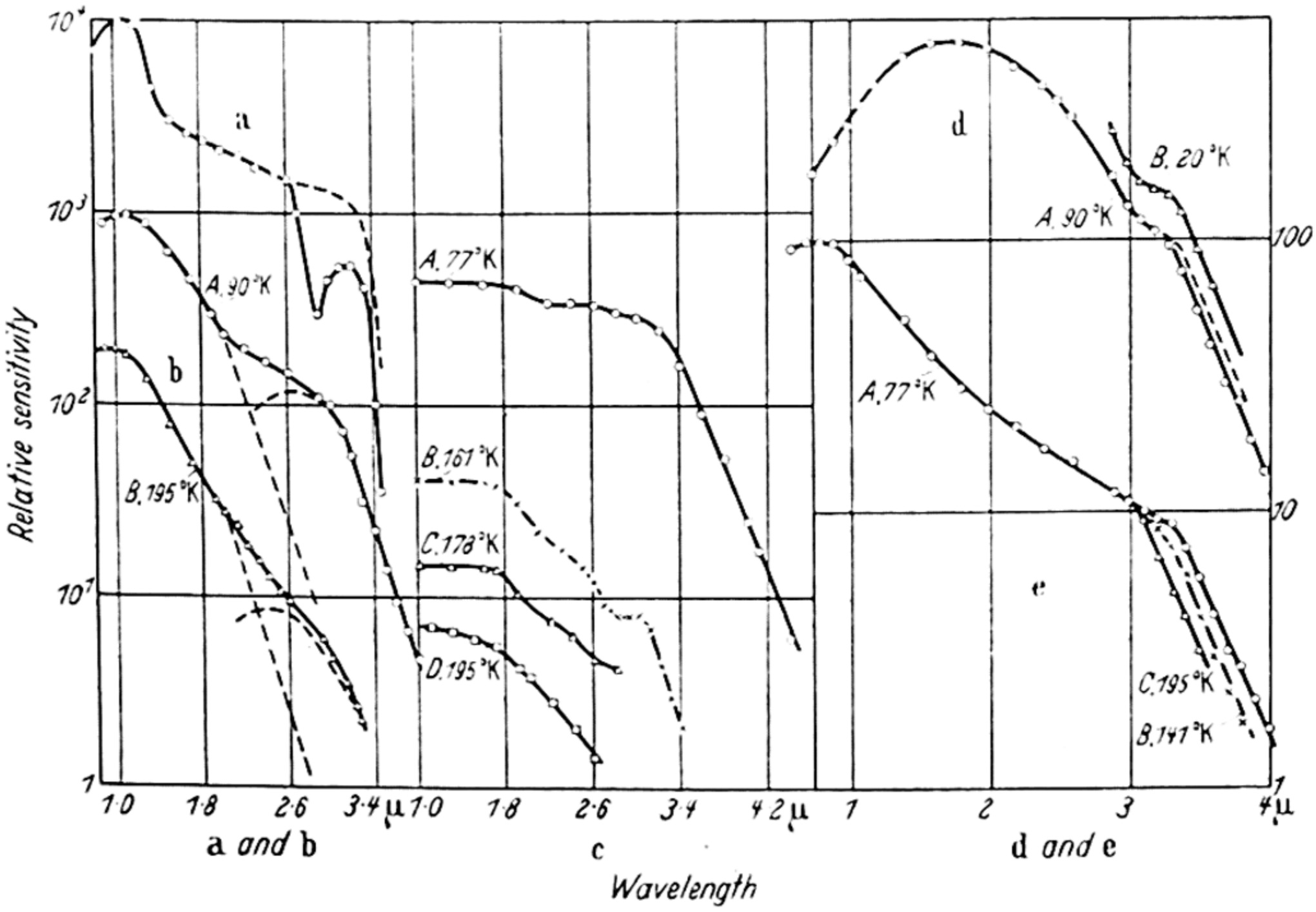

Figure 45. Spectral sensitivity curves for tellurium

Two bands of sensitivity are apparent, with threshold wavelengths $\lambda_{\frac{1}{2}} = 1{\cdot}4\ \mu$ and $3{\cdot}3\ \mu$. When the cell was opened the sign of the thermoelectric power was observed. This showed the current carriers to be positive holes.

Cell 2

This cell was made in the same manner as the previous one, and had a sensitive area 4 mm × 2 mm. The resistance was

5·8 kΩ at 292°K and 65 kΩ at 90°K. At the latter temperature the cell showed high sensitivity, and it was possible to measure its response time using a pulsed neon lamp, wide-band amplifier, and oscilloscope. The response time, which was measured on the falling edge of the pulse, was found to be 800 μsec (for a fall to 1/e).

The limiting sensitivity of the cell was measured at 90°K using radiation chopped at 800 c/s. The source was a 3 W bulb with a filament temperature ~2,000°C. With 3×10^{-6} W total radiation incident on the layer the resulting signal–noise ratio was 560 : 1 for 20 c/s bandwidth. Hence signal = noise for $5{\cdot}3 \times 10^{-9}$ W for 20 c/s bandwidth, or approximately $1{\cdot}2 \times 10^{-9}$ W for 1 c/s bandwidth. The a.c. signal from the cell was found to be proportional to the applied d.c. field for field strengths up to about 100 V/cm.

The spectral sensitivity curve was measured, with results very similar to those found for the first cell. On correcting for the loss in the cell window, it was found that $\lambda_i = 3{\cdot}4\ \mu$.

Cell 3

In view of the fact that measurements on cells 1 and 2 had shown that sensitivity extended to wavelengths longer than those transmitted by *Pyrex* of millimetre thicknesses, this cell was made with a 'bubble' window of very thin *Pyrex*, such as would give good transmission for wavelengths up to 4·5 μ. The electrodes were 4 mm × 1·5 mm gap, and the layer resistance 1 kΩ at room temperature, and 6 kΩ at 90°K. After redistilling the layer from the electrodes to the window and back again several times, the values became constant at 1·1 kΩ and 11 kΩ respectively.

The sign of the thermoelectric power was observed (by warming one side of the layer through the glass backing). As before the carriers were found to be positive holes.

Spectral Sensitivity

Conditions were the same as for the previous measurements, except that the interruption frequency was reduced to 85 c/s and the bandwidth reduced to 6 c/s, as this was found to

improve the signal–noise ratios. The results obtained for a layer temperature of 90°K are shown in *Figure 45*b, curve *A*. Two bands of sensitivity are again observed. As the curve has no flat part in the long-wave region which may be used as a datum to find the half-value wavelength, the curve has been analysed into its two component bands (as shown by the broken lines) assuming that the edge of the short wavelength band of sensitivity falls exponentially with the same slope as that observed for the long-wave band.

The threshold wavelength is now taken at half the value at the peak of the broken curve, and is found to be $\lambda_{\frac{1}{2}} = 3{\cdot}2\ \mu$. The value is relatively insensitive to the precise way in which the edge of the first band is extrapolated. The long wavelength part of the curve is fairly linear over a range of 30 : 1 indicating an exponential fall in sensitivity with wavelength.

In curve *B* measurements obtained at 195°K are shown. The sensitivity was much lower at this temperature, particularly at longer wavelengths. It was possible, however, with care, to measure out to 3·2 μ. By extrapolating the short wavelength band as before we may again isolate the long wavelength band. The results are not so accurate at this temperature, but the method serves to give an estimate of the spectral shift. The shift is found to be 0·18 μ for 105°C, the wavelength *increasing* on cooling. This is the only element found to give a positive energy shift with temperature, the value being $\mathrm{d}E/\mathrm{d}T \sim 2 \times 10^{-4}\mathrm{eV}/°\mathrm{C}$. The 195°K curve should give a fairly accurate figure for the threshold wavelength for the short wavelength band, since the long wavelength band is comparatively small. The value is $\lambda_{\frac{1}{2}} = 1{\cdot}4\ \mu$.

Relation between signal and radiant power— Several measurements were made of the relation between the a.c. photocurrent and incident radiation. A tungsten lamp was used as the source, the radiation being interrupted at 85 c/s. Results with the layer cooled by liquid oxygen are shown in *Figure 46*, curve *A*. As will be seen, the points lie mainly on two straight lines of slopes, half and unity, so that at low energy levels the response is linear, while at high levels the relation becomes photocurrent $\propto$ (Power)$^{\frac{1}{2}}$. The results are therefore in accord with the photo-response theory of Chapter 6.

Cell 4

This cell was made with a ' bubble ' window, the layer being formed in the same manner as for the previous cells. Extensive spectral sensitivity measurements were carried out on this cell with the particular aim of measuring the temperature shift of the threshold wavelength. The difficulty in performing this measurement lies in the fact that the sensitivity of the cell falls rapidly with increasing temperature, and furthermore the sensitivity of the long wavelength band—which is the part of greatest interest—falls more than that of the short wavelength band. Since the energy of the monochromator is low at long wavelengths the signal–noise ratio becomes very small. As a result of these factors it was not possible to extend the measurements to sufficiently long wavelengths at temperatures much above 150°K. Since the lowest convenient temperature to use was that of boiling nitrogen (77°K), measurements could only be made over a rather restricted range of temperature, with correspondingly small shifts and low accuracy.

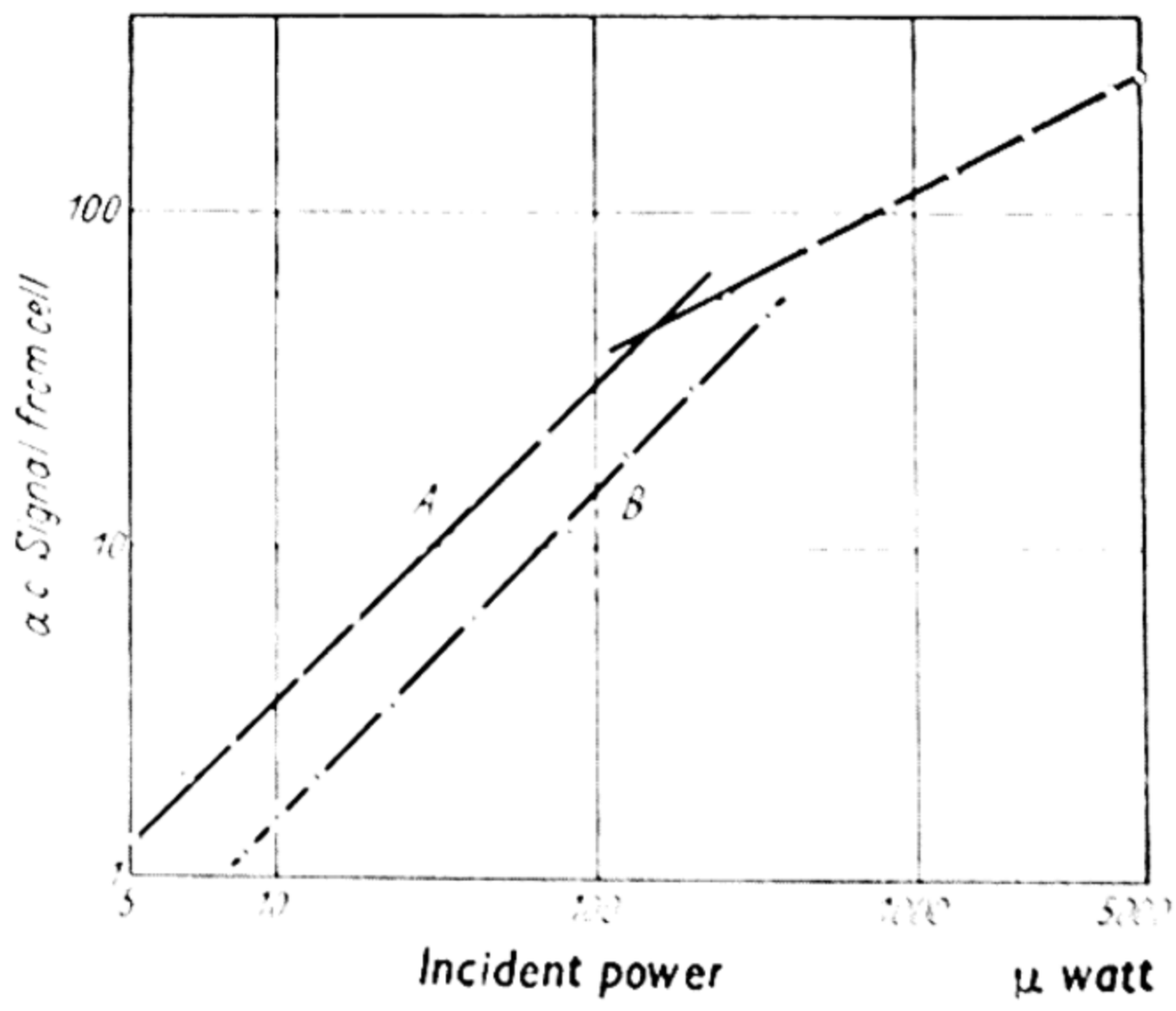

Figure 46. Photo-response of tellurium

Measurements were made at the following temperatures: *A*, 77°K, boiling point of liquid nitrogen; *B*, 161°K, melting point of carbon bisulphide; *C*, 178°K, melting point of acetone; *D*, 195°K, solid CO_2 in acetone. The resulting spectral sensitivity curves are plotted in *Figure 45c*. At 77°K the curve is

roughly flat from 1 to 3 μ, with slight evidence of band structure. This structure is shown more clearly at higher temperatures, where there is a band of sensitivity stretching from 0·9 μ to nearly 2·0 μ, the sensitivity then falling until a small ' plateau ' on the curve at 3·0 μ, with a final fall at longer wavelengths. At 77°K the curve falls exponentially over a 40 : 1 range.

Only on the two curves at lowest temperatures can the half-value wavelength be determined. Taking it relative to the plateau in the 2·8 to 3·0 μ region gives:

$$77°\text{K}, \lambda_{\frac{1}{2}} = 3{\cdot}45\ \mu \quad 161°\text{K}, \lambda_{\frac{1}{2}} = 3{\cdot}28\ \mu$$

Hence the corresponding energy shift is

$$\mathrm{d}E/\mathrm{d}T = +\ 2{\cdot}2 \times 10^{-4}\text{eV}/°\text{C}.$$

At 178°K the measurements just reached the plateau at 3 μ, at 195°K only the first band of sensitivity appears. As the sensitivities on the curves plotted are in terms of signal–noise ratio per 10 μW incident energy (referred to 1 c/s bandwidth) it may readily be seen that the limiting sensitivity of the cell at 77°K is $2{\cdot}2 \times 10^{-8}$ W.

Cell 5

This cell had a ' bubble ' window and platinum electrodes of 4·5 mm × 1 mm gap. The cell was kept at low pressure (with the tellurium in the form of a layer) for some hours with the temperature at 250°C, and the material then distilled to the ' bubble ' at 300°C. By this means impurities volatile below 260°C or non-volatile at 300°C should be removed. The material was finally evaporated by a flame on to water-cooled electrodes to give a layer of resistance 3·5 kΩ at room temperature, and 38 kΩ at 90°K. Spectral sensitivity curves were obtained at 90°K and 195°K which closely resembled those of *Figure 45*b. Using the same method of analysing the curves as for cell 3, the threshold wavelength is $\lambda_{\frac{1}{2}} = 3{\cdot}2\ \mu$ at 90°K, and the spectral shift $\Delta\lambda \simeq 0{\cdot}13\ \mu$. Hence $\mathrm{d}E/\mathrm{d}T \simeq +\ 1{\cdot}8 \times 10^{-4}\text{eV}/°\text{C}$.

The dependence of the a.c. photocurrent on intensity was found to confirm the results for cell 3, namely that the response was linear at low levels of illumination (over a 100 : 1 range), with a (Power)$^{\frac{1}{2}}$ law at high levels.

At 90°K the response time was found to be $\tau = 460$ μsec. At 195°K the signal–noise ratio was very poor, but it was estimated that $\tau = 150$ μsec ± 20 per cent.

Cell 6

This cell was made as for cell 5 except that the layer was rather thicker. Spectral sensitivity measurements were carried out at 77°K, 161°K and 195°K. The curves obtained were similar to those shown in *Figure 45*c. At 77°K the response was nearly constant from 1 μ to 3 μ, with a steady exponential fall from 3·2 μ to 4·2 μ, and $\lambda_{\frac{1}{2}} = 3{\cdot}4$ μ. At 161°K, however, the sensitivity of the long wavelength band was only 1/5 of that for the short wavelength band. At 195°K it was not possible to plot the long wavelength band in sufficient detail to determine $\lambda_{\frac{1}{2}}$, so that the shift could only be estimated for the temperature range 77 to 161°K. The value was $\mathrm{d}E/\mathrm{d}T \simeq +1{\cdot}7 \times 10^{-4}$eV/°C.

Limiting Sensitivity and Response Time

At 77°K the limiting sensitivity at 1·5 μ was $4{\cdot}5 \times 10^{-9}$ W for 1 c/s bandwidth. The signal fell to 1/e of its maximum value in 350 μsec.

Dependence of Photocurrent on Field and Intensity

It was found that both dark and photocurrents were proportional to the applied field, until the electrical power dissipated in the layer became great enough to cause appreciable heating.

The variation of a.c. photocurrent with radiant power falling on the layer is shown by curve *B* of *Figure 46*. It will be seen that the points lie on a straight line of slope unity, showing that the response of the cell is linear throughout this region.

Cell 7

This cell was made with a different design of electrodes in order to increase the resistance of the layer and so make it comparable with the noise resistance of the amplifier. Instead of the usual sensitive area of ~ 5 mm × 1 mm gap (which is a convenient shape to use when focusing an image of a spectrometer slit on to the layer), the area was made ~ 1 mm

wide with ~ 5 mm gap between electrodes. This procedure would increase the cell resistance by about 25 : 1. To make the cell with this electrode configuration a narrow ridge of glass was formed on the end of the inner part of the Dewar, of about 1 cm height. The surface of this ridge was then ground flat and polished, and electrodes of platinum applied to the ends of the ground portion. The resulting area between the electrodes was 4·6 mm long × 0·9 mm wide. The cell was fitted with a ' bubble ' window, and the layer formed in the manner described for earlier cells. The layer was photosensitive and its resistance at various temperatures was:

330	298	195	90°K
8	11	40	120 kΩ

The response time was 800 μsec at 90°K, and the limiting sensitivity 1×10^{-9} W for 1 μ radiation at this temperature.

The spectral sensitivity curve was measured between 0·8 μ and 3·8 μ. There was no well-defined long wavelength threshold, so no spectral shift measurements were carried out. There was a sharp bend in the curve at 3·2 μ (where the most rapid exponential fall commenced) which may be taken as a rough value for the threshold wavelength. At short wavelengths, the sensitivity fell to half its maximum value at $\lambda_{\frac{1}{2}} = 1{\cdot}4\ \mu$.

Cell 8

This cell used the same electrode configuration as cell 7. The layer was made considerably thicker by using 2 to 3 times as much tellurium. Its resistance was 5 kΩ at 20°C and 20 kΩ at 90°K.

Spectral Sensitivity

The results for 90°K are shown in *Figure 45*d, curve *A*, from which it is seen that the sensitivity has a broad maximum near 1·6 μ. The long wavelength threshold, taken as half the sensitivity at 3·2 μ is $\lambda_{\frac{1}{2}} = 3{\cdot}5\ \mu$. Curve *B* shows results obtained with the layer cooled by liquid hydrogen. Unfortunately, the hydrogen boiled away very rapidly—due primarily to the absence of silvering or any other radiation screening—and consequently readings only covered a restricted wavelength range.

To estimate the spectral shift, which is very small, the points on curve *B* have been scaled down to give the broken curve. It will be seen that this curve coincides with the 90°K curve from 2·9 to 3·2 μ, but lies above it at longer wavelengths. The shift is taken as the horizontal distance between the broken curve and the 90°K curve at longer wavelengths, and is approximately 0·08 μ. With such a small shift, the percentage accuracy is low; and considering the particular difficulties of performing the measurements at liquid hydrogen temperatures, it is felt that the value may well be in error by as much as 0·03 μ.

After the liquid hydrogen measurements were completed the cell became more noisy, and the signal-noise ratios were inadequate to enable spectral sensitivity measurements to be carried out over the wavelength range required at any higher temperature than that of liquid oxygen. Even at the relatively low temperature of 141°K (attained by working at the melting point of solid *n*-pentane) useful signal–noise values could only be obtained up to 3·0 μ.

Cell 9

This cell was made of similar design to cell 8, except that the ridge of glass carrying the electrodes was formed in such a manner as to give better thermal contact to the layer. It was also recessed within the end of the inner part of the Dewar flask, so that the solid angle over which radiation would fall on to the layer was reduced.

The preparation of the cell was carried out in the usual way, and a layer of good sensitivity obtained.

Spectral sensitivity— Extensive measurements were carried out on this cell at various temperatures. The results are plotted in *Figure 45*c. The main curve *A* (at 77°K), shows a steady fall from the region of 1·0 μ to a shoulder on the curve at 3·3 μ. The threshold wavelength, taken at half the sensitivity at this shoulder region is $\lambda_{\frac{1}{2}} = 3{\cdot}5\ \mu$. For the short wavelength band, $\lambda_{\frac{1}{2}} = 1{\cdot}4\ \mu$.

The results of curve *B* were obtained at 141°K, the melting point of *n*-pentane. The vertical scale of this curve has been adjusted to coincide with curve *A* from 2·6 to 3·0 μ. The same

procedure was used for curve *C*, which gives the sensitivity for 195°K. The wavelength separation of the straight lines drawn for the three curves represents the spectral shift, the values being:

77°K to 141°K, 0·12 μ
141°K to 195°K, 0·09 μ

Hence the total shift for 118°C is 0·21 μ, which gives $dE/dT = +1{\cdot}9 \times 10^{-4}$eV/°C. This is the most accurate value obtained from the spectral shift measurements on any of the tellurium cells, and it is thought unlikely to be in error by more than ± 20 per cent.

Conduction— It was found that the layer obeyed Ohm's law for a range of applied voltages of 0·05 to 100 V. The fact that the layer was ohmic for such small potentials means that barrier effects at the electrodes cannot be of much importance. The sign of the thermoelectric power showed, as before, that the conduction was by positive holes.

Response time and signal–intensity relation— The response time of the cell was found to be 450 μsec at 90°K, and 550 μsec at 77°K. Measurements of the variation of a.c. photocurrent with intensity were carried out with the cell cooled by liquid oxygen. For low power levels the response was linear with incident power over a range of 100 : 1. At higher powers the results fitted a (Power)$^{\frac{1}{2}}$ law over a range of 30 : 1 in intensity.

21.4. TEMPERATURE VARIATION OF SENSITIVITY

Cell 9 was the most sensitive tellurium cell made, and when cooled to 77°K it gave signal–noise in 1 c/s bandwidth for an incident energy of $1{\cdot}2 \times 10^{-10}$ W of monochromatic radiation at 1 μ. As the cell sensitivity was so high (with the layer cooled) its temperature dependence could be measured over a wide range. It was just possible to detect a signal at room temperature.

Mercury was put in the cell, and a thermocouple junction immersed in it. The mercury was then cooled with liquid nitrogen and readings of the signal taken as the cell warmed slowly to room temperature. Monochromatic radiation of 1·0 μ wavelength, chopped at 80 c/s, was used to produce the signal. The signal was found to alter over such an enormous

range that it was necessary to vary the amplifier gain (over 1,000 : 1 range), the energy incident on the cell, and the cell current, in order to make continuous measurements. The energy was kept small when the sensitivity was high so that there would be no question of non-linearity in response.

The results obtained are shown in *Figure 47*, where log (relative sensitivity*) is plotted as a function of temperature. It will be seen that between 77°K and 287°K the cell sensitivity falls by a quarter of a million times. This change is even more surprising when it is considered that the resistance of the

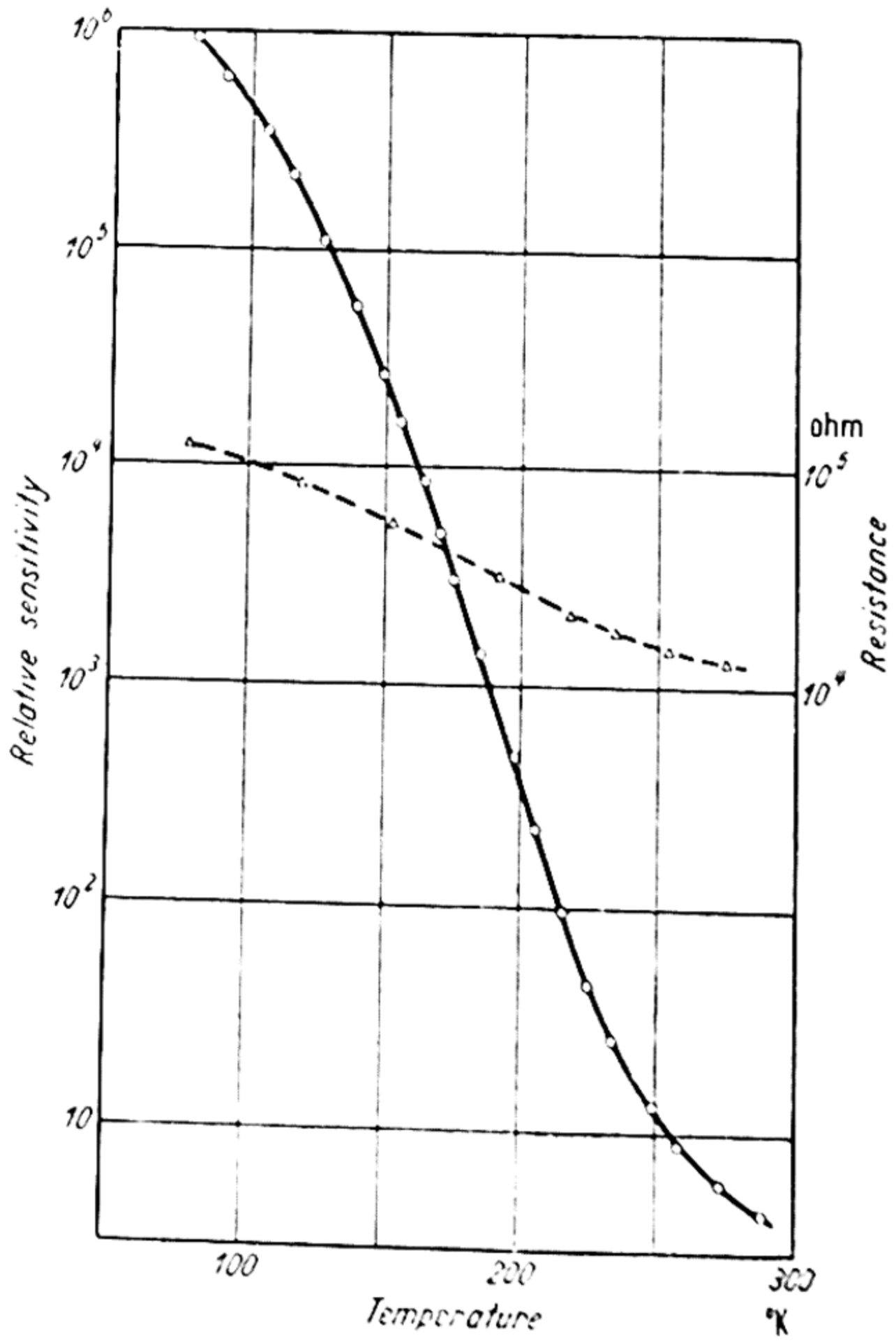

Figure 47. Temperature variation of sensitivity in tellurium

layer (shown by the broken curve) changes by < 10 over the same temperature range.

* Note, the 'sensitivity' plotted is the a.c. voltage signal across the cell when operated in series with a high resistance load. Under these conditions the signal is proportional to the resistance change of the cell on illumination.

Some of the increase in sensitivity on cooling was probably due to increase of response time, but it was not possible to measure this at temperatures above 90°K. It may be noted that the effect is in the opposite direction to that observed in the alkali halides (MOTT and GURNEY, 1948), and to that shown for arsenic in *Figure 34*.

21.5. PHOTO-EMISSIVE MEASUREMENTS

APKER *et alii* (1948) have reported measurements on photo-emission from films of tellurium evaporated in high vacuum on to various metal substrates. Films of thickness 10^{-5} to 10^{-2}cm were used, some layers having random structures whilst others had highly oriented crystallites.

It was observed that for high voltages (*i.e.* 10 to 1,000 V) the photocurrent varied as $V^{\frac{1}{2}}$ as expected for the Schottky effect. The curves of energy distribution of the photoelectrons were corrected for this effect in order to obtain the saturation potential. The energy distribution of the photoelectrons was found to fit a relation of the form of equation 66 with the parameter $r = 1{\cdot}5$. This value of r leads to values of the gap between the Fermi level and the full band of $\Delta = 0{\cdot}12$ eV.

From the spectral distribution curves (again interpreted by equation 66) the best value of r was 2, the photo-yield being proportional to $(h\nu - 4{\cdot}89)^4$. As the work function was found to be $\phi_c = 4{\cdot}76$ within close limits, this result gives $\Delta = 4{\cdot}89 - 4{\cdot}76 = 0{\cdot}13$ eV. APKER *et alii* point out that the data are insufficient to determine r uniquely, and that the results could equally well be explained by a series of superimposed characteristics with $r = 1$. For this case the energy gap would be $\Delta = 0{\cdot}18$ eV.

These results thus indicate a forbidden zone width of 0·24 to 0·36 eV, if we assume the specimens used were well in the intrinsic range of conductivity, so that the Fermi level lay midway between the full and conduction bands. As evaporated tellurium layers are normally *p*-type, the Fermi level would be lowered, and smaller values of Δ (as observed) would be expected.

Photoemissive measurements on tellurium at different temperatures have been reported by ARSENEVA–GEIL (1949).

21.6. OPTICAL PROPERTIES OF TELLURIUM

Absorption

Little information has been published on direct measurements of transmission of tellurium, the only works known being:

i RUTTER (1930) who found that a film of unquoted thickness gave 10 per cent transmission at 1 μ, and 80 per cent at 2·5 μ.

ii SOEZIMA (1949) who measured films (again of unspecified thickness) in the visible and near ultra-violet and found a very flat absorption maximum near 0·4 μ.

iii PFUND (1933) who gave infra-red transmission measurements on films of unknown thickness.

Measurements are now described on thin films of *Specpure* tellurium evaporated *in vacuo* on to plates of artificial sapphire. Plates of the thickness used ($\sim \frac{1}{2}$ mm) give good transmission in the infra-red for wavelengths $< 6\,\mu$. By the use of films of various thicknesses down to 0·26 μ, measurements could be made at wavelengths as low as 1 μ. A lithium fluoride prism monochromator was used because of its good dispersion. As the absorption decreased rapidly with increasing wavelength, scatter in the spectrometer tended to give spuriously high transmission readings. This effect was minimized by using as the detector a lead sulphide cell, which was sensitive only to wavelengths less than 3 μ. This detector determined the long wavelength limit of the measurements.

The value of the thickness was found by weighing the films. The nominal density of tellurium is 6·25 g/cm^3, but the value for an evaporated film is inevitably somewhat lower. A measurement by BRATTAIN and BRIGGS (1949) on a germanium film showed that the density was only 1 per cent less than the bulk density. However, the long wavelength value of refractive index obtained by these workers is 7 per cent greater than the precise value obtained by BRIGGS (1950), and it would seem probable that the major source of error was the determination of film thicknesses by weighing. Hence for germanium the density of films can probably be taken as 3 per cent less than the bulk density, with an error of ± 3 per cent. By analogy the specific gravity of tellurium films will be taken as 6·1 ± 3 per cent.

The absorption A is defined by the relation

$$A = \frac{\text{Incident radiation}}{\text{Transmitted radiation}} = e^{Kd}$$

where K is the absorption constant in cm^{-1}. Measurement of the incident and transmitted energies thus gives K directly, if the thickness d is known. Some correction must be applied for reflection losses at the tellurium–air–sapphire interfaces. It was not convenient to measure these individually, but they may be estimated from the Fresnel formula $R = [(n_1 - n_2)/(n_1 + n_2)]^2$. Hence for air–sapphire, with $n = 1{\cdot}7$, $R_1 = 7{\cdot}5$ per cent; for air–tellurium, with $n \simeq 5{\cdot}5$, $R_2 = 48$ per cent; for sapphire–tellurium, $R_3 = 28$ per cent. It may be remarked that the full formula for reflection involves the absorption index $k = K\lambda/4\pi$*. However at 3μ (using the value of absorption constant quoted later), $k = 0{\cdot}6$, and inclusion of this term only increases the reflection coefficient by $\frac{1}{2}$ per cent. At $2\ \mu$ the reflection coefficient would be 6 per cent greater, with negligible effect on the calculated absorption constant. At $1\ \mu$ it is estimated that k might be as high as 4 or 5, which would increase the reflection loss 1·5 : 1. As the measured absorption at $1\ \mu$ was approximately 1,000 : 1 for the thinnest film used, the correction would still have little effect on the absorption constant.

From the product $(1 - R_1)(1 - R_2)(1 - R_3)$ we see that the three reflections represent a total loss of 3 : 1. In view of possible errors in this value and other possible insertion losses, only measured absorptions of 10 : 1 or more were considered satisfactory for the calculation of K. For very thin films the thickness was determined relative to a thicker film, utilizing the absorption equation in the form $(1/d_1)\log A_1 = (1/d_2)\log A_2$. Thus a graph of $\log A_1$ against $\log A_2$ for various wavelengths (using values of absorption corrected for reflection losses) should give the thickness ratio d_1/d_2. Such a graph is shown in *Figure 48*, where the ratio is 1·5 : 1.

The resulting curve of absorption constant against λ is shown in *Figure 49* (curve A). It will be seen that at $1\ \mu$ the absorption constant exceeds $2 \times 10^5 cm^{-1}$. Such a high value must be due to absorption in the main crystal lattice. The

* See Appendix.

absorption falls rapidly with increasing wavelength to a value of $10^4 cm^{-1}$ at 2·5 μ.

Experiments with slabs of tellurium ground very thin and polished, showed transmission measurements on bulk samples to be possible. At the longest wavelength used, 12 μ, the absorption constant was only 130 cm^{-1}. Results of bulk measurements are plotted as curve *B* in *Figure 49*. It will be

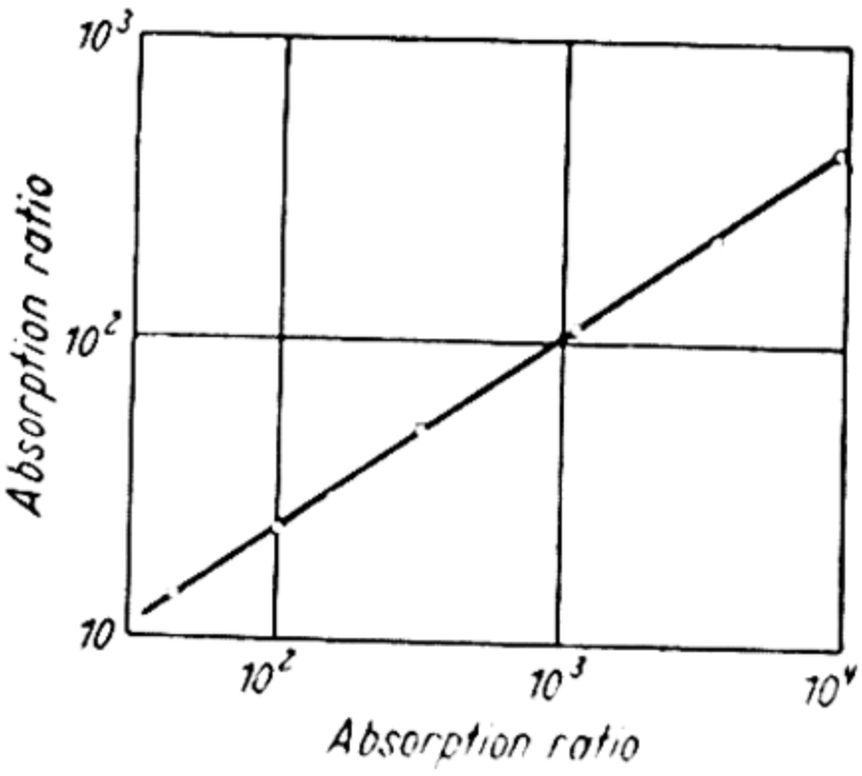

Figure 48. Relative absorption in two tellurium films of thickness ratio 1·5 : 1

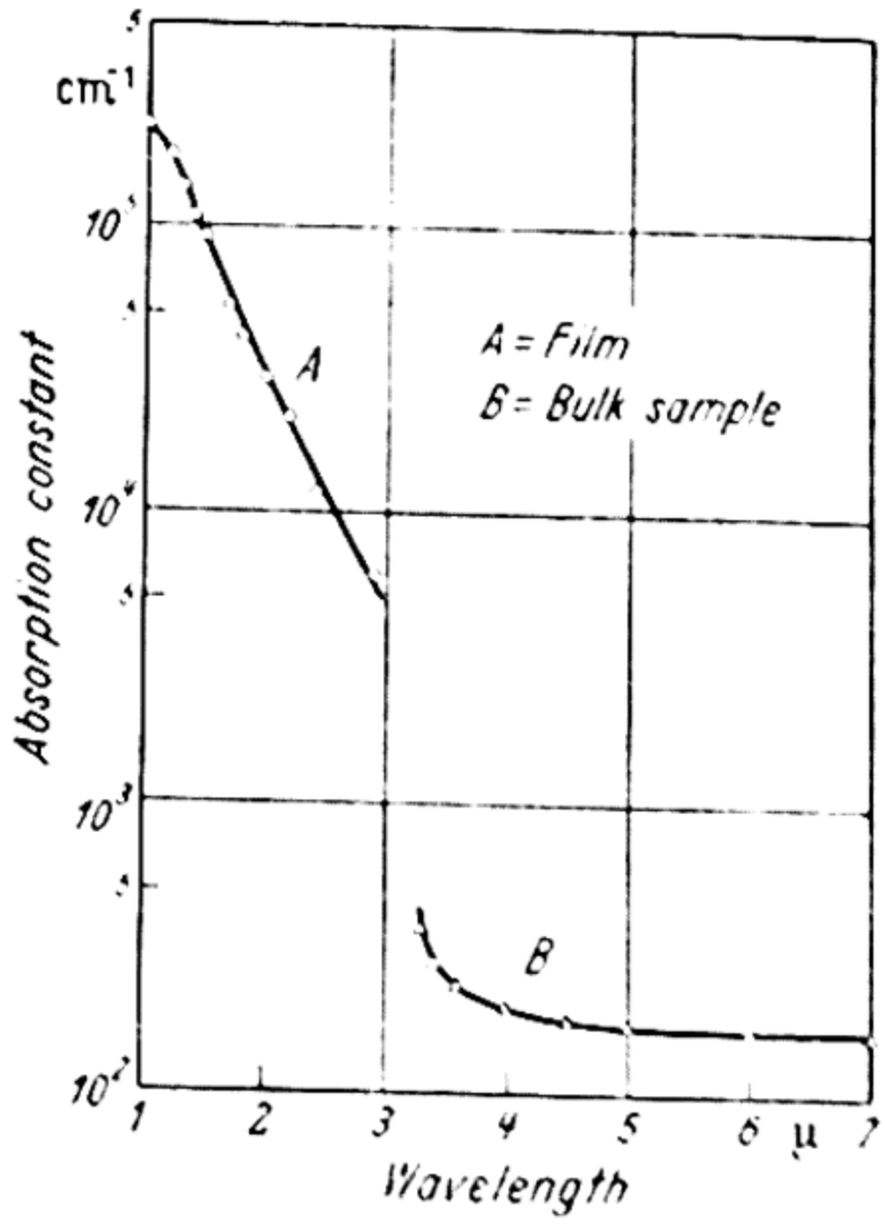

Figure 49 (Reproduced by kind permission of the Physical Society)

seen that the absorption is practically constant at long wavelengths but that it rises rapidly as the wavelength is reduced below 3·5 μ. These measurements thus indicate the presence of an absorption edge in the region 3 μ to 3·5 μ, which would coincide approximately with the threshold wavelength of the photoconductive effect. Loferski and Miller (1951) have reported briefly on the transmission of bulk tellurium. They estimate the absorption edge as 4·2 μ, and have obtained as much as 25 per cent transmission through samples 0·7 mm thick.

From measurements by Gibson (1950, 1952) on evaporated layers and single crystals of lead sulphide, it seems that the absorption edge is not well defined in layers, possibly as a result of some scattering process.

Refractive Index

The refractive index was determined by measurement of interference fringes. Reflection fringes were used in order to increase the ratio of maxima to minima, and to make measurements with backing plates possible at longer wavelengths. The plates used were discs of artificial sapphire for which the reflection is low except for wavelengths between 11 μ and 13 μ. Using a rock–salt prism monochromator and thermopile detector, fringes could be plotted for wavelengths up to 14 μ. For wavelengths less than 3 μ, increasing absorption rendered the fringes insignificant.

The frequencies f of the reflection minima are given by $2nd\cos\theta = N/f$ where d is the film thickness, n the refractive index, N the order of the fringe, and θ is the angle between the normal and the direction of a ray inside the film. All the measurements were carried out near normal incidence so that $\cos\theta = 1$. (It may be noted that with such a high refractive index, even an angle of incidence of 30° would reduce $\cos\theta$ by only $\frac{1}{2}$ per cent.) Hence $2nd = N/f_1 = (N+1)/f_2 = 1/(f_2 - f_1)$.

Now $f_2 - f_1$ is the fringe separation, which for a typical film was found to be 237 cm^{-1} in the non-dispersive region. Hence $2nd \simeq 42\ \mu$. More accurate values of $2nd$ may now be obtained by inserting the relevant integral values of N, as shown by *Table XII*. The thickness of the film was 4·0 μ, this being the value used in calculating n.

Table XII

N	f cm^{-1}	λ microns	$2nd$	n
3	~770	~13	~39	—
4	1,004	9·97	39·8	4·97
5	1,245	8·03	40·1	5·01
6	1,477	6·77	40·6	5·08

Note: The minimum near 770 cm^{-1} is still in the region of high reflectivity from the sapphire, and is thus only approximate

The main error in the results lies in the determination of the thickness, due to uncertainties in the value of the density, as discussed previously. There is relatively little error in the

determination of values of $2nd$. Hence, to plot a representative dispersion curve, the values of refractive index in the 10 μ region have been averaged, and all the results then normalized to this average value by correction of the measured values of d. The composite curve thus obtained is shown as *Figure 50*a. It may be seen that there is high dispersion at 3 μ, but that the index has become practically constant at the longer wavelengths.

Plotting a dispersion curve in the form $1/(n^2 - 1) = a - b/\lambda^2$ (using the values taken from the smooth curve of *Figure 50*a), gives a straight line as shown by *Figure 50*b. From the graph

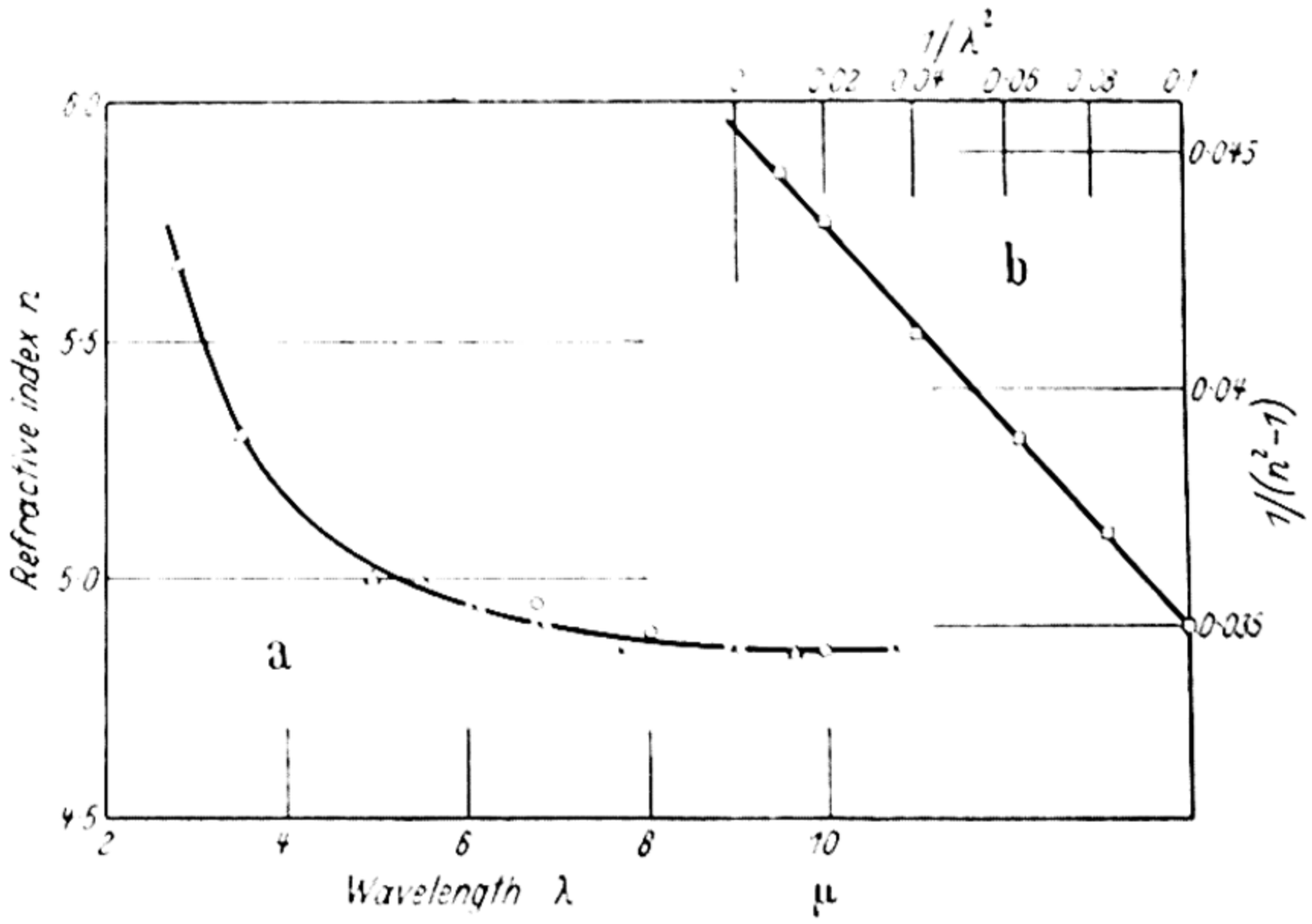

Figure 50 (Reproduced by kind permission of the Physical Society)

the values $a = 0{\cdot}045$ and $b = 0{\cdot}10$ are obtained, and on extrapolating to $1/\lambda = 0$, we find $n_0 = 4{\cdot}8$. This is a remarkably high value of refractive index (considering that it is for the non-dispersive region) and is much higher than any other known refractive index*. This figure is presumably the mean of the two indices for the two crystal directions.

Measurements have previously been made of the refractive index in the visible region by reflection methods using polarized light (MILLER, 1925; VAN DYKE, 1922). The values found

* It has recently been reported by AVERY (1951) that the refractive index of PbTe is approximately 5·3.

lie in the region of 2·0 to 3·5. Such measurements are inevitably susceptible to the precise state of the surface of the specimen, and may be inaccurate for this reason. However, since the main lattice absorption band lies largely between the visible region and the infra-red region where the interference measurements were made, the refractive index should be greater in the infra-red, so that the two sets of measurements are not necessarily in disagreement.

It may be noted that COBLENTZ (1911) has measured the reflectivity of tellurium in the infra-red. The very high values obtained ($\sim$ 50 per cent) are in reasonable agreement with $n = 5$ on the basis of the Fresnel reflection formula. FRAGSTEIN (1933) also records reflectivities of more than 50 per cent.

From the results of MILLER (1925) and VAN DYKE (1922) the absorption (*i.e.* the imaginary part of the dielectric constant) rises steadily from 0·3 μ to 0·6 μ. As only one point was measured beyond 0·6 μ, it is not certain where the maximum absorption lies, but it is probably at $\lambda > 0{\cdot}6\ \mu$. This is a very long wavelength for an absorption peak, and it would indicate that at not inconveniently short wavelengths (*i.e.* $\leqslant 0{\cdot}2\ \mu$) tellurium should be relatively transparent again, and hence, according to standard optical theories, should have a refractive index of unity. As the refractive index of tellurium is so high, it would be interesting to check it by precise prism measurements. From the data given by LOFERSKI and MILLER (1951) it is clear that adequate transmission can be obtained through samples up to 1 mm thick, so that a prism of 1 cm $\times$ 1 cm face and 5° angle is possible.

There are serious experimental difficulties in the way of measuring the dielectric constant at radio frequencies. The resistivity of the material is so low that the angular frequency (ω) where a 'condenser' would have a capacitive reactance equal to the resistance would be given by $\omega\epsilon/4\pi = \sigma$, with ω equivalent to 5×10^{11}c/s (or about 1 mm wavelength), for $\epsilon = 25$ and $\sigma = 1\ \Omega^{-1}\text{cm}^{-1}$. At the present time it is feasible to carry out measurements at frequencies 5 to 10 times lower than this, so that by the use of cooled specimens, where σ is lower, a value for the dielectric constant might be obtained.

21.7. SUMMARY AND CONCLUSIONS

When prepared in a sufficiently pure state, tellurium layers and single crystals are intrinsic semiconductors at room temperature. The conductivity is anisotropic, being twice as great along the *c* axis as perpendicular to it. At room temperature the conductivity along the *c* axis is approximately 3 $\Omega^{-1}cm^{-1}$.

Photoconductivity occurs in evaporated layers, but only to a significant degree when the layers are cooled with liquid air. An increase in photosensitivity of as much as 250,000 times has been observed to occur on cooling from room temperature to 77°K. It is interesting to compare the sensitivities of the best tellurium cells with conventional radiation detectors. DALY and SUTHERLAND (1949) give the following limiting sensitivities for unselective radiation detectors:

Bolometer (semiconducting)	$\sim 10^{-9}$ W
Bolometer (superconducting)	$\sim 10^{-12}$ W
Golay Cell	$\sim 10^{-9}$ W
Thermopile	$\sim 10^{-10}$ W

The best tellurium cell described, which had a limiting sensitivity of $1{\cdot}2 \times 10^{-10}$ W, is thus similar to the best thermopiles, and probably superior to bolometers (except the superconducting type) and pneumatic detectors, within its spectral range. The response times of the photoconductive process were found to lie in the range 300 to 700 μ sec at liquid air temperatures, falling by a factor of 3 at solid carbon dioxide temperature.

The relation between the a.c. signal output from the cell and the d.c. current passed through the cell, was found to be linear in the cases measured. The law between the cell signal and power incident on the layer was investigated, and in all cases the response was linear at low signal levels. At higher levels the signal became proportional to $(\text{Power})^{\frac{1}{2}}$.

Activation Energy

From measurement of the spectral distribution of photoconductivity on nine cells the average value of the optical activation energy was found to be 0·37 eV, the λ_t values

ranging from 3·15 to 3·45 μ. From Hall effect and conductivity measurements the thermal activation energy lies in the range 0·34 to 0·38 eV. There is thus good agreement between the two energy values. Photoemissive measurements give a similar value of activation energy, and support the conclusion that the measured energy is in fact the width of the forbidden zone. Absorption measurements on bulk samples show an edge at wavelengths corresponding to quantum energies of 0·3 to 0·35 eV, which is therefore identified with the threshold of photoconductivity.

The activation energy was found to *decrease* on cooling, in contradistinction to all other elements measured. The measurements of the energy shift (*i.e.* the temperature variation of the photoconductive threshold wavelength) were difficult, and only by working to the limits both in the experimental procedure and in the interpretation of the results obtained, was it possible to obtain definite values. The data are summarized in *Table XIII*. From the table the average energy shift is $dE/dT = +2 \times 10^{-4}$eV/°C.

Table XIII

Cell number	*Wavelength Shift* μ	*Energy Shift* eV	*Temperature range* °C	eV/°C $\times 10^{-4}$
3	0·17	$2{\cdot}2 \times 10^{-2}$	105	+ 2·1
4	0·17	$1{\cdot}8 \times 10^{-2}$	84	+ 2·2
5	0·13	$1{\cdot}9 \times 10^{-2}$	105	+ 1·8
6	0·13	$1{\cdot}4 \times 10^{-2}$	84	+ 1·7
9	0·21	$2{\cdot}3 \times 10^{-2}$	118	+ 1·9

These results may be compared with measurements carried out on the change of resistance with pressure, which has been measured by BRIDGMAN (1938) for pressures up to 30,000 kg/cm², the resistance at this pressure being less than 1/500 of its normal value. Measurements were made at two temperatures (30°C and 75°C) and hence, as pointed out by BARDEEN (1949), the thermal activation energy may be calculated at any pressure on the assumption that the sample is in the range of intrinsic

conductivity. This latter condition is not fulfilled at the lowest pressures, but the value of 0·37 eV found from other measurements may be used for the zero-pressure activation energy. If the energy values so obtained are plotted as a function of the dilatation (BRIDGMAN, 1940) corresponding to the applied pressure, *Figure 51* is obtained. It will be observed that the graph is an excellent straight line even down to an activation energy of 0·02 eV, so that the change of activation energy is

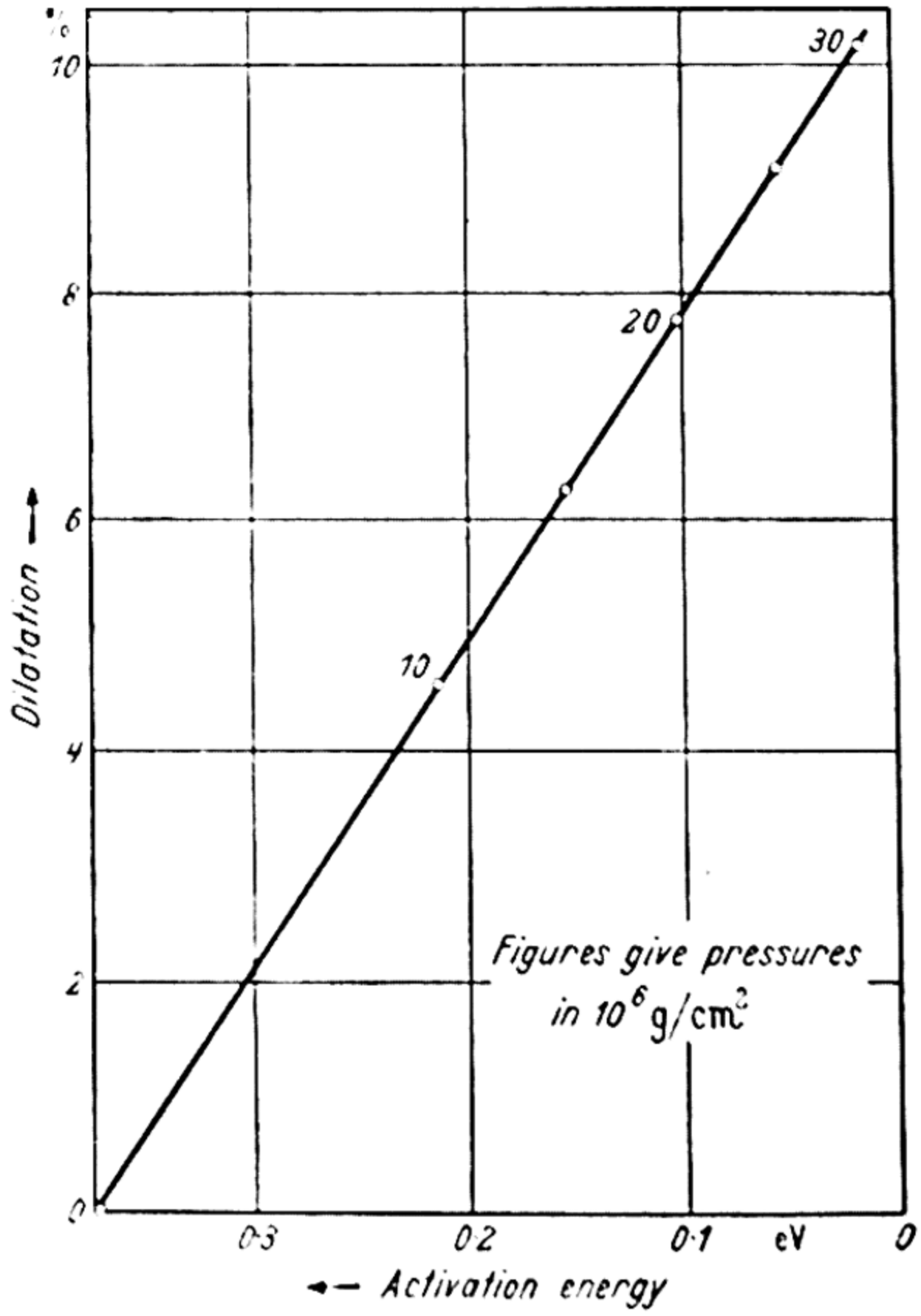

Figure 51. Pressure dependence of activation energy for tellurium

directly proportional to the dilatation. From the slope of the curve, the energy shift is $\delta E/(\delta V/V) = 0{\cdot}035$ eV per 1 per cent dilatation. The value of the energy shift found from the optical measurements can also be put in terms of dilatation, taking the coefficient of thermal expansion as $\delta V/(V.\delta T) = 53 \times 10^{-6}$ (BRIDGMAN, 1925). Hence from the optical data $\delta E/(\delta V/V) = 0{\cdot}036$ eV per 1 per cent dilatation. There is thus

close agreement between the two values found by the different methods, so that the change in activation energy must be determined almost entirely by the dilatation, the lattice broadening effect being relatively unimportant in tellurium.

Using equations 56 and 57, with the value of the sound velocity deduced by SHOCKLEY (1951) from the compressibility, *i.e.* $\rho c^2 = 0{\cdot}5 \times 10^{12}$ dynes^2 cm^{-2}, we can calculate the shift contributions of the full and conduction bands. With the mobility values found by FUKUROI *et alii* (1949–50) of $b_h = 1{,}100$ and $b_e = 1{,}650$, the contributions from dilatation only should be 0·9 and $0{\cdot}74 \times 10^{-4}$ eV/°C. Taking both shifts as positive as suggested by Shockley gives $(\mathrm{d}E/\mathrm{d}T)_2 = +\ 1{\cdot}64$ eV/°C, which compares favourably with the observed value.

22

IODINE

22.1. GENERAL PROPERTIES

IODINE forms strongly doubly refracting crystals which belong to the rhombic system. WAHL (1913) found no evidence of a transition on cooling to — 180°C, and concludes that this rhombic form is stable at all temperatures. The crystals are molecular in nature, the I_2 molecules being bound by van der Waals forces to form the solid (RICE and TELLER, 1949). The intra-molecular distance is almost the same in the solid (2·70 Å) as in the vapour (2·65 Å), while the distance between the molecules is at least 3·54 Å (WYCKOFF, 1948).

The thermal expansion is extremely high, being 250×10^{-6} for the volume coefficient at liquid air temperature and 220×10^{-6} over the range from room temperature to the melting point at 114°C. This property tends to make backed layers rather unstable. The vapour pressure is also high, even at room temperature; being 0·2 mm Hg at 20°C, and 2 mm Hg at 50°C (GMELIN, 1933). The material is thus pumped away very rapidly in a vacuum system.

Little information has appeared in the literature so far concerning either the conductivity or photoconductivity of iodine. Experimental measurements of these properties have now been made on both melted and evaporated layers.

22.2. PREPARATION OF SPECIMENS

For measurements on melted samples, the cells used were simple tubes with flat depressions into which the molten iodine was allowed to run (see *Figure 13c*). Graphite electrodes painted in the centre of the depression made contact with the iodine and with glass covered tungsten leads. Resublimed iodine was used to form the layers. Because of the high vapour pressure of iodine, prolonged pumping or outgassing was not possible. The cells were pumped for approximately one

minute with a mechanical backing pump, and then sealed off. The iodine was melted by placing the cell in an oven, and allowed to flow into the depression to form layers $\sim \frac{1}{2}$ mm thick. The vapour in the cell was condensed into the depression by cooling the latter with an air jet before the rest of the cell cooled. Cells made in this manner had resistances $\sim 10^8\,\Omega$ at room temperature, and showed considerable a.c. and d.c. photoconductivity.

For evaporated layers, Dewar flask type cells similar to that shown in *Figure 13a* were used. The evaporation was carried out with the cell sealed off after pumping for one or two minutes. The inner part of the Dewar flask was water cooled (or ice cooled) while the cell was heated in an oven. The layer thicknesses, estimated from the amount of iodine evaporated and the area of the layer, were about 0·05 to 0·1 mm. Evaporated cells showed greater d.c. sensitivity than the melted layers, it being possible to double the conductivity by the light of a 100 W lamp.

22.3. PHOTOCONDUCTIVE MEASUREMENTS

Cell 1

This cell was the melted layer type, of thickness 0·5 mm. It was found that if potential differences much in excess of 10 V were used across the layer the resistance began to drift, but in the range 1·5 to 10 V Ohm's law was obeyed quite closely, with a resistance of 90 MΩ at 19°C. As the layer area was 6×1 mm^2, the specific resistance was $2{\cdot}7 \times 10^7\,\Omega$ cm. The a.c. photocurrent, produced by monochromatic radiation of 0·55 μ wavelength chopped at 80 c/s, was measured for the same range of currents. The results showed the a.c. signal to be proportional to the d.c. current through the layer.

Measurements of spectral sensitivity were carried out using radiation chopped at 80 c/s, in conjunction with a tuned amplifier. Lithium fluoride was used as the prism material in the spectrometer. In order to plot the peak of the sensitivity curve it was necessary to extend the measurements to below 0·4 μ, whilst at long wavelengths suitable signals were obtained up to a wavelength of 1·17 μ. The resulting spectral sensitivity curve, plotted as (a.c. signal)/(incident intensity) on

a logarithmic scale, is shown in *Figure 52*a. It will be seen that the results cover a range of 5,000 : 1 in sensitivity. Two bands of sensitivity appear, the first having its peak at 0·45 μ, after which the curve falls exponentially over a range of 50 : 1. The second band is only about 1 per cent of this main band, but is quite clearly defined and again has an exponential fall. The $\lambda_{\frac{1}{2}}$ values are 0·53 μ for the first band, and 0·93 μ for the second band—the latter figure being determined by subtraction of the extrapolated tail of the short wavelength band, as shown by the broken line. The optical activation energies for this layer are thus 2·3 eV and 1·33 eV.

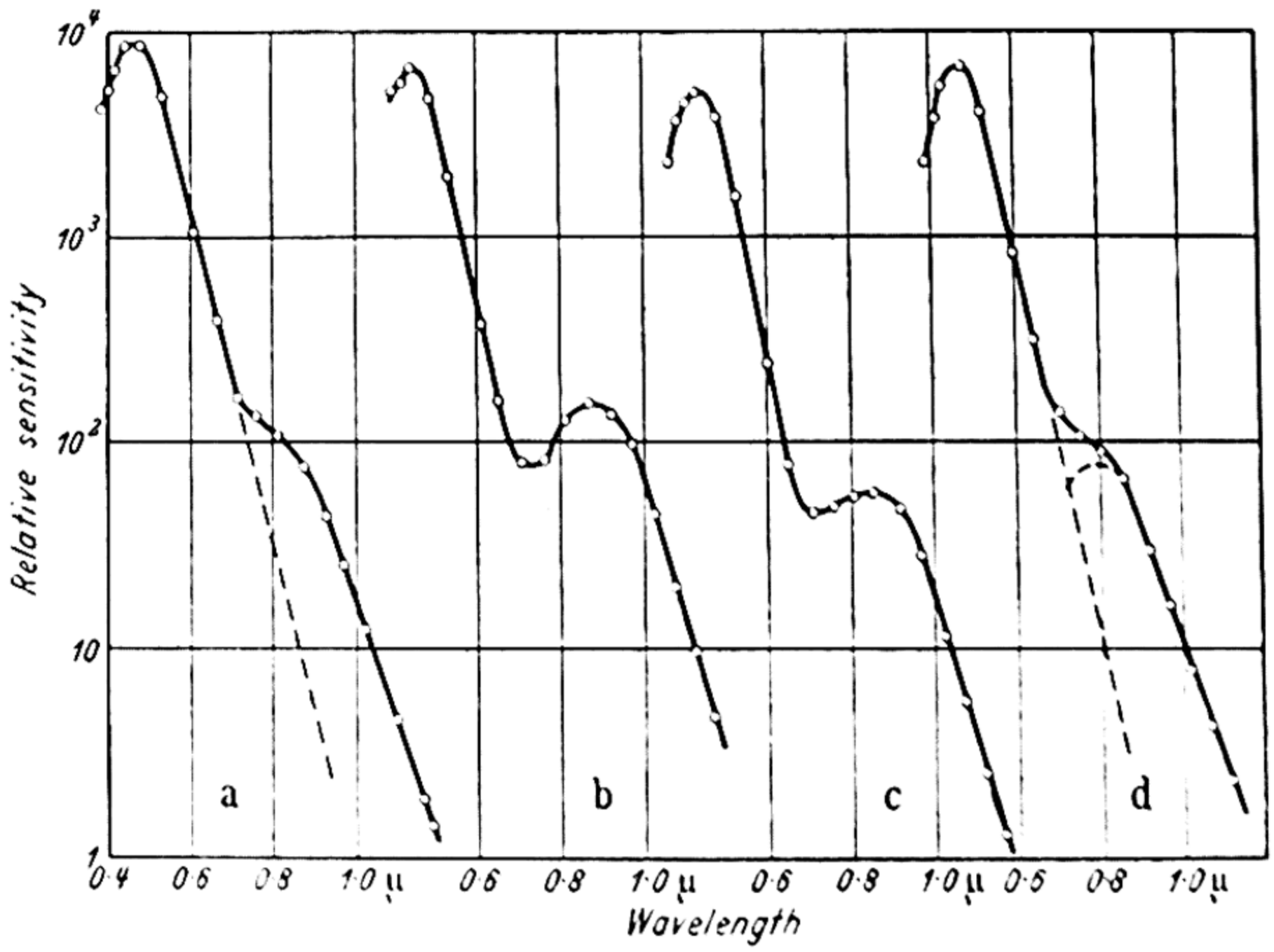

Figure 52. Spectral sensitivity curves for iodine

The cell was not sufficiently sensitive to enable an accurate measurement of its response time to be made. However, an upper limit was estimated by passing the cell signal through an untuned amplifier followed by a homodyne detector. As the speed of the chopper was decreased it was found that there was no change in the signal amplitude. Hence the signal must have reached its full amplitude in a time considerably less than the duration of a pulse of radiation through the chopper *i.e.* $< 6 \times 10^{-3}$ sec. As less than 10 per cent amplitude variation was observed then $\tau < 3 \times 10^{-3}$ sec.

Cell 2

This cell was of the evaporated type. It was more stable with applied voltages than the first iodine cell, and measurements with fields of up to 2,000 V/cm were made. The results showed that Ohm's law was obeyed over the whole range of applied voltages, giving a layer resistance of $8{\cdot}5 \times 10^9\,\Omega$. The layer thickness was estimated to be about 0·1 mm, giving a specific resistance of $5 \times 10^8\,\Omega$ cm. This is much higher than for the previous cell and may well be due to the additional purity of this layer by virtue of it being distilled *in vacuo*, and not simply melted.

The spectral sensitivity of this cell was measured in the same manner as for cell 1. As shown by *Figure 52*b the sensitivity again varies over a wide range between 0·4 and 1·2 μ. The two bands of sensitivity are clearly defined, the second peak occurring at a wavelength of 0·87 μ, and being approximately 2 per cent of the amplitude of the main band. Both bands show exponentially falling sensitivity with wavelength. The $\lambda_{\frac{1}{2}}$ values are 0·51 μ and 0·99 μ.

Cell 3

This cell was made by distillation, using ice-cooling. The bottom of the inner part of the Dewar flask was maintained at 0°C during the subsequent measurements to reduce evaporation of the layer. The cell resistance at 0°C was $7{\cdot}5 \times 10^{10}\,\Omega$. From the amount of material used and the layer area the thickness was estimated to be $\sim$ 1/20 mm, giving specific resistance $\sim 4 \times 10^9\,\Omega$ cm.

The spectral sensitivity curve was measured under the same conditions as for the previous cells, except that the layer was maintained at 0°C. The results again show two well-defined bands, with the long wavelength band of sensitivity about 1 per cent of that for the main band. The edge of the main band falls exponentially over a wide range. From the curve the two threshold wavelengths are $\lambda_{\frac{1}{2}} = 0{\cdot}50$ and 0·99 μ.

Cell 4

The iodine was again distilled on to an ice-cooled surface, forming a layer of $3 \times 10^9\,\Omega$ resistance. The layer was

maintained at 0°C whilst the spectral sensitivity curve shown in *Figure 52*c was measured. The results are again characterized by two bands of photoconductivity with the second band about 1 per cent of that of the first band. Both bands show exponential falls for a range of about 50 : 1 in sensitivity. The threshold wavelengths lie at $\lambda_{\frac{1}{2}} = 0{\cdot}51\ \mu$ and $0{\cdot}97\ \mu$.

Cell 5

This cell was of the simple tube type, as for the first cell. The electrodes were $7 \times 1\ mm^2$, and the thickness 0·8 mm. After cooling to 19°C the resistance was $1{\cdot}1 \times 10^8\ \Omega$. The cell was filled with nitrogen at atmospheric pressure to reduce evaporation of the iodine, and resealed. On measuring the resistance again it was found to have changed only to $1{\cdot}2 \times 10^8\ \Omega$, so it was considered that the introduction of the nitrogen had not influenced the layer properties significantly. Both the dark current and a.c. photocurrent were found to be proportional to the applied d.c. voltage for this cell.

The spectral sensitivity curve was plotted at room temperature with the experimental details as before, the results obtained being shown in *Figure 52*d. The curve is similar to the earlier ones, although the long wavelength band is not so well defined as for the majority of the cells. The threshold wavelengths—found by subtraction as shown by the broken line in the case of the long wavelength band—are $\lambda_{\frac{1}{2}} = 0{\cdot}53\ \mu$ and $0{\cdot}91\ \mu$.

With this cell it was just possible to measure the response time using a pulse of radiation from a neon lamp, although even under optimum conditions the signal–noise ratio was only $\sim 3 : 1$. The time for the signal to decay to half value was found to lie between 200 and 300 μ sec. Hence for an exponential decay (as expected), $\tau = 300$ to 450 μ sec.

The intensity dependence of the a.c. photocurrent was observed over a range of intensities of 4,000 : 1. Two sources of radiation were used, a 2 W lamp for measurements at low levels, and a 75 W lamp to give high intensities. The observed cell outputs are plotted as a function of the incident power in *Figure 53*, curve *A*. It will be seen that over the lower power region the points lie well on a line of slope unity, indicating a

linear variation of signal with power. At the higher intensities the signal increases less rapidly than the power. Measurements taken with the 75 W source are plotted in curve *B*. Here the slope of the curve is steadily decreasing, until at the highest intensities the points lie near a line of slope 0·5. These results are thus in agreement with the theory of photo-response given in §6.1. From comparison of the signal magnitudes with those obtained in the spectral sensitivity measurements, it is concluded that for the latter the layer would be operating in the linear region.

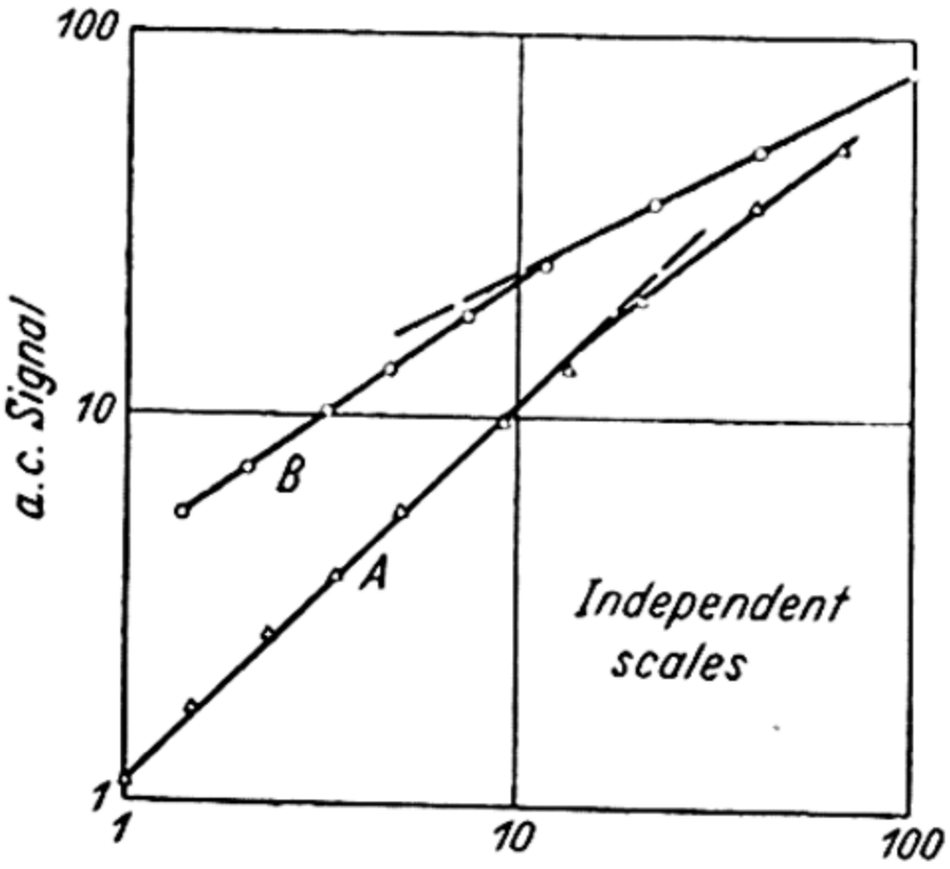

Figure 53. Signal–energy relation for iodine

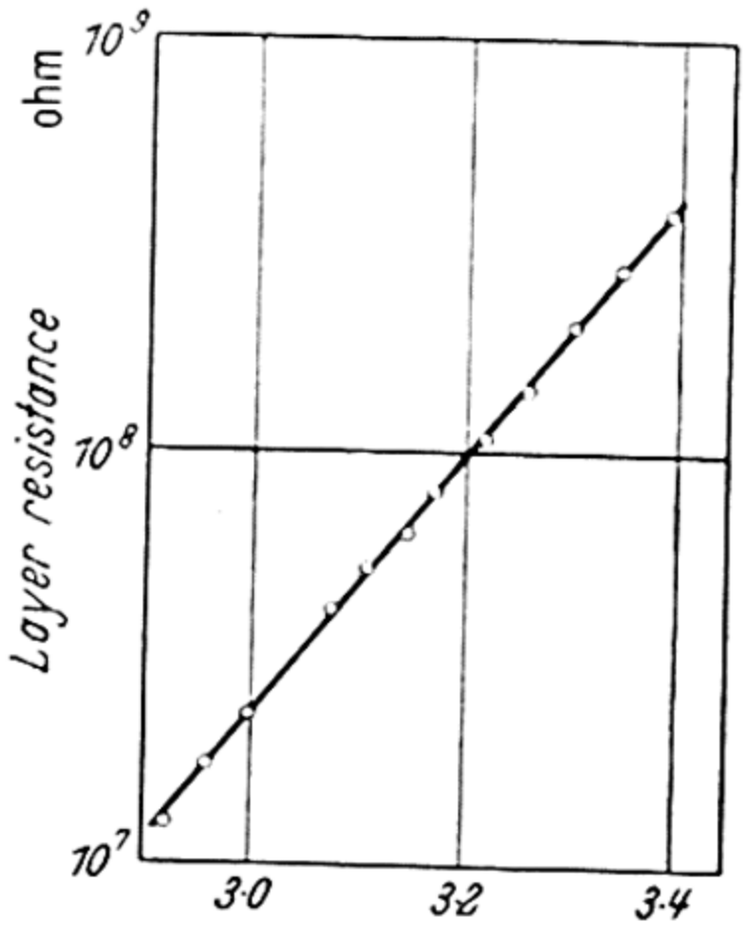

Figure 54. Resistance of iodine

22.4. RESISTANCE–TEMPERATURE MEASUREMENTS

For these measurements, cell 5 had the end containing the layer immersed in a bath of mercury. The cell leads were clear of the bath, one lead being glass covered for a considerable length to give good insulation against surface leakage. A *Chromel–Alumel* thermojunction was placed in the mercury immediately below the layer. The mercury was initially heated to 80°C, little evaporation of iodine occurring at this temperature because the cell was filled with nitrogen. Readings were taken during the slow cooling from 70°C to room temperature. Over this temperature range the resistance varied by about 200 : 1, as shown by *Figure 54*, where log (resistance) is plotted as a function of reciprocal temperature. All the points lie on a straight line of slope 0·62 eV,

which leads to a value of thermal activation energy of 1·24 eV. This value is in close agreement with the optical activation energy found for the long wavelength band of photoconductivity, namely 1·3 eV.

If for the conductivity we put $\sigma = \sigma_0 e^{-E/2kT}$, then with $E = 1{\cdot}24$ eV and $\sigma = 10^8\,\Omega^{-1}\,cm^{-1}$ at 312°K, we find $\sigma_0 = 100$. This indicates a value of mobility of ~ 25 cm sec^{-1}/V cm^{-1}, which is a reasonable value for a polycrystalline layer. The only measurements of resistance at different temperatures to be found in the literature are those of POCHETTINO and FULCHERIS (1923). Their values, if plotted as log (resistance) against reciprocal temperature, give a fairly good straight line, indicating an activation energy of $\sim 1{\cdot}9$ eV. These measurements however, are not self consistent as they lead to a value of $\sigma_0 = 10^7$, which is clearly impossible.

22.5. OPTICAL PROPERTIES OF IODINE

Absorption

Transmission measurements on thin films of solid iodine have been carried out by COBLENTZ (1903), BOVIS (1927) and HILSCH and POHL (1928). All these workers used films made by melting iodine between glass or quartz plates. By this means films only a few microns thick can be obtained. Values of absorption constant calculated from the data are plotted in *Figure 55*. The curve has a broad maximum in the ultra-violet, with the relatively small peak value of $1{\cdot}5 \times 10^5$ cm^{-1}. For wavelengths beyond 1 μ the transmission is high even for layers of 1 mm thick, and the long wavelength absorption edge may be taken as somewhat less than 1 μ. This value is thus in agreement with the long wavelength threshold of photoconductivity. The broken curve in *Figure 55* shows results obtained by MEIER (1910) from reflection measurements.

Both Coblentz and Bovis found that if polarized light was used the absorption was greatly dependent on the plane of polarization. The directions of the crystal axes were not known, but observations were made with the plane of polarization set alternately for maximum and minimum absorption. At 0·54 μ the absorption constants for the two conditions were found to be $8{\cdot}2 \times 10^4$ and $3{\cdot}1 \times 10^4$ cm^{-1}. The relative

magnitudes of the absorption were found to be reversed at 1·1 μ *i.e.* the plane of polarization which gave maximum absorption at 0·54 μ gave minimum absorption at 1·1 μ.

These data therefore emphasize the marked optical anisotropy of the crystals, and indicate the presence of two absorption bands (corresponding to different crystal directions) which may be related to the two bands of photoconductivity. Hence using a single crystal and polarized light, it might be possible to separate the two bands of photoconductivity, or at least to alter the relative contributions from the two bands.

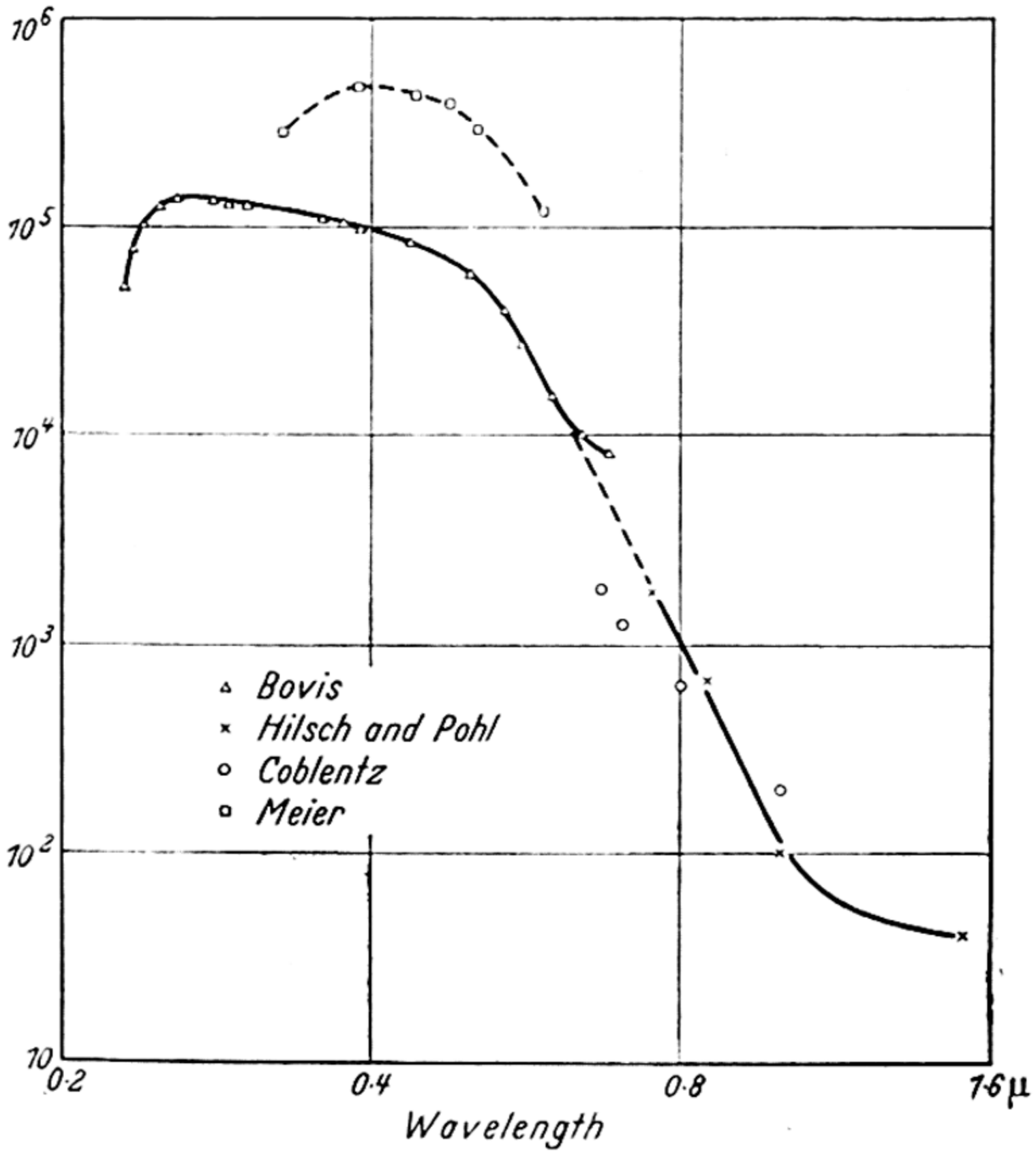

Figure 55. Absorption in iodine

It has been observed by Bovis (1929) that a layer of iodine 0·1 mm thick transmits radiation of wavelength $> 0{\cdot}67\ \mu$ when cooled to 20°K. From the data of *Figure 55*, a film of this thickness at room temperature would transmit < 1 per cent at 0·85 μ. We may thus assume a shift of at least this

amount (*i.e.* 0·4 eV) for a temperature change of 270°C. Hence $dE/dT = -15 \times 10^{-4}$ eV/°C. This is a very high figure compared with the other elements, possibly as a consequence of the extremely high coefficient of expansion possessed by this material. For example, cooling to 20°K would give about 2 per cent linear contraction of the lattice, which is of the same order as the difference in intra-molecular spacing between the solid and the gas.

Refractive Index and Dielectric Constant

There are several measurements of dielectric constant and refractive index quoted in the literature, with considerable discrepancies among the values quoted. For the dielectric constant, SCHLUNDT (1901) gave 10·3, while SCHMIDT (1903) gave 4·0. For the refractive index, the results of MEIER (1910) show that the value rises steadily from the ultra-violet to 0·589 μ, where $n = 3{\cdot}34$ and is apparently approaching a maximum. This latter wavelength is still in the region of high absorption, which explains why the index is still rising with wavelength. It should of course fall again at longer wavelengths. Using equation 16, Meier's data give satisfactory agreement when $\nu_0 = 6{\cdot}4 \times 10^{14}$ and $\gamma = 3{\cdot}3 \times 10^{14}$c/s. Extrapolation to $\nu = 0$ then gives the refractive index $n_0 \simeq 3{\cdot}0$.

From work on solutions of iodine, DAMIEN (1881) and HURION (1877) deduce values of 2·11 and 2·08 respectively, for $\lambda = 0{\cdot}656\,\mu$, COBLENTZ (1903) made measurements on thin prisms of solid iodine, and found $n = 2{\cdot}07$ at 0·65 μ. There is thus agreement between the value of Coblentz, the estimated values of Hurion and Damien, and the dielectric constant of Schmidt. The results of Schlundt and Meier (the latter being the most thorough set of measurements) agree in a value near 3 for the long wavelength refractive index. The explanation of the difference may lie in the great anisotropy and marked double refraction of the material. Coblentz states that the double refraction is at least 0·5. If the value were about unity, then measurements in different crystal directions might give the two sets of results observed. It seems possible therefore that iodine has two refractive indices, being approximately 2 and 3, for long wavelengths.

22.6. SUMMARY AND CONCLUSIONS

There is little data published in the literature on photoconductivity in iodine, although both COBLENTZ and ECKFORD (1923), and VOLMER (1917), had observed that the effect existed. Both workers were unable to plot spectral sensitivity curves, although Coblentz with the aid of filters, was able to estimate that the maximum effect was in the region of 0·5 μ. BERGMANN (1932) observed a slight photovoltage in solid iodine, but again no specific results are given.

The measurements now described establish that pure iodine layers are very photosensitive, and that the effect occurs with a time lag of only a few hundred microseconds. Quantitative measurements of the variation of a.c. photocurrent with applied field and intensity of irradiation show linear relations over a small range. At high illuminating intensities, a $(\text{Power})^{\frac{1}{2}}$ law is obeyed.

The spectral sensitivity measurements show two well-defined bands of sensitivity in all layers (whether melted layers $\sim$ 1 mm thick, or evaporated films), with maximum sensitivity at 0·46 μ. Close agreement is found between the threshold wavelengths for the different layers. The $\lambda_{\frac{1}{2}}$ values correspond to optical activation energies 2·4 eV and 1·3 eV with a maximum deviation of $\pm$ 4 per cent. The relative intensities of the two bands are similar in all layers, the long wavelength band being approximately 1 per cent of the main band. The temperature variation of activation energy is estimated as $\mathrm{d}E/\mathrm{d}T = -15 \times 10^{-4}$ eV/°C.

Regarding the significance of these two optical activation energies, it seems probable that the 2·4 eV value is related to the intra-molecular energy of the I_2 molecules in the solid. Measurements of the absorption spectrum of iodine vapour show that there is a well-defined absorption limit at 0·50 μ or 2·5 eV (RICE and TELLER, 1949). This is very near to the value for the optical activation energy found above. As the intra-molecular distance varies little from gas to solid, so the intra-molecular energy in the solid state would be expected to be only slightly less than that in the gaseous state. This suggestion therefore fits readily with the experimental results. The

lower activation energy is likely to be associated with the lattice as a whole, corresponding to the band to band transitions found for semiconductors with more normal crystal structures. A suggestion that such behaviour would be expected in molecular crystals was put forward by SEITZ (1940).

From the slope of the resistance temperature curve the thermal activation energy is found to be 1·24 eV, in close agreement with the lower value of optical activation energy. The specific resistance for melted layers is $\sim 10^8\,\Omega$ cm, which is about the same as the early value given by EXNER (1882). For evaporated layers the specific resistance is considerably higher, probably as a result of increased purity produced by the vacuum distillation, the value being $\sim 5 \times 10^8\,\Omega$ cm at 20°C. From the specific resistance and activation energy, the mobility of the carriers is estimated to be $\sim 25\,\mathrm{cm\,sec^{-1}/V\,cm^{-1}}$.

Consideration of the data in the literature indicates that there are two refractive indices for solid iodine, with values near 2 and 3.

It is concluded that solid iodine is a semiconductor with a lattice activation energy of 1·24 to 1·3 eV.

23

DISCUSSION

23.1. OCCURRENCE OF PHOTOCONDUCTIVITY

PHOTOCONDUCTIVITY has now been observed in most of the elements which are not metals and which have a high refractive index (*i.e.* greater than about 2). Measurements of the spectral distribution of photosensitivity have been made on the elements boron, carbon, silicon, germanium, phosphorus, arsenic, sulphur, selenium, tellurium and iodine. For antimony, although such measurements have been carried out, there is still doubt whether the effect observed is bolometric or photoconductive. Photoconductivity has not yet been observed in grey tin, but study of the other properties of this material makes it seem probable that photoconductivity would occur under appropriate conditions.

Table XIV shows the part of the periodic table containing the photoconductive elements. By each material is given the $\lambda_{\frac{1}{2}}$ value in microns. It will be observed that the wavelengths always increase on proceeding either from right to left, or downwards, through the table. Thus in a given column, the wavelength increases with the atomic weight; whilst in a given row, the wavelength increases with the negative valency.

23.2. GENERAL PROPERTIES OF THE PHOTOCURRENT

For the variation of photocurrent with applied voltage (or field) the relation is found to be linear, at least at low voltages. For the relation between the photocurrent and intensity of irradiation, all the elements have been found to give a linear law at low intensities. For most of the elements a (Power)$^{\frac{1}{2}}$ law holds at high power levels. For phosphorus and selenium complex laws have been observed, but for measurements with monochromatic light the behaviour is found to fit the simple relations.

The response times of the photoconductors have been estimated with varying degrees of accuracy. For diamond $\tau \simeq 10^{-8}$ sec and for amorphous selenium $\tau < 50$ μsec. Values in the range 100 to 1,000 μsec have been generally found for Si, Ge, As, Te and I. For boron, sulphur and phosphorus, one can only say at present that the values are less than 3×10^{-3}, 0·1, and one second respectively.

Table XIV

B 1·1	C 0·23			
	Si 1·08	P 0·50 and 0·85	S 0·5	
	Ge 1·7	As 1·03	Se 0·5 and 0·8	
	Sn 3·3	Sb	Te 0·52 and 0·96	I

23·3. COMPARISON OF THERMAL AND OPTICAL ACTIVATION ENERGIES

For the majority of the elements the agreement between optical and thermal activation energies is very good. The values obtained (in eV), are summarized in *Table XV*. In addition to the values found from photoconductivity and resistance–temperature measurements, approximate values deduced from the specific resistance (when this resistance is sufficiently high for the results to be fairly accurate), and from photoemissive measurements, are given. The last column shows values of the temperature shift of activation energy.

It will be seen that for seven of the elements the two energy values agree within 5 per cent. For the other three elements, the difference between the average values of the two energies is still less than the scatter about these average values. It is to be concluded therefore, that for all the photoconductive elements, the optical and thermal activation energies are substantially the same.

Table XV. Agreement between Thermal and Optical Activation Energies

Element	*Photo-conductivity*	*Resist./ Temp.*	*Sp. Resist.*	*Photo-electric*	*Shift* (10^{-4}eV/°C)
Boron ..	0·96–1·27	0·88–1·28	1·0	1·0	− 3 to −4
Diamond ..	5·3	5·2 ± 0·3	~ 5·8	—	− 2
Silicon ..	1·15	1·13	—	—	− 4 ± 1
Germanium ..	0·73	0·74	—	—	~ − 3
Phosphorus ..	1·39–1·56	1·51–1·64	—	—	—
Arsenic ..	1·2	1·2	1·1	1·0	− 5
Sulphur ..	2·4	2·6	2·5	—	~ − 10
Selenium ..	(*a*) 1·5–1·9	~ 1·7	—	—	− 4 to − 6
	(*b*) 2·5	2·3			~ −7
Tellurium ..	0·37	0·36	—	~ 0·36	+ 2
Iodine ..	1·30	1·24	1·35	—	~ − 15

(*a*) Red or metallic selenium (*b*) Amorphous

No difference in the activation energies should occur in consequence of the Franck–Condon principle provided the polarizabilities at high and low frequencies are the same, and hence $\epsilon = n^2$. By correlation of various measurements reported in the literature, it is established that for sulphur, diamond, and phosphorus, this relation is correct to ~ 1 per cent. Also for germanium, n^2 agrees with the value of dielectric constant derived from conductivity measurements.

Estimates of the temperature dependence of activation energy are given for nine elements, the information being derived from various types of measurement. It is found that, with the exception of tellurium, all the shifts are negative *i.e.* the energy gap decreases with rising temperature.

23.4. RELATION BETWEEN ACTIVATION ENERGY AND OTHER PROPERTIES

It has been shown that for photoconductive compounds there are theoretical reasons and experimental evidence for a relation between the threshold wavelength of the photoconductive effect and the refractive index, namely n^4/λ = constant. It is of interest to see if a similar relation exists for any of the elements; particularly for the carbon–silicon series which all have the same crystal structure. To be more specific, the dielectric constant (ϵ) and activation energy (E) are considered, so that the relation $E\epsilon^2$ = constant would be expected. The values are given in *Table XVI* and are seen to lie within $\pm$ 8 per cent of 173, while E varies by more than 7 : 1; so the agreement may be considered relatively good.

Table XVI

Element	E	ϵ	$E\epsilon^2$
Diamond ..	5·3	5·67	170
Silicon ..	1·14	11·8	160
Germanium ..	0·73	16·0	186

A further estimate of $E\epsilon^2$ may be made for silicon carbide, which although a compound, is clearly similar to the above elements in that it is non-polar, and crystallizes in the same tetrahedral lattice (except that each atom of one element is surrounded by 4 atoms of the other element)*. Measurements of photoconductivity have been made on SiC by LOSEV (1940), from whose results $\lambda_t = 0{\cdot}35\ \mu$, and hence the activation energy is 3·5 eV. Refractive indices are given by MERWIN†, which on extrapolating to zero frequency give $n_0 = 2{\cdot}57$ and 2·60. Taking the dielectric constant as the product of these indices we have $\epsilon = 6{\cdot}7$, and $E\epsilon^2 = 160$. Thus this value also lies within the range 173 $\pm$ 8 per cent. We may therefore conclude

* SEITZ and JOHNSON (1937) say the band structure of SiC is like that of diamond.
† MERWIN, see LANDOLT-BORNSTEIN, *Physical-Chemical Tables*.

that for this series of materials, the activation energy varies inversely as the square of the dielectric constant.

The refractive index is not known for grey tin—in fact very few parameters are known for this material. One of the few data which has been measured is the lattice constant, which is $a = 6{\cdot}49$ Å. It is of interest to find some way of plotting the observed activation energies for the whole series, including grey tin, in order to illustrate the progressive decrease. In a general way the interatomic distance will be representative of

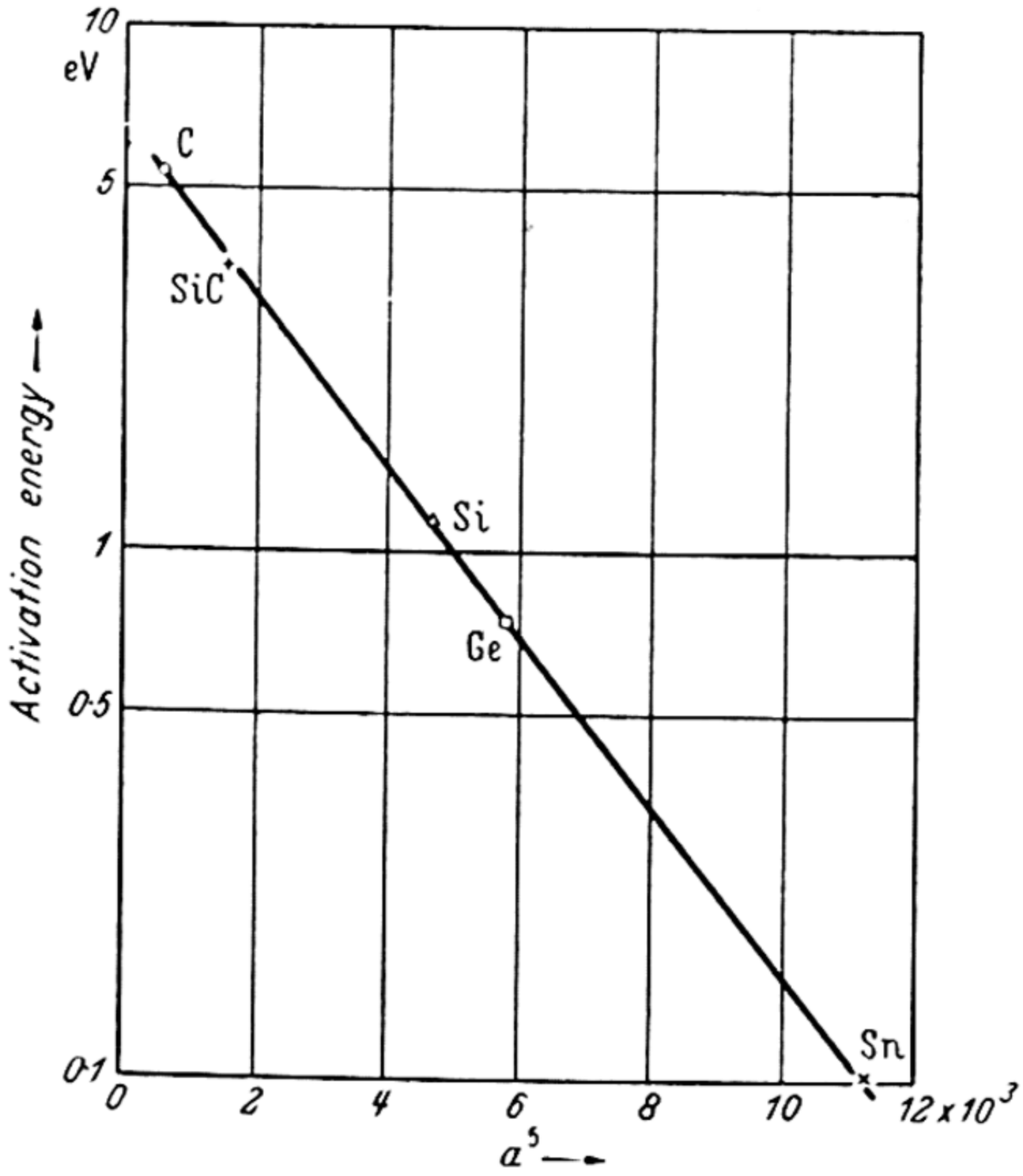

Figure 56. Activation energy and lattice constant

the tightness of binding between the atoms, and the activation energy may therefore be expected to decrease as some fairly high power of the interatomic distance (or lattice constant, a). By trial it was found that plotting activation energy against a^5 on a semi-log scale was most satisfactory. From *Figure 56* it may be seen that all five points lie very close to a straight line, so that we are led to an empirical relation between activation energy and lattice constant, $E = 6{\cdot}6 \exp(-a^5/2{,}670)$.

The fact that the point for grey tin fits on the line of *Figure 56* shows that it behaves similarly to the other four

materials, and hence we should expect it to obey the $E\epsilon^2 \simeq 173$ relation. Using this formula to estimate the dielectric constant gives $\epsilon = 42$ and $n_0 = 6{\cdot}5$.

For the remaining elements the value of $E\epsilon^2$ varies widely within the columns of the periodic table. Considering that these elements have different crystal structures, the lack of constancy is not surprising. For the elements in general however, it still appears that the more highly refractive materials are photoconductive at the longer wavelengths. Tellurium for example, has the highest refractive index, and is photoconductive at the longest wavelength. The photoconductive elements are listed in *Table XVII* in order of decreasing $\lambda_{\frac{1}{2}}$, with the refractive indices quoted for comparison. As will be seen, there is a general tendency for the refractive index to decrease as the $\lambda_{\frac{1}{2}}$ value decreases, the only definite discrepancy being the last element on the list, diamond.

Table XVII

Element	Te	Ge	B	Si	As	I	P	Se	S	C
$\lambda_{\frac{1}{2}}$	3·3	1·7	1·1	1·08	1·03	0·96	0·85	0·8	0·5	0·23
n	4·8	4·0	>3	3·43	3·35	~3	2·6	2·45	2·0	2·4

As discussed in § 9.3, the frequency of maximum absorption is directly related to the refractive index when this is high, and by making the simplifying assumption of a constant difference (B) in quantum energy between the threshold wavelength and the wavelength of maximum absorption for all elements, we obtain (as equation 61) $E = U/n - B$, where U is a constant. With the values $U = 9$ and $B = 1{\cdot}5$ this expression gives the following energy values:

Element	Te	Ge	Si	As
Calculated Energy	0·37	0·75	1.12	1·18
Observed Energy	0·36	0·73	1·14	1·2

Thus for the elements of highest refractive index, this simple relation appears to hold well.

Further evidence of the inter-relation between activation energy and refractive index may be obtained by consideration

of the effect of the shift of the absorption edge on refractive index. Consider a simplified absorption curve which is an isosceles triangle for $2nk$ when plotted against energy, with a maximum absorption of 'a' at energy E_0, and zero absorption at $E_0 \pm \gamma$. Then, as given in § 3.3, the refractive index (at zero frequency) is:

$$\frac{\pi}{2}(n_0^2 - 1) = \int_0^\infty 2nk \frac{\mathrm{d}E}{E}$$

which gives

$$\frac{\pi}{2a}(n_0^2 - 1) = \frac{E_0}{\gamma} \log \frac{(E_0^2 - \gamma^2)}{E_0^2} + \log \frac{(E_0 + \gamma)}{(E_0 - \gamma)}$$

For silicon, the observed absorption data would give reasonable parameters for the equivalent triangle as $E_0 = 3{\cdot}5$ eV, $\gamma = 2$ eV, and $a = 27$ approximately. With these values the calculated n_0^2 is $11{\cdot}7$, in good agreement with the observed figure.

Now suppose that on cooling E_0 increases to $E_0 + \Delta$ while γ decreases to $\gamma - \Delta$ *i.e.* assuming that the shift of the absorption edge due to lattice broadening (Δ) is half the total shift of the edge (2Δ), as is approximately true for silicon, then the change in refractive index is given by

$$\frac{\pi}{2}(n^2 - n_0^2) = \frac{a\Delta}{\gamma}(1 + E_0/\gamma) \log (1 - \gamma^2/E_0^2) = -0{\cdot}54a\Delta.$$

Thus $(n^2 - n_0^2)/n_0^2 = -0{\cdot}8\,\Delta = -0{\cdot}9\,\Delta/E$ where E is the threshold energy for silicon *i.e.* $1{\cdot}14$ eV.

Hence $(n^4 - n_0^4)/n_0^4 = -1{\cdot}8\,\Delta/E = -0{\cdot}9(2\Delta/E)$, so that the relative shift of the absorption edge of $2\Delta/E$ is approximately equal to the relative change in n^4, as of course would follow if the $En^4 = constant$ relation were obeyed. This calculation therefore shows that the theoretical variation of refractive index is consistent (in sign and magnitude) with such a relation between refractive index and activation energy.

It is to be concluded therefore that on the basis of information available at present, the parameter most closely associated with the activation energy is the refractive index, the correlation being particularly good for materials like silicon where there is no anisotropy, and where the absorption curve has a simple symmetrical form.

APPENDIX

OPTICAL INTERFERENCE AND REFRACTIVE INDEX

CONSIDER a ray of light incident on a thin parallel sheet of material of refractive index n and thickness d. For an incident ray of unit amplitude, if the reflection coefficient is r, and t and t' are the transmission coefficients into and out of the material then the amplitudes* of the various reflected rays will be r, rtt', r^3tt', r^5tt' *etc*, and of the transmitted rays, tt', r^2tt', r^4tt' and so on. The only phase change on reflection will be that of the first reflected ray.

In transmission all the rays will be in phase and produce a maximum of transmission when $2nd = N\lambda$ (for almost normal incidence), where N is an integer. The total transmission then is

$$t_m = tt' + r^2tt' + r^4tt' + \ldots\ldots\ldots = tt'/(1 - r^2)$$

Now $tt' = 1 - r^2$, and hence the maximum transmission is unity —as it clearly must be. When $2nd = (2N + 1)\lambda/2$, destructive interference occurs, giving a transmission minimum, with $t_0 = tt'/(1 + r^2) = (1 - r^2)/(1 + r^2)$.

In reflection, when $2nd = N\lambda$, the net reflection is a minimum with

$$r_0 = -r + rtt' + r^3tt' + r^5tt' \ldots\ldots\ldots$$

$$= -r\left(1 - \frac{tt'}{1 - r^2}\right) = 0$$

Similarly at $2nd = (2N + 1)\lambda/2$ the reflection is a maximum with

$$r_m = -r\left(1 + \frac{tt'}{1 + r^2}\right) = -\frac{2r}{1 + r^2}.$$

A more complicated case results if absorption in the film is considered. The simplest way of introducing absorption is to

* The *intensities* are given by the squares of the *amplitudes*.

assume a transmission of α for each traversal of the film. We then obtain for the amplitude of the transmitted ray for maximum

$$t_m = \alpha(1 - r^2)/(1 - r^2\alpha^2)$$

and for minimum

$$t_0 = \alpha(1 - r^2)/(1 + \alpha^2 r^2)$$

For the reflected amplitude, at maximum we find

$$r_m = -r(1 + \alpha^2)/(1 + \alpha^2 r^2)$$

and for minimum

$$r_0 = -r(1 - \alpha^2)/(1 - \alpha^2 r^2)$$

In finding the value of refractive index from interference fringes, there is the difficulty that in general the order of the fringe *i.e.* the value of N, is not known. However, for consecutive fringes we have:

$$2nd = N\lambda_1$$
$$2nd = (N + 1)\lambda_2$$

Hence $2nd(1/\lambda_2 - 1/\lambda_1) = 1$, so that the value of $2nd$ may be obtained from the wave number separation of consecutive fringes.

The intensity of reflection at a surface where interference phenomena are not of importance is given by the Fresnel formula $R = r^2 = (n - 1)^2/(n + 1)^2$, provided the material is not highly absorbing. When absorption is important, $R = \{(n - 1)^2 + k^2\}/\{(n + 1)^2 + k^2\}$ where k is given in terms of the absorption constant (K) by $k = \lambda K/4\pi$. The effect of absorption on the reflectivity is thus important for highly refractive materials only if $K \sim 10^5 \text{cm}^{-1}$ or more.

REFERENCE LIST AND AUTHOR INDEX

NOTE—The numbers in heavy type refer to the pages in this book

ACCORDO, C. A. see LEHOVEC, K., 1951
ADAMS, W. G. and DAY, R. E. *Proc. roy Soc.* 25 (1877) 113, **50**
AFANASEV, N. W. *J. tech. Phys., Moscow*, 19 (1950) 225, **193**
AHEARN, A. J. *Phys. Rev.* 84 (1951) 798, **101**
AKA, E. Z. see STRAUMARIS, M. E., 1952
APKER, L. and TAFT, E. *Phys. Rev.* 75 (1949) 1181, **158**, **171**
— — and DICKEY, J. *ibid* 74 (1948) 1462, **71**, **94**, **219**
ARSENEVA-GEIL, A. N. *C. R. Acad. Sci., U.R.S.S.* 68 (1949) 245, **219**
AVERY, D. G. *Proc. phys. Soc. B* 64 (1951) 1087, **62**, **224**
BAILLY, R. *Bull. Acad. Belg. Cl. Sci.* 24 (1938) 791, **62**
BALTENSPERGER, W. *Phys. Rev.* 83 (1951) 1055, **64**
BARDEEN, J. see HALL, H., 1951; PEARSON, G. L., 1949: *Phys. Rev.* 71 (1947) 717, **42**, **54**; 75 (1949) 1777, **227**; 79 (1950) 216, **134**
— and BRATTAIN, W. H. *ibid* 75 (1949) 1208, **126**, **128**, **130**, **131**
— and SHOCKLEY, W. *ibid* 80 (1950) 72, **58**, **115**, **131**, **132**
BARNARD, G. P. *The Selenium Cell* London, 1930, **185**, **195**
BECKER, A. and SCHAPER, I. *Z. Phys.* 122 (1944) 49, **190**
BECKER, J. A. *Elect. Engng., N.Y.* 68 (1949) 937, **120**, **171**
BECKER, M. see FAN, H. Y., 1950, 1951
— and FAN, H. Y. *Phys. Rev.* 76 (1949) 1531, **114**, **121**, **133**; 78 (1950) 301, **39**, **41**, **54**, **123**, **131**
— — and LARK-HOROVITZ, K. *ibid* 85 (1952) 730, **112**
BELL, R. P. see EMELÉUS, H. J., 1948
BENZER, S. *Phys. Rev.* 70 (1946) 105, **123**; 72 (1947) 1267, **123**; *J. appl. Phys.* 20 (1949) 804, **124**
BERGMANN, L. *Naturwissenschaften* 20 (1932) 15, **239**
BERNDT, G. *Phys. Z.* 5 (1904) 121, **196**
BERNDT, W. see SUHRMANN, R., 1940
BHAGAVANTAM, S. *Nature, Lond.* 161 (1948) 729, **102**
BIDWELL, C. C. *Phys. Rev.* 19 (1922) 447, **125**
BILLIG, E. *Proc. phys. Soc. B* 65 (1952) 216, **194**, **202**
BILLINGS, B. H. and HYMAN, M. *J. opt. Soc. Amer.* 37 (1947) 119, **62**
BIRNBAUM, G. *Phys. Rev.* 76 (1949) 178, **22**
BLEULER, E. see LARK-HOROVITZ, K., 1948 and Teal, G. K., 1951
BLUM, A. I. and GORYUNOVA, N. A. *C. R. Acad. Sci., U.R.S.S.* 75 (1950) 367, **136**
BODE, H. W. *Network Analysis and Feedback Amplifier Design* London and New York, 1945, **22**
BOER, F. DE *Philips Res. Rep.* 2 (1947) 352, **193**
BOLTAKS, I. V. *J. tech. Phys., Moscow* 20 (1950) 3, **107**
BOLTZMANN, L. *S.B. Akad. Wiss. Wien.* 70 (1874) 342, **183**
BOTTOM, V. E. *Phys. Rev.* 74 (1948) 1218, **205**; 75 (1949) 1310, **205**
BOVIS, P. *C. R. Acad. Sci., Paris* 184 (1927) 1237, **236**; *Commun. Kamerlingh Onnes Lab. Leiden* 191 (1929) 3, **237**
BRATTAIN, W. H. see BARDEEN, J., 1949
— and BRIGGS, H. B. *Phys. Rev.* 75 (1949) 1705, **18**, **21**, **133**, **134**, **220**
BRIDGMAN, P. W. *J. Amer. chem. Soc.* 36 (1914) 144, **141**; 38 (1916) 609, **141**; *Proc. Amer. Acad. Arts Sci.* 60 (1925) 305, **228**; 72 (1938) 157, **204**, **227**; 74 (1940) 21, **228**; 77 (1949) 189, **131**; 79 (1951) 127, **115**
BRIGGS, H. B. see BRATTAIN, W. H., 1949; *Phys. Rev.*, 77 (1950) 287, 727, **111**, **112**, **114**, **116**, **133**, **220**
BROWN, F. C. see SIEG, L. P., 1914
— and MACMAHON, A. M. *International Critical Tables* New York, 1929, **208**
— and SIEG, L. P. *Phys. Rev.* 4 (1914) 48, **35**, **195**, **197**
BROWNLEE, L. D. *Nature, Lond.* 166 (1950) 482, **136**
BURSTEIN, E., OBERLY, J. J., DAVISSON, J. W. and HERVIS, B. W. *Phys. Rev.* 82 (1951) 764, **111**

Busch, G. *Helv. phys. acta.* 19 (1946) 198, **32**; *Z. angew. Math. Phys.* 1 (1950) 3, **13**
— Flury, H. and Merz, W. *Helv. phys. acta.* 21 (1948) 212, **65**
— and Mooser, E. *Z. phys. Chem.* 198 (1951) 23, **140**
— Wieland, J. and Zoller, H. *Helv. phys. acta.* 23 (1950) 528; 24 (1950) 49, **136**; *Semi-conducting Materials* London, 1951, **136**
Castellan, G. W. and Seitz, F. *ibid*, **10**
Cartwright, C. H. and Haberfeld-Schwarz, M. *Proc. roy. Soc. A* 148 (1935) 648, **204**, **205**
Cheesman, I. C. *Proc. phys. Soc. A* 65 (1952) 25, **17**, **57**, **58**
Chentsov, R. A. *J. exp. theor. Phys.* 18 (1948) 374, **205**
Chynoweth, A. G. *Phys. Rev.* 83 (1951) 254, 264, **102**, **106**
Coblentz, W. W. *Phys. Rev.* 16 (1903) 72, **236**, **238**; *Supplementary Investigation of Infra-Red Spectra* Washington, 1908, **152**, **201**; *Bull. U.S. Bur. Stand.* 7 (1911) 198, **225**; 14 (1918) 591, **208**; 16 (1920) 595, **62**, **66**
— and Eckford, J. F. *Bull. U.S. Bur. Stand.* 18 (1923) 489, **62**, **239**
— and Kahler, H. *ibid* 15 (1919) 121, 231, **28**, **62**; 18 (1922) 265, **62**
Conwell, E. and Weisskopf, V. F. *Phys. Rev.* 69 (1946) 258, **14**
Cope, A. D. see Forgue, S. V., 1951; and Weimer, P. K., 1951
Corson, D. R., Mackenzie, K. R. and Segre, E. *Phys. Rev.* 57 (1940) 1087, **76**
Cotton, P. *J. Phys. Radium* 11 (1950) 375, **112**
Curl, G. W. and Danielson, G. C. *Phys. Rev.* 85 (1952) 729, **95**
Daly, E. F. and Sutherland, G. B. B. M. *Proc. phys. Soc.* 62 (1949) 205, **226**
Damien, B. C. *Ann. sci. Éc. norm. sup., Paris* 10 (1881) 233, 265, 298, **153**, **238**
Danforth-Cope, A. see Cope, A. D.
Danielson, G. C. see Curl, G. W., 1952
Davis, R. see Lark-Horovitz, K., 1948
Davisson, J. W. see Burstein, E., 1951
Day, R. E. see Adams, W. G., 1877
Dechene, G. *C. R. Acad. Sci., Paris* 208 (1939) 95, **62**
Dember, H. see Mendelssohn, T., 1940
De Sorbo, W. and Dunlap, W. C. *Phys. Rev.* 83 (1951) 879, **118**, **128**
Dexter, D. L. and Heller, W. R. *ibid* 84 (1951) 377, **61**
Dickey, J. see Apker, L., 1948
Dowd, J. J. *Proc. phys. Soc. B.* 64 (1951) 783, **190**, **198**, **200**
DuBridge, L. A. see Hughes, A. L., 1932
Dunlap, W. C. see De Sorbo, W., 1951; *Phys. Rev.* 79 (1950) 286, **126**, **129**; 82 (1951) 329, **129**; 85 (1952) 945, **128**
Du Pre, F. K. see Hutner, R. A., 1950
Dupuy, E. and Hackspill, L. *C. R. Acad. Sci., Paris* 179 (1933) 229, **78**
Eckart, F. and Kittel, A. *Naturwissenschaften* 29 (1941) 371, **194**
— and Schmidt, A. *Z. Phys.* 118 (1941) 199, **195**
Eckford, J. F. see Coblentz, W. W., 1923
Edmunds, C. K. *Phys. Rev.* 18 (1904) 193, **200**
Elliot, D. S. *ibid* 5 (1915) 53, **196**
Emeléus, H. J. and Bell, R. P. *Quart. Rev. chem. Soc., Lond.* 2 (1948) 132, **84**
Engelhard, E. *Ann. Phys.* 17 (1933) 501, **29**
Estermann, I. and Foner, A. *Phys. Rev.* 79 (1950) 365, **129**
Exner, F. *Ann. Phys.* 15 (1882) 412, **240**
Faltz, G. *ibid* 30 (1937) 193, **62**
Fan, H. Y. see Becker, M., 1949, 1950, 1952 and Johnson, V. A., 1950; *Phys. Rev.* 75 (1949) 1631, **53**; 78 (1950) 808, **116**, **132**; 82 (1951) 900, **58**, **116**
— and Becker, M. *ibid* 78 (1950) 178, **112**, **115**, **121**; *Semi-conducting Materials* London, 1951, **114**, **115**, **116**, **132**
Fassbender, J. *Naturwissenschaften* 34 (1947) 212, **28**; *Ann. Phys.* 5 (1949) 3, **46**, **48**
— and Lehmann, H. *ibid* 6 (1949) 215, **40**
Fedorus, G. A. see Lashkarev, V. E., 1949
Fischer, F., Gudden, B. and Treu, M. *Phys. Z.* 39 (1938) 127, **36**

FISHER, J. R. see TEAL, G. K., 1946
FLURY, H. see Busch, G., 1948
FONER, A. see ESTERMANN, I., 1950
FORGUE, S. V., GOODRICH, R. R. and COPE, A. D. *R.C.A. Rev.* 12 (1951) 335, **27**
FORNSTECHER, M. and RYSKEVIC, E. *C. R. Acad. Sci. Paris* 221 (1945) 749, **78**
FOURNIER D'ABLE, E. E. *Proc. roy. Soc.* 89 (1913) 75, **197**
FOUSSEREAU, G. *C. R. Acad. Sci., Paris* 97 (1883) 996, **141-2**, **144**, **156**; *Ann. Chim. (Phys.)* 5 (1885) 317, **141-2**, **144**, **182**
FOWLER, R. H. *Statistical Mechanics* Cambridge, 1936, **11**
FOX, J. J. see Robertson, R., 1934
FRAGSTEIN, K. VON *Ann. Phys.* 17 (1933) 1, **225**
FRANK, —.Dissertation, Berne, 1912, see MELLOR, J. W. 1929, **158**
FREEMAN, G. P. and VAN DER VELDEN, H. A. *Physica, Eindh ven* 18 (1952) 1, **102**
FRENKEL, J. and JOFFÉ, A. *Phys. Rev.* 39 (1932) 530, **55**
FREYMANN, R. and STIEBER, A. *C. R. Acad. Sci., Paris* 199 (1934) 1109, **91**, **92**
FRIEDBERG, S. A. *Phys. Rev.* 82 (1951) 764, **128**
FUKUDA, M. *Mem. Coll. Sci. Kyoto* 4 (1921) 351, **182**
FUKUROI, T., TANUMA, S. and TOBISAWA, S. *Sci. Rep. Res. Insts. Tôhuku Univ. A* 1 (1949) 365, 375, **205**, **229**; *A* 2 (1950) 233, 239, **205**, **229**.
FULCHERIS, G. see POCHETTINO, A., 1923
FULLER, C. S., THEURER, H. C. and ROOSBROECK, W. VAN *Phys. Rev.* 85 (1952) 678, **118**
GEBBIE, H. A. and KIELY, D. G. *Proc. phys. Soc. B* 65 (1952) 553, **201**
— and SAKER, E. W. *ibid B* 64 (1951) 360, **189**, **200**
GERRITSEN, A. N. *Physica, Eindhoven* 15 (1949) 427, **128**
GIBSON, A. F. *Proc. phys. Soc. B* 63 (1950) 756, **63**, **222**; *B* 64 (1951) 603, **41**, **44**; *B* 65 (1952) 196, 378, **46**, **56**, **63**, **222**
— LAWSON, W. D. and Moss, T. S. *ibid A* 64 (1951) 1054, **62**
GILLEO, M. A. *J. chem. Phys.* 19 (1951) 1291, **189**, **195**, **198**
GIVENS, M. and SIEGMUND, W. P. *Phys. Rev.* 85 (1952) 313, **203**
GLEISSMAN, J. R. see HUNG, C. S., 1950
GMELIN'S *Handbuch der anorganische Chemie* Berlin, 1933, *Jod* **230**; 1940, *Tellur*, **204**
GOODMAN, B., LAWSON, A. W. and SCHIFF, L. I. *Phys. Rev.* 71 (1947) 191, **9**
GOODRICH, R. R. see FORGUE, S. V., 1951
GORLICH, P. *Photo-elements*, Moscow, 1948, **196**; *Photocells*, Leipzig, 1951, **196**
GORYUNOVA, N. A. see BLUM, A. I., 1950
GOUCHER, F. S. *Phys. Rev.* 78 (1950) 646, 816, **27**, **120**, **130**
— PEARSON, G. L., SPARKS, M., TEAL, G. K. and SHOCKLEY, W. *ibid* 81 (1951) 637, **54**, **122**
GUDDEN, B. see FISCHER, F., 1938; *Lichtelektrische Erscheinungen* Berlin, 1927/8, **24**, **28**, **63**, **191**
— and POHL, R. W. *Z. Phys.* 3 (1920) 123, **62**, **97**; 7 (1921) 65, **26**; 17 (1923) 331, **27**, **75**, **95**, **97**, **98**; 20 (1924) 14, **27**; 35 (1925) 243, **188**, **196**; 37 (1926) 881, **61**; 48 (1928) 384, **62**;
GURNEY, R. W. see MOTT, N. F., 1948
GYULAI, Z. *Z. Phys.* 33 (1925) 251, **27**
HABERFELD-SCHWARZ, M. see CARTWRIGHT, C. H., 1935
HACKETT, W. see WHITEHEAD, S., 1939
HACKSPILL, L., see DUPUY, E., 1933
HALL, G. G. *Phil. Mag.* 43 (1952) 338, **95**
HALL, H., BARDEEN, J. and PEARSON, G. L. *Phys. Rev.* 84 (1951) 129, **131**
Handbook of Chemistry and Physics Cleveland, Ohio, 1948, **62**
HASS, G. H. and SCOTT, N. W. *J. Phys. Radium* 11 (1950) 394, **112**
HAYNES, J. R. see SHOCKLEY, W., 1949
— and SHOCKLEY, W. *Phys. Rev.* 81 (1951) 835, **41**, **129**
— and WESTPHAL, W. C. *ibid* 85 (1952) 680, **110**
HECHT, K. *Z. Phys.* 77 (1932) 235, **96**

HELLER, W. R. see DEXTER, D. L., 1951
— and MARCUS, A. *Phys. Rev.* 84 (1951) 808 (see also DEXTER, D. L. and HELLER, W. R., 1951) **61**
HENISCH, H. K. *Metal Rectifiers* London, 1949. **51**
— and SAKER, E. W. *Proc. phys. Soc. B* 65 (1952) 149, **193**
HENKELS, H. W. *Phys. Rev.* 76 (1949) 1737, **193**; 77 (1950) 734, **193**; *J. appl. Phys.* 21 (1950b) 725, **199**
HENNINGER, F. P. *Ann. Phys., Lpz.* 28 (1937) 245, **91**
HERMAN, F. see MOORE, A. R., 1951
HEYWANG, W. VON *Z. Naturf.* 4 (1949) 654, **10**
HERVIS, B. W. see BURSTEIN, E., 1951
HILSCH, R. and POHL, R. W. *Z. Phys.* 48 (1928) 384, **236**
HIPPEL, A. R. VON *J. chem. Phys.* 16 (1948) 372, **180**, **185**, **191**, **202**, **204**
— and RITTNER, E. S. *ibid* 14 (1946) 370, **38**, **40**
HOARD, J. L. see LAUBENGAYER, A. W., 1943
HOJENDAHL, K. *K. Danske vidensk Selsk.* 16 (1938) No. 2, 59, **62**
HOLMES, D. K. *Phys. Rev.* 76 (1949) 178, **115**
HUGHES, A. L. and DUBRIDGE, L. A. *Photoelectric Phenomena* New York, 1932, **35**, **62**, **71**, **195**
HUNG, C. S. and GLEISSMAN, J. R. *Phys. Rev.* 79 (1950) 726, **128**
HUNTER, L. P. see KLAHR, C. N., 1951
HURD, D. T. see LAUBENGAYER, A. W., 1943
HURION, A. *Ann. sci. Éc. norm. sup. Paris* 6 (1877) 394, **238**
HUTNER, R. A. see SAXON, D. S., 1949
— RITTNER, E. S. and DU PRE, F. K. *Philips Res. Rep.* 5 (1950) 188, **14**
HYMAN, M. see BILLINGS, B. H., 1947
INGERSOLL, L. R. *Astrophys. J.* 32 (1910) 265, **111**
International Critical Tables New York, 1926–1930, **62**, **208**
JAMOCHIAN, E. see LEHOVEC, K., 1951
JOFFÉ, A. F. see FRENKEL, J., 1932; *The Physics of Crystals* New York, 1928, **75**, **180**
JOHNSON, E. W. see KRAUS, C. A., 1928
JOHNSON, R. P. see SEITZ, F., 1937
JOHNSON, V. A. *Phys. Rev.* 74 (1948) 1255, **205**
— and FAN, H. Y. *ibid* 79 (1950) 899, **126**, **131**
— and LARK-HOROVITZ, K. *ibid* 82 (1951) 763, **119**
KAHLENBERG, H. H. *Trans. Amer. electrochem. Soc.* 47 (1925) 55, **80**
KAHLER, H. see COBLENTZ, W. W., 1919, 1922
KANDA, E. see SUGAWARA, T., 1949
KAPP, G. *Ann. Phys.* 22 (1935) 257, **62**
KECK, P. H. *Optik, Stuttgart* 1 (1946) 42, **197**
KENDALL, J. T. *Proc. phys. Soc. B* 63 (1950) 821, **138**
KIELY, D. G. see GEBBIE, H. A., 1952
KIMBALL, G. E. *J. chem. Phys.* 3 (1935) 560, **6**, **95**
KITTEL, A. see ECKART, F. E., 1941
KLAHR, C. N. and HUNTER, L. P. *Phys. Rev.* 81 (1951) 1059, **14**
KLEINSCHROD, F. G. *Ann. Phys.* 27 (1936) 97, **18**
KLICK, C. C. and MAURER, R. J. *Phys. Rev.* 76 (1949) 179, **101**; 81 (1951) 124, **101**
KOENIGSBURGER, J. and SCHILLING, K. *Ann. Phys., Lpz.* 32 (1910) 179, **110**
KOLOMIETS, B. T. and RYVKIN, S. M. *J. tech. Phys., Moscow* 18 (1947) 987, **181**
KOZLOUSKI, I. L. and NASLEDOV, D. N. *J. tech. Phys., Moscow* 13 (1943) 627, **193**
KRAUS, C. A. and JOHNSON, E. W. *J. phys. Chem.* 32 (1928) 1281, **205**
KREBS, H. *Semi-conducting Materials* London, 1951, **158**, **185**
KRISHNAN, R. S. *Proc. Indian Acad. Sci. A* 24 (1946) 33, **105**
KUBO, R. *J. phys. Soc. Japan* 3 (1948) 254, **64**
KURRELMEYER, B. *Phys. Rev.* 30 (1927) 893, **63**, **75**, **180**
LABHART, H. *Helv. phys. acta.*, 19 (1946) 463, **11**
LANDOLT-BORNSTEIN *Physical Chemical Tables* Berlin, 1927, 1935, **62**, **168**, **244**

LANGE, B., *Photoelements* New York, 1938, **35, 55**
LARK-HOROVITZ, K. see BECKER, M., 1952; JOHNSON, V. A., 1951; SCANLON, W., 1947; THORNHILL, J. W., 1951: *N.D.R.C. Rep.* 14/585 (1942–45) **133**; *Elect. Engng., N.Y.* 68 (1949) 1047, **118**, **126**; *Semi-conducting Materials* London, 1951 **112, 119, 121**
— BLEULER, E., DAVIS, R. and TENDAM, D. *Phys. Rev.* 23 (1948) 1256, **121**
— and MEISSNER, K. W. *ibid* 76 (1949) 1530, **133**
— MIDDLETON, A. E., MILLER, E. P. and WALDERSTEIN, I. *ibid* 69 (1946) 258, **126**
LASHKAREV, V. E., POTAMENKO, I. R. and FEDORUS, G. A., *J. exp. theor. Phys.* 10 (1949) 887, **39**
LAUBENGAYER, A. W., HURD, D. T., NEWKIRK, A. E. and HOARD, J. L. *J. Amer. chem. Soc.* 65 (1943) 1924, **91**
LAWSON, A. W. see GOODMAN, B., 1947
LAWSON, W. D. see GIBSON, A. F., 1951
LEHFELDT, W. *Götting. Nach. Fach.*, II, I (1935) 171, **27**
LEHMANN, H. see FASSBENDER, J., 1949
LEHOVEC, K., ACCORDO, C. A. and JAMOCHIAN, E. *Phys. Rev.* 83 (1951) 603, **72**
LENZ, H. *Ann. Phys., Lpz.* 77 (1925) 449, **27**, **100**; 83 (1927) 941, **97, 98**
LIZELL, B. *J. chem. Phys.* 20 (1952) 672, **199**
LOFERSKI, J. J. and MILLER, P. H. *Phys. Rev.* 83 (1951) 876, **222, 225**
LORD, R. C. *ibid* 85 (1952) 140, **114, 134**
LOSEV, O. V. *C. R. Acad. Sci. U.R.S.S.* 29 (1940) 360, 363, **244**
MACKENZIE, K. R. see CORSON, D. R., 1940
MACMAHON, A. M. see BROWN, F. C., 1929
MALYSHEV, E. K. see NASLEDOV, D. N., 1946
MARCUS, A. see HEILER, W. R., 1951
MARTENS, F. F. *Ann. Phys., Lpz.* 8 (1902) 459, **102**
MARTIN, A. E. see ROBERTSON, R., 1934
MASON, W. H. see VONWILLER, O. U., 1907
MAURER, R. J. see KLICK, C.C., 1949, 1951
MAXWELL, C. R. *J. chem. Phys.* 17 (1949) 1288, **76**
MCKAY, K. G. *Phys. Rev.* 74 (1948) 1606, **96**; 77 (1950) 816, **41, 96, 101**; 84 (1951) 829, 833, **102, 125**
MEIER, W. *Ann. Phys., Lpz.* 31 (1910) 1017, 1033, **201, 236, 238**
MEISSNER, K. W. see LARK-HOROVITZ, K., 1949
MELLOR, J. W. *Inorganic and Theoretical Chemistry* London, 1924, **104**; 1929, **158**, **167**; 1930, **183**
MENDELSSOHN, T. and DEMBER, H. *Rev. Fac. Sci. Univ. Istanbul A* 6 (1940) 18, **98, 100**
MERWIN, —. see LANDOLT-BORNSTEIN *Physical-Chemical Tables*; **244**
MERZ, W. see BUSCH, G., 1948
MICHELS, W. C. and WILFORD, S. E. *Phys. Rev.* 76 (1949) 174, **76**
MIDDLETON, A. E. see LARK-HOROVITZ, K., 1946
MILLER, E. P. see LARK-HOROVITZ, K., 1946
MILLER, P. H. see LOFERSKI, J. J., 1951
— and TAYLOR, J. H. *Phys. Rev.* 76 (1949) 179, **131**
MILLER, R. F. *J. opt. Soc. Amer.* 10 (1925) 621, **199, 224, 225**
MINCHIN, G. M. *Nature, Lond.* 77 (1908) 173, **196**
MOGLICH, F., RIEHL, N. and ROMPE, R. *Z. tech. Phys.* 21 (1940) 6, 128, **57**
— and ROMPE, R. *Z. Phys.*, 119 (1942) 472, **66**
MONCH, G. *Phys. Z.* 40 (1939) 487, **191**
MOORE, A. R. and HERMAN, F. *Phys. Rev.* 82 (1951) 763, **129**
MOOSER, E. see BUSCH, G., 1951
MOSS, T. S. see GIBSON, A. F., 1951; *Nature, Lond.* 159 (1947) 476, **39, 62**; 161 (1948) 776, **67**; *Proc. Phys. Soc. A* 62 (1949) 264, **160**; *B* 62 (1949b) 741, **30, 35, 36, 56, 57, 62**; B63 (1950) 167, **57, 65, 67**; Dissertation, Cambridge, 1950 (b) **76**

MOTT, N. F. *Proc. Instn. elect. Engrs.* 96 (1949) I 253, **61**
— and GURNEY, R. W. *Electronic Processes in Ionic Crystals* Oxford, 1948, **21**, **22**, **43**, **61**, **64**, **219**
— and SNEDDON, I. N. *Wave Mechanics and its Applications* Oxford, 1948, **18**
MULLANEY, J. F. *Phys. Rev.* 66 (1944) 326, **107**, **115**
MULLER, T. *S. B. phys.-med. Soz. Erlangen* 70 (1938) 7, **193**
MUNESUE, S. see SAKURAI, T., 1952
MUTO, T. and OYAMA, S. *Progr. theor. Phys., Osaka* 6 (1951) 61, **105**, **132**
NARAY-SZABO, S. VON *Nature, Lond.* 24 (1936) 77, **78**
NASLEDOV, D. N. see KOZLOUSKI, I. L., 1943
— and MALYSHEV, E. K. *J. tech. Phys., Moscow* 16 (1946) 1127, **185**
NEUMANN, H. *Z. Phys.* 45 (1927) 717, **182**
NEWKIRK, A. E. see LAUBENGAYER, A. W., 1943
NEWTON, R. R. *Phys. Rev.* 75 (1949) 234, **97**
OBERLY, J. J. see BURSTEIN, E., 1951
OYAMA, S. see MUTO, T., 1951
PANT, D. D., *Proc. Indian Acad. Sci.* 19 (1944) 315, **75**, **95**, **97**
PARTINGTON, J. R. *General and Inorganic Chemistry* London, 1949, **142**
PAULING, L. *Nature Lond.* 161 (1948) 1019, **136**
PEARLSTEIN, E. A. and SUTTON, R. B. *Phys. Rev.* 79 (1950) 907, **97**, **101**
PEARSON, G. L. see GOUCHER, F. S., 1951, HALL, H., 1951, SHOCKLEY, W., 1949:
Elect. Engng. N.Y. 66 (1947) 638, **109**
— and BARDEEN, J. *Phys. Rev.* 75 (1949) 865, **10**, **14**, **64**, **108**, **109**, **110**, **115**
— READ, W. T. and SHOCKLEY, W. *ibid* 85 (1952) 1055, **133**
— and SHOCKLEY, W. *ibid* 71 (1947) 141, **127**
— STRUTHERS, J. D. and THEUERER, H. C. *ibid* 77 (1950) 809, **118**, **129**
— and SUHL, H. *ibid* 83 (1951) 768, **12**, **129**, **130**
PELABON, H. *C. R. Acad. Sci. Paris* 173 (1921) 295, **199**
PENSAK, L. *Phys. Rev.* 79 (1950) 171, **188**
PETER, F. *Z. Phys.* 15 (1923) 358, **102**
PFESTORF, G. *Ann. Phys., Lpz.* 81 (1926) 906, **111**
PFUND, A. H. *Phys. Rev.* 34 (1912) 370, **197**; *J. opt. Soc. Amer.* 23 (1933) 375, **220**
PICK, H. *Ann. Phys., Lpz.* 3 (1948) 17, **38**, **40**
PIETENPOL, W. J. *Phys. Rev.* 82 (1951) 121, **123**
PINCHERLE, L. *Proc. phys. Soc. A* 64 (1951) 603, **10**
PIGULEWSKY, V. *J. Soc. phys.-chim. russe* 44 (1912) 105; **180**
PLESSNER, K. W. *Proc. phys. Soc. B.* 64 (1951) 671, 681, **194**
POCHETTINO A. and FULCHERIS, G. *Atti Accad. Torino* 58 (1923) 493, **236**
POHL, R. W. see GUDDEN, B., 1920, 1921, 1923, 1924, 1925, 1926, 1928 and HILSCH, R., 1928
POTAMENKO, I. R. see LASHKAREV, V. E., 1949
PRESTON, J. S. *Proc. roy. Soc. A* 202 (1950) 449, **197**
PUTLEY, E. H. *Proc. phys. Soc. A* 62 (1949) 284, **127**; *T.R.E. Jl* Jan. 1952, **207**
PUTSEIKO, E. K. *C. R. Acad. Sci. U.R.S.S.* 67 (1949) 1009, **29**; *Bull. Acad. Sci. Russ. (Phys.)* 13 (1949) 224, **196**
RADHAKRISHNAN, T. see RAMACHANDRAN, G. N. 1952
RADKOWSKY, A. *Phys. Rev.* 73 (1948) 749, **57**
RAMACHANDRAN, G. N. *Proc. Indian Acad. Sci. A* 25 (1947) 208, 266, **104**, **105**
— and RADHAKRISHNAN, T. *Phil. Mag.* 43 (1952) 317, **105**
RAMBERG, E. G. see ZWORYKIN, V. K., 1949
READ, W. T. see PEARSON, G. L. ,1952
REINKOBER, O. *Ann. Phys., Lpz.* 34 (1911) 243, **103**
REKALOVA, G. see TARTAKOVSKY, P., 1940
RETGERS, J. W. *Z. anorg. Chem.* 3 (1893) 399, **142**
RICE, F. O. and TELLER, E. *The Structure of Matter* New York, 1949, **230**, **239**
RICHARDSON, O. W. *Phil. Mag.* 23 (1912) 615; 24, 570, **35**
RIEHL, N. see MOGLICH, F., 1940
RIES, C., 1918, see BARNARD, 1930, **196**

RINGER, W. and WELKER, H. *Z. Naturf.* 3a (1948) 20, **129**
RISTAU, K. see WOLF, L., 1925
RITTNER, E. S. see HIPPEL, A. VON, 1946 and HUTNER, R. A., 1950: *Science* 111 (1950) 685, **41**
ROBERTSON, R., FOX, J. J. and MARTIN, A. E. *Phil. Trans. A* 232 (1934), 463, **75**, **95**, **99**, **102**, **103**
ROMPE, R. see MOGLICH, F., 1940, 1942
ROOSBROECK, W. VAN see FULLER, C. S., 1952
ROSE, A. *R.C.A. Rev.* 12 (1951) 362, **32**, **40**
ROSENFELD, L. *Theory of Electrons* Amsterdam, 1951, **21**
ROTH, L. Dissertation, Erlangen, 1938, **36**
ROTHLEIN, B. J. *Phys. Rev.* 83 (1951) 228, **123**
— and STAHL, F. A. *Sylvan. Tech.* 3 (1950) 8, **124**
ROY, S. C. *Proc. roy. Soc.* (1926) 112, 599, **35**
RUTTER, E. *Z. Phys.* 60 (1930) 1, **220**
RYDER, E. J. *Phys. Rev.* 82 (1951) 330, **130**; (see also RYDER, E. J. and SHOCKLEY, W. *ibid* 81 (1951) 139)
RYSKEVIC, E. see FORNSTECHER, M., 1945
RYVKIN, S. M. see KOLOMIETS, B. T., 1947; *C. R. Acad. Sci. U.R.S.S.* 68 (1949) 487, **39**
SAKAMOTO, Y. see SUGAWARA, T., 1949
SAKER, E. W. see GEBBIE, H. A., 1951 and HENISCH, H. K., 1952
SAKURAI, T. and MUNESUE, S. *Phys. Rev.* 85 (1952) 921, **207**
SAXON, D. S. and HUTNER, R. A. *Philips Res. Rep.* 4 (1949) 81, **8**, **10**
SCAFF, J. H. see THEUERER, H. C., 1951
SCANLON, W. and LARK-HOROVITZ, K. *Phys. Rev.* 72 (1947) 530, **204**, **205**
SCHAPER, I. see BECKER, A., 1944
SCHIFF, L. I. see Goodman, B., 1947
SCHILLING, K. see Koenigsburger, J., 1910
SCHLUNDT, H. *J. phys. Chem.* 5 (1901) 514, **238**; 8 (1904) 122, **154**
SCHMIDT, A. see ECKART, F., 1941
SCHMIDT, W. *Ann. Phys., Lpz.* 11 (1903) 114, **201**, **238**
SCHONWALD, B. *ibid* 15 (1932) 395, **63**
SCHOTTKY, W. *Z. Phys.* 113 (1939) 367, **42**, **54**
— *Schweiz. Arch. angew. Wiss.* Jan., 1941, **42**
SCHRAUF, A. *Z. Krystallogr.* 18 (1890) 113, **183**
SCHULZE, A. *Phys. Z.* 31 (1930) 1062, **110**
SCHWEICKERT, H. *Z. Phys.* 128 (1950) 47, **193**
SCOTT, N. W. see HASS, G. H., 1950
SEGRE, E. see CORSON, D. R., 1940
SEITZ, F. see CASTELLAN, G. W., 1951; *Modern Theory of Solids* New York, 1940, **5**, **16**, **23**, **240**; *Phys. Rev.* 73 (1948) 549, **14**, **101**, **110**; 79 (1950) 372, **12**
— and JOHNSON, R. P. *J. appl. Phys.* 8 (1937) 186, **244**
SELLA, A. see MELLOR, 1924
SERIN, B. *Phys. Rev.* 70 (1946) 104, **8**
SHARWIN, G. *J. Phys., Moscow* 9 (1945) 350, **136**
SHIFRIN, K. *ibid* 8 (1944) 242, **11**
SHIVE, J. N. *Phys. Rev.* 76 (1949) 575, **120**; *Bell Lab. Rec.* 28 (1950) 337, **125**; *The Transistor, Bell Teleph. Syst. tech. Publ.*, 1951, **125**
SHOCKLEY, W. see BARDEEN, J., 1950; GOUCHER, F. S. 1951; HAYNES, J. R., 1951; PEARSON, G. L., 1947, 1952; RYDER, E. J., 1951, and SUHL, H., 1949; *Bell Syst. tech. J.* 28 July, 1949, **54**; *Electrons and Holes* New York, 1950, **12**, **52**, **123** **125**, **128**, **130**, **229**
— and BARDEEN, J. *Phys. Rev.* 77 (1950) 407, **105**, **132**
— PEARSON, G. L. and HAYNES, J. R. *Bell Syst. Tech J.* 28 (1949) 344, **40**, **129**
— SPARKS, M. and TEAL, G.K. *Phys. Rev.* 83 (1951) 151, **125**
SIEG, L. P. see BROWN, F. C., 1914; *J. opt. Soc. Amer.* 6 (1922) 448, **199**
— and BROWN, F. C. *Phys. Rev.* 4 (1914) 507, **195**

SIEGMUND, W. P. see GIVENS, M., 1952
S.I.G.E.S.O., 1945, Report of German War-Time Research, **62**
SIMON, I. *J. opt. Soc. Amer.* 41 (1951) 336, **21**
SIMPSON, J. H. *Proc. roy. Soc. A* 197 (1949) 269, **64**
SKINNER, C. H. *Phys. Rev.* 9 (1917) 148, **199**
SKINNER, H. W. B. *Rep. Progr. Phys.* 5 (1938) 271, **6**
SMEKAL, A. *Z. Phys.* 55 (1929) 289, **61**
SMITH, R. W. *R.C.A. Rev.* 12 (1951) 350, **38**
SMITH, W. *Nature Lond.* 7 (1873) 303, **75**, **195**
Smithsonian Physical Tables Washington, 1933, **103**, **184**
SNEDDON, I. N. see MOTT, N. F., 1948
SOEZIMA, Y. *J. sci. Res. Inst., Tokyo* 44 (1949) 68, **189**, **220**
SOSNOWSKI, L. *Phys. Rev.* 72 (1947) 641, **54**
SPARKS, M. see GOUCHER, F. S., 1951, SHOCKLEY, W., 1951 and TEAL, G. K., 1951
STAHL, F. A. see ROTHLEIN, B. J., 1950: *Elect. Engng., N.Y.* 70 (1951) 518, **124**
STIEBER, A. see FREYMANN, R., 1934
STOCKMAN, F. *Naturwissenschaften* 37 (1950) 85 and *Z. Phys.* 128 (1950) 185, **28**, **111**
STRAUMARIS, M. E. *Z. Krystallogr.* 102 (1940) 432, **192**
— and AKA, E. *Z. J. appl. Phys.* 23 (1952) 330, **115**, **131**
STRUTHERS, J. D. see PEARSON, G. L., 1950
SUGAWARA, T., SAKAMOTO, Y. and KANDA, E. *Sci. Rep. Res. Inst. Tôhu'u Univ.* I (1949) 29, 153, **141**
SUHL, H. see PEARSON, G. L., 1951
— and SHOCKLEY, W. *Phys. Rev.* 75 (1949) 1617, **41**
SUHRMANN, R. and BERNDT, W. *Z. Phys.* 115 (1940) 17, **178**
SUTHERLAND, G.B.B.M. see DALY, E. F., 1949
SUTTON, R. B. see PEARLSTEIN, E. A., 1950
TAFT, E. see APKER, L., 1948, 1949
TAMMANN, G. *Z. anorg. Chem.* 197 (1931) 1, **201**
TANUMA, S. see FUKUROI, T., 1949, 1950
TARTAKOVSKY, P. and REKALOVA, G., *J. exp. theor. Phys.* 10 (1940) 1025, **181**
TAYLOR, J. H. see Miller, P. H., 1949; *Phys. Rev.* 80 (1950) 919, **131**
TEAL, G. K. see GOUCHER, F. S., 1951 and SHOCKLEY, W., 1951
— FISHER, J. R. and TREPTOW, A. W. *J. appl. Phys.* 17 (1946) 879, **75**, **107**, **110**
— SPARKS, M. and BLEULER, E. *Phys. Rev.* 81 (1951) 637, **119**, **123**
TELLER, E. see RICE, F. O., 1949
TENDAM, D. see LARK-HOROVITZ, K., 1948
THEURER, H. C. see FULLER, C. S., 1952 and PEARSON, G. L., 1950
— and SCAFF, J. H. *Trans Amer. Inst. min. (metall.) Engrs.* 189 (1951) 59, **118**
THORNHILL, J. W. and LARK-HOROVITZ, K. *Phys. Rev.* 82 (1951) 763, **15**, **130**
TOBISAWA, S. see FUKUROI, T., 1949, 1950
TORREY, H. C. and WHITMER, C. A. *Crystal Rectifiers* New York, 1948, **14**, **51**, **108**, **130**
TREPTOW, A. W. see TEAL, G. K., 1946
TREU, M. see FISCHER, F., 1938; Report of Wartime Work at Erlangen University, **35**
TREUTING, R. G. *J. opt. Soc. Amer.* 41 (1951) 454, **114**
VALLANCE, R. H. *Textbook of Inorganic Chemistry*, London, 1938, **158**
VAN DER VELDEN, H. A. see FREEMAN, G. P., 1952
VAN DYKE, G. D. *J. opt. Soc. Amer.* 6 (1922) 917, **224**, **225**
VAN VLECK, J. H. *Electric and Magnetic Susceptibilities* Oxford, 1932, **21**
VOLMER, M. *Z. wiss. Photogr.* 16 (1917) 152, **62**, **239**
VONWILLER, O. U., and MASON, W. H. *Proc. roy. Soc.* 79 (1907) 175, **201**
WAHL, W. *ibid* 88 (1913) 348, **230**
WALDERSTEIN, I. see LARK-HOROVITZ, K., 1946
WALTER, B. *Ann. Phys., Lpz.* 42 (1891) 505, **102**
WANNIER, G. H. *Phys. Rev.* 52 (1937) 191, **16**
WARBURTON, F. W. *ibid* 29, (1927) 905; 30 (1927) 673, **205**

WARTENBERG, H. *Phys. Z.* 13 (1912) 1123, **99**, **100**
WARTH, A. H. *Bull. Md Acad. Sci.* 3 (1923) 3. **91** ; *Trans. Amer. electrochem. Soc.* 47 (1925) 62, **91**
WEIMER, P. K. *Phys. Rev.* 79 (1950) 171, **186**, **188**
— and DANFORTH-COPE, A. *R.C.A. Rev.* 12 (1951) 314, **188**
WEINTRAUB, E. *Trans. Amer. electrochem. Soc.* 16 (1909) 165, **78**, **89**; *J. industr. Engng. Chem.* 3 (1911) 299, **78**; 5 (1913) 107, **89**, **91**,
WEISSKOPF, V. F. see CONWELL, E., 1946
WELD, L. D. *J. opt. Soc. Amer.* 6 (1922) 67, **199**
WELKER, H. see RINGER, W., 1948
WESOLOWSKI, J. *Bull. int. Acad. Cracovic* (*Acad. p. l. Sci.*). 6–7*A* (1938) 290, **201**
WESTPHAL, W. C. see HAYNES, J. R., 1952
WHITEHEAD, S. and HACKETT, W. *Proc. phys. Soc.* 51 (1939) 173, **102**
WHITMER, C. A. see TORREY, H. C., 1948
WIELAND, J. see BUSCH, G., 1950, 1951
WILFORD, S. E. see MICHELS, W. C., 1949
WOLD, P. I. *Phys. Rev.* 7 (1916) 169, **205**
WOLF, L. and RISTAU, K. *Z. anorg. Chem.* 149 (1925) 403, **141**
WOOD, R. W. *Phil. Mag.* 3 (1902) 607, **200**
WYCKOFF, R. W. G. *Crystal Structures* New York, 1948, **78**, **230**
ZOLLER, H. see BUSCH, G., 1950, 1951
ZWICKY, F. *Proc. nat. Acad. Sci. Wash.* 15 (1929) 816, **61**
ZWORYKIN, V. K. and RAMBERG, E. G. *Photoelectricity and its Applications* New York, 1949, **195**, **197**

SUBJECT INDEX